Scuola Internazionale Superiore di Studi Avanzati - Trieste

"ABDUS SALAM" INTERNATIONAL CENTRE FOR THEORETICAL PHYSICS
SCUOLA INTERNAZIONALE SUPERIORE DI STUDI AVANZATI

ASTROPARTICLE PHYSICS JOINT PHD PROGRAMME

The Abdus Salam
International Centre
for Theoretical Physics

Scuola Internazionale
Superiore di Studi
Avanzati

DARK MATTER AND GALAXY ROTATION CURVES

Candidate: Ernesto López Fune. **Supervisor:** Prof. Paolo Salucci.

Thesis submitted for the degree of Doctor Philosophiae.
Trieste, Italy.
Sept 14, 2017.

SISSA - Via Bonomea 265 - 34136 TRIESTE - ITALY

“ABDUS SALAM” INTERNATIONAL CENTRE FOR THEORETICAL PHYSICS
SCUOLA INTERNAZIONALE SUPERIORE DI STUDI AVANZATI

ASTROPARTICLE PHYSICS JOINT PHD PROGRAMME

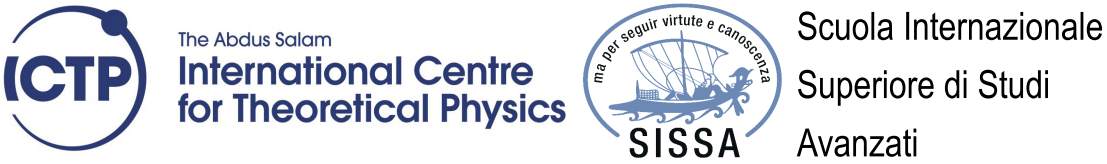

DARK MATTER AND GALAXY ROTATION CURVES

Candidate: Ernesto López Fune. **Supervisor:** Prof. Paolo Salucci.

Thesis submitted for the degree of Doctor Philosophiae.

Trieste, Italy.

Sept 14, 2017.

Acknowledgments:

I want to say thanks to Prof. Paolo Salucci for introducing me to the subject of dark matter and being my mentor during this time, from which I learned many topics in the field of astrophysics and dark matter phenomenology, and would be a honor to keep working and collaborating with him. Also to the Astroparticle Physics department for having me during these four years, even when I wasn't enough visible. To SISSA and ICTP in general for making me a part of their lists of graduated students, which I feel very proud. To the ICTP director F. Quevedo and Prof. K. Narain for doing more than the impossible to bring me to the institute as a diploma student. Also to all the SISSA and ICTP diploma professors, my classmates and in general SISSA and ICTP staff.

Abstract

Cosmological N-body simulations on structure formation in a $\Lambda-$CDM scenario point to a mass density distribution of dark matter, in local objects like galaxies, that are in strong tension with recent observations on low surface brightness galaxies. Modified theories of gravity lack of this problem but also find tensions with observations at larger scales. In this thesis we study the main methods for galaxy rotation curve fitting, from modified theories of gravity such as MOND and $f(R) = R^n$, and considering dark matter halos, such as the one derived from the $\Lambda-$CDM numerical simulations and the phenomenological Burkert cored halo profile. To investigate the properties of the dark matter halo that surrounds galaxies, two methods are examined: the standard mass modeling and the local density method. All these methods are applied to the study of the rotation curve of the galaxy M33, which is well extended and measured with an unprecedent high spatial resolution. Later on, we present a unified parameterization of the circular velocity which accurately fits 887 galactic rotation curves without needing in advance the knowledge of the luminous matter components, nor a fixed dark matter halo model. A notable feature of this parametrization is that the associated gravitational potential increases with the distance from the galactic center, giving rise to a length scale indicating a finite size of a galaxy, and after, the keplerian fall-off of the velocity is recovered, making possible for the prediction of the total mass enclosed by the galaxy. As the keplerian regime is reached after a finite length scale, based on isotropy and homogeneity arguments, we considered a static and spherically symmetric Schwarzschild-like space time embedding each galaxy, such that any massive particle moving in geodesic circumferences in the equatorial plane, turns around origin of coordinates with the newly found parameterized velocity formula. Appealing to the General Relativity field equations, for a perfect fluid with pressure anisotropies, we found that the dark matter halo behaves like a cosmological constant in the outer parts of galaxies and controls the distribution shape of the luminous matter component by means of the anisotropic pressure in the azimuthal direction.

Published papers

The work presented in this thesis has been partially published in scientific papers.

- "The radial dependence of dark matter distribution in M33," E. L. Fune, P. Salucci and E. Corbelli, Mon. Not. R. Astron. Soc. **468** (2017), 147-153, [arXiv:1611.01409].
- "Empirical velocity profiles for galactic rotation curves," E. L. Fune and P. Salucci, in preparation for Mon. Not. R. Astron. Soc.

Contents

Chapter 1

General Introduction

1.1 The dark matter problem

For more than already 80 years, the scientific community have been struggling on decipher about the way galaxies and other cosmic structures appear to gravitate toward something invisible in the Universe. The earliest indications that scientists are concerned with this phenomenon date back to the XIXth century when Lord Kelvin first estimated the number of faint stars in the Milky Way from the observed velocity dispersion of the visible stars. The velocity at which the visible stars were orbiting around the center of the galaxy and their velocity dispersion give an estimate of the mass of the galaxy. His main conclusion was that the mass of the galaxy was greater than the total mass inferred from the visible stars, which means that a great majority of the total amount of stars in the Milky Way should be very faint or dark bodies.

Later on, in 1915, Ernst Öpik [1] developed a method to determine the density of matter near the galactic plane by using the vertical oscillations of stars. Öpik was curious about the densities of visual binary stars, in particular, he measured the density of o^2 Eridani and determined it as 25.000 times the density of the Sun, but soon he concluded that his result was impossible, and the only explanation was that however high the temperature of the star is, the surface brightness or radiating power was very low, leading to the absorption of light in the galaxy by the possible presence of absorbing invisible matter near the Milky Way. A bit more later, in 1932, the dynamical density of matter in the Solar vicinity was investigated by Oort [2], who arrived to a different answer. According to his analysis the total density exceeds the density of visible stellar populations by a factor of up to 2. This limit is often called the Oort limit and it means that the amount of invisible matter in the Solar vicinity could be approximately equal to the amount of visible matter.

Another indication of the possible existence of a sort of invisible matter came from more extended cosmic objects like galaxy clusters. In 1933, Fritz Zwicky measured the radial velocities of galaxies in the Coma cluster [3], where he found that the velocities of the individual galaxies with respect to the cluster mean velocity were much larger than those expected from the estimated total mass of the cluster, calculated from the sum of the individual mass of each galaxy.

A bit more later, in 1939, Horace W. Babcock reported the rotation curve (hereafter RCs) for the Andromeda nebula, giving the first robust indications that the mass-to-light ratio in this galaxy was larger than unity [4]; even more, he suggested that the mass-to-luminosity ratio increases radially. Babcock, attributed this phenomenon to either light absorption within the galaxy or modified dynamics in the outer portions of Andromeda but not to invisible matter.

The consolidation point where this invisible matter became a real problem in Physics was brought by Vera Rubin, Kent Ford and Albert Bosma in the 1960s-1970s. These scientists provided strong evidences of the existence of an invisible form of matter from the observations on galaxy RCs [5, 6, 7]. The works of Rubin in measuring accurately the circular velocity of stars and gas of edge-on spiral galaxies, lead to the conclusion that most galaxies must contain about six times as much dark as visible mass. In the '80s, the apparent need for dark matter (hereafter DM) was widely recognized as a major and unsolved problem in observational astronomy. The term for Dark Matter or Matière Obscure (in French), appeared for the first time in the manuscripts "The Milky Way and Theory of Gases" of Henri Poincaré in 1906 as he referred when discussing Lord Kelvin works. At the end of the 80's, a stream of new observations not only on galaxy RCs but also including the gravitational lensing of background objects by galaxy clusters, the temperature distribution of hot gas in galaxies and clusters, and the pattern of anisotropies in the Cosmic Microwave Background (CMB) with the early observations of COBE, indicated the presence of the DM in the Universe. This hypothetical invisible form of matter seems to outweigh all visible matter by a five-to-one ratio, which suggests that we barely know our Universe. The main consensus in the scientific community is that the DM is composed primarily by a unknown-yet-type of subatomic particle of non-baryonic nature, constituting nowadays the biggest challenge of the Standard Model of Particle Physics and the Concordance Model in Cosmology.

1.2 Particles or gravity?

The DM scenario looks pretty seductive for the particle physics point of view due to the necessity of postulating a new sector of new particles and a new physics beyond the Standard Model, which is also needed to explain other high-energy phenomena. Hence, to find a solution to this puzzling problem, both, theoretical and experimental efforts should be done, which include astrophysical and accelerator experiments as well.

Large surveys about cosmic structures, suggest that the DM particles should not carry electric nor color charges, since there are no evidences at present of DM heavy isotopes; therefore, if the DM is the distribution of congregates of elementary particles, they should be composed by neutral particles interacting very weakly with ordinary particles. They must be produced in the early universe via thermal processes or from the decay of their parent particles before the radiation-to-matter dominance transition, with their correct relic abundances. One of the most important property is that since their effects are present at this precise moment, then they have to stable against the cosmic time scale.

The kinematical properties of the DM clearly affect the CMB anisotropy spectrum and play important roles in the structure formation in the Universe. According to their velocities at the decoupling time, the DM can be divided into three kinematical categories [8]:

1. The Hot Dark Matter (HDM) is composed by abundant light particles and the best candidates are the light neutrinos from the Standard Model. Since the light neutrino masses are of the order of 1 eV or less, then, when free streaming, they are in the ultra-relativistic regime at the decoupling time and remain in this state when the galaxy formation process starts to take place at the cosmic photon temperature of 1 KeV. Highly relativistic particles generate high pressure fluids, so they can wash out small dense chunks of matter suppressing the formation of galaxies by destroying small scale structures of the Universe, as supported as well by N-body simulations. This is obviously in conflict with cosmological observations of large scale structures, disfavoring this hypothesis. Worths to mention that HDM, despite it certainly exists in the Universe, in the form of neutrinos, can only be a small part of the total amount of matter.

2. The Cold Dark Matter (CDM) is the extreme opposite of the HDM in the mass-velocity spectrum. The main features are: it is non-relativistic at the decoupling time and its mass can be of the order of the GeVs or even larger. The best candidates come from the supersymmetric extensions of the Standard Model which include the so called WIMPs (Weakly Interacting Massive Particles) like neutralinos, or other exotic particles like WIMPZILLAs, solitons, etc. A fluid of non-relativistic particles may exerts very little pressure and may form small scale structures. Later on, I will continue the discussion on CDM.

3. The Warm Dark Matter (WDM) lies between the HDM and CDM mass-velocity spectrum and it is formed by a fluid of particles in the mass range around the KeV or even higher. It is relativistic at decoupling time but then becomes non-relativistic at the radiation-to-matter dominance transition. The possible candidates for WDM include the sterile neutrino, light gravitinos and photino.

Physics beyond the Standard Model provides a whole new set of particles from which there are some well-qualified candidates for non-baryonic DM. However, parallel to individual elementary particles, there exist large astronomical bodies, most of them are no longer viable, which can also fulfill the DM necessities, such as the Massive Compact Halo objects (MACHOs), Masive Compact Objects (MCOs), Black Holes (BHs) and Primordial Black Holes (PBHs), etc. The MACHO class involves very dim stars, brown dwarfs which have small masses, less than 10% of that of the Sun, and dense chunks of heavy elements, which can be observed via gravitational lensing; however, studies about the big bang nucleosynthesis rule-out the possibility of MACHOs being a candidate to solve the DM problem and they should be only a very small fraction of the total DM mass. On the other hand, MCOs are clumps of dense and very dim luminous matter similar to MACHOs, and they can be detected (if they are distributed in the Universe) as well by gravitational lensing from supernovae explosions. The light coming from supernovae will be scattered when encounters MCOs yielding a distribution map; however, observations of more than 300 distant supernovae shown show no signs of MCOs with a mass

greater than 1% the solar mass, and they can be rule-out as well from the DM candidate list [9]. Last but not least, large scale BHs and PBHs are ruled-out as well by the gravitational lensing data, however, small-sized BHs are not totally excluded from the list of DM candidates [10].

The main tool for theoretical astrophysics to investigate the properties of the DM as a particle relies in N-body simulations, where a heavy calculational approach is necessary [11, 12, 13]. This approach has already yielded some important results on the kinematical properties of the DM, which provide important constraints for the particle physics approach, such as the impossibility of a hot DM scenario, which leave place only for cold or warm DM. Maybe the most successful model of DM is provided within the $\Lambda-$CDM Cosmology, whose current paradigm is that it assumes that DM is made of WIMPs, forming a cold and collisionless fluid [11, 12, 13]. This is strongly supported by the largely smooth CMB radiation as measured by the satellites COBE and WMAP. In this framework, numerical simulations of structure formation, taking only into account WIMPs (not including baryons) suggest that galaxies are embedded celestial bodies in a DM halo, which to the extent of the particle resolution in every simulation, can be considered as spherical, such that the extrapolated (locally in galaxies) mass density $\rho_{DM}(r)$ distribution of DM is nearly universal, i.e. dependent only on the mass of the halo.

Despite of the success of the $\Lambda-$CDM model, it suffers from two main problems when matching with local observations such as the overabundance of dwarf galaxy satellites and the cuspy halo problem. The dwarf galaxy problem or as it is usually addressed as the missing satellite problem consists in the fact that numerical simulations predict a large number of dwarfs satellite galaxies than the observed in galaxy clusters. For example, in the nearby of the Milky Way there were observed around 11 dwarfs galaxies orbiting the Milky Way, however, numerical simulations predict around 500 satellites. The cuspy halo problem, also addressed as the core-cusp problem, refers to the fact that numerical simulations predict a local density with a characteristic steep slope (cusp) in the inner regions of the galaxies which can be approximated by a power-law $\rho(r)/\rho_c \simeq (r/r_c)^{-\gamma}$, with ρ_c a characteristic constant density, γ of order unity, and r_c a constant scaling radius. This cuspy density profile has not been inferred for several dwarfs, spirals and LSB galaxies [14, 15, 16, 17, 18, 19, 20] whose RCs favor a much shallower cored profile, as showed in Fig.(1.1).
In addition, independent evidence for a cored distribution comes from stacked RCs which lead to almost solid body profile $V \propto r$ at $r \to 0$ [21, 22, 23], see Fig.(1.1) as well. All this evidence, though remarkable, still needs some investigations because the inner regions of galaxies are dominated by the luminous matter. The cusp-core issue in galaxy DM density profiles is also related to the investigation of the nature of the DM itself and to the galaxy evolution. Numerical simulations have in fact shown that baryonic feedback occurring at later times than the galaxy formation epoch can transform the original cuspy profiles into cored ones [11, 24]. Hence, the existence of cores for DM halo density distributions in dwarf galaxies may not be sufficient to disprove the $\Lambda-$CDM scenario. Specifically, one needs, for the same galaxy, very accurate mass models and a high quality RCs which traces, with high resolution, the inner disk kinematics

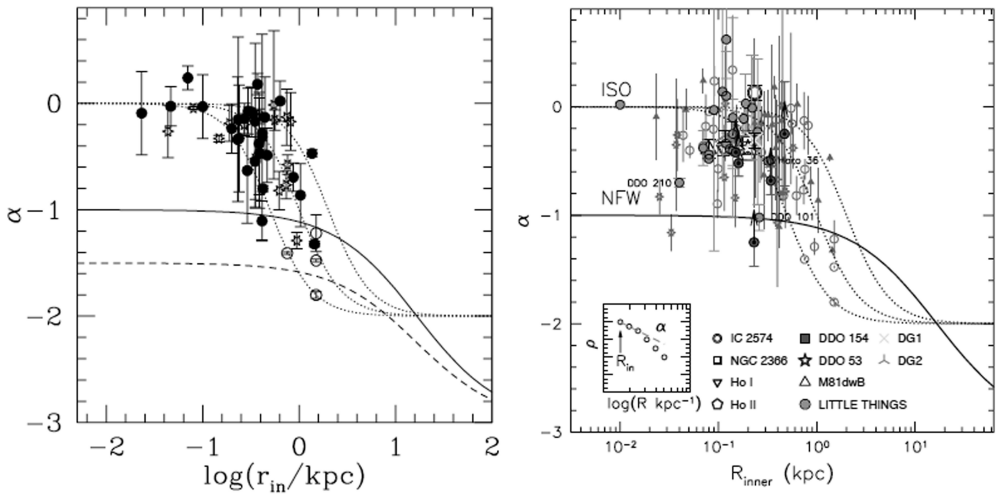

Figure 1.1: The inner slope of the DM density profile inferred from numerical N-body simulations as a function of the radius R_{in} in the innermost region of a galaxy. Solid and dashed lines correspond to the theoretical predictions of the Navarro-Frenkel-White (hereafter NFW) and Isothermal Sphere halo mass density profiles respectively. In the left panel is shown these inferred halo density profiles and a sample of Low Surface Brightness (LSB) galaxies as the experimental points as described in [25], while the right panel shows the galaxy samples presented in [20].

(using mm or optical line tracers) and extends radially for several disk scale lengths (thanks to the outer disk 21-cm line emission of neutral hydrogen).

Not mentioned in the above mass-velocity spectrum, recently it has been considered that DM could be even self-interacting. This DM model, proposed initially in [26], pretends to solve the cusp-core issue within the CDM framework, by considering non-negligible the microscopic interactions of the DM particles, which should suppress high density fluctuations at small scales that could affect the dynamics of the DM halo formation [27, 28, 29]. The Bullet Cluster could be an interesting cosmic object to prove the viability of this self-interacting DM model and to constrain the particle spectrum of possible DM candidates.

On the other hand, present WDM N-body simulations suggest the suppression of the growth of structures at small scales, which alleviate the cuspy mass density profile problem arising in the framework of the $\Lambda-$CDM cosmology [30, 31]. In the WDM framework, cuspy or small-sized cores are obtained for the extrapolated mass density profiles at small scales; the core sizes are even smaller than the ones predicted from the direct fittings of the experimental RCs [32, 33, 34]. However, in [31] is suggested that if quantum corrections of the WDM are taken into account, simulations should be able to reconstruct the correct small scale (even below 1 kpc) structure of cosmic objects.

1.2.1 Direct and indirect method for the dark matter search

The direct and indirect searches of DM candidates has grown up in last decades, but so far, experimental reports give mostly negative results. Most searches of DM in form of WIMPs performed to date, involving direct, indirect, and accelerator searches, have set tighter limits on the mass-cross section spectrum. The interactions between DM with SM particles can be split into: spin-dependent or spin-independent interactions. Most of the DM detection experiments are based in spin-independent interactions, however, spin-dependent scattering processes between DM particles and nuclei are also important. The motivation of this subsection is, although out of the main scope of the present thesis, to give an overview of the most know experiments for DM search.

One of the most important projects in searching directly DM candidates is the DAMA collaboration, which is an observatory for rare processes based on scintillator techniques, located in the Gran Sasso underground laboratory. The first project was called DAMA/NaI which contained a scintillator of thallium-doped sodium iodide (NaI Tl, hence the name) crystals. It has been one of earliest detectors used in direct investigation of DM particles in the Milky Way galactic halo.

Since the Earth orbits around the Sun and this last drags the whole solar system around the center of the galaxy, the Earth is exposed to a higher flux of DM particles around June, when it is closer to the Sun and its orbital velocity is added to the one of the solar system with respect to the center of the galaxy, and to a smaller flux around December, when the two velocities are subtracted. Its main feature is that it is a model independent detector and became the first DM search experiment. In 1997 claimed a direct signal of DM due to the annual modulation in the relative velocity between the WIMP fluid that forms the halo surrounding the galaxy and the DAMA detector because of the Earth orbital motion [35]. The obtained results were compatible with the wide DM particle spectrum such as neutralinos, self-interacting DM, and heavy neutrinos. The annual modulation can be interpreted as that of the WIMP velocity in the earth frame and this collaboration agrees that the observed annual modulation is a clear evidence of the presence of a DM halo surrounding the Milky Way.

A new upgrade of the DAMA/NaI detector is called DAMA/LIBRA which uses the same technique as the former. The collected data can be well fitted to a WIMP-nucleon cross-section compatible with the predictions from the Minimal Super-symmetric Standard Model (MSSM), which implies [36] either a WIMP of mass $m_\chi = 50$ GeV with the elastic WIMP-proton cross section $\sigma_{\chi p} \approx 7 \times 10^{-6}\ pb$, or a lighter WIMP of mass $6 - 10$ GeV with $\sigma_{\chi p} \approx 7 \times 10^{-3}\ pb$. However, it has been found that the DAMA data is not longer compatible with current upper limits from other experiments which have higher resolution.

Other direct detection experiments are the Cryogenic Dark Matter Search (hereafter CDMS), the Collaboration Germanium Neutrino Technology (hereafter CoGeNT) and the Cryogenic Rare Event Search with Superconduction Themometers (hereafter CRESST-II). The CDMS

uses Germanium-Silicon technologies to detect WIMP DM particles. Its first experiment, usually called CDMS-I was located in a tunnel under the Stanford University campus. The second generation experiment or CDMS-II is located underground in the Soudan Mine in Norther Minnesota, U.S.A, which is better shielded from cosmic rays and other cosmogenic events. The CDMS-II experiment, kept at very low temperatures to avoid possible thermal noise, uses a crystal detector of phonon-produced elastic collisions between nuclei and WIMPs. The energy deposited in the detector by an incident WIMP may be as low as a few tens of keV. The CDMS-II collaboration had observed two candidate events even when the expected background was 0.9 ± 0.2 events. Despite the high expectations of the community, these two events are not statistically significant as a direct DM signal and the likelihood analysis indicated that they are likely leakage events rather than a WIMP signal [37].

On the other hand, the experiment CoGeNT [38] is in the search of low mass WIMPs y using a high-purity and low radioactivity Germanium source for ionization signal. It is, as well as CDMS, located in the Soudan Mine but it is a smaller setup compared to the CDMS-II. The detector is calibrated to detect WIMP mass in a much lower range than most of the other direct search experiments, and the techniques are as well ideal to search for annual modulation signatures due to low mass WIMPs as DAMA/LIBRA. The data collection started by the end of 2009 and detected of the order of hundred of particle signals which were first interpreted as light WIMPs with mass in the range of $7 - 11$ GeV and cross section $\sigma_{\chi p} \approx 10^{-4}\ pb$. There's no final consensus as they could be identified as well as background of residual events [39, 40] (and references therein).

The CRESST-II [41] collaboration consists in a direct detection experiment of phonons and scintillation signals via WIMP scattering on target nuclei of $CaWO_4$ crystals. Phonons provide the measurements of the energy recoil due to the interactions and the scintillation light discriminate different types of interacting particles, and to screen out possible background events. The collaboration found 67 acceptable events, and all the possible estimated background events were unable to explain these results. The collaboration announced a WIMP candidate signal of a statistical accuracy more than 4σ, however a background reduction is needed for better clarifications.

In parallel, there are other indirect experiments in the search of DM particles by looking at the sub-products of their interactions with SM particles. DM signals can be detected by charged particles such as positrons, electrons, antiprotons, anti-deuterons, etc. Annihilation channels of WIMPs can be measured by the flux shapes of positrons and antiprotons, which are completely determined by the WIMP mass (in the corresponding channel). One of these experiments is the Payload for Antimatter Matter Exploration and Light-Nuclei Astrophysics or best known as PAMELA, which consists in a satellite which was launched in 2006 and observed a sharp increase in the energy spectrum of the positron fraction $e^+/(e^+ + e^-)$ in the range of 10 GeV to 100 GeV [42, 43], which is thought to be a possible sign of DM annihilation process. Another possible explanation of this sharp increase is the production of electron-positron pairs on pulsars with subsequent acceleration in the vicinity of the pulsar. The first two years of data collections

were released in 2008, where the positron excess was confirmed but no excess of antiprotons was found. This is in contrast with the predictions since the positron and antiproton excesses should be correlated.

Another indirect search experiment is the Fermi Large Area Telescope or FermiLAT satellite which confirmed, in their more recent data, the PAMELA observations on the positron fraction and extended the energy of the excess up to 200 GeV. Although an astrophysical origin for the sharp increase of the positron fraction cannot be ruled out, a DM explanation could be possible. According to the measurements, the DM particle that could fit the data has to be very massive, mass of the order of a few TeVs in order to fit the electron plus positron spectrum; it has to be also leptohilic, which means that they have to annihilate only giving leptons as the final state, not quarks which would result in an enhancement in the antiproton and proton spectrum, which is not observed; and the corresponding annihilation rate of the DM particles into the lepton channel has to be signficantly larger than the thermal relic benchmark cross section of $\sigma \approx 3 \times 10^{-26}$ cm$^3/s$, which is, with a velocity of $v = 0.1c$, about $1pb$. More recent, the Alpha Magnetic Spectrometer (AMS-02) on the International Space Station has announced their first result on the positron spectrum, which confirms the trend of the excess position up to 350 GeV with no sign of turn over.

Photons will be produced indirectly (from secondary emissions) after the annihilation of the DM particles. Diffuse gamma rays are secondary photons of DM annihilation into charged particles, which are hadronized to produce, say, high energy neutral pions which decay into two photons of high energies, carrying the information of the mass and energy of the DM particles. The spatial distribution of these photons follows the distribution of the DM particles, therefore there's a high probability to find those diffuse gamma rays where higher concentrations of DM is expected, such as in the center of the galaxies and satellite dwarf galaxies, also called Dwarf Spheroidals (dSphs). The latter are expected to have high concentrations of DM. Several experiments like FermiLAT, Hess telescope, and the VERITAS telescope have been looking for these diffuse gamma rays in the energy range of GeV and above; however, no DM signals have been presented by any of the above mentioned experimental collaborations.

Heavy DM annihilation processes may produce high energy neutrinos and anti-neutrinos coming from the center of the Milky Way where a high concentration of DM is expected. The advantage of neutrino detectors is based in the fact that the firsts have a very long mean free path due to their very weak interactions so they can reach the Earth-shielded detectors, isolated from other background events like cosmic rays. Neutrinos can be detected in a controlled environment of underground laboratories, under water, or in ice. Neutrino detectors include Super-Kamiokande (Super-K), ICECUBE and ANTARES. To date there are no relevant signals in the neutrino channel from Super-K and ICECUBE. The absence of high energy neutrinos from the galactic center and from the Sun sets useful constraints on the DM particle mass and annihilation cross sections.

Two double phase (liquid-gas) Xenon-based indirect search experiments that are currently on the look for DM particles as WIMPs are the Large Underground Xenon (LUX) and the

XENON1T experiments [36]. The DM interactions in liquid Xenon generate gamma rays and ultra-relativistic electrons that are immediately detected by arrays of photomultiplier (photons) and drifted upwards (electrons) towards the Xenon gaseous phase by a strong electric field. The accelerated electrons onto the gas produce electroluminescence photons, which along with the primary gamma rays, can reconstruct the particle interaction in the liquid Xenon. The LUX experiment, 368 kg of pure and liquified Xenon, is located 1.510 m underground at the Sanford Underground Laboratory in the Homestake Mine (South Dakota), and being operated at the Sanford Laboratory. LUX is a time-projection chamber which allows 3D positioning of interactions occurring within its active volume and operates as a liquid Xenon scintillator [44]. The events registered by LUX so far are all consistent with electron recoil backgrounds, which means no low-mass WIMP interactions [45]. Till the final run, from October 2014 to May 2016, LUX hasn't detected DM candidate as WIMPs [45].

On the other hand, the XENON1T project, operated at Gran Sasso, is also a deep underground detector which looks for rare interaction events via nuclear recoils in a liquid Xenon target chamber. Xenon1T aims to detect both: scintillation and ionization produced when the WIMP particles interact with the liquid Xenon to look for an excess of nuclear recoils over known backgrounds. The most recent results date from May, 2017, when was presented the collected data from 34 days. Unfortunately, no signals of WIMPs or other DM candidates were officially detected, but they achieved a record of low reduction in the background radioactivity levels [46].

The experimental high energy physics community is tirelessly looking for such invisible particles; however, in parallel, there is a another community that proposes Modifications of Gravity (MOG) to explain the phenomenon of the mass discrepancy without having to resort to new particles beyond those predicted by the well-known Standard Model. From the particle physics point of view, the DM phenomenology explanation is based on General Relativity (GR) which at the same time is rooted on the Newtonian classical gravity. However, as pointed out by many authors, it may not be the only approach to resolve the problem. There are three different directions in the modification of gravity, which include the modified Newtonian dynamics (hereafter MOND), $f(R)$ theories and Quantum Gravity. In this thesis I will review only the first two theories of modified gravity since they are relevant in explaining the flatness of galaxy RCs.

MOND was first proposed in [47] and relativistically generalized to the Tensor-Vector-Scalar theory (hereafter TeVeS) scheme in [48], such that in its construction, flat RCs are implemented with the help of an acceleration scale a_0 separating the Newtonian and Modified-Newtonian (MONDIAN) regimes, and an interpolating function smoothly joining both. $f(R)$ theories promote a generalization of the Hilbert-Einstein action to a general function $f(R)$ of the Ricci scalar R [49], containing GR when $f(R) = R$ (f is identity function). However, recent observations on gravitational lensing from galaxy clusters, disfavor MOND/TeVeS and $f(R)$, and the conclusion is that in order to accommodate all observations, a DM component is needed in the MOND/TeVeS and $f(R)$ frameworks.

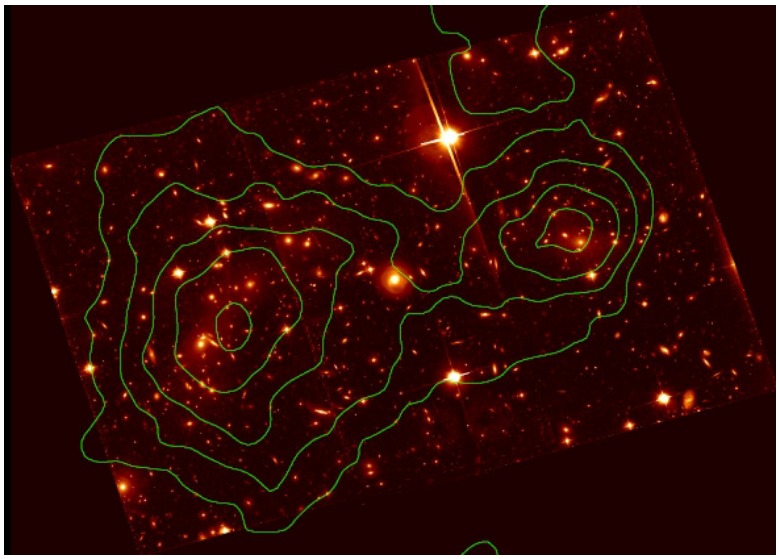

Figure 1.2: Hubble Space Telescope photograph of the Bullet Cluster and the mass density contours superimposed, inferred from the gravitational lensing.

The most serious and recent problem facing MOND (and generalizations) came in the 2006 observations of a pair of colliding galaxy clusters also known as the Bullet Cluster [50]. It poses a significant challenge for, not only MOND but also for every modified theory of gravity proposing a solution to the missing mass problem in the Universe. Astrophysicists measured the density distribution of stars and gas in the clusters using visible and X-ray light techniques, respectively, and with the gravitational lensing, the inferred DM density was mapped. In MOND, one would expect the missing mass to be centred on the visible mass, however, an offset was found in the observations as the lensing source is misplaced with respect to the baryons, see Fig.(1.2). This new fact leaves an alternative: or a sort of unseen non-baryonic mass must exist in galaxy clusters, which detracts from the elegance of MOND, or to take MOND altogether with 2 eV sterile neutrinos, which could account for the cluster observations and preserves the theory's successes at the galaxy scale [51, 52]. This last idea initially appeared as promising since sterile neutrinos along with MOND were able to solve the Bullet Cluster problem and reproduce correctly the CMB power spectrum [53, 54]; however, more recent MOND cosmological simulations with sterile neutrinos showed that too many too massive galaxy clusters are formed [55]. In the case of $f(R)$ theories, recent studies have proven the equivalence between $f(R)$ gravity to a scalar-tensor gravity theory, so, the previous efforts on this model attempt to look for a model of DM as a matter scalar field [56, 57, 58, 59, 60]. Most of the works in this direction concentrate on models of the form $f(R) = l_0 R^n$. In [61, 62] was studied a theory of this form with $n = 1 - \alpha/2$ by using spherically symmetric solutions to approximate galaxies. Performing the corresponding fittings with a large sample of galaxies, they found $\alpha = (3.07 \pm 0.18) \times 10^{-7} \left(M/10^{10} M_{\odot}\right)^{0.494}$, being M the mass of the galaxy. As argued in [63], the fact of having α depending on the mass of each individual galaxy, makes the whole approach highly implausible since with one fixed choice of $f(R)$ one cannot find reasonable fits for all galaxies.

This thesis is organized in four chapters. Chapter 1 is intended to give a review of the most used methods in galaxy RC fitting in order to study these cosmic objects. Either using MOG such as MOND and $f(R)$ theory, or considering a DM halo (such as the NFW or the BRK mass density profiles) that harbors galaxies, the standard method consists in finding the best fitting parameters of each model such that they minimize the χ^2 distribution concerning the experimental data. From the DM point of view, two methods are discussed: the standard dynamical mass modeling and the local density method whose difference strikes in the fact that in the second method one can study the DM halo properties only relying on the experimental data and not knowing in advance the luminous matter distribution such as stars and gas; the inconvenience of this method is that one needs an analytical formula to represent the circular velocity experimental points, problem that will be solved in the third chapter. Chapter 2 contains a direct application of the above mentioned methods applied to the galaxy M33. The RC of M33 is studied in the context of MOG and DM halo models, with the corresponding results. Chapter 3 is dedicated to present a general method to fit RCs without knowing in advance the luminous matter distribution nor a specific DM halo. A velocity formula is proposed such that provides outstanding fits for the experimental RCs for later use in the local density method. Finally, Chapter 4 is dedicated for the conclusions of this thesis and the prospects for future research.

Chapter 2

Galaxy rotation curves as modified gravity or dark matter tracers

2.1 Galaxy rotation curves

A galactic rotation curve (hereafter RC) is a two-dimensional diagram which shows the circular velocity fields of stars and gas as a function of the distance from the center of the galaxy. They are directly given from experimental observation of the lines Hα of stars and the 21-cm emission line of the atomic Hydrogen HI respectively, via their Doppler shifts. If the measured velocity fields are nearly circular and confined to a disk, then, from the astrometry one needs to determine the disk orientation, the position angle of the major axis PA (the angle measured counter-clockwise between the north direction on the sky and the major axis of the receding half of the galaxy), the inclination angle with respect to the line-of-sight i, the systemic velocity $V_{\rm sys}$, the center position (x_c, y_c) and circular velocity $V_C(r)$ inferred by the Doppler shift $\lambda_{\rm obs}(r)/\lambda_{\rm emit}(r) = 1 + V_C(r)/c$, being c the speed of light in vacuum. The measured circular velocity at the point (x, y) can be computed via the formula:

$$V(x,y) = V_{\rm sys} + V_C(r)\sin i\cos\theta, \tag{2.1}$$
$$\cos\theta = -\frac{(x-x_c)\sin PA - (y-y_c)\cos PA}{r}, \quad \sin\theta = -\frac{(x-x_c)\cos PA + (y-y_c)\sin PA}{r\sin i}.$$

There are many cases in which the gaseous disk shows different orientations than the inner ones, so the disk is said to be warped and the above parameters parameters vary with the distance from the center of the galaxy. The final extended RC is build by stacking the circular velocity of stars and gaseous disks, see for example Fig.(2.1).

Before the development of the modern techniques of radio-astronomy, RCs were build up only by the optical velocities of stars, till the optical extent of the galaxy, which can be quantified by means of the Holmberg radius [64]: the major-axis radius at a surface brightness of 26.5 $mag\, arcsec^{-2}$. Later on, M. S. Roberts [65] found that the median extent of optical RCs published up to 1975 was only till 0.3 of their Holmberg radii. These curves typically showed

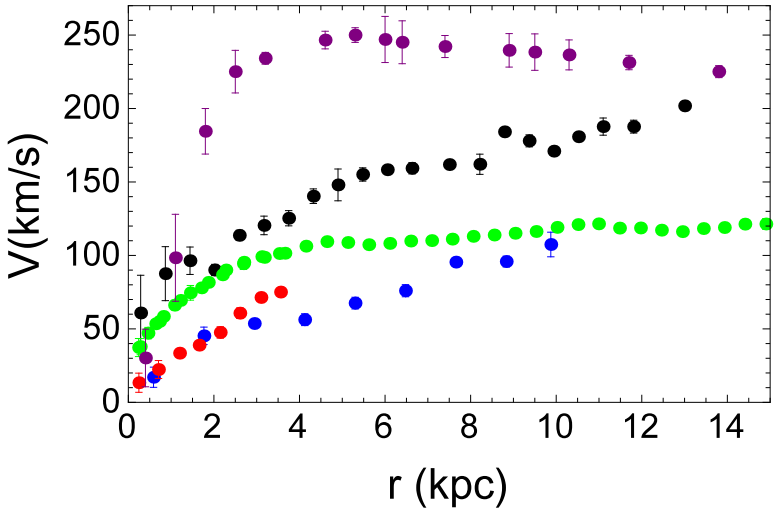

Figure 2.1: Examples of extended RCs of different spiral galaxies.

a circular velocity[1] with a steep slope near the galactic center and then a short decrease. At this point, the available data ended, usually because the surface brightness of the galaxy was so low that further measurements with the resolution of the equipments developed at that time were impossible. Beyond the last measurement point, it was assumed that the turnover of the rotation curve was achieved and the circular velocity was reaching asymptotically the Keplerian regime $V \propto r^{-1/2}$, at large distances. Soon after, theoretical models were developed to reproduce the experimental curve and from it, infer the mass distribution and total mass enclosed inside the galaxy, but it was not till 1978 when Bosma [5] provided useful insights about the Toomre galactic disk models [66].

One of the pioneers of rotation curve fitting was Brandt [67], who proposed a simple approximate parameterized formula given by:

$$V_{\rm rot}(r) = \frac{V_{\rm max} \times (r/r_{\rm max})}{(1/3 + 2/3(r/r_{\rm max})^n)^{3/2n}}, \tag{2.2}$$

where $V_{\rm max}$ is the maximum rotational velocity, $r_{\rm max}$ is a length scale, i.e. the radius at which the circular velocity reaches $V_{\rm max}$ and n is a shape parameter that determines how rapidly the curve approaches the Keplerian regime. Performing the fittings of the experimental points, the value of n gets fixed. Moreover, if by extrapolation it is assumed that the circular velocity beyond $r_{\rm max}$ is adequately approximated by Eq.(2.2), then the total mass of the galaxy can be computed as $M_0 = (3/2)^{\frac{3}{n}}\, V_{\rm max}^2 r_{\rm max}/G$.

In extragalactic astronomy the Brandt's model and many others were an empirical way to describe, by extrapolation, the RCs of spiral galaxies since the light was fainting off quickly

[1]Worth to mention that stars in general don't move in circular orbits due to the asymmetric drift.

nearly the last measured point, and several other galaxies were behaving in the same fashion. However, at that time it was realized that since an extrapolation method was being used, it might not represent the reality in all galaxies. With the recent developments of radio-astronomy techniques, specially, with the radio 21-cm observations, it allowed astrophysicists to measure the extension of the rotation curves beyond the Holmberg radius. The gas component of each galaxy extends larger than the Holmberg radius and the 21-cm line of neutral hydrogen helps in determining the velocity fields, which altogether with the velocity field of stars, provides an extended RC with a great angular resolution, corresponding to smaller errors in the measured velocity.

Contrary to what was expected, the new measurements of RCs did not agree with the extrapolation made with Eq.(2.2), since they remain mainly flat[2] or even increasing to the new limit of observations, which indicates a much larger total mass than the one given by M_0. These results strongly suggested that, or general relativity fails at larger scales than the Solar System [47], or either there is, or there are, unknown Dark Matter particles [5, 6, 7] which are transparent to the sensitivity of the measurement equipments but dominate the dynamics of the galaxy in the outer parts.

2.2 The luminous matter distribution in spiral galaxies

According to the Hubble sequence or morphological classification, based on their visual appearance (originally on photographic plates), there are three main types of galaxies: Elliptical, Spirals, and Irregulars. Elliptical galaxies appear as an ellipsoidal globe on the photographic plates, showing a smooth and featureless light distribution with a surface brightness decreasing as one moves farther out from the center. They are usually denoted by the letter "E", followed by an integer number n representing their degree of ellipticity on the Sky, for example, a galaxy of classification of $E0$ appears to be perfectly spherical, while a classification of $E7$ is very oblate. The elliptical scale varies from $E0$ to $E7$ and they have no particular axis of rotation.

Spiral galaxies on the other hand, show a flattened two-spiral-arms disk structure with dust, gas, and younger stars; a central distribution also known as the bulge and contains older stars; the halo which is a loose spherical structure located around the bulge and some of the disk that contains old clusters of stars, also known as globular clusters. In the Hubble sequence classification[3] they are denoted by the letter "S".

Finally, there are irregular galaxies, denoted by "I", which do show any regular or symmetrical structures like in the case of disk-like or ellipsoidal galaxies. They are divided into two

[2]RCs differ in shape according to the morphology of each galaxy (see Fig.(2.1)), and recent observational facts suggest that they are not always asymptotically flat, as it is usually assumed in the related literature.

[3]There is a subclassification in this group as roughly half of all spirals are also observed to have a bar-like structure (denoted by "SB") extending from the central bulge, lenticular galaxies (denoted by "$S0$") which contain a bright central bulge surrounded by an extended disk-like structure but unlike spiral, the disks of lenticular galaxies have no visible spiral arms and are not actively forming stars in any significant quantity.

groups, "$IrrI$" and "$IrrII$". $IrrI$ galaxies have molecular hydrogen regions and many young hot stars. "$IrrII$" galaxies on the other hand, seem to have large amounts of dust that absorbs most of the light from the stars, which makes almost impossible to observe distinct stars in these type of galaxies.

Almost 80% of the large amount of observed nearby galaxies possess a disk of some kind. They are usually thin disks with a nearly circular distributions of stars, gas, and dust, which move on nearly circular orbits about a common center. Galaxy disks may exhibit beautiful spiral arms as a result of this rotation, and some have bulges and/or pronounced bars crossing their centers. Other disks, however, show a fuzzy structure and can only be identified by the characteristic falloff of the surface brightness with the distance from the center. The evolution of disk galaxies is still a subject of intense debate within the structure formation theories. Progresses in this field has come by combining global observations of the motions of the stars, their compositions, and ages, but still one cannot offer a definitive account of the evolution of disk galaxies.

Optical observations suggests that the stellar surface density follows an exponential profile or as usually called Freeman disk given by

$$\sigma_s(r) = \frac{M_s}{2\pi R_d^2} e^{-r/R_d}, \tag{2.3}$$

being M_s the stellar disk mass and R_d the disk length scale, related to the optical radius R_o (the radius enclosing 83% of the total light) by $R_o = 3.2R_d$. The Freeman disk model assumes the mass is distributed isotropically in a flat disk, depending only the surface density on the radial coordinate r. On the other hand, the surface density of stars in the bulge is usually modeled as a Sérsic profile:

$$\sigma_b(r) = \frac{M_b \alpha^{2n}}{2\pi R_b^2 n \Gamma(2n)} e^{-\alpha(r/R_b)^{1/n}}, \tag{2.4}$$

with M_b the total projected mass, R_b is the bulge length scale, the integer number n is called Sérsic index of the profile related to α by $\alpha \sim 2n - 0.324$ and $\Gamma(x)$ is the gamma function. The Sérsic bulge model assumes the mass is distributed isotropically and spherically, with the corresponding dependence of the surface density only on the radial coordinate r. As a special case $n = 4$, is the Vaucouleurs profile which describes how the surface brightness $I(r)$, and surface density for constant mass-to-light ratio, of an elliptical galaxy varies as a function of the apparent distance r from the galactic center.

Following [66], one can compute the circular velocity of a massive particle induced gravitationally by a disk surface mass density $\sigma(r)$ with the aid of the formulas:

$$V_s^2(r) = 2\pi G r \int_0^{+\infty} J_1(kr) k S(k) dk, \quad S(k) = \int_0^{+\infty} J_0(ku) u \sigma(u) du, \tag{2.5}$$

where r is the radial coordinate on the disk, G is the gravitational constant and $J_0(z), J_1(z)$ are the zero- and first-order Bessel functions. The velocity of stars in the Freeman disk is then given by:

$$V_s^2(r) = \frac{2GM_s}{R_d} x^2 (I_0(x)K_0(x) - I_1(x)K_1(x)),\ x = r/2R_d, \tag{2.6}$$

being $I_n(z)$ and $K_n(z)$ the modified Bessel functions of first and second kind respectively.

For the bulge, supposing a spherically distribution, [68] shows the formulas to compute the velocity

$$V_b^2(r) = \frac{G\,M_b(r)}{r},\ \ M_b(r) = 4\pi \int_0^r s^2 \rho_b(s) ds,\ \ \rho_b(s) = -\frac{1}{\pi} \int_s^{+\infty} \frac{d\sigma_b(u)}{\sqrt{u^2 - s^2}}, \tag{2.7}$$

being $M_b(r)$ the total mass enclosed in a radius r and $\rho_b(r)$ the de-projected mass density. The velocity in this case has to be computed numerically due to the lack of an analytical function to represent it.

As an important remark, the circular velocity due to a Freeman [69] stellar disk given by Eq.(2.6) has a flattish region between 2 and 3 disk scale-lengths. At first sight one may think that a flat RC is not necessarily a proof for the existence of DM, however, the most solid evidence of the existence of DM comes from the fact that even in very faint galaxies the RCs are often steeply rising already in their optical regions, as also shown in Fig.(2.1).

Empirical results in spiral galaxies suggest that the galaxy's total luminous mass (the sum of its mass in stars and gas) and the maximum circular velocity measured from the RCs are correlated by the law $d\log M/d\log V \sim 3.5 - 4$. This empirical relation was first published in 1977 by the astronomers R. Brent Tully and J. Richard Fisher [70] and carries the name: Baryonic Tully-Fisher relation. Its applications in astrophysics are numerous, as it can be used to estimate the distance from Earth to spiral galaxies. In the DM paradigm, in galaxy RCs, the velocity is primarily determined by the mass of the DM halo that harbors the galaxy, which makes the Tully-Fisher relation a manifestation of the connection between the luminous and DM masses. The analogues of the Tully-Fisher relation for non-rotationally-supported galaxies, such as ellipticals, are known as the Faber-Jackson relation and the Fundamental Plane.

In the innermost parts of galaxy disks the luminous matter dominates the dynamics: light traces the mass inferred from disk rotation [71, 72, 73] out to a radius ranging between 1 and 3 disk exponential scale length (depending upon the galaxy luminosity [74]), such that the total luminous matter velocity contribution is given in quadrature by

$$V_d^2(r) = V_s^2(r) + V_g^2(r) + V_b^2(r), \tag{2.8}$$

where $V_s(r),\ V_g(r)$ and $V_b(r)$ are the stellar, gas and the bulge contributions.

Instead, in the outskirts, far from galaxy centres, circular velocities are found to be constant or even rising with radius despite the sharp radial decrease of the stellar or gaseous surface brightness. This contradicts the well known Keplerian-like expectations of the standard Newtonian Gravity if light traces the mass. It is well known that, in order to explain this anomaly, a DM halo is routinely added in the computation of the gravitational potential [5, 6, 7]. The luminous and DM contributions to the RC can explain the observed velocities as traced by star light or gas emission, even at large galactocentric distances where circular velocities are flat or keep increasing with radius.

2.3 Rotation curves in MOND

An alternative to explain the flatness of galaxy RCs comes from modifications of gravity at larger scales than the solar system. One of the most successful models is the Modified Newtonian Dynamics, or as it is currently addressed as MOND [47]. In its original formulation it was a pure phenomenological description to explain two observational systematics of spiral galaxies: flat RCs and the Tully-Fisher relation, although nowadays it is believed that DM also can have an increasing RC as well, and MOND can explain it by the means of the gaseous disk contributions.

The phenomenological approach to derive such modification of the Newtonian dynamics can be described as follows. Since GR is well proven to work very well at small scales and its Newtonian limit as well, then one can postulate that below some length scale r_0 kpc, the RC can be well described by the Newtonian velocity of stars plus gas. Beyond that scale, the Newtonian velocity is known to behave as $V_N^2(r) \sim r^{-1}$, therefore, to reproduce a flat RC, the behavior of this velocity should be modified. The simplest way is by multiplying $V_N^2(r)$ times the distance. These two conditions, in terms of accelerations can be written as:

$$\frac{V^2(r)}{r} = \begin{cases} \dfrac{V_N^2(r)}{r}, & r \ll r_0; \\ \\ \dfrac{V_N^2(r)}{r}(r/r_0), & r \gg r_0. \end{cases}$$

The above relation attempts to explain RCs without relying in extra matter, this is, based only on modifications of the Newtonian dynamics applied to the luminous matter which moves with circular velocity $V_N^2(r)$. Notice as well that it is purely kinematical relation and could be transformed into a dynamical one by introducing a characteristic acceleration scale a_0, related to r_0 by a dimensional analysis argument $r_0 a_0 = V_0^2$, being V_0 the constant velocity where the Newtonian regime starts to fail.

The main question now is: how to connect both regimes through a smooth process? The change from one regime to the other should be smooth, with a sufficiently good transient function or as it is called in the literature: *interpolating function*. Writing $a(r) = V^2(r)/r$ and $a_N(r) = V_N^2(r)/r$, and recalling that in the regime $r \gg r_0$, $a(r) = V_0^2/r$, then Eq.(2.3) can be rewritten as

$$a(r) = \begin{cases} a_N(r), & r \ll V_0^2/a_0; \\ \\ \sqrt{a_N(r)a_0}, & r \gg V_0^2/a_0. \end{cases}, \quad \text{or,} \quad a_N(r) = \begin{cases} a(r), & r \ll V_0^2/a_0; \\ \\ a(r)\dfrac{a(r)}{a_0}, & r \gg V_0^2/a_0. \end{cases}$$

The connection between both regimes now is easier to find by writing $a_N(r) = a(r)\mu(a(r)/a_0)$, where $\mu(x)$ is the above mentioned interpolating function and should satisfy

$$\mu(x) = \begin{cases} 1, & x \ll 1; \\ x, & x \gg 1. \end{cases}$$

The regime $x \gg 1$ is usually called MONDIAN regime, to distinguish from the Newtonian one $x \ll 1$. In the related literature there are many interpolating functions proposed by several studies of galaxy RCs; the two most known are:

$$\mu_I(x) = \frac{x}{\sqrt{1+x^2}}, \tag{2.9}$$

$$\mu_{II}(x) = \frac{x}{1+x}, \tag{2.10}$$

where $\mu_I(x)$ and $\mu_{II}(x)$ are called *Standard* and *Simple Interpolating functions* respectively, and the corresponding modified velocities are then given by

$$V_I^2(r) = \frac{V_N^2(r)}{\sqrt{2}}\sqrt{1+\sqrt{1+\left(\frac{2a_0 r}{V_N^2(r)}\right)^2}}, \tag{2.11}$$

$$V_{II}^2(r) = \frac{V_N^2(r)}{2}\left(1+\sqrt{1+\frac{4a_0 r}{V_N^2(r)}}\right). \tag{2.12}$$

To roughly estimate the value of a_0 one may take the typical galactic length scale $r_0 \sim 1$ kpc and the flat velocities are around 100 km s^{-1}, therefore $a_0 = V_0^2/r_0 \sim 10^{-8}$ cm s^{-2}. A more realistic estimate should come from the RC fittings; for example, in [75] was found, with Eq.(2.11) $a_0 = 1.2 \times 10^{-8}$ cm s^{-2}; however, in [76] was obtained with Eq.(2.12) a value of $a_0 = 1.35 \times 10^{-8}$ cm s^{-2} instead.

The other prediction of the MOND prescription is the Tully-Fisher relation as it was already mentioned. If in the MONDIAN regime $r \gg V_0^2/a_0$ a massive particle moves in a circular orbit, then the Universal Gravitation and Third Newton Laws convey to

$$a_N(r)m = \frac{GMm}{r^2}, \quad \frac{a^2(r)}{a_0} = \frac{GM}{r^2}, \tag{2.13}$$

$$V_0^4 = Ga_0 M, \tag{2.14}$$

being M the mass of the point-source of gravity.

In order to create a theory of modified gravity, Milgrom's law requires a covariant formulation such that it satisfies conservation laws and provide a unique solution for the time evolution of any physical system, not only to galaxy RCs. The first attempt to solve this problem was a non-relativistic lagrangian formulation dubbed AQUAL (acronym of AQUAdratic Lagrangian), constructed by Milgrom and Jacob Bekenstein [77]. AQUAL explains the MONDIAN regime by modifying the gravitational term in the classical lagrangian from being quadratic in the gradient of the Newtonian potential to a more general dimensionless function $F(x)$:

$$\mathcal{L}_{Newton} = -\rho(\vec{r},t)\Phi(\vec{r},t) - \frac{1}{8\pi G}\cdot\|\vec{\nabla}\Phi(\vec{r},t)\|^2, \tag{2.15}$$

$$\mathcal{L}_{AQUAL} = -\rho(\vec{r},t)\Phi(\vec{r},t) - \frac{1}{8\pi G}\cdot\|\vec{\nabla}\Phi(\vec{r},t)\|^2\cdot F\left(\frac{\|\vec{\nabla}\Phi(\vec{r},t)\|^2}{a_0^2}\right), \tag{2.16}$$

where $\Phi(\vec{r},t)$ is the standard Newtonian gravitational potential. The Euler-Lagrange equations applied to this lagrangian lead to a non-linear generalisation of the Newton-Poisson equation:

$$\vec{\nabla}\cdot\left[\mu\left(\frac{\left\|\vec{\nabla}\Phi(\vec{r},t)\right\|}{a_0}\right)\vec{\nabla}\Phi(\vec{r},t)\right] = 4\pi G\rho(\vec{r},t), \tag{2.17}$$

with $\mu(x) = dF(x^2)/dx$. To solve this non-linear equation one needs suitable boundary conditions and a particular choice of the function $F(x)$ to yield Milgrom's law, of course, up to a curl field correction which vanishes in situations of high symmetry.

The other non-relativistic MOND formulation is QUMOND [78]. Its gravitational potential $\Phi_Q(\vec{r},t)$ is the solution of the system of equations

$$\nabla^2\Phi_Q(\vec{r},t) = \vec{\nabla}\cdot\left(\nu\left(\|\vec{\nabla}\Phi_N(\vec{r},t)\|/a_0\right)\vec{\nabla}\Phi_N(\vec{r},t)\right), \tag{2.18}$$

$$\nabla^2\Phi_N(\vec{r},t) = 4\pi G\rho(\vec{r},t), \tag{2.19}$$

being $\Phi_N(\vec{r},t)$ the Newtonian gravitational potential, $\nabla^2 = \vec{\nabla}\cdot\vec{\nabla}$ is the Laplacian operator and the function $\nu(x)$ is related to the interpolating function $\mu(x)$ by $\nu(y) = 1/\mu(x),\ y = x\mu(x)$. The advantage of QUMOND over AQUAL relies in the fact that the first involves to solve two linear Poisson equations instead of one which is non-linear.

The phenomenological way MOND was constructed to explain the flatness of galaxy RCs (relying only on the baryonic mass distribution) allowed to fit many observational facts, including the correct agreement with many of scaling relations present at the galaxy level [75, 79, 80, 81, 82, 83, 84]. A covariant completion of AQUAL was created under the name of RAQUAL (Relativistic-AQUAL), which is a Scalar-Tensor theory that aimed to explain as well the light deflection phenomena, not included in the non-relativistic version. In this case, the dimensionless function $F(x)$ is changed by the covariant generalization $F\left(\|\vec{\nabla}\Phi(\vec{r},t)\|^2/a_0^2\right) \mapsto F\left(l_0^2 g^{\mu\nu}\,\partial_\mu\phi\,\partial_\nu\phi\right)$, where $g_{\mu\nu}$ is the metric tensor ($g_{00}\sim 1-2\Phi(\vec{r},t)$ in the Newtonian limit),

ϕ is an auxiliary scalar field, and $l_0 = c^2/a_0$ is the MOND length scale. However, as empirical as all these models are, soon the caveats started to bloom. For example, they face some conceptual difficulties in analyzing composite systems as they violate the linear and angular momenta conservation. Moreover, within a star, the characteristic accelerations $a_i(\vec{r}, t) \gg a_0$ of the constituent atoms are never in the MONDIAN regime, while the whole star is moving with acceleration $a_e(\vec{r}, t) \ll a_0$. This conceptual problem is known in the literature as the "external field effect" and it implies a violation of the strong equivalence principle (but not necessarily the weak equivalence principle) as well. Despite RAQUAL was formulated to include computations of the light deflection, many inconsistencies started to arise when computing the gravitational lensing from galaxy clusters.

The first relativistic theory with MONDIAN behavior was formulated in 2004 by Jacob Bekenstein under the name of TeVeS (Tensor-Vector-Scalar) [48]. It is constructed from a local Lagrangian which is Lorentz invariant, and introduces an Einstein metric tensor $g_{\mu\nu}$ with a well defined inverse metric $g^{\mu\nu}$, a time-like vector field A_μ ($g_{\mu\nu}A^\mu A^\nu = -1$), a dynamical and non-dynamical scalar field $\phi(r)$ and $\sigma(r)$ respectively, and a free function $F(x)$. Despite TeVeS enjoys some success in generalizing MOND to make contact with gravitational lensing and structure formation observations [85], it faces some other problems when confronted with the CMB anisotropies [86], the lifetime of compact objects [87], and the relationship between the lensing and matter overdensity potentials [88].

Despite the lack of success of the MOND formulation, there are several numerical cosmological coincidences related to the acceleration scale a_0, but it is unknown if these coincidences have a deeper reason. It was already noticed by Milgrom [47] that $2\pi a_0 \approx cH_0 \approx c^2\sqrt{\Lambda/3}$ where H_0 is the present value of the Hubble constant and Λ the cosmological constant. The combination $c^4/Ga_0 \approx 10^{54}$ kg is the total mass of the observable part of the Universe, and the length $c^2/a_0 \approx 7.5 \times 10^{30}$ m is of the order of the current Hubble radius. Worth to mention that in the bimetric formulation of MOND (one of the MOND relativistic completion), the coincidence between a_0 and Λ is a direct consequence of the theory [78].

2.4 Rotation curves in $f(R)$ gravity

The second modified gravity theory applied to explain the flatness of galaxy RCs is called $f(R)$ gravity and the early aim was to generalize the Hilbert-Einstein action to overcome the emerging problems of the singularities and the lack of a full quantization scheme [49]. $f(R)$ gravity is set of theories, each one is fixed by a different function $f(R)$ of the Ricci scalar R . The simplest and more familiar case is when $f(R) = R$ (f is identity function) which corresponds to General Relativity. The first consequence of this kind of theories is the freedom one has by choosing an adequate function $f(R)$ depending on the specific problem one needs to solve, for example, the accelerated expansion and structure formation of the Universe without adding unknown forms of DE or DM [89]. Despite the large variety of functions $f(R)$ proposed in the current

literature, many of them can now be ruled out based on observational grounds, or because of pathological theoretical problems.

$f(R)$ gravity seeks to generalise the Hilbert-Einstein action as follows:

$$S_f(g_{\mu\nu}) = \int \frac{c^4}{16\pi G} d^4x\sqrt{-g}f(R), \tag{2.20}$$

where $g = det(g_{\mu\nu})$ is the determinant of the metric tensor and $f(R)$ is some previously specified function of the Ricci scalar R. When deriving the equations of motion, two possibilities may arise:

1. the connection coefficients $\Gamma^{\lambda}_{\mu\nu}$ are given by the Christoffel symbols of the metric tensor (metric $f(R)$ gravity), or
2. the connection coefficients $\Gamma^{\lambda}_{\mu\nu}$ are independent of the metric tensor:
   (a) one varies the action with respect to the metric tensor and the connection coefficient independently, but the matter Lagrangian is assumed to be independent of the connection (Palatini $f(R)$ theories), or
   (b) one varies the action with respect to the metric tensor and the connection coefficient independently, but assuming the matter Lagrangian depending on the connection as well (metric-affine $f(R)$ gravity).

Recent theoretical studies suggest that the Palatini $f(R)$ formulation might be ruled out since it appears to be in conflict with the Standard Model [90, 91] in the sense that it introduces non-perturbative corrections to the matter-field action and strong couplings between gravity and matter in the local frame and at low energies. On the other hand, from the astrophysical point of view, in [92] was also shown that for generic choices of $f(R)$, there are widely used equations of state (for example: the polytropic equation which describes white dwarf stars) for which one cannot find satisfactory physical solutions of the field equations within this framework, apart of those provided by the special case of General Relativity. Even more, other conflicts come from a missmatch with the observational evidences in the Solar System [93]. Worth to mention that Palatini $f(R)$ theories are equivalent to a Brans-Dicke theory with $\omega = -3/2$.

In the case of metric $f(R)$ gravity, as mentioned above, one can derive the field equations by varying with respect to the metric and not treating the connection independently from the total action $S(g_{\mu\nu}, \psi) = S_f(g_{\mu\nu}) + S_m(g_{\mu\nu}, \psi)$, where $S_f(g_{\mu\nu})$ is given by Eq.(2.20) and $S_m(g_{\mu\nu}, \psi)$ is the matter-field action. Following the same steps as in the Hilbert-Einstein action

$$\delta\sqrt{-g} = -\frac{1}{2}\sqrt{-g}g_{\mu\nu}\delta g^{\mu\nu}, \quad \delta\Gamma^{\lambda}_{\mu\nu} = \frac{1}{2}g^{\lambda a}\left(\nabla_\mu\delta g_{a\nu} + \nabla_\nu\delta g_{a\mu} - \nabla_a\delta g_{\mu\nu}\right), \tag{2.21}$$

$$\delta R = R_{\mu\nu}\delta g^{\mu\nu} + g_{\mu\nu}\Box\delta g^{\mu\nu} - \nabla_\mu\nabla_\nu\delta g^{\mu\nu} \tag{2.22}$$

where ∇_ν is the covariant derivative and $\Box = g_{\mu\nu}\nabla_\mu\nabla_\nu$ is the D'Alembertian operator, one can write the variation of $S_f(g_{\mu\nu})$ as:

$$\delta S_f(g_{\mu\nu}) = \int \frac{c^4}{16\pi G} d^4x \left(\delta f(R)\sqrt{-g} + f(R)\delta\sqrt{-g}\right), \tag{2.23}$$

$$= \int \frac{c^4}{16\pi G} d^4x \left(f'(R)\delta R\sqrt{-g} - \frac{1}{2}\sqrt{-g}g_{\mu\nu}\delta g^{\mu\nu} f(R)\right) \tag{2.24}$$

$$= \int \frac{c^4}{16\pi G} d^4x\sqrt{-g}\delta g^{\mu\nu}\left(f'(R)R_{\mu\nu} - \frac{1}{2}g_{\mu\nu}f(R) + [g_{\mu\nu}\Box - \nabla_\mu\nabla_\nu]f'(R)\right) \tag{2.25}$$

where $f'(R) = \partial f(R)/\partial R$ and the surface terms have been dropped out. The stationary action condition $\delta S(g_{\mu\nu}, \psi)$ demands

$$f'(R)R_{\mu\nu} - \frac{1}{2}f(R)g_{\mu\nu} + [g_{\mu\nu}\Box - \nabla_\mu\nabla_\nu]\, f'(R) = \frac{8\pi G}{c^4}T_{\mu\nu}, \tag{2.26}$$

with $T_{\mu\nu}$ the matter field stress-energy tensor defined by $T_{\mu\nu} = -\frac{2}{\sqrt{-g}}\delta(\sqrt{-g}L_m(g_{\mu\nu}, \psi))/\delta g^{\mu\nu}$, being $L_m(g_{\mu\nu}, \psi)$ the matter field Lagrangian. Obviously, from Eq.(2.26) Einstein equations emerge by fixing $f(R) = R$, $f'(R) = 1$. For direct applicability it is better the traced version

$$3\Box f'(R) + Rf'(R) - 2f(R) = \frac{8\pi G}{c^4}T, \tag{2.27}$$

with $T = g^{\mu\nu}T_{\mu\nu}$ the trace of $T_{\mu\nu}$.

An example of a vacuum solution for the metric $f(R)$ gravity, widely applied to fit galaxy RCs can be found in [94]. For a static and spherically symmetric space-time, with Schwarzschild-like line element

$$ds^2 = -c^2e^{\nu(r)}dt^2 + e^{-\nu(r)}dr^2 + r^2d\Omega^2, \tag{2.28}$$

where $e^{\nu(r)}$ is the principal metric coefficient depending only on the radial coordinate r and $d\Omega^2 = d\theta^2 + \sin^2\theta d\phi^2$ the line element on the three-dimensional unit sphere.

Supposing a vacuum model with $f(R) = l_0R^n$ being n any real number and l_0 a convenient constant to get the right dimension of the action integral, in [94] was proposed an approximate solution to the vacuum equation, which works great at the scale of the Solar System and galaxies:

$$e^{\nu(r)} - 1 = \frac{2\Phi(r)}{c^2} = \frac{2GM}{c^2r}\left[1 + \frac{1}{2}\left(\left(\frac{r}{r_c}\right)^\beta - 1\right)\right], \tag{2.29}$$

where $\Phi(r)$ is the gravitational potential depending only on the radial coordinate r, β is supposed to be a universal constant, function of n given by

$$\beta = \frac{12n^2 - 7n - 1 - \sqrt{36n^4 + 12n^3 - 83n^2 + 50n + 1}}{6n^2 - 4n + 2}, \tag{2.30}$$

and r_c is a scale length parameter which depends on the particular gravitating system being studied. Notice that in the case $n = 1$ one recovers the usual Newtonian gravitational potential. Since n could be in principle any real number, then β is bounded to $-0.41 \leq \beta < 1$, or $1 < \beta \leq 1.78$, since the square-root in the definition of β in Eq.(2.30) has to be a real-valued quantity. As argued in [94], this approximated solution solves the field equations up to order 10^{-6} which is more than sufficient in the above mentioned astrophysical situations.

The advantage from Eq.(2.29) is that the gravitational potential can be read directly, and from the usual relation $V_c^2(r) = r\, d\Phi(r)/dr$, one can write the circular velocity of any massive point particle as:

$$V_c^2(r) = \frac{GM}{r}\left[\frac{1}{2} + \frac{1-\beta}{2}\left(\frac{r}{r_c}\right)^{\beta}\right]. \tag{2.31}$$

As can be easily seen, the first term equals half the Newtonian contribution, while the second contribution, for $\beta \neq 0,\ r > r_c(1-\beta)^{\frac{1}{\beta}}$ is higher than half classical one, which means that the tail of the velocity curve is higher than the Newtonian part. Moreover, for $\beta = 0$ both terms sum up to reproduce the expected classical result. These results make possible the explanation of the flatness of galactic RCs without relying on extra matter, but only on modifications of the laws of gravity.

The solution Eq.(2.31) corresponds to the circular velocity in the case of a point-like particle, but it can be easily generalized to the case of extended systems. The gravitational potential for extended systems is

$$\Phi(\vec{r}) = -G\int d^3r' \frac{\rho(\vec{r'})}{\|\vec{r}-\vec{r'}\|}\left(1 + \frac{1}{2}\left(\frac{\|\vec{r}-\vec{r'}\|^{\beta}}{r_c^{\beta}} - 1\right)\right), \tag{2.32}$$

where $\rho(\vec{r})$ is the matter density and $\|\vec{x}\|$ is the norm of the vector $\vec{x}$. Once the gravitational potential has been obtained, the RC may be easily evaluated and then compared with observations.

To a good extent, the luminous matter in galaxies is distributed cylindrically with a density $\Sigma(r, z)$, so Eq.(3.5) becomes

$$\Phi(\vec{r}) = -G\int_0^{+\infty}\int_{-h}^{h} dr'dz'r'\Sigma(r', z')\int_0^{2\pi} d\theta \frac{1}{\|\vec{r}-\vec{r'}\|}\left(1 + \frac{1}{2}\left(\frac{\|\vec{r}-\vec{r'}\|^{\beta}}{r_c^{\beta}} - 1\right)\right), \tag{2.33}$$

being h the half-thickness of the disk distribution. Since $\|\vec{r}-\vec{r'}\|^2 = \|\vec{r}\|^2 + \|\vec{r'}\|^2 - 2\|\vec{r}\|\|\vec{r'}\|\cos\alpha$, where α is the angle between $\vec{r}$ and $\vec{r'}$, and since one is interested in computing the potential at $z = 0$ to find the circular velocity $V^2(r) = r\partial\Phi/\partial r|_{z=0}$, then $\|\vec{r}-\vec{r'}\|^2 = r^2 + (r'^2 + z'^2)^2 -$

$2r\sqrt{r'^2+z'^2}\cos\alpha$. Moreover, setting the direction where one wants to measure the velocity as the $x-$axis, then $\cos\alpha = r'\cos\theta/\sqrt{r'^2+z'^2}$ and $\|\vec{r}-\vec{r'}\|^2 = [r^2+(r'^2+z'^2)^2]\,(1-k^2\cos\theta)$, being θ the angular coordinate and $k^2 = 2rr'/\,[r^2+(r'^2+z'^2)^2]$. Taking this into account, the gravitational potential gives

$$\Phi(r) = -\frac{G}{2}\int_0^{+\infty}\int_{-h}^{h} dr'dz'r'\Sigma(r',z')(\mathcal{I}_0(r,r',z')+\mathcal{I}_\beta(r,r',z')), \tag{2.34}$$

$$\mathcal{I}_\beta(r,r',z') = \frac{I_\beta(r,r',z')}{r_c^\beta(r^2+r'^2+z'^2)^{\frac{1-\beta}{2}}},\ I_\beta(r,r',z') = \int_0^{2\pi}\frac{d\theta}{(1-k^2\cos\theta)^{\frac{1-\beta}{2}}} \tag{2.35}$$

$$I_\beta(r,r',z') = \frac{\pi}{(1-k^2)^{\frac{1-\beta}{2}}}\,{}_2F_1\left(\frac{1}{2},\frac{1-\beta}{2};1;-\frac{2k^2}{1-k^2}\right)+\frac{\pi}{(1+k^2)^{\frac{1-\beta}{2}}}\,{}_2F_1\left(\frac{1}{2},\frac{1-\beta}{2};1;\frac{2k^2}{1+k^2}\right),$$

being $\mathcal{I}_0(r,r',z') = \mathcal{I}_{\beta=0}(r,r',z')$ and ${}_2F_1(a,b,c,z)$ the hypergeometric function. Once computed the gravitational potential, one can compute as well the circular velocity with the corresponding formula and fit the experimental RCs to find the values of β and r_c. In the next chapter I will perform this type of calculation applied to the galaxy M33.

2.5 Dark matter

Despite the theories of modified gravity provide good fits for galaxy RCs, they fail at explaining larger and more complex objects like galaxy clusters. To alleviate this issue, astrophysicists propose a second point of view which involve extra particles, which by now its nature is uncertain, but they play an essential role in structure formations in the Universe. This section is devoted to explain the main methods of RCs fitting taking different models of DM.

2.5.1 Dark matter mass modeling method

The standard dynamical analysis of the RCs is carried out by modeling the galaxy as a stellar and gaseous disk and a bulge all embedded in a DM halo, all together in centrifugal equilibrium. Concerning the DM halo mass density model, in the current literature two different DM density distributions are considered. The first one is a spherical halo with a NFW density profile for structures growing in a $\Lambda-$CDM hierarchical Universe [12, 13, 95, 96, 97, 98] given by:

$$\rho_{NFW}(r) = \frac{\rho_c}{\frac{r}{r_c}\left(1+\frac{r}{r_c}\right)^2}, \tag{2.36}$$

where ρ_c and r_c are the scaling density and radius respectively, which are internal parameters to the DM halo. Appealing to Newtonian gravity and invoking Gauss equation for a homogeneous and isotropic mass distribution, the circular velocity around the galactic center of any DM

massive particle at a distance r from the center and in the $z = 0$ plane can be obtained from $V^2_{NFW}(r) = r\partial\Phi_{NFW}(\vec{r})/\partial r|_{z=0}$, and it is given by the analytical formula:

$$V^2_{NFW}(r) = \frac{4\pi G\rho_c r_c^2}{r/r_c}\left(\ln(1+r/r_c) - \frac{r/r_c}{1+r/r_c}\right). \tag{2.37}$$

In the literature, for this specific DM halo model, one encounters frequently another parameterization in terms of the virial mass $\mathrm{M_{vir}}$ and the concentration parameter $c = r_{vir}/r_c$, which are related to ρ_c and r_c by:

$$\rho_c = \frac{97.2}{3}\frac{c^3}{\ln(c+1) - \frac{c}{c+1}}\rho_{\rm crit} \ \ \mathrm{g\ cm^{-3}}, \tag{2.38}$$

$$r_c = \frac{1}{c}\left(\frac{3}{97.2}\frac{\mathrm{M_{vir}}}{4\pi\rho_{\rm crit}}\right)^{1/3} \ \ \mathrm{kpc}. \tag{2.39}$$

where $r_{\rm vir}$ is the virial radius and $\rho_{\rm crit} = 9.3\times10^{-30}\ \mathrm{g\,cm^{-3}}$ is the critical density of the Universe.

Another widely used DM halo density profile, which do not come from numerical simulations but from phenomenology of galaxy dynamics is the cored BRK density distribution, that successfully fits individual galaxy RCs (e.g. [19] and references therein), as well as the Universal Rotation Curve of spirals. This cored halo profile, also known as the Burkert halo profile [15, 99] has a radial density distribution given by

$$\rho_{BRK}(r) = \frac{\rho_c}{\left(1+\frac{r}{r_c}\right)\left(1+\frac{r^2}{r_c^2}\right)} \tag{2.40}$$

where ρ_c and r_c are the central core density and the core radius respectively. As in the previous DM halo model, appealing to Newtonian gravity and invoking Gauss equation for a homogeneous and isotropic mass distribution, the circular velocity around the galactic center of any DM massive particle at a distance r from the center and in the $z = 0$ plane can be obtained from $V^2_{BRK}(r) = r\partial\Phi_{BRK}(\vec{r})/\partial r|_{z=0}$, which gives:

$$V^2_{BRK}(r) = \frac{2\pi G\rho_c r_c^2}{r/r_c}\left(\ln(1+r/r_c) + \ln\sqrt{1+(r/r_c)^2} - tan^{-1}(r/r_c)\right). \tag{2.41}$$

Appealing to the local centrifugal equilibrium condition

$$\frac{V^2(r)}{r} = a_h(r) + a_d(r) = \frac{V^2_{DM}(r)}{r} + \frac{V^2_d(r)}{r}, \tag{2.42}$$

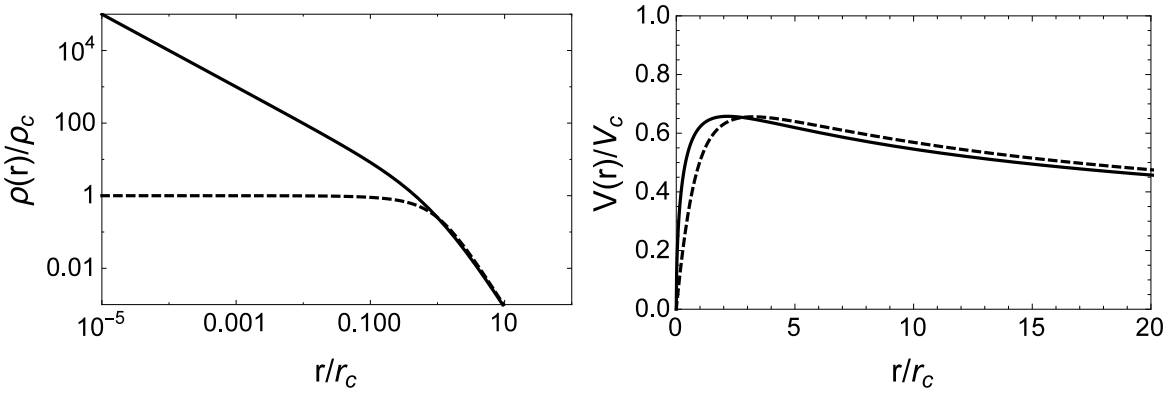

Figure 2.2: In the left panel are shown the NFW (continuous line)and BRK (dashed line) DM halo density profiles in log-log scale. The right panel shows their respecting velocity formulas as given by Eq.(2.37) (continuous line) and Eq.(4.2) (dashed line), with $V_c^2 = 2\pi G\rho_c r_c^2$.

where $V_{DM}^2(r)$ can be either $V_{NFW}^2(r)$ or $V_{BRK}^2(r)$, the velocity contribution from the DM density profile adds in quadrature to the luminous mass contribution given by Eq.(2.8) to yield the total circular velocity $V(r)$. The current DM mass modeling method aims to find the best fitting values of $(c, \mathrm{M_{vir}})$ or (r_c, ρ_c) and possible additional parameters in $V_d^2(r)$ such as the constant stellar mass-to-light ratio Υ, by minimizing the χ^2 distribution between the experimental points of the RCs and the total circular velocity formula obtained for $V(r)$.

In the NFW halo density profile, the free parameters, c and $\mathrm{M_{vir}}$ can be considered as independents during the fitting process, however, one has to check the consistency of the best fitting values with the relations obtained by numerical simulations of structure formation in a $\Lambda-$CDM Universe, which suggest that in fact c and $\mathrm{M_{vir}}$ are not independents from each other [100, 101], but correlated by

$$c = 10.6 \left(\frac{1}{10^{12} h^{-1}} \frac{\mathrm{M_{vir}}}{\mathrm{M_\odot}} \right)^{-0.097}, \tag{2.43}$$

where $h = 0.678$ the dimensionless value of the Hubble parameter [102]. On the other hand, for the BRK DM halo density, the central core density ρ_c and the core radius r_c are not independents either, as shown in [22], and the following relation holds:

$$\log \left(\frac{\rho_c r_c}{\mathrm{M_\odot pc^{-2}}} \right) = 2.15 \pm 0.2. \tag{2.44}$$

Through the dynamical analysis of individual RCs, one needs to find the best fitting values of $(c, \mathrm{M_{vir}})$ or (ρ_c, r_c) and Υ, where this last free parameter is constrained by the derived stellar mass surface densities which comes from the photometry properties of each individual galaxy.

It could be the case to find no compatible values of Υ, predicting higher stellar masses which can be easily attributed to the fact that in galaxies, even beyond some lengthscale, the influence of the luminous matter might not be negligible so that any derivation of the DM density profile would be fraught with the uncertainties inherent to such a component. More precisely, since in the inner regions $r \lesssim 2R_D$ (being R_D the disk length scale) of most spirals, the stellar disk dominates over the dark component, even small uncertainties in the mass determination of the former induces large uncertainties in the values of the structural parameters of the dark components. By using a second method for fitting the RCs data, in the next section we hope to alleviate this degeneracy. We will see that the fits related to the second method is less dependent on the luminous matter distribution and thus hopefully it will help us to clarify better the properties of the DM halo that host spirals.

2.5.2 Dark matter local density method

The idea behind this method, brought by Salucci et.al [103] is to resort the equation of centrifugal equilibrium, which holds the spiral galaxies:

$$\frac{V^2(r)}{r} = a_h(r) + a_s(r) + a_g(r), \tag{2.45}$$

where $a_h(r), a_s(r)$, and $a_g(r)$ are the radial accelerations, generated by the DM halo, stellar and gaseous disks respectively.

Under the approximation of a spherical DM halo, one has

$$\rho_h(r) = \rho(r) - \Upsilon\rho_s(r) - \rho_g(r) = \frac{X_q}{4\pi G r^2}\frac{d}{dr}\left(rV^2(r) - r\Upsilon V_s^2(r) - rV_g^2(r)\right), \tag{2.46}$$

$$\rho(r) = \frac{1}{4\pi G r^2}\frac{d}{dr}\left(rV^2(r)\right), \tag{2.47}$$

$$\rho_s(r) = \frac{1}{4\pi G r^2}\frac{d}{dr}\left(rV_s^2(r)\right), \tag{2.48}$$

$$\rho_g(r) = \frac{1}{4\pi G r^2}\frac{d}{dr}\left(rV_g^2(r)\right), \tag{2.49}$$

where X_q is a factor correcting the spherical Gauss law used above in case of an oblate DM halo and it takes values between 1.05 and 1.00 (see details in [103]), $V(r)$ is the velocity given by the experimental RC, $V_s(r)$ and $V_g(r)$ are the stellar and gas velocities and Υ the usual stellar mass-to-light ratio. The strength of this method lies in the fact that we have transformed the surface mass density of the stellar and gaseous disks in equivalent bulk densities with the aid of Gauss's law. Moreover, at large distances the bulge plays no role and Eq.(2.6) for the stellar and gaseous disks has the asymptotic expansion

$$V_{s,g}^2(r \gg R_d) = \frac{GM_{s,g}}{r} + o(r^{-2}), \tag{2.50}$$

which is nothing but the expected Keplerian behavior of the circular velocity. Therefore, appealing to Eq.(2.48), for $r > R_d$ we expect a sharp fall-off of the equivalent three-dimensional densities of the luminous matter components $\rho_s(r)$ and $\rho_g(r)$, leaving only the contribution of the DM to the observed RC. From this fact, one can infer the DM halo properties directly from the experimental data and not relying on the luminous matter component, which can introduce large uncertainties due to the stellar mass-to-light ratio, as discussed in the previous subsection.

An issue left to treat is to derive an analytical expression for the total velocity $V(r)$ from the available discreet set of the RC data. Having an analytic function will avoid artifact due to the numerical computation of the derivative of $V(r)$ needed for the later computation of the total density as given by Eq.(2.47). In the next chapter I propose an appropriate empirical smooth curve to solve this problem for the particular case of the galaxy M33, and in Chap.(4) a generalization for 887 galaxies of different morphologies.

Chapter 3

The radial dependence of dark matter distribution in M33

In this chapter we study in detail the DM distribution in M33, a Local Group low-luminosity spiral galaxy, rich in gas and very much DM dominated. Its rotation curve is very extended due to the presence of a large gaseous disc and has an excellent spatial resolution due to M33 proximity and to the presence of CO-lines that trace the inner kinematics [104, 105]. The high resolution RC of this galaxy gives us the possibility to derive the DM halo distribution from the inner regions out to large galactocentric distances and therefore to uniquely test the $\Lambda-$CDM cosmological scenario. M33 hosts no bulge nor a prominent bar [106]: the absence of these concentrated stellar distributions much alleviates the usual uncertainty in deconvolving the disk contribution from that of a bulge, and in modeling correctly non circular motion.

The fitting method throughout this thesis is based in minimizing the χ^2 function, which depends on the model parameters. Defining hereafter $\chi^2_{\rm red} = \chi^2/d.o.f$, where $d.o.f = N-P+C$ is the number of degrees of freedom, being N the total number of experimental points, P the number of free parameters and C the number of constrains or correlations among the parameters; we find the global minimum of the function $\chi^2_{\rm red}$ (which is proportional to χ^2) to obtain the P best fitting values and estimate the errors σ_i in each parameter a_i ($i = 1, 2, \ldots, P$), as described in [107] for nonlinear fitting methods, by $\sigma_i^2 = 2(\partial\chi^2/\partial a_i^2)^{-1}$.

3.1 The luminous matter distribution in M33

In this section we introduce the stellar and gaseous components of the M33 disk and discuss the radial-dependence of the luminous surface mass density as derived by [105]. We then briefly summarize how these luminous mass distributions are used for the standard RC fitting method in M33 and the implications for the DM distribution.

3.1.1 Stellar disk

Thanks to the tight correlations between the colour and the apparent stellar mass-to-light ratio M/L [108], the stellar mass, to a first approximation, can be determined using multi-band optical imaging measurements of the whole galaxy luminosity in several bands. However, due to likely radial variations of the stellar mass-to-light ratio, as galaxy disks grow with time, references [109, 110, 111] have been using chemo-photometric models for a large samples of spatially resolved, disk-dominated galaxies to determine the radial dependence of the stellar mass surface density. A radially decreasing mass-to-light ratio is found based on galaxy colour gradients and spectral synthesis techniques. Being M33 the second closest spiral, in [105] was implemented an extension of the ZCR09 method to build up a detailed map of the stellar surface mass density using mosaic maps in the B (blue band), V (visible band), I (infrared band), g (green band) and i (infrared band) bands from the Local Group Survey [112] and from the Sloan Digital Sky Survey [113]. After processed the images, a pixel-by-pixel synthesis model of the stellar population allowed to obtain a stellar mass surface density map of the M33 disk out to 5 kpc which showed a clear radial gradient of the mass-to-light ratio in the inner regions. This finding is consistent with the negative radial metallicity gradient which supports an inside-out formation scenario and underlines the importance of carrying out a careful analysis of the stellar mass distribution in disks before computing their contribution to RCs [109]. By fitting the resulting radial averages of the stellar surface mass density of M33, with analytic functions, namely exponential functions with with different scale-lengths r_s, in [105] was obtained the following approximation for the radial distribution of the stellar mass surface density in units of $M_\odot\,\mathrm{pc}^{-2}$:

$$\sigma_{BVIgi}(r) = \begin{cases} \exp(-2.010\,r + 6.24), & 0.0\,\mathrm{kpc} < r \leq 0.3\,\mathrm{kpc}; \\ \exp(-1.239\,r + 6.01), & 0.3\,\mathrm{kpc} < r \leq 0.77\,\mathrm{kpc}; \\ \exp(-0.758\,r + 5.64), & 0.77\,\mathrm{kpc} < r \leq 1.85\,\mathrm{kpc}; \\ \exp(-0.515\,r + 5.19), & 1.85\,\mathrm{kpc} < r \leq 10\,\mathrm{kpc}; \\ \exp(-0.161\,r + 1.65), & 10\,\mathrm{kpc} < r \leq 23\,\mathrm{kpc}, \end{cases} \tag{3.1}$$

where r is the galactocentric radius in kpc units. The fits to the radial distribution of the stellar mass density are shown in Fig.(3.1) (dashed line), where we can notice the drop of the stellar mass density by more than 3 orders of magnitudes from the centre to the outskirts of the M33 disk. The amplitude of $\sigma_{BVIgi}(r)$ is uncertain by a 30%, while its radial trend has negligible uncertainties. As in [105], in order to compute the dynamical contribution of the stellar mass density to the rotation curve, we consider the stellar disk perpendicular to the galactic plane as a flaring disk with a radially varying half thickness: this is only 100 pc at the centre and it reaches 1 kpc at the outer disk edge. The method for computing the induced velocity can be found in [114].

3.1.2 The HI and H_2 gaseous disks

The gaseous disk of M33 is made of atomic and molecular gas (mostly hydrogen and helium) and it warps beyond 8 kpc. The high resolution $21-cm$ data for the atomic hydrogen gas in M33, the best fitting tilted ring model, and the radial averages of the HI surface density distribution, $\sigma_{HI}(r)$, have been presented in [105] and it is given by the formula

$$\sigma_{HI}(\hat{r}) = \exp(0.45 - (1. + 0.0026\,\hat{r}^{2.7})^{0.37037}) + \exp\left(-100. + \frac{100.}{(1. + 7.5 \times 10^{-7}\hat{r}^4)}\right) + \\ + \exp\left(-100. + \frac{101.64}{(1. + 3.2 \times 10^{-8}\hat{r}^6)}\right) \ \ \mathrm{M}_\odot/\mathrm{pc}^{-2}, \tag{3.2}$$

where $\hat{r} = r/\mathrm{kpc}$. In the same paper, the authors summarize the results of the CO surveys for the determination of the H_2 surface mass density. The molecular gas surface density is well represented by the following relation:

$$\sigma_{H_2}(\hat{r}) = 10 \exp\left(-\hat{r}/2.2\right) \ \ \mathrm{M}_\odot/\mathrm{pc}^{-2} \tag{3.3}$$

where $\hat{r} = r/\mathrm{kpc}$ [104, 115, 116]. For the dynamical contribution of the gaseous disk to the rotation curve, the gaseous disk has been considered vertically thick with half thickness of 0.5 kpc. As in the stellar case, the method for computing the induced velocity is explained in [114].

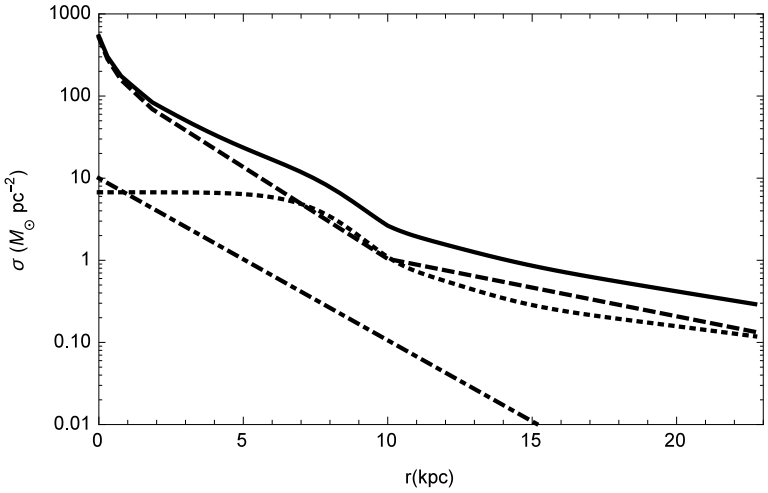

Figure 3.1: Radial dependence of the baryonic mass surface densities of the M33 disk: stellar surface density inferred from BVIgi maps (dashed line), neutral hydrogen surface density (dotted line), molecular hydrogen surface density (dotted-dashed line) and total baryonic mass surface density (continuous line) namely stars, atomic and molecular gas.

Using the accurate determination of the stellar mass surface density via chemo-photometric methods, one can determine the total luminous matter surface density in M33 shown in Fig.(3.1).

In the inner regions of the galaxy ($r \lesssim 7$ kpc, see Fig.(3.1)), the stellar mass surface density dominates over the gaseous mass surface density. For 7 kpc $\lesssim r \lesssim$ 10 kpc, stars and the atomic gas have a similar mass surface densities and beyond 10 kpc, they decrease with radius with a similar slope. Moreover, the molecular gas contribution is negligible compared to the atomic gas and stars surface densities.

In the standard RC fitting method, the stellar and gaseous disk velocity contributions add in quadrature as follows:

$$V_d^2(r) = \Upsilon V_s^2(r) + V_g^2(r), \tag{3.4}$$

where $\Upsilon = \Upsilon_*/\Upsilon_*^{\rm BVIgi} = {\rm M}_*/{\rm M}_*^{\rm BVIgi}$, is the ratio between the stellar disk mass and that given by Eq.(3.1), which is 4.9×10^9 $\rm M_\odot$ out to $r = 23$ kpc. The parameter Υ takes into account the uncertainties in the stellar disk mass and hence, the total stellar disk mass is allowed to vary in the interval $3.4 - 6.4 \times 10^9$ $\rm M_\odot$. The terms $V_s(r)$ and $V_g(r)$ indicate the contributions to the rotation curve of the stellar disk, as given by Eq.(3.1), and of the Helium corrected HI and H_2 gas mass.

3.2 The rotation curve of M33 in modified gravity

The experimental RC of the galaxy M33 constitutes a great example to study the phenomenon of the DM grace to the fact that it is traced with a unprecedent spatial resolution. As the galaxy M33 exhibits a warped HI disk, in [117] was fitted a tilted-ring model to the 21-cm line data over the full extent of the disk. A set of free rings was considered, each ring being characterized by its radius r and by 7 additional parameters: the HI surface density, the circular velocity $V_C(r)$, the inclination i (variable as the disk wraps) and the position angle PA, the systemic velocity $V_{\rm sys}$ and the position and velocity shifts of the orbital centers with respect to the galaxy center (x_c, y_c). The final RC of M33 consists of stacking the measurements inside and outside the optical disk. In this section I will explain some of the most recurrent methods to explain the mass discrepancies observed in galaxy RCs by taking two approaches: first from the modifications of gravity point of view, and then directly introducing the unknown yet DM through a mass density model obtained by numerical simulations based in the $\Lambda-$CDM cosmology and later a phenomenological DM density profile introduced to alleviate the core-cusp problem.

3.2.1 The rotation curve of M33 in MOND

As introduced in the previous chapter, an alternative explanation for the mass discrepancy in galaxies has been proposed by Milgrom, introducing the modified Newtonian dynamics or MOND [77]. According to this phenomenological model, the dynamics of the galaxy becomes non-Newtonian below an acceleration scale a_0, where the effective gravitational acceleration is given by $a(r) = a_N(r)/\mu(a(r)/a_0)$, where $\mu(x)$ is interpolating function. For the galaxy M33, one can test the two most popular interpolating functions $\mu(x)$ given by Eq.(2.9) and Eq.(4.4.2)

respectively. We have used both velocity formulas Eq.(2.11) and Eq.(2.12), and in particular one finds that the corresponding to the standard interpolating function ($V_I(r)$) provides better fits to the M33 data than the simple one ($V_{II}(r)$), however, the values of the constant stellar mass-to-light ratio of the former, lies outside of the range allowed by the BVIgi maps.

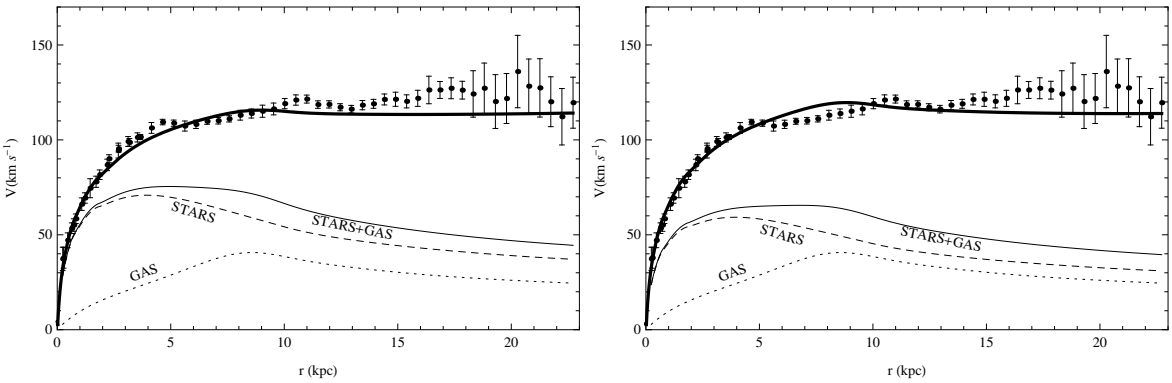

Figure 3.2: RC of M33 and best fittings considering the standard and simple interpolating functions. The different luminous components are labeled correspondingly.

For the standard interpolating function was obtained $\chi^2_{\rm red} = 1.79$ with $\Upsilon = 1.33$, that corresponds to a stellar mass of $M_s = 6.52 \times 10^9$ M$_\odot$ as obtained in [105], but it is just outside the $3-\sigma$ region. For the simple interpolating function was obtained $\chi^2_{\rm red} = 2.40$ with $\Upsilon = 0.93$, which corresponds to a stellar mass of $M_s = 5.83 \times 10^9$ M$_\odot$ compatible with the BVIgi maps, but the fit does not improve. As also argued in [105], the fits of the RC of the galaxy M33 provided by MOND do not improve considerably by increasing the stellar disk mass.

3.2.2 The rotation curve of M33 in $f(R)$ gravity

The distribution of the luminous matter in spiral galaxies, to a good extent, can be considered as cylindrically symmetric with surface density $\Sigma(\vec{r})$, hence, using cylindrical coordinates, the gravitational potential Eq.(3.5), generated by each disk component i, reads

$$\Phi_{i,\beta}(r) = -\frac{G}{2}\int_0^{+\infty}\int_0^{2\pi}\int_{-h_i}^{h_i} dr'dz'd\theta \frac{\|\vec{r'}\|\Sigma_i(\vec{r'})}{\|\vec{r}-\vec{r'}\|}\left(1+\frac{1}{2}\left(\frac{\|\vec{r}-\vec{r'}\|^\beta}{r_c^\beta}-1\right)\right), \tag{3.5}$$

where h_i is the disk half-thickness of each component, and $\Sigma_i(\vec{r'}) = 0.66\sigma_i(r')\cosh^{-2}(z'/h_i)/h_i$ is the volume mass density for the thick disk i, being $\sigma_i(r')$ their corresponding surface mass densities. For the galaxy M33, as discussed in [105], there are mainly three disk components: the stellar with a half-thickness of 0.1 kpc, a HI and H_2 gaseous disk which have 0.5 kpc half-thickness each respectively. The total gravitational potential will be

$$\Phi_\beta(r) = \Phi_{s,\beta}(r) + 1.33 \times (\Phi_{HI,\beta}(r) + \Phi_{H_2,\beta}(r)), \tag{3.6}$$

with the 1.33 correcting the Helium presence in the galaxy. Plugging the values of the half-thickness of the stellar and gaseous components, one can fit the circular velocity $V_\beta^2(r) = rd\Phi_\beta(r)/dr$ directly from the experimental data, to determine the parameters Υ, β and r_c.

In [118] were analyzed several galaxy RCs and obtained the best fitting value for $\beta = (0.70 \pm 0.25)$, however, this parameter is well constrained from SNeIa to be $\beta = 0.87$. For the analysis of the RC of the galaxy M33, I fixed the values of β to $\beta = 0.70$ as supported by [118, 119], and later at $\beta = 0.87$. For $\beta = 0.7$ the best fitting values obtained for r_c and Υ were: $r_c = (0.038 \pm 0.002)$ kpc while $\Upsilon = (0.70 \pm 0.25)$, compatible with the BVIgi mass maps, and a $\chi^2_{\rm red} = 5.58$. On the other hand, for $\beta = 0.87$ the fits improve as in this case $\chi^2_{\rm red} = 3.33$ with the best fitting values: $r_c = (0.097 \pm 0.012)$ kpc and $\Upsilon = (1.30 \pm 0.61)$, which is still compatible with the BVIgi mass maps.

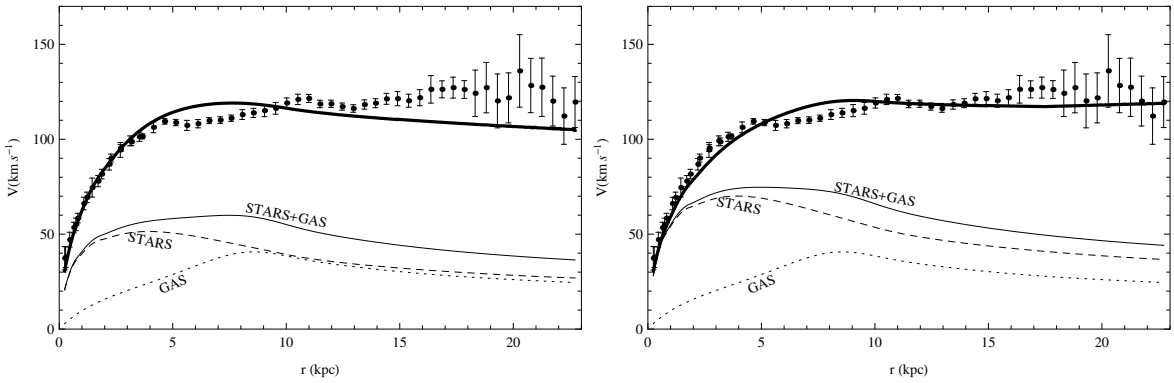

Figure 3.3: RC of M33 and best fittings (black continuous lines) considering the $f(R)$ model with $\beta = 0.70$ (left panel) and $\beta = 0.87$ (right panel). The stellar and gas Newtonian velocities are correspondingly labeled.

As can be seen, from the point of view of modified theories of gravity, the fits obtained in both: in MOND and $f(R) = R^n$ are not favorable for this galaxy, whose RC is well extended and rich in data. However, from these two models of modified gravity, we can conclude that MOND is favored against $f(R) = R^n$. In the next section I will study again the problem of the flatness of the RC of this galaxy assuming that this is due to an excess of mass made by particles that have not yet been directly observed.

3.3 Dark matter halo models and dynamical analysis of the rotation curve

In Chap.(2) was presented the DM mass modeling method, which consist in fitting directly the experimental RC of galaxies with the total circular velocity induced by a prescribed DM halo model and the luminous matter distribution. For the galaxy M33 this was already done in [105]

by taking into account the disk velocity decomposition $V_d^2(r) = \Upsilon V_s^2(r) + V_g^2(r)$, being Υ the stellar mass-to-light ratio, constrained by the BVIgi maps to vary in the range $0.7 \leq \Upsilon \leq 1.3$. $V_s(r)$ and $V_g(r)$ are the stars and helium corrected gas circular velocities. Since this galaxy has a negligible bulge and no prominent bars, then the model for the total circular velocity is given by $V^2(r) = V_d^2(r) + V_{DM}^2(r)$ where $V_{DM}^2(r)$ could be either given by Eq.(2.37) or Eq.(4.2).

For the NFW halo profile, the following values have been obtained by [105]: $c = (9.5 \pm 1.5)$, $\mathrm{M_{vir}} = (4.3 \pm 1.0) \times 10^{11}$ $\mathrm{M_\odot}$, and $\mathrm{M_*} = (4.9 \pm 0.6) \times 10^9$ $\mathrm{M_\odot}$ by considering a composite probability, which takes into account the fit to the RC, the synthesis models of the stellar population and the $c-\mathrm{M_{vir}}$ relation found by numerical simulations.

Through the dynamical analysis of the M33 RC, [105] found no compatible values of the stellar mass surface densities using Eq.(3.1). However, considering only the B, V, I color maps of M33, the synthesis models predict somewhat higher stellar masses than Eq.(3.1): $5.5{\times}10^9$ $\mathrm{M_\odot}$. Given the uncertainties in the models, the likely M33 stellar mass is in this case within the interval 3.9-7.2$\times 10^9$ $\mathrm{M_\odot}$. Using the corresponding stellar mass surface density the following RC best fitting values for the BRK halo and the stellar mass have been found: $r_c = 7.5$ kpc, $\rho_c = 18.0 \times 10^6$ $\mathrm{M_\odot}$ $\mathrm{kpc^{-3}}$ and $\mathrm{M_*} = 7.2 \times 10^9$ $\mathrm{M_\odot}$. The global χ^2 value is larger than that found when using the NFW DM profile but still acceptable. Therefore, even for this galaxy, despite we have accurate and extended RC data tracing the gravitational potential, and a good determination of the luminous mass surface density, both DM mass models are compatible with the data. This can be easily attributed to the fact that in M33, even beyond 10 kpc, the influence of the luminous matter is not negligible so that any derivation of the DM density profile would be fraught with the uncertainties inherent to such a component.

3.4 Model-independent method for the local density estimation

A new method to determine the DM density distribution in spiral galaxies has been introduced by [103]. This method was applied first to estimate the value of the DM density at the Sun's location [103], and extended in [120] to the study of the DM distribution in the galaxy NGC 3198. The goal of this section is to derive, for the spiral galaxy M33, a model independent DM density using this method which deals with the RC at large radii, where the influences of the stellar and gaseous disks are weak.

3.4.1 Empirical velocity profile

With the aid of the local density method, we can study, directly from the experimental data, the DM halo properties by computing the densities given by Eq.(2.47), Eq.(2.48) and Eq.(2.49) respectively. Just with the purpose of deriving a smooth profile of dV/dr, we introduce the

following empirical velocity formula to describe the rotation curve of M33:

$$V(r) = V_0 \frac{r/r_0 + d}{r/r_0 + 1}. \tag{3.7}$$

This is a simple, rational, 3-parameter-dependent velocity profile that reproduces at large galactocentric distances a flat velocity curve and as we will see immediately, it describes genuinely the RC in the range allowed by the experimental data. The three free parameters, namely the terminal velocity V_0, the scaling radius r_0 and $d < 1$, an additional parameter to prevent $V(r)$ to be constant, make the degree of freedom of the fit to be similar to that of the standard RC fitting method (see previous Section) when considering the uncertainties on the stellar surface mass density. The empirical velocity formula can be used when considering both for the BRK halo plus luminous disk and the NFW halo plus luminous disk mass models.

By minimizing the χ^2 distribution for fitting the RC data with its measurement errors, with the above analytic function, we obtain the best fit parameters: $V_0 = (130.2 \pm 1.0)$ km s^{-1}, $r_0 = (1.3 \pm 0.1)$ kpc, and $d = (0.12 \pm 0.03)$, giving a $\chi^2_{\rm red} = 0.75$. In Fig.(3.4) we show the fit to the RC data of the derived analytic function. For comparison we show also the fits obtained by [105] using the BRK DM profile (left panel) and the NFW DM profile (right panel) discussed in the previous section. Moreover, in Figs.(3.5) we show the $1, 2, 3\sigma$ confidence levels for such three free parameters.

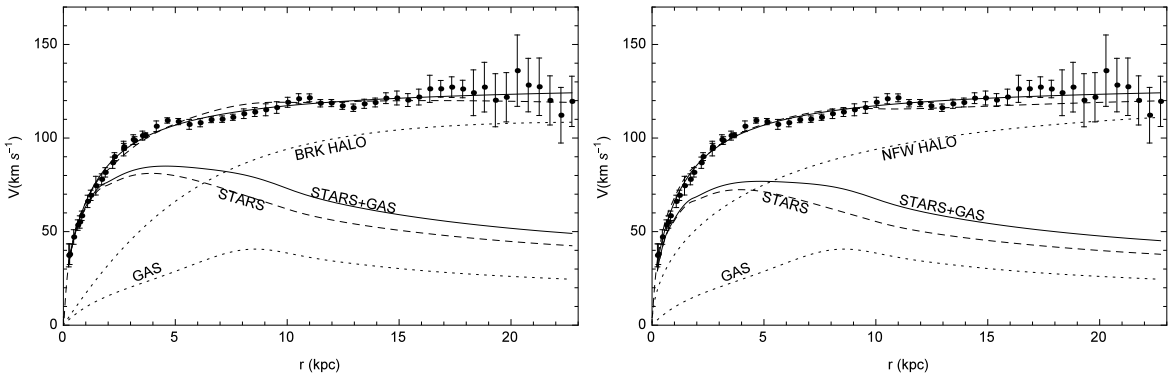

Figure 3.4: RC of M33 (black dots with error bars) with the analytical best fit to it as given by Eq.(3.7) (continuous line) with $V_0 = 130.2$ km s^{-1}, $r_0 = 1.3$ kpc, and d = 0.12. In both panels are also shown (in dashed lines with no labels), for comparison, the solutions to the RC fit obtained by [105] using the BRK (left panel) and NFW (right panel) profiles respectively, as discussed in the previous section. The halo, stellar, gas and total disk contributions are shown as well with their corresponding labels.

3.4.2 Dark matter profiles and effective densities

Given the goodness of the fit of the RC data with the analytic function given by Eq.(3.7), the goal of this subsection is to use this continuous smooth curve to compute $\rho(r)$ as given by

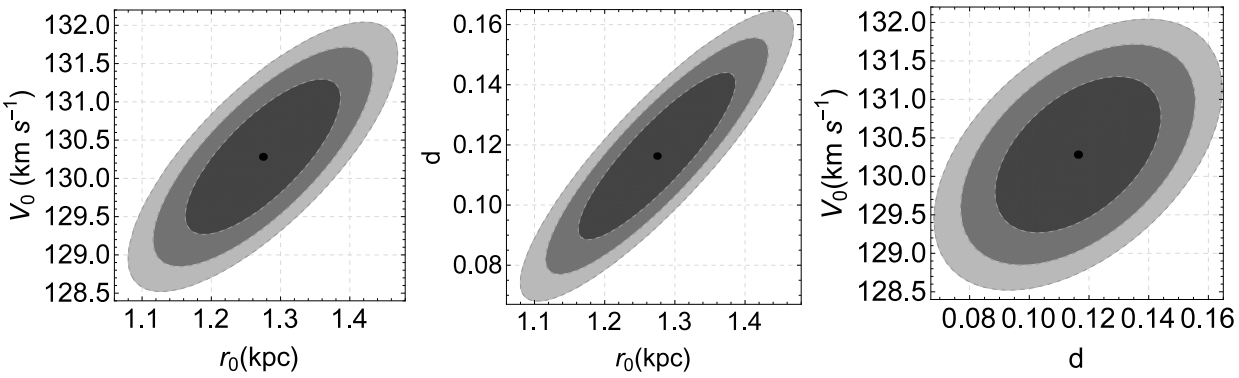

Figure 3.5: 1, 2 and 3σ confidence ellipses (from dark to light) for the best fitting parameters $V_0,\ r_0,\ d$ in fitting the analytic function in Eq.(3.7) to RC data. The black central dots indicate the best fitting values.

Eq.(2.47) and the effective baryonic disk densities. As mentioned before, for $r \gtrsim 9$ kpc the contributions of the star and gas densities are negligible in Eq.(2.46) and we are left only with the DM halo contribution.

In the range of galactocentric distances $9.5\,\mathrm{kpc} \leq r \leq 22.72\,\mathrm{kpc}$, we fit the derived density profile using the BRK and NFW DM radial density distribution. In the case of the BRK profile, we obtain the best fitting values: $r_c = (9.6 \pm 0.5)$ kpc and $\rho_c = (12.3 \pm 1.0) \times 10^6\ \mathrm{M}_\odot$ kpc^{-3} respectively, giving a $\chi^2_{\mathrm{red}} = 0.8$ and the halo virial mass is $\mathrm{M}_{\mathrm{vir}}(3.0 \pm 0.8) \times 10^{11}\,\mathrm{M}_\odot$. In Fig.(3.6) (left panel) we show the corresponding fit in log-log scale. Framed by this solution, let us stress again that close to $r \sim 9 - 9.5$ kpc the stars and gas contributions drop sharply more than two orders of magnitude, therefore, in the radial range $9.53\,\mathrm{kpc} \leq r \leq 22.72\,\mathrm{kpc}$ the stellar mass-to-light ratio Υ plays no role in this analysis and we can obtain the two halo parameters also if the baryonic disk mass has some uncertainties. In the right panel of Fig.(3.6) we show the corresponding $1, 2, 3\sigma$ confidence levels for the two BRK halo parameters. In the same panel, the continuous line shows the correlation found (Eq.(4.4)) and the shaded area its 1σ region. Clearly the solution obtained for the parameters ρ_c and r_c lies inside the uncertainties associated with the correlation, as reported in [22].

We performed the same analysis using the NFW profile. In this case we obtained the best fitting values $c = (9.5 \pm 0.7)$ and $\mathrm{M}_{\mathrm{vir}} = (5.4 \pm 0.6) \times 10^{11}\ \mathrm{M}_\odot$, giving a $\chi^2_{\mathrm{red}} = 1.0$. In the left panel of Fig.(3.8) we show the corresponding fit in log-log scale. In the right panel we display the corresponding $1, 2, 3\sigma$ confidence levels for the two free parameters of the NFW profile, as well as their correlation relation found by numerical simulations and its uncertainties as given by Eq.(2.43) (shaded area).

It is worth to discuss the present result. We can trace the distribution of matter in M33 using the RC observational data starting from the innermost radius $r = 0.24$ kpc. Inside this radius, no information can be inferred except by extrapolating the best fitting models and testing the predicted RC velocities with follow up higher resolution observations. In the radial range $0.24\ \mathrm{kpc} \leq r \lesssim 9$ kpc, the stellar component is dynamically very relevant with respect to the DM halo component. For both DM halo models tested, the structural parameters of

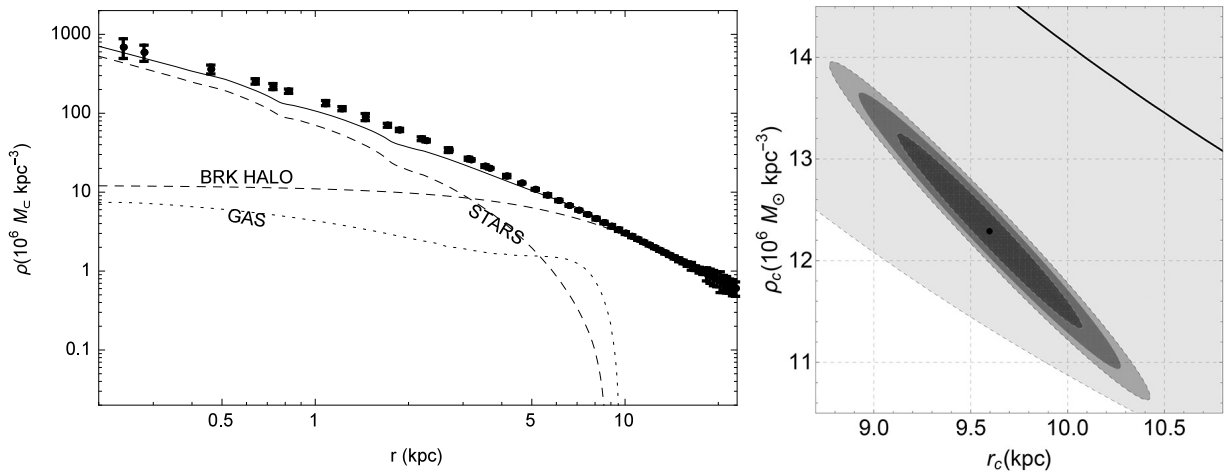

Figure 3.6: The left panel shows the dependence of various effective densities on galactocentric radius: the black points with error bars correspond to $\rho(r)$ as derived from Eq.(2.47). The continuous line marks the total density given by the BRK halo plus stars and gas. We also plot the effective densities of stars and gas given by Eq.(2.48) and Eq.(2.49) respectively and the best fitting BRK DM halo density. The right panel shows the 1, 2 and 3σ confidence ellipses (from dark to light) for the best fitting parameters r_c and ρ_c, as well as the correlation relation between these two (continuous line) given by Eq.(4.4) with a 20% of uncertainty (shaded area).

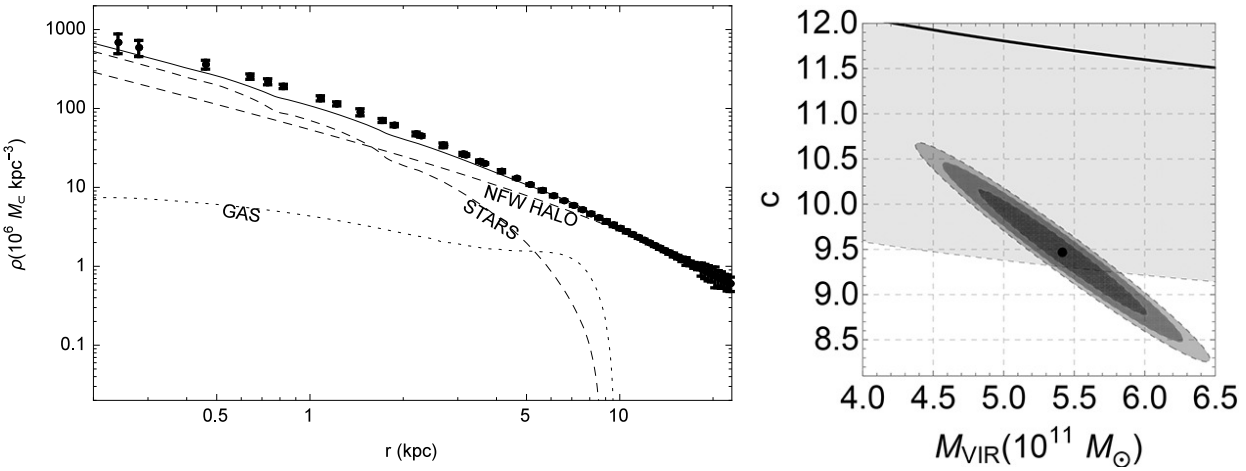

Figure 3.7: The left panel shows the dependence of various effective densities on galactocentric radius: the black points with error bars correspond to $\rho(r)$ as derived from Eq.(2.47). The continuous line marks the total density given by the NFW halo plus stars and gas. We also plot the effective densities of stars and gas given by Eq.(2.48) and Eq.(2.49) respectively and the best fitting NFW DM halo density. The right panel shows the 1, 2 and 3σ confidence ellipses for the best fitting halo parameters c and $\mathrm{M_{vir}}$, where the black central point corresponds to the best fitting values of c and $\mathrm{M_{vir}}$. The continuous line and shaded area in the right panel correspond to the $c - \mathrm{M_{vir}}$ correlation given by Eq.(2.43).

the DM distribution are mingled with the unknown value of the disk mass. In both cases, no information can be extracted either since any measurements of DM distribution would be fraught with the uncertainties due to the stellar contribution (i.e. the stellar disk accounts for most of the total gravitational potential of the galaxy). Around 9 kpc, the luminous matter still competes against DM to dominate over the total mass, given the RC uncertainties. But beyond 9.5 kpc, at $\simeq 3.5R_D$, the exponential decrease of the stellar matter density and the negligible contribution of the gaseous component, which never plays a role even if its total mass is about half of that of the stars, assure that only the DM component balances the radial accelerations, which the gaseous disk is engaged with.

In Fig.(3.8) we show the best fits of the BRK and NFW profiles to the outer disk effective matter densities. As we can notice, the values and radial gradients of the matter density of the two DM halo models are similar, in agreement with our finding that both halos are compatible with the data. This is because the core of the BRK best fitted halo does not extend much beyond the optical disk, where DM is the dominant dynamical component.

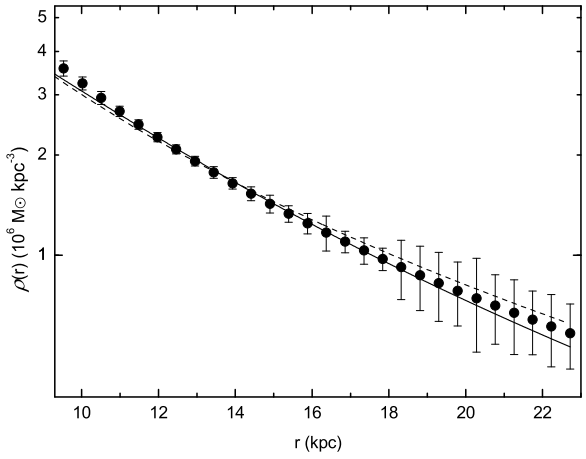

Figure 3.8: The observed DM halo density profile in the outer disk is shown using black dots with error bars. For comparison the BRK (continuous line) and NFW (dashed line) best fitting halo models to the effective densities inferred from the dynamical analysis of RC data are also displayed.

In this section were deepened the results of [105] which obtained a global fit of the RC of M33, after an accurate mass modelling of its stellar disk, by considering a DM halo with a cuspy NFW or a cored BRK profile. The results of the global fits to the RC favour a cuspy $\Lambda-$CDM halo despite a cored one is still compatible with the data when a heavier stellar disk is considered. Following [103] and [120], it was used a new approach to investigate the DM content of M33. Relying on the centrifugal equilibrium condition, assuming a spherical DM halo, the DM density was traced by using only the experimental RC. This method relies on fitting the DM density distribution of M33 in the radial range $9.53\,\mathrm{kpc} \leq r \leq 22.72\,\mathrm{kpc}$, where the stellar and

gaseous contributions to the RC are negligible. According to this method, the BRK profile with the following parameters: $r_c = (9.6 \pm 0.5)$ kpc and $\rho_c = (12.3 \pm 1.0) \times 10^6$ $M_\odot$ kpc^{-3} provides an excellent fit to the M33 data. The BRK halo virial mass is $M_{vir} = (3.0 \pm 0.8) \times 10^{11}\, M_\odot$ and it is only $6.7 \pm 1.2 \times 10^{10} M_\odot$ out to about 23 kpc. When testing the NFW DM profile through the local density estimator method it was found instead a higher virial mass for the halo and therefore an extremely low baryonic fraction. With the analysis presented in this section, one may conclude that the possibility that M33 harbors a cored DM halo seems still suitable. Even though the determination of the stellar disk mass via synthesis models has eliminated most of the disk-halo degeneracies in this low luminosity spiral, it is shown that the cuspy or cored dark matter density profiles degeneracy still hold because different dynamical methods used in modelling RC data favour different DM density distributions and halo masses.

Chapter 4

Empirical velocity profiles

In order to apply to any galaxy the local density method as introduced in Sec.(2.5.2) and applied in the previous chapter, a very important issue left to treat is to derive an analytical expression for the total circular velocity $V(r)$ from the available discreet set of the observational points of the experimental RC. An analytic expression for $V(r)$, will make easier the numerical computation of the total density as given by Eq.(2.47). In order to alleviate this issue and as shown in the previous chapter, in [121] was proposed an empirical velocity profile (see Eq.(3.7)) to fit the total RC of the spiral galaxy M33. As discussed in the previous chapter, this empirical velocity profile has three free parameters and it is the simplest velocity profile that reproduces the observational RC and gives an asymptotically flat rotation curve at large galactocentric distances.

The empirical velocity profile given by Eq.(3.7) has a limited use since it doesn't show the usual bumps of the bulge-to-disk transition in the inner regions of the RCs, nor reproduce slightly declining nor increasing RCs. Despite this issue, its application in the local density method is valid since one only needs to know the velocity profile in the distant regions of the galactic centre, free from the influences of the luminous matter. The motivation in this chapter is to introduce a more generalized velocity profile that overcome this issue and could help to express the density and other physical quantities from the experimental RCs, so that one can study in a deeper way the nature of the DM that surrounds the galaxies.

4.1 Empirical velocity profile

There are many situations in which one needs a simple fitting formula for a RC between the initial and the final experimental points such that by extrapolation, it converges to the Keplerian velocity at very large distances. In order to do so, we propose a new empirical formula for the rotational velocity as:

$$V_n(r) = \frac{V_0 d^n (r/r_c)^{\frac{3}{2}} (1 + r/r_c)^{-(n+\frac{1}{2})}}{\sqrt{1 + (r/r_c)^2}} \sum_{i=0}^{n} \left(\frac{r/r_c}{d} \right)^i , \tag{4.1}$$

where again V_0 is the constant velocity of the outskirts of the galaxy, r_c is a radial length-scale, d is a dimensionless parameter and we have introduced an additional free parameter $n \geq 1$ which is a positive integer number. This simple fit enlarges the number of RCs that one can analyze with respect to the main approach, that is to fit the data with physical halo plus disk model velocity components, and although the functional fit might not have a direct physical meaning, mathematically it carries the properties of the RCs.

For this circular velocity profile, similarly as in Eq.(3.7), at large distances $r \gg r_c$ the velocity profile approaches asymptotically the constant value V_0 independent of d and n, and reproduces a flat RC. At small distances $r \ll r_c$ the behavior is $V_n(r \ll r_c) \sim V_0 d^n (r/r_c)^{\frac{3}{2}}$, which is always increasing and the RC starts at $r = 0$ regardless of the values of d and n. Even more interesting is the fact that expanding the sum in Eq.(4.1), for every $0 \leq i \leq n$ each term reaches a local maximum at $r/r_c = s$ where s satisfies the cubic equation $2(n-i)s^3 - (2i+1)s^2 + 2(n-i-1)s - (2i+3) = 0$ which for $i \neq n$ always has, at least, one real solution and it is positive for $n \geq 1$ (this last can be easily checked using Descartes' sign rule). This means that the class of RCs we could fit, include also those with prominent bulges. It worth also to notice that as in Eq.(3.7) was needed $0 \leq d < 1$ to reproduce an increasing RC, for Eq.(4.1), this restriction has no meaning since the velocity always increases near $r = 0$, which allows us also to use Eq.(4.1) as an extrapolation of the experimental RC towards the centre of the galaxy.

4.2 Gravitational potential

The total gravitational potential is related with the velocity by means of the differential equation

$$\left.\frac{\partial \Phi_n(\vec{r})}{\partial r}\right|_{z=0} = -\frac{V_n^2(r)}{r}. \tag{4.2}$$

Assuming spherical symmetry, the geodesics lines, which describe the motion of particles are confined to the $\theta = \pi/2$ plane, so we can get rid of the partial derivative and write Eq.(4.2) as

$$\frac{d\Phi_n(r)}{dr} = -\frac{V_0^2 d^{2n}}{r_c} \frac{(r/r_c)^2 (1 + r/r_c)^{-(2n+1)}}{1 + (r/r_c)^2} \sum_{i=0}^{2n} C_{(i,n)} \left(\frac{r/r_c}{d}\right)^i, \tag{4.3}$$

$$C_{(i,n)} = \begin{cases} i+1, & \text{if } 0 \leq i \leq n; \\ 2n-i+1, & \text{if } n \leq i \leq 2n. \end{cases} \tag{4.4}$$

Notice that to the gravitational potential contribute $2n+1$ components, but there is one which is not conventional to the physics we know; to see this more in details, let's expand $\Phi(r)$ as:

$$\begin{aligned} \Phi_n(r) = \Phi_n(+\infty) + \int_{r/r_c}^{+\infty} \frac{GM_0 d^{2n}}{r_c} \frac{s^2 (1+s)^{-(2n+1)}}{1+s^2} \sum_{i=0}^{2n-1} C_{(i,n)} \left(\frac{s}{d}\right)^i ds + \\ + \int_{r/r_c}^{+\infty} \frac{GM_0}{r_c} \frac{s}{1+s^2} \left(\frac{s}{1+s}\right)^{2n+1} ds, \end{aligned} \tag{4.5}$$

being $M_0 = V_0^2 r_c/G$ a constant with mass unit and G is the universal gravitational constant.

Assuming the factor GM_0/r_c to be a constant, the integrating function in the first term of the above formula satisfies:

$$\left|\frac{s^2 s^i}{(1+s)^{(2n+1)}(1+s^2)}\right| \leq \left|s^{(i-2n-1)}\right| \leq \left|1/s^2\right|, \tag{4.6}$$

for $0 \leq i \leq 2n-1$, therefore the integral converges in the improper sense. Meanwhile in the second term we have the integrating function

$$\frac{s}{1+s^2}\left(\frac{s}{1+s}\right)^{(2n+1)} = \frac{s}{1+s^2}\left(1-\frac{1}{1+s}\right)^{(2n+1)} = \frac{s}{1+s^2} + \sum_{j=1}^{2n+1}\binom{2n+1}{j}(-1)^j \frac{s}{(1+s)^j(1+s^2)}$$

where in the last step the binomial formula was used. The second integral in the gravitational potential then can be written as

$$\begin{aligned}\int_{r/r_c}^{+\infty} \frac{GM_0}{r_c}\frac{s}{1+s^2}\left(\frac{s}{1+s}\right)^{2n+1} ds = \int_{r/r_c}^{+\infty} \frac{GM_0}{r_c}\sum_{j=1}^{2n+1}\binom{2n+1}{j}(-1)^j \frac{s}{(1+s)^j(1+s^2)} ds + \\ + \int_{r/r_c}^{+\infty} \frac{GM_0}{r_c}\frac{s}{1+s^2} ds.\end{aligned} \tag{4.7}$$

Following the same convergence analysis, we find that

$$\left|\frac{s}{(1+s)^j(1+s^2)}\right| \leq \left|1/s^{j+1}\right| \leq \left|1/s^2\right|, \tag{4.8}$$

therefore the first integral in the above expression converges in the improper sense, while the second diverges logarithmically. The total gravitational potential can thus be written as

$$\Phi_n(r) = \Phi_n(+\infty) + \Phi_{n\,c}(r) + \int_{r/r_c}^{+\infty} \frac{GM_0}{r_c}\frac{s}{1+s^2} ds, \tag{4.9}$$

with

$$\begin{aligned}\Phi_{n\,c}(r) = \int_{r/r_c}^{+\infty} \frac{GM_0 d^{2n}}{r_c}\frac{s^2(1+s)^{-(2n+1)}}{1+s^2}\sum_{i=0}^{2n-1} C_{(i,n)}\left(\frac{s}{d}\right)^i ds + \\ + \int_{r/r_c}^{+\infty} \frac{GM_0}{r_c}\sum_{j=1}^{2n+1}\binom{2n+1}{j}(-1)^j \frac{s}{(1+s)^j(1+s^2)} ds\end{aligned} \tag{4.10}$$

being $\Phi_{n\,c}(r)$ the convergent part. Under the assumption that GM_0/r_c is constant throughout the galaxy, the divergent part of the potential, responsible for the flatness of the rotation curve, will always bound the orbit of any massive particle and no possibility of escape will be possible,

which in turn means that the Universe should be populated by a single galaxy and everything should be bounded to it. This is clearly not true and a finite escape velocity should exist even in the presence of a large DM component.

This issue can be easily solved by relaxing the condition of constancy of the parameters r_c and V_0 at large distances. Indeed, to guarantee the total convergence of every integral in the potential, it is enough to suppose that r_c is constant, or slowly varying with the galactic radius till some characteristic length scale $r_{\rm edge}$, and after, increases linearly with r, while keeping constant d, n and the factor GM_0. Notice that higher powers of r will improve faster the convergence, but the minimum power required to make the gravitational potential well defined, is at the linear order. If one attains to this prescription, since $V_0^2 = GM_0/r_c$, then, for $r > r_{\rm edge}$ one expects the Keplerian fall of the velocity as $V_n(r > r_{\rm edge}) \propto \sqrt{GM_0/r}$, where the proportionality constant depends on n, d, $r_{\rm edge}$ and $\langle r_c\rangle$ (the constant part of r_c for $r \ll r_{\rm edge}$).

Notice the power of this method. First of all, it resembles a generalization of the Brandt's model, but including the flatness effect, which was not present in Eq.(2.2). Moreover, one recovers the Keplerian fall-off of the velocity after some length-scale and all these effects are explained within the same formula, which also allows to make predictions on the mass of the galaxies. Even more curious is the fact that the prescription of introducing a sliding scale $r_{\rm edge}$ to recover the Keplerian behavior at large distances resembles a renormalization procedure in the IR regime.

As a toy example of such a variation for r_c and V_0 which respects the continuity of the velocity and its derivative one could propose:

$$r_c(r) = \langle r_c\rangle f(r), \quad V_0(r) = \langle V_0\rangle/\sqrt{f(r)} \tag{4.11}$$

$$f(r) = \left(1 + r/r_{\rm edge} + \sqrt{(r/r_{\rm edge} - 1)^2 + \langle r_c\rangle^2/r_{\rm edge}^2} - \sqrt{1 + \langle r_c\rangle^2/r_{\rm edge}^2}\right), \tag{4.12}$$

where $GM_0 = \langle V_0\rangle^2\langle r_c\rangle$, $\langle V_0\rangle$ and $\langle r_c\rangle$ are constants. Recall that $\langle V_0\rangle$ and $\langle r_c\rangle$ are the constant parts of $V_0(r)$ and $r_c(r)$ for $r \ll r_{\rm edge}$ respectively. In Figs.(4.1) are shown the radial dependence of $r_c(r)$ and $V_0(r)$ for the above prescription. Notice that for small values of $r/\langle r_c\rangle$, $r_c(r)$ and $V_0(r)$ are almost constants and then, they start to vary such to make the gravitational potential finite at large distances as needed. The Newtonian gravitational potential is recovered for large values of $r/\langle r_c\rangle$ and how quick this regime is reached, it depends on the ratio $\langle r_c\rangle/r_{\rm edge}$. This means that beyond $r_{\rm edge}$ the circular velocity of any massive particle is the same as if the particle is moving in vacuum, influenced by the gravitational field created by a point-like particle of mass M_T.

Moreover, in Figs.(4.2) are shown the velocity profiles as given by Eq.(4.1) (continuous lines) and the same Eq.(4.1) but with the renormalized coefficients as given by Eq.(4.12) (dashed lines) for $d = 0.7$ (left panel) and $d = 1.3$ (right panel), and n from 1 to 7.

With the prescription Eq.(4.12), all the integrals in Eq.(4.10) now are well define and one can compute them numerically by setting $\Phi_n(+\infty) = 0$. In Fig(4.3) are shown the graphics of the gravitational potential for $d = 0.7$ (left panel) and $d = 1.3$ (right panel), for n from 1 to 7.

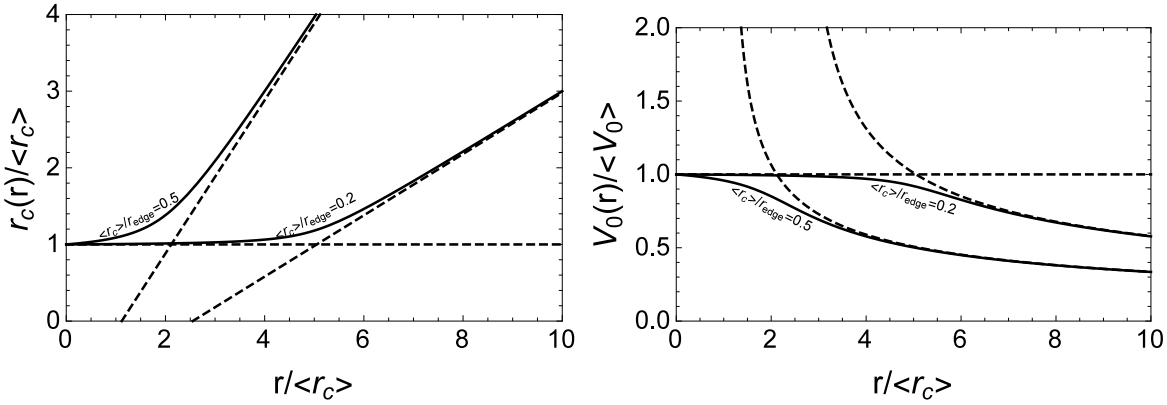

Figure 4.1: The left panel shows the dependence with $r/\langle r_c\rangle$ of $r_c(r)/\langle r_c\rangle$ as given by Eq.(4.12), for different values of the ratio $\langle r_c\rangle/r_{\rm edge}$: 0.2 and 0.5 respectively (see labels); the dashed lines correspond to their linear asymptotes. The right panel shows as well the dependence with $r/\langle r_c\rangle$ of $V_0(r)/\langle V_0\rangle$ as given by Eq.(4.12), taking again the ratio $\langle r_c\rangle/r_{\rm edge}$: 0.2 and 0.5 (see labels); as before, the dashed lines correspond to their $\sim 1/\sqrt{r}$ asymptotes.

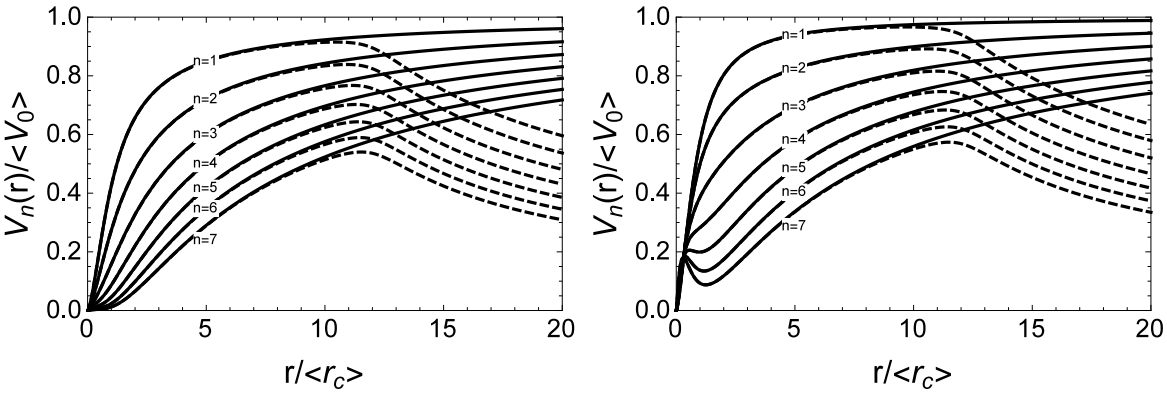

Figure 4.2: In both panels are shown the velocity formula for $d = 0.7$ (left) and $d = 1.3$ (right) for several integer values of $n : 1 \leq n \leq 7$ with their corresponding labels for the prescription Eq.(4.12). The continuous lines are given by Eq.(4.1), while the dashed lines correspond to the Newtonian renormalized ones with $r_{\rm edge}/\langle r_c\rangle = 12$.

The total mass M_T can be computed from Eq.(4.1) substituting the renormalized coefficients $r_c \mapsto r_c(r)$ and $V_0 \mapsto V_0(r)$ by taking the limit of $r_c(r)V^2(r)/G$ (keeping GM_0, d and n constants) with a suitable election of the renormalization conditions for $r_c(r)$ and $V_0(r)$. The values of M_T will depend for sure on how one chooses the dependence of $r_c(r)$ with r, keeping GM_0 constant as required for the convergence of the integrals in the gravitational potential expression. For example, for the renormalization prescription in Eq.(4.12), M_T is given by:

$$M_T = M_0 \frac{d^{2n} x^4 \left(1+x\right)^{-(2n+1)}}{1+x^2} \sum_{i=0}^{2n} C_{(i,n)} \left(\frac{x}{d}\right)^i,\ M_0 = \frac{\langle V_0\rangle^2 \langle r_c\rangle}{G},\ x = \frac{r_{\rm edge}}{2\langle r_c\rangle}. \tag{4.13}$$

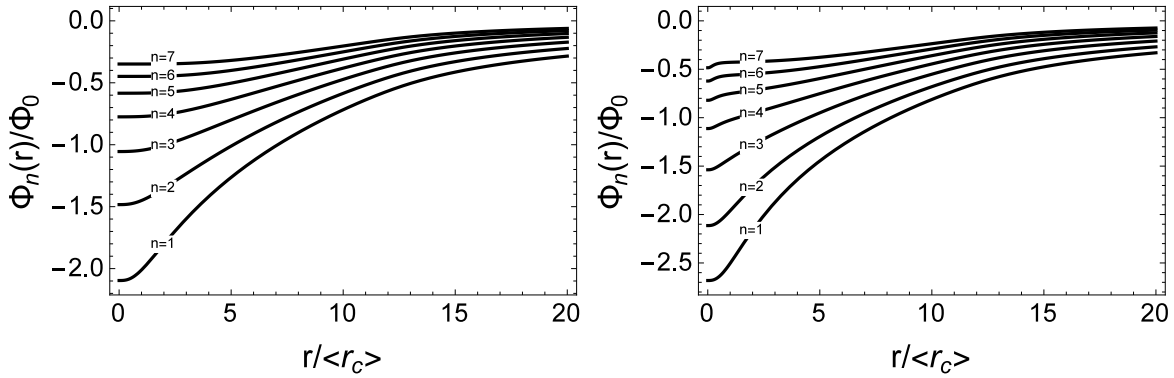

Figure 4.3: In both panels are shown the gravitational potential in units of $\Phi_0 = \langle V_0 \rangle^2$ for $d = 0.7$ (left panel) and $d = 1.3$ (right panel) for several integer values of $n : 1 \leq n \leq 7$ with their corresponding labels for the prescription Eq.(4.12) and $r_{\rm edge}/r_c = 12$.

The physical interpretation of the length-scale $r_{\rm edge}$, as mentioned above, is that any point-like massive particle moving in orbits far beyond this scale, will feel like it is moving in vacuum by the effects of the gravitational field produced by a point-like particle with mass M_T. This means that beyond the scale $r_{\rm edge}$ no luminous nor DM influence the state of motion and one can identify $r_{\rm edge}$ with the DM halo virial radius $r_{\rm vir}$, as it represents a measure of the edge of a galaxy. Moreover, since the total mass M_T is the sum of the DM halo virial mass $\mathrm{M_{vir}}$ and luminous matter mass $\mathrm{M_L}$ components, and if one uses the relation between the virial mass and virial radius given by Eq.(2.38),

$$r_{\rm edge} = \left(\frac{3}{97.2} \frac{\mathrm{M_{vir}}}{4\pi\rho_{\rm crit}} \right)^{1/3} \ \ \text{kpc}. \tag{4.14}$$

then:

$$\frac{M_T}{\frac{4\pi}{3}\rho_{\rm crit} r_{\rm edge}^3} = \frac{\mathrm{M_{vir}} + \mathrm{M_L}}{\frac{4\pi}{3}\rho_{\rm crit} r_{\rm edge}^3} = \frac{\mathrm{M_{vir}}}{\frac{4\pi}{3}\rho_{\rm crit} r_{\rm edge}^3} \left(1 + \frac{\mathrm{M_L}}{\mathrm{M_{vir}}} \right). \tag{4.15}$$

Since the ratio $\mathrm{M_L/M_{vir}}$ is in principle constrained to $0 < \mathrm{M_L/M_{vir}} < 1$, then the scale length $r_{\rm edge}$ is constrained to satisfy the inequalities

$$97.2 < \frac{M_T}{\frac{4\pi}{3}\rho_{\rm crit} r_{\rm edge}^3} < 2 \times 97.2, \tag{4.16}$$

where recall that M_T depends on $r_{\rm edge}$ as well.

4.3 Results from the fittings with 887 galaxies.

In the Figs.(4.6) are shown the experimental RCs and the corresponding fits using Eq.(4.1) (continuous black lines) and with the renormalization prescription described above to get the

Keplerian decay of the circular velocity (dashed black lines). For such a study, a sample of 887 different RCs was taken from Refs.[20, 25, 121, 105, 120, 122, 123, 124, 125, 126, 127, 128]. Our galaxy sample covers a wide range of different morphological types of galaxies, which include from dwarf spiral galaxies such as DDO154, DDO52 and NGC2366 [20], low surface brightness (LSB) spiral galaxies such as F5631, F5683, F5718 [25], till barred and lenticular spirals [126]. In the RC plots Figs.(4.6), there are RCs with error bars and with open symbols. All galaxies with error bars meet the excellence criterium since their approaching and receding arms are very symmetric and their RCs are extended out to (at least) the optical radius. The RCs with open symbols, as clearly explained in [126], they fail in at least one of the criteria stated above and therefore may be not suitable for accurate and direct mass modeling. However, they constitute a large database for those methods able to recover the DM properties by needing less stringent requirements on the RC quality.

Since there are 4 free parameters to fit with Eq.(4.1), from the list of 900 different galaxies analyzed in [126] another selection criterium was used such that the RCs fitted contain 8 or more experimental points. We performed first a χ^2 minimization procedure[1] to determine the parameters (V_0, r_c, d, n) regarding the formula given by Eq.(4.1) which throughout all the computation procedures were considered as free, which means, uncorrelated.

Given the goodness of the first fits with Eq.(4.1), a second fit was performed to the above mentioned experimental RCs by using again Eq.(4.1), this time r_c and V_0 are scale-dependents as given in Eqs.(4.12) but fixing the new parameters as equal to those of the first fits ($\langle V_0\rangle$, $\langle r_c\rangle$, d, n) = (V_0, r_c, d, n), and constraining $r_{\rm edge}$ in the range given by the inequality Eq.(4.16). In Table.(4.1) are tabulated the best fitting values (and their errors) of the free parameters
($\langle V_0\rangle$, $\langle r_c\rangle$, d, $n, r_{\rm edge}$), including the total predicted mass M_T and the values of the reduced χ^2-distribution for each galaxy analyzed in this thesis.

The relatively large amount of parameters is justified by the fact that the circular velocity model used during the fitting process contains already all the information from the DM halo, bulge, stellar and gaseous disks and possible bars or other structures that will contribute to the experimental RCs by their composite probabilities. Moreover, in Figs.(4.4) are shown the best fitting values as points (with error bars) in a two dimensional graphics of $\langle V_0\rangle - \langle r_c\rangle$, $\langle r_c\rangle - d$, $\langle r_c\rangle - M_T$ and $d - M_T$ for all values of the integer parameter n. As one may also see in Figs.(4.4), there exist large dispersions between the best fitting values of the pairs of parameters ($\langle V_0\rangle, \langle r_c\rangle$) (top-left), ($\langle r_c\rangle, d$) (top-right), ($\langle r_c\rangle, M_T$) (bottom-left) and ($d, M_T$) (bottom-right); however, from the above mentioned graphics, one can extract interesting informations about the range of variability of the parameters.

One can see bounds of each parameter as they take a finite range of values for all the galaxies analyzed in this thesis. In the $\langle V_0\rangle - \langle r_c\rangle$ plane, the range of the possible values of $\langle V_0\rangle$ doesn't exceed 10^3 km s^{-1} and statistically the mean value of this parameter is more concentrated around 10^2 km s^{-1}, with a very few values in the range $0 \sim 10$ km s^{-1}. The

[1]The fitting procedure and the parameter error estimation is already explained in Chapter 3.

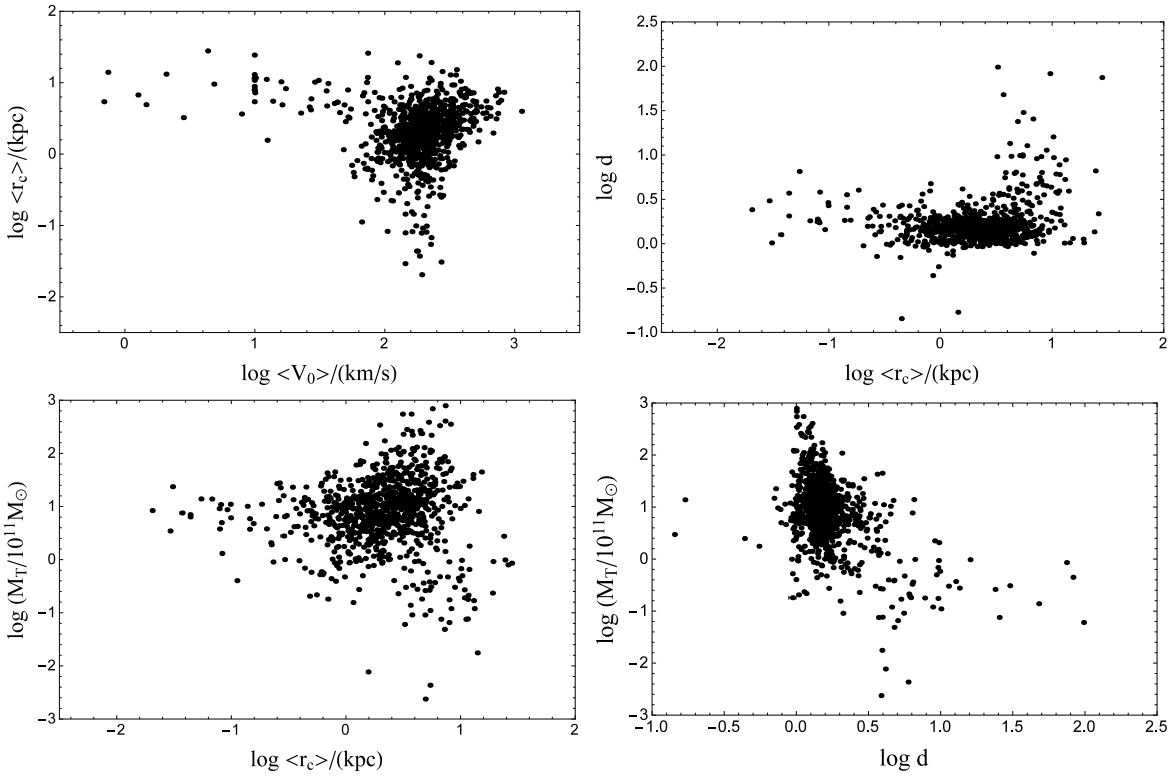

Figure 4.4: Best fitting parameters plots for all value of n. Large dispersions are observed in the $\langle V_0\rangle - \langle r_c\rangle$ (top-left panel), $\langle r_c\rangle - d$ (top-right panel), $\langle r_c\rangle - M_T$ (bottom-left panel) and $d - M_T$ (bottom-right panel) planes.

parameter $\langle r_c\rangle$ doesn't reach the values $\sim 10^2$ kpc despite of the size of the RCs, and its mean value is concentrated below the 10 kpc. The largest values of $\langle r_c\rangle$ are connected with the lowest values of $\langle V_0\rangle$. In the $\langle r_c\rangle - d$ plane one can see that both parameters are uncorrelated as d is almost constant with $\langle r_c\rangle$

However, one can observe in Figs.(4.5) the plot of the best fitting values of $\langle V_0\rangle$ and the total predicted mass M_T (left panel), as well as the pair $(\langle V_0\rangle, d)$ (right panel). For the pair $(\langle V_0\rangle, M_T)$, one finds a correlation relation compatible with a power-law as a Tully-Fisher-like formula:

$$\log\left(\frac{M_T}{10^{11}M_\odot}\right) = -(5.84 \pm 0.01) + (2.96 \pm 0.01)\log\left(\frac{\langle V_0\rangle}{km/s}\right). \tag{4.17}$$

Notice that in the left panel of Figs.(4.5), there is an island of points with $\log\langle V_0\rangle \sim 1$. As can be easily see in Figs.(4.6), all these points correspond to galaxies which RCs are not so extended, i.e. RCs with open symbols, with the exception of the three galaxies UGC11820, NGC2366 and ua394, which are not so extended either. To obtain this power-law relation Eq.(4.17), as it is shown in Figs.(4.5) (left panel), all the galaxies with $\langle V_0\rangle$ were removed from the fittings, although they are shown in the graphics.

In the right panel of Figs.(4.5) one can see that the parameter d is negatively correlated to $\langle V_0 \rangle$ and the best fitting formula is given by

$$\log d = (2.48 \pm 0.01) - (0.93 \pm +0.01) \log \left(\frac{\langle V_0 \rangle}{km/s} \right). \tag{4.18}$$

As in the previous case, all the galaxies with $\langle V_0 \rangle$ were removed from the fittings, although they are shown in the graphics. This means that despite there are five free parameters to make the general fit, only three of them are independent.

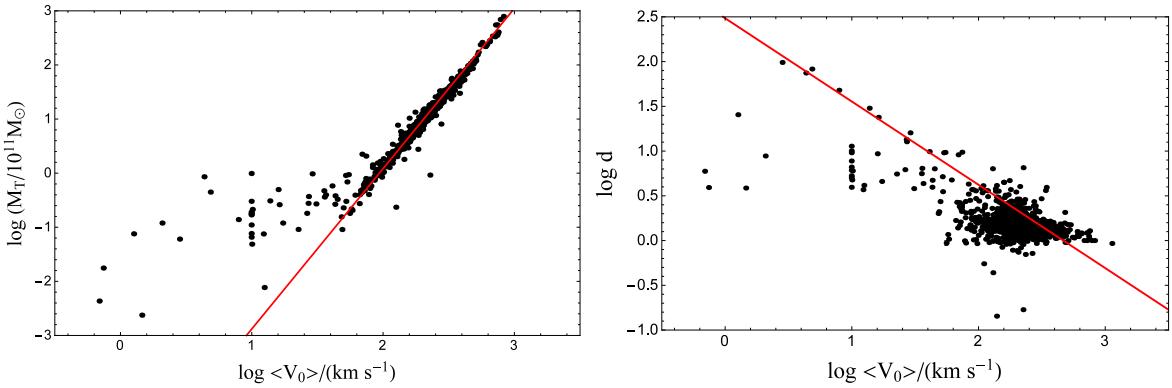

Figure 4.5: Correlations between $\langle V_0 \rangle$ and M_T (left panel), and $\langle V_0 \rangle$ and d (right panel). In the left panel, the red line corresponds to Eq.(4.17). In the right panel, the red line corresponds to Eq.(4.18).

In the previous chapter was computed the virial mass of the galaxy M33 using the standard mass modeling and the local density method. Along with the stellar mass reported in [105], the total mass in the mass modeling method corresponding to the NFW DM halo density profile as the best fit one has $M_T = (4.36 \pm 1.00) \times 10^{11}$ $M_\odot$, while for the local density method $M_T = (3.06 \pm 0.80) \times 10^{11}$ $M_\odot$. Notice that both computed masses, with different methods, are compatible with the total mass computed via Eq.(4.13) evaluated at the corresponding best fitting values: $M_T = (2.785 \pm 0.003) \times 10^{11}$ $M_\odot$. The compatibility window between the mass obtained for M33 using the empirical mass formula Eq.(4.13) and the BRK profile in the local density method is wider than the NFW one in the standard mass modeling method.

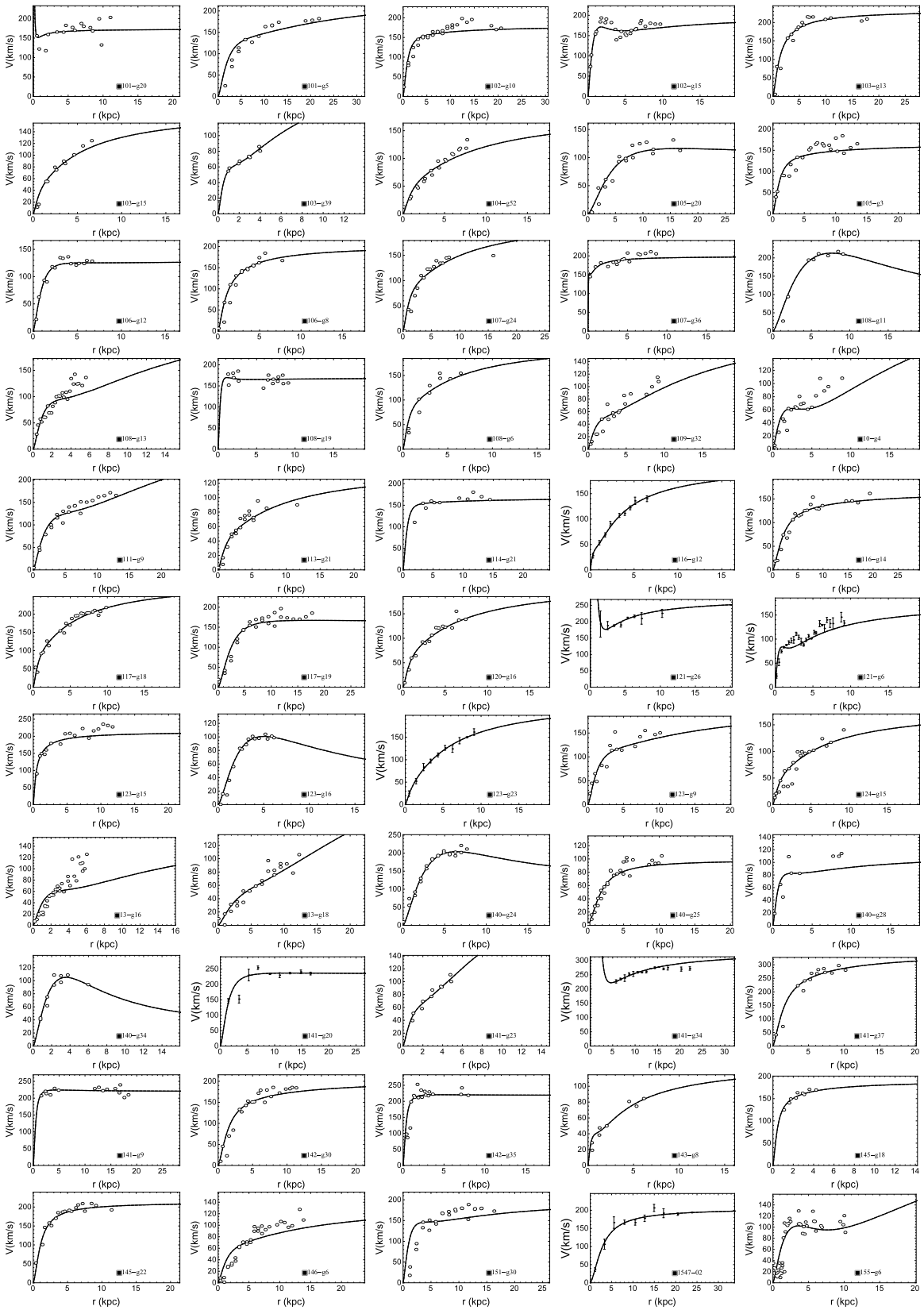
V(km/s)
r (kpc)
101−g20
101−g5
102−g10
102−g15
103−g13
103−g15
103−g39
104−g52
105−g20
105−g3
106−g12
106−g8
107−g24
107−g36
108−g11
108−g13
108−g19
108−g6
109−g32
10−g4
111−g9
113−g21
114−g21
116−g12
116−g14
117−g18
117−g19
120−g16
121−g26
121−g6
123−g15
123−g16
123−g23
123−g9
124−g15
13−g16
13−g18
140−g24
140−g25
140−g28
140−g34
141−g20
141−g23
141−g34
141−g37
141−g9
142−g30
142−g35
143−g8
145−g18
145−g22
146−g6
151−g30
1547−02
155−g6

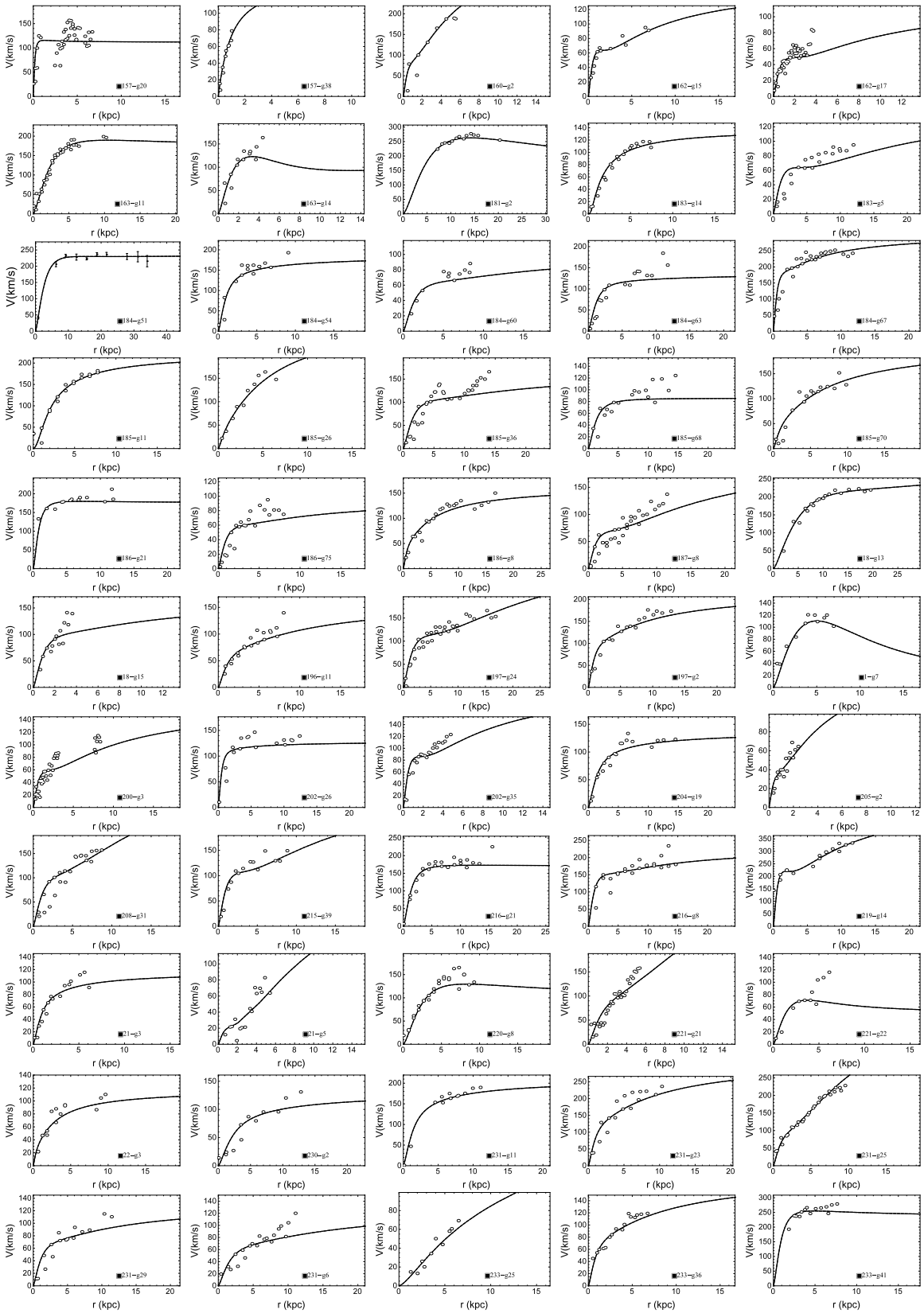
V(km/s)
r (kpc)
157−g20
157−g38
160−g2
162−g15
162−g17
163−g11
163−g14
181−g2
183−g14
183−g5
184−g51
184−g54
184−g60
184−g63
184−g67
185−g11
185−g26
185−g36
185−g68
185−g70
186−g21
186−g75
186−g8
187−g8
18−g13
18−g15
196−g11
197−g24
197−g2
1−g7
200−g3
202−g26
202−g35
204−g19
205−g2
208−g31
215−g39
216−g21
216−g8
219−g14
21−g3
21−g5
220−g8
221−g21
221−g22
22−g3
230−g2
231−g11
231−g23
231−g25
231−g29
231−g6
233−g25
233−g36
233−g41

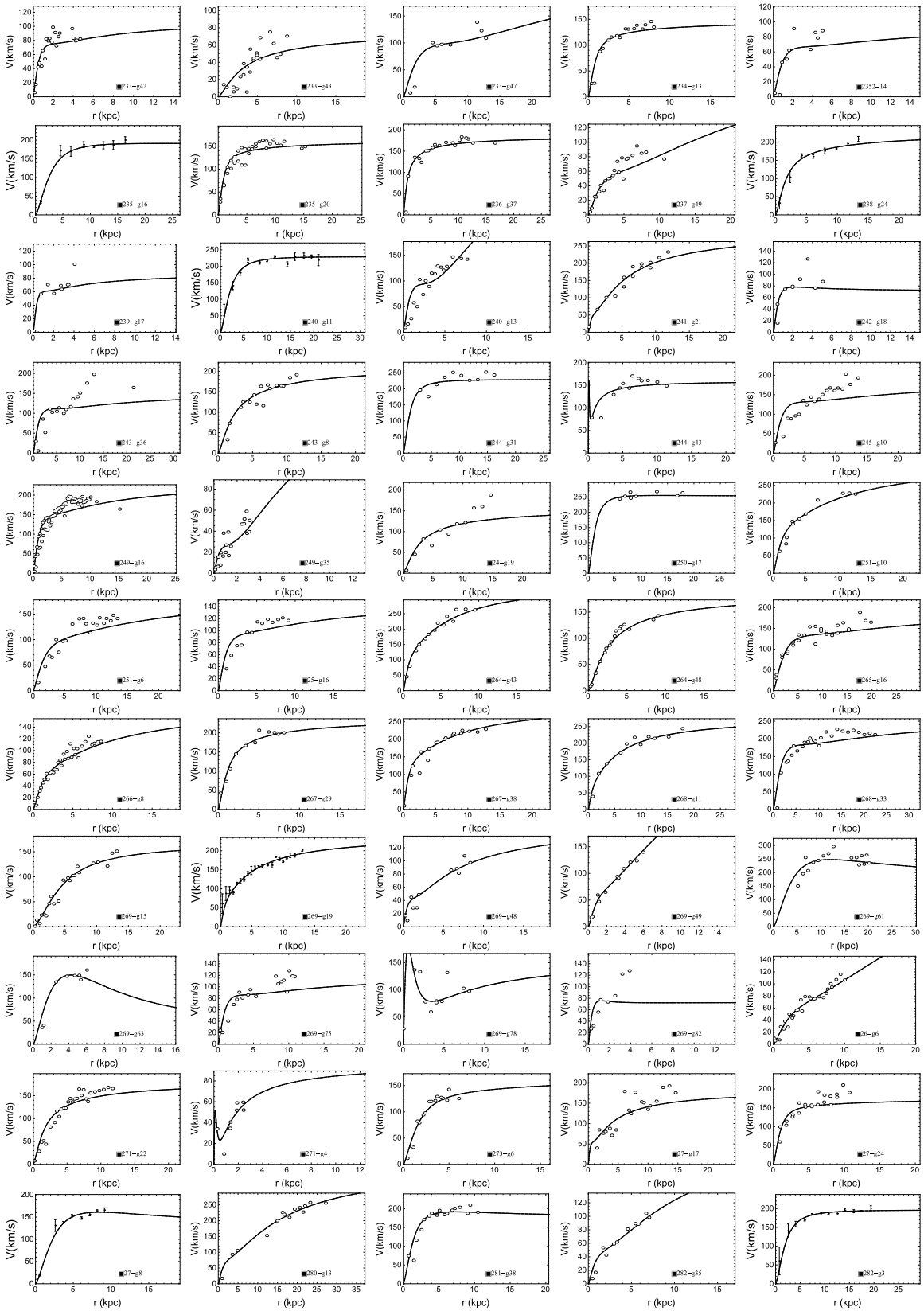
V(km/s)
r (kpc)
233−g42
233−g43
233−g47
234−g13
2352−14
235−g16
235−g20
236−g37
237−g49
238−g24
239−g17
240−g11
240−g13
241−g21
242−g18
243−g36
243−g8
244−g31
244−g43
245−g10
249−g16
249−g35
24−g19
250−g17
251−g10
251−g6
25−g16
264−g43
264−g48
265−g16
266−g8
267−g29
267−g38
268−g11
268−g33
269−g15
269−g19
269−g48
269−g49
269−g61
269−g63
269−g75
269−g78
269−g82
26−g6
271−g22
271−g4
273−g6
27−g17
27−g24
27−g8
280−g13
281−g38
282−g35
282−g3

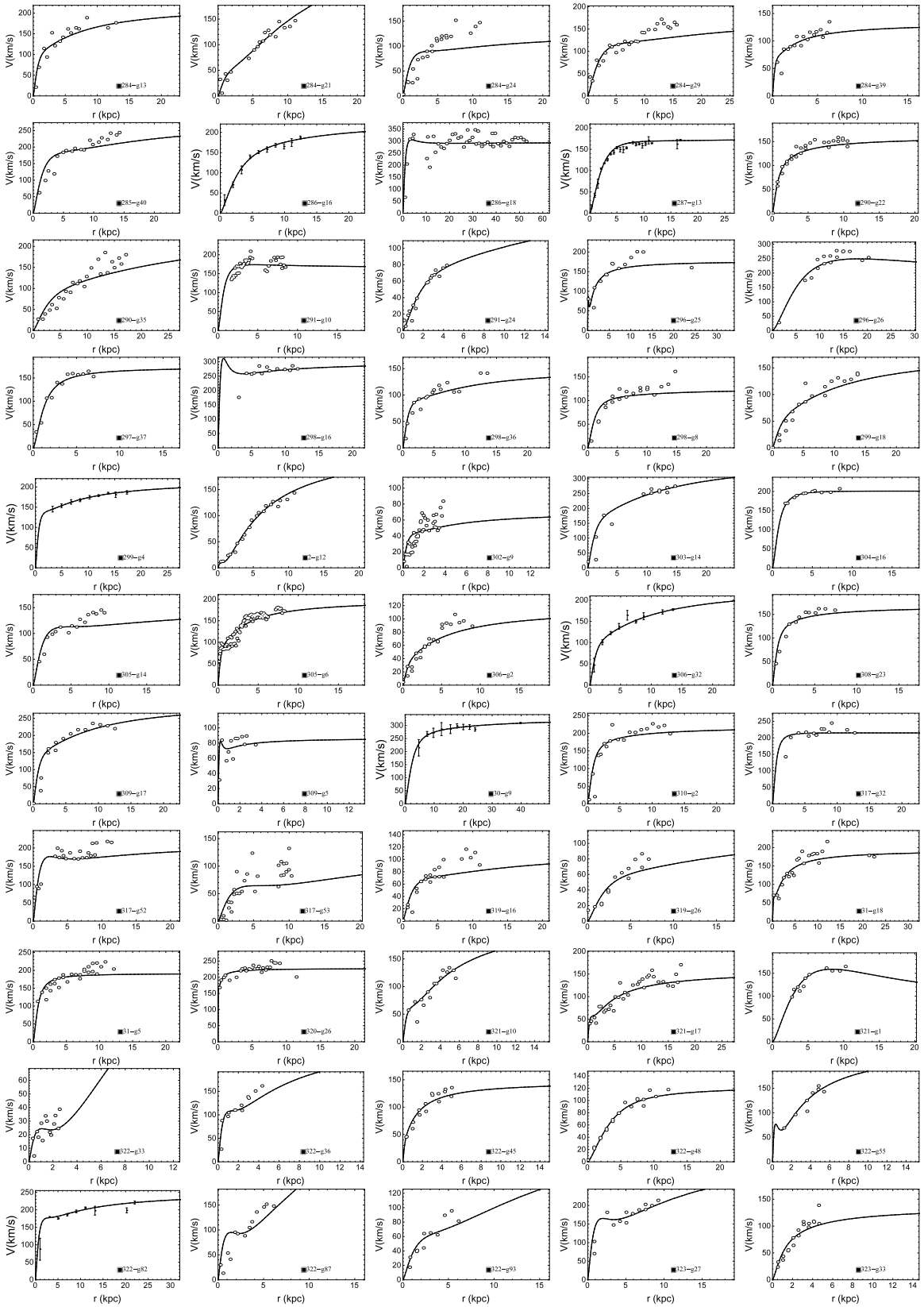
V(km/s)
r (kpc)
284−g13
284−g21
284−g24
284−g29
284−g39
285−g40
286−g16
286−g18
287−g13
290−g22
290−g35
291−g10
291−g24
296−g25
296−g26
297−g37
298−g16
298−g36
298−g8
299−g18
299−g4
2−g12
302−g9
303−g14
304−g16
305−g14
305−g6
306−g2
306−g32
308−g23
309−g17
309−g5
30−g9
310−g2
317−g32
317−g52
317−g53
319−g16
319−g26
31−g18
31−g5
320−g26
321−g10
321−g17
321−g1
322−g33
322−g36
322−g45
322−g48
322−g55
322−g82
322−g87
322−g93
323−g27
323−g33

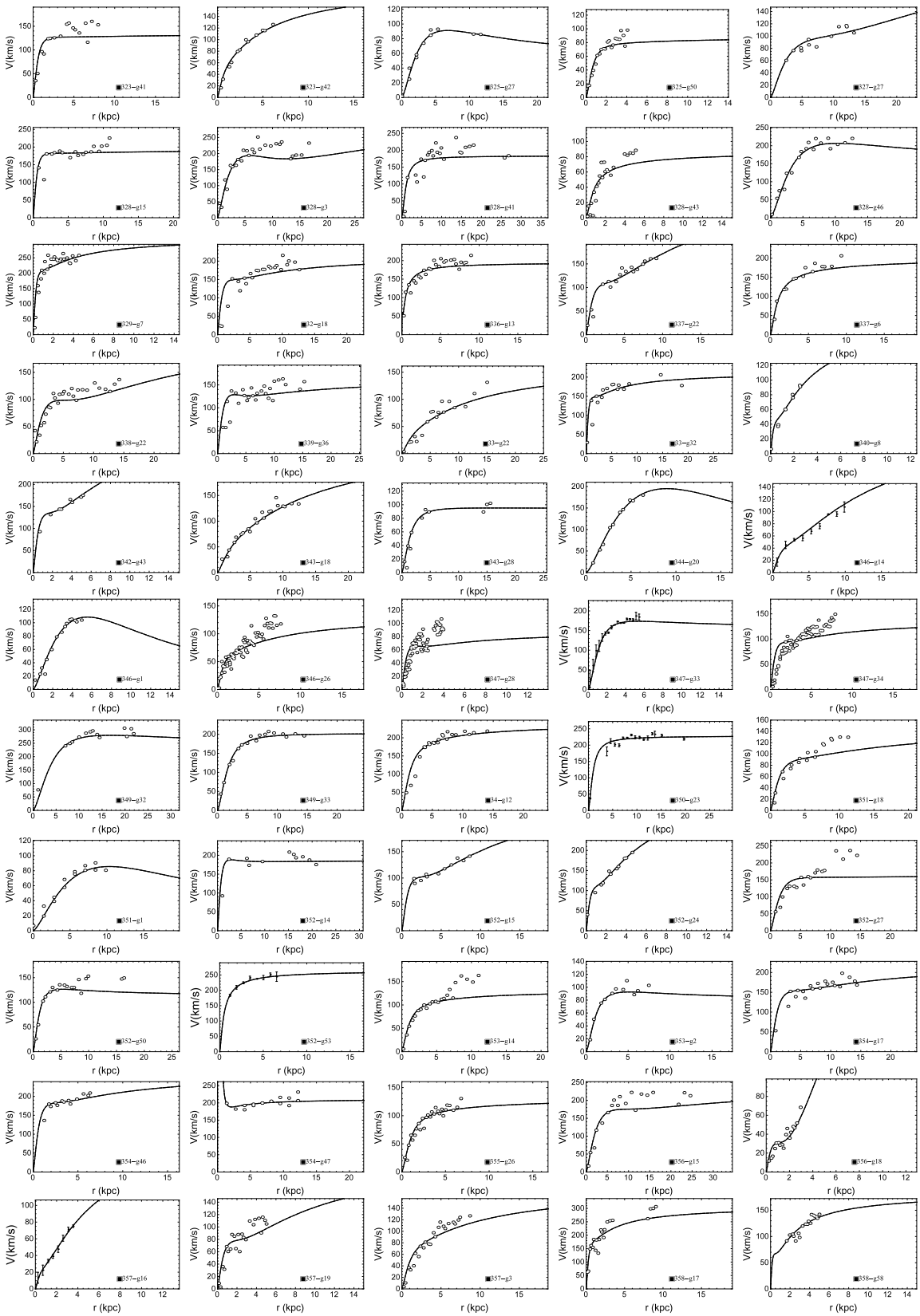
V(km/s)
r (kpc)
323−g41
323−g42
325−g27
325−g50
327−g27
328−g15
328−g3
328−g41
328−g43
328−g46
329−g7
32−g18
336−g13
337−g22
337−g6
338−g22
339−g36
33−g22
33−g32
340−g8
342−g43
343−g18
343−g28
344−g20
346−g14
346−g1
346−g26
347−g28
347−g33
347−g34
349−g32
349−g33
34−g12
350−g23
351−g18
351−g1
352−g14
352−g15
352−g24
352−g27
352−g50
352−g53
353−g14
353−g2
354−g17
354−g46
354−g47
355−g26
356−g15
356−g18
357−g16
357−g19
357−g3
358−g17
358−g58

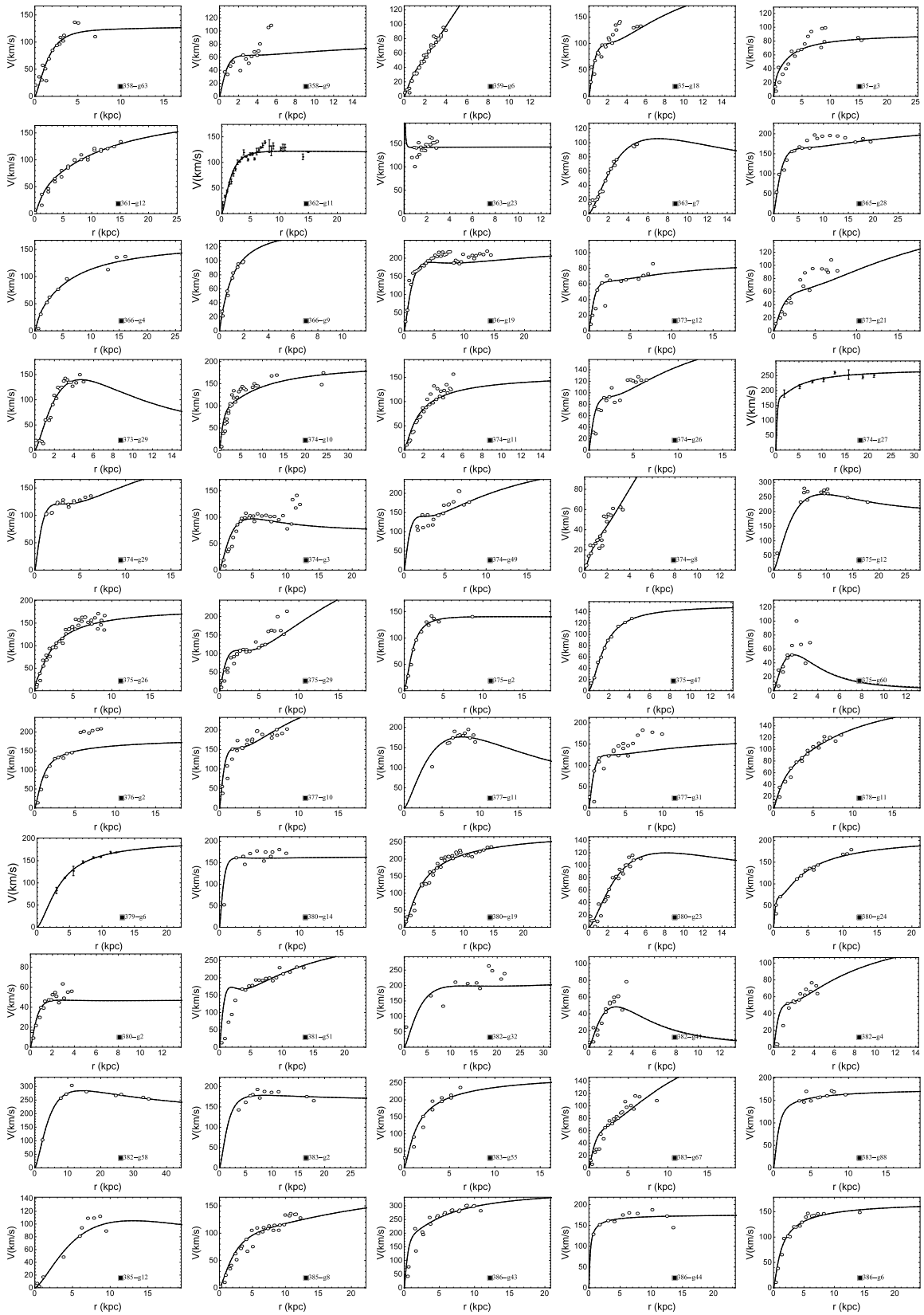
V(km/s)
r (kpc)
358–g63
358–g9
359–g6
35–g18
35–g3
361–g12
362–g11
363–g23
363–g7
365–g28
366–g4
366–g9
36–g19
373–g12
373–g21
373–g29
374–g10
374–g11
374–g26
374–g27
374–g29
374–g3
374–g49
374–g8
375–g12
375–g26
375–g29
375–g2
375–g47
375–g60
376–g2
377–g10
377–g11
377–g31
378–g11
379–g6
380–g14
380–g19
380–g23
380–g24
380–g2
381–g51
382–g32
382–g44
382–g4
382–g58
383–g2
383–g55
383–g67
383–g88
385–g12
385–g8
386–g43
386–g44
386–g6

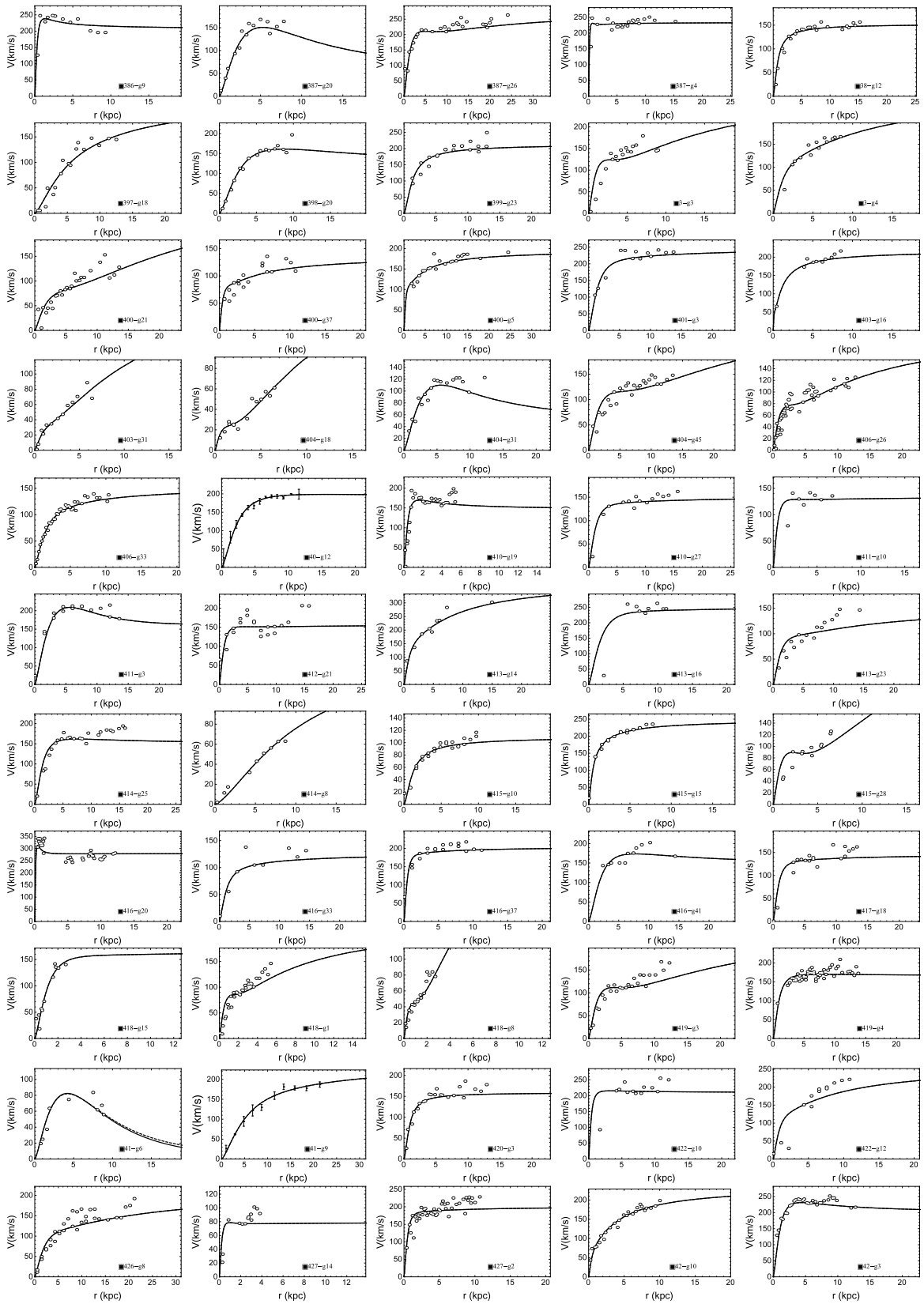
V(km/s)
r (kpc)
386−g9
387−g20
387−g26
387−g4
38−g12
397−g18
398−g20
399−g23
3−g3
3−g4
400−g21
400−g37
400−g5
401−g3
403−g16
403−g31
404−g18
404−g31
404−g45
406−g26
406−g33
40−g12
410−g19
410−g27
411−g10
411−g3
412−g21
413−g14
413−g16
413−g23
414−g25
414−g8
415−g10
415−g15
415−g28
416−g20
416−g33
416−g37
416−g41
417−g18
418−g15
418−g1
418−g8
419−g3
419−g4
41−g6
41−g9
420−g3
422−g10
422−g12
426−g8
427−g14
427−g2
42−g10
42−g3

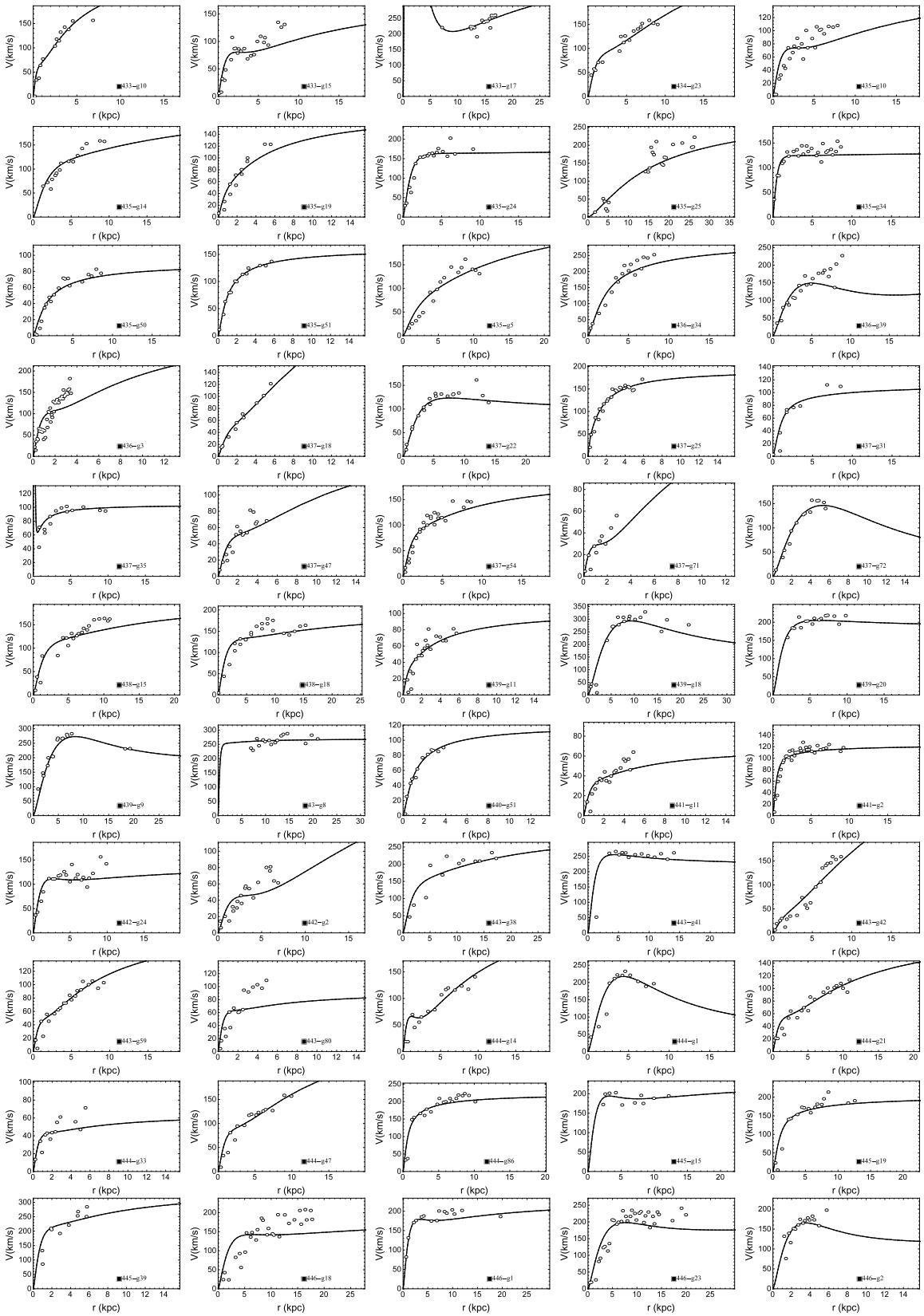
V(km/s)
r (kpc)
433−g10
433−g15
433−g17
434−g23
435−g10
435−g14
435−g19
435−g24
435−g25
435−g34
435−g50
435−g51
435−g5
436−g34
436−g39
436−g3
437−g18
437−g22
437−g25
437−g31
437−g35
437−g47
437−g54
437−g71
437−g72
438−g15
438−g18
439−g11
439−g18
439−g20
439−g9
443−g8
440−g51
441−g11
441−g2
442−g24
442−g2
443−g38
443−g41
443−g42
443−g59
443−g80
444−g14
444−g1
444−g21
444−g33
444−g47
444−g86
445−g15
445−g19
445−g39
446−g18
446−g1
446−g23
446−g2

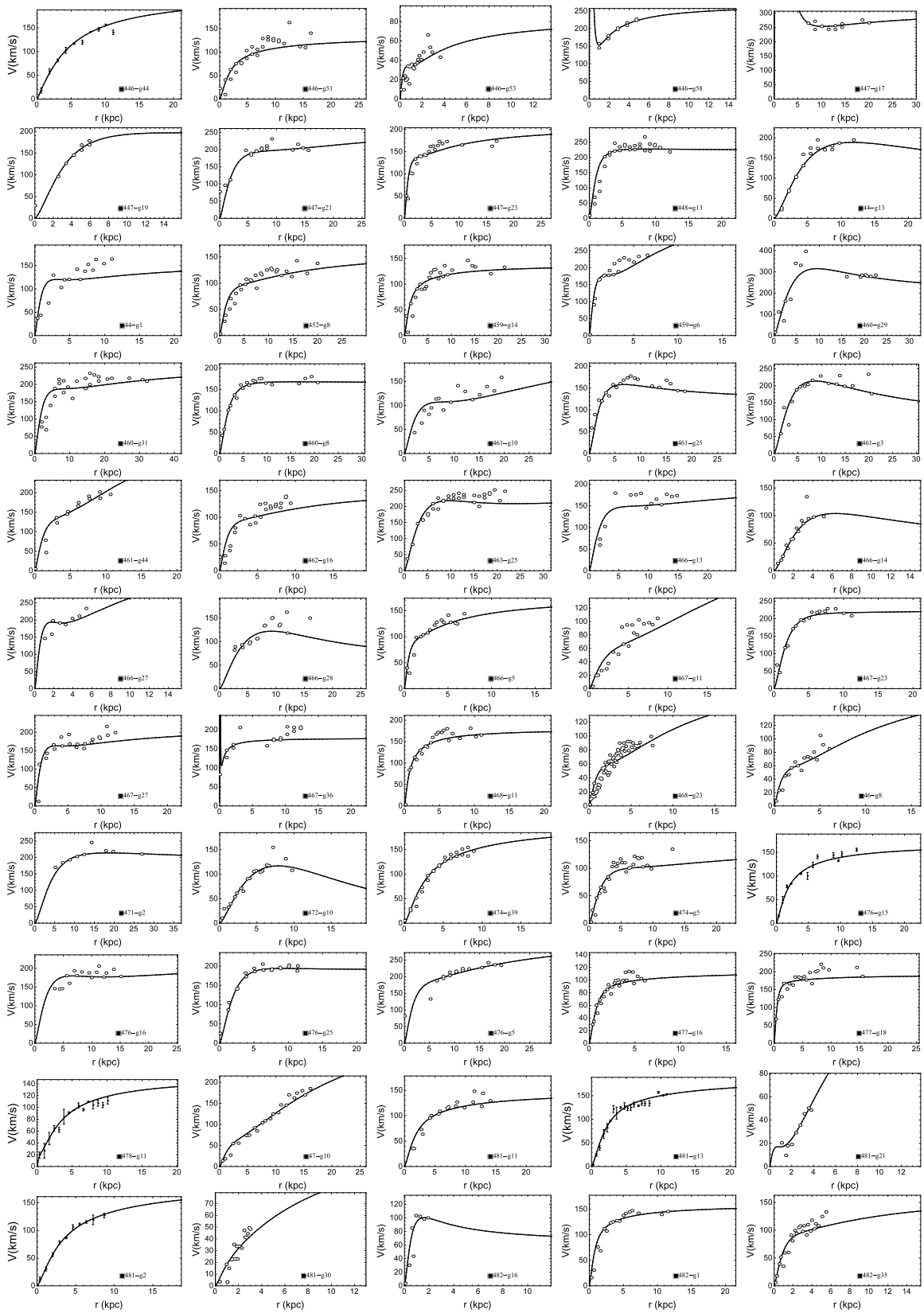
V(km/s)
r (kpc)
446−g44
446−g51
446−g53
446−g58
447−g17
447−g19
447−g21
447−g23
448−g13
44−g13
44−g1
452−g8
459−g14
459−g6
460−g29
460−g31
460−g8
461−g10
461−g25
461−g3
461−g44
462−g16
463−g25
466−g13
466−g14
466−g27
466−g28
466−g5
467−g11
467−g23
467−g27
467−g36
468−g11
468−g23
46−g8
471−g2
472−g10
474−g39
474−g5
476−g15
476−g16
476−g25
476−g5
477−g16
477−g18
478−g11
47−g10
481−g11
481−g13
481−g21
481−g2
481−g30
482−g16
482−g1
482−g35

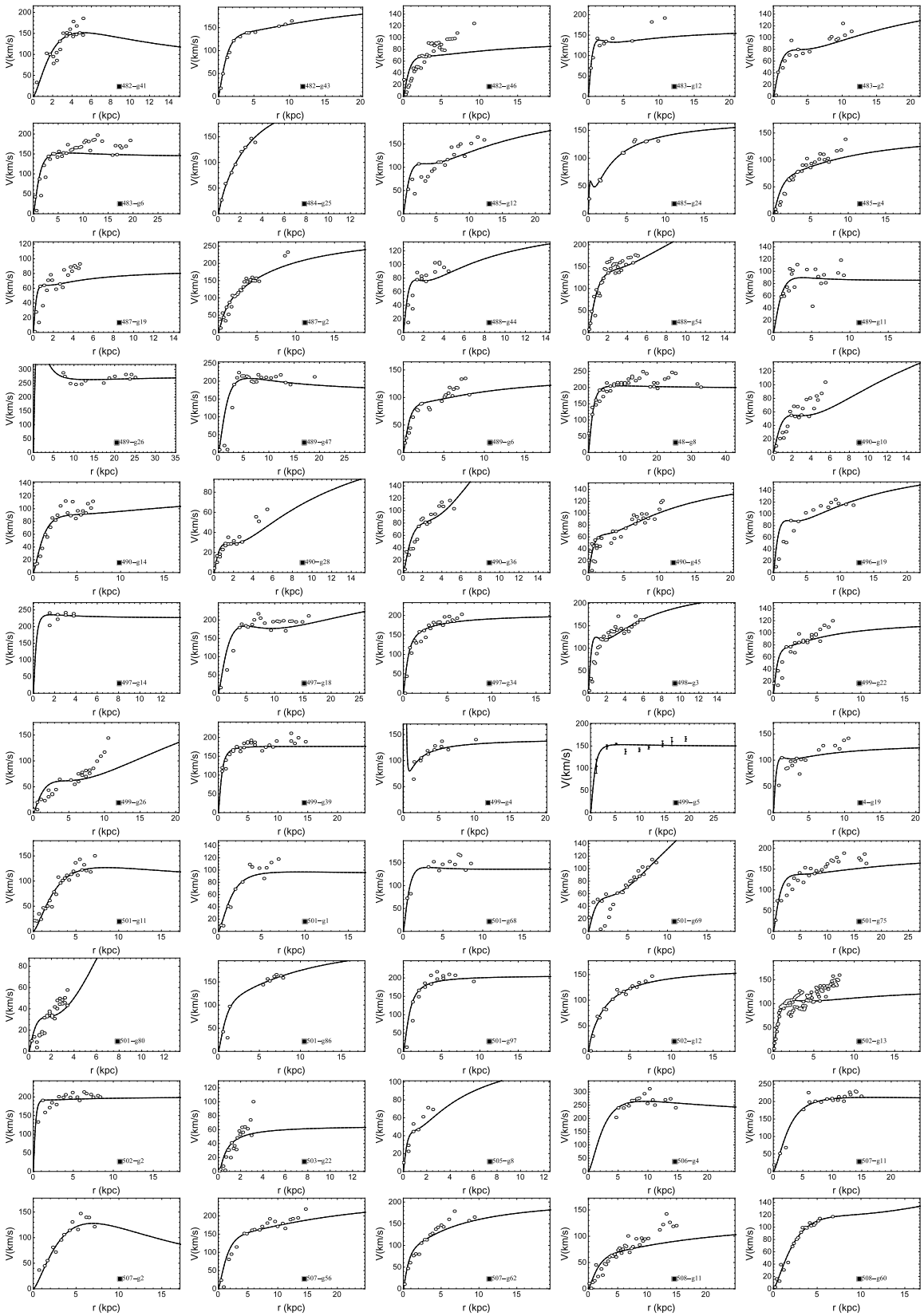
V(km/s)
r (kpc)
482−g41
482−g43
482−g46
483−g12
483−g2
483−g6
484−g25
485−g12
485−g24
485−g4
487−g19
487−g2
488−g44
488−g54
489−g11
489−g26
489−g47
489−g6
48−g8
490−g10
490−g14
490−g28
490−g36
490−g45
496−g19
497−g14
497−g18
497−g34
498−g3
499−g22
499−g26
499−g39
499−g4
499−g5
4−g19
501−g11
501−g1
501−g68
501−g69
501−g75
501−g80
501−g86
501−g97
502−g12
502−g13
502−g2
503−g22
505−g8
506−g4
507−g11
507−g2
507−g56
507−g62
508−g11
508−g60

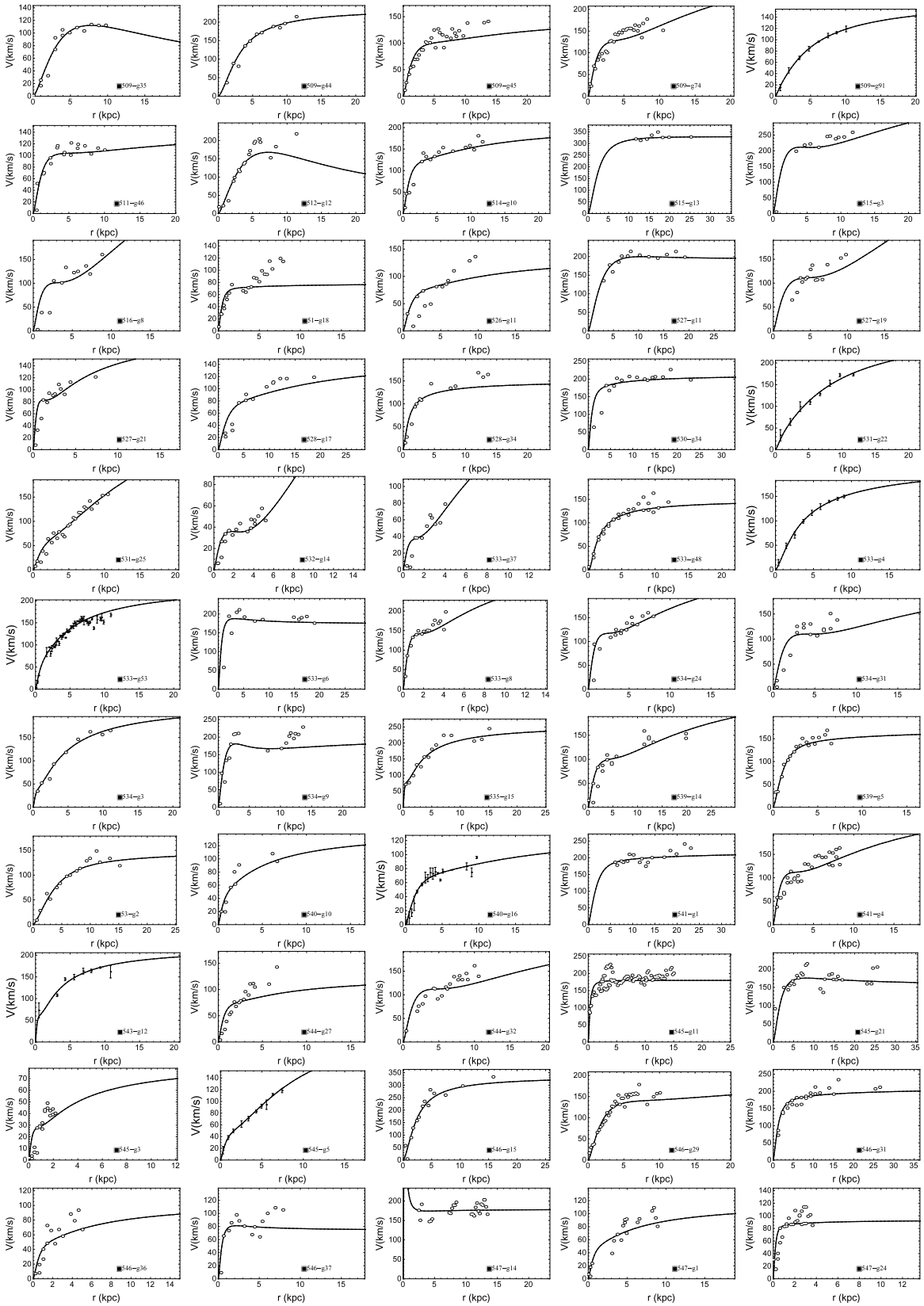
V(km/s)
r (kpc)
509−g35
509−g44
509−g45
509−g74
509−g91
511−g46
512−g12
514−g10
515−g13
515−g3
516−g8
51−g18
526−g11
527−g11
527−g19
527−g21
528−g17
528−g34
530−g34
531−g22
531−g25
532−g14
533−g37
533−g48
533−g4
533−g53
533−g6
533−g8
534−g24
534−g31
534−g3
534−g9
535−g15
539−g14
539−g5
53−g2
540−g10
540−g16
541−g1
541−g4
543−g12
544−g27
544−g32
545−g11
545−g21
545−g3
545−g5
546−g15
546−g29
546−g31
546−g36
546−g37
547−g14
547−g1
547−g24

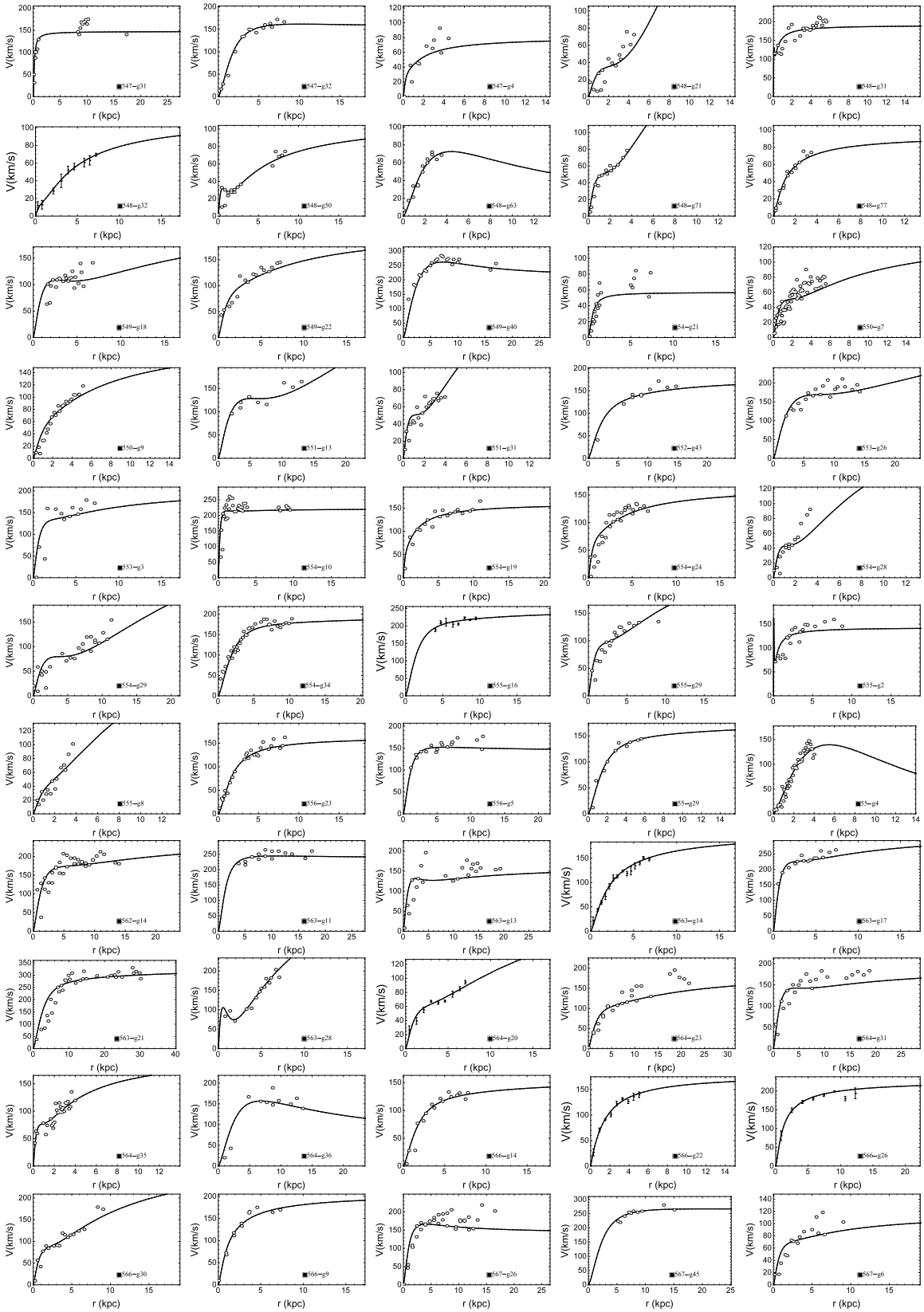
V(km/s)
r (kpc)
547−g31
547−g32
547−g4
548−g21
548−g31
548−g32
548−g50
548−g63
548−g71
548−g77
549−g18
549−g22
549−g40
54−g21
550−g7
550−g9
551−g13
551−g31
552−g43
553−g26
553−g3
554−g10
554−g19
554−g24
554−g28
554−g29
554−g34
555−g16
555−g29
555−g2
555−g8
556−g23
556−g5
55−g29
55−g4
562−g14
563−g11
563−g13
563−g14
563−g17
563−g21
563−g28
564−g20
564−g23
564−g31
564−g35
564−g36
566−g14
566−g22
566−g26
566−g30
566−g9
567−g26
567−g45
567−g6

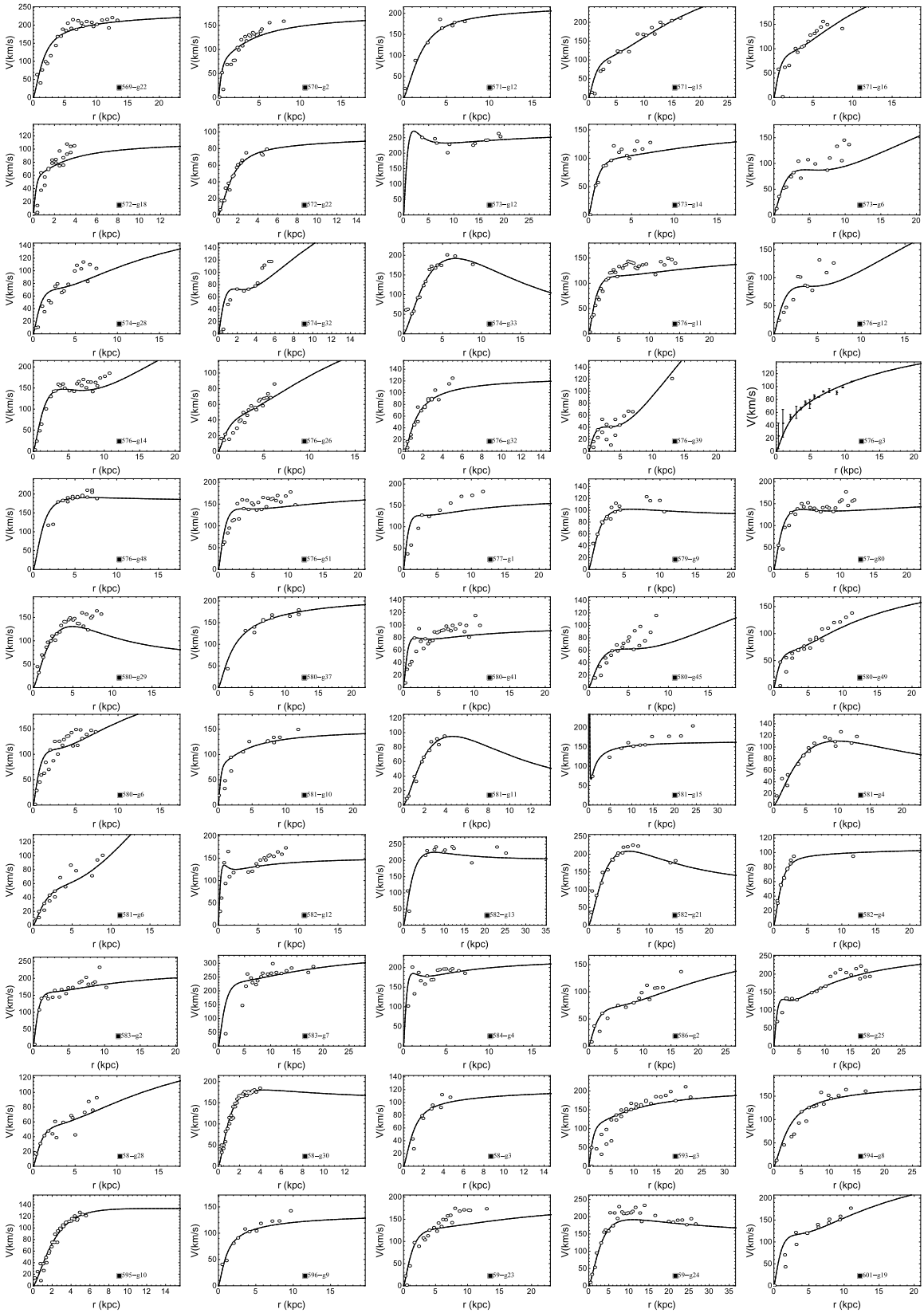
V(km/s)
r (kpc)
569−g22
570−g2
571−g12
571−g15
571−g16
572−g18
572−g22
573−g12
573−g14
573−g6
574−g28
574−g32
574−g33
576−g11
576−g12
576−g14
576−g26
576−g32
576−g39
576−g3
576−g48
576−g51
577−g1
579−g9
57−g80
580−g29
580−g37
580−g41
580−g45
580−g49
580−g6
581−g10
581−g11
581−g15
581−g4
581−g6
582−g12
582−g13
582−g21
582−g4
583−g2
583−g7
584−g4
586−g2
58−g25
58−g28
58−g30
58−g3
593−g3
594−g8
595−g10
596−g9
59−g23
59−g24
601−g19

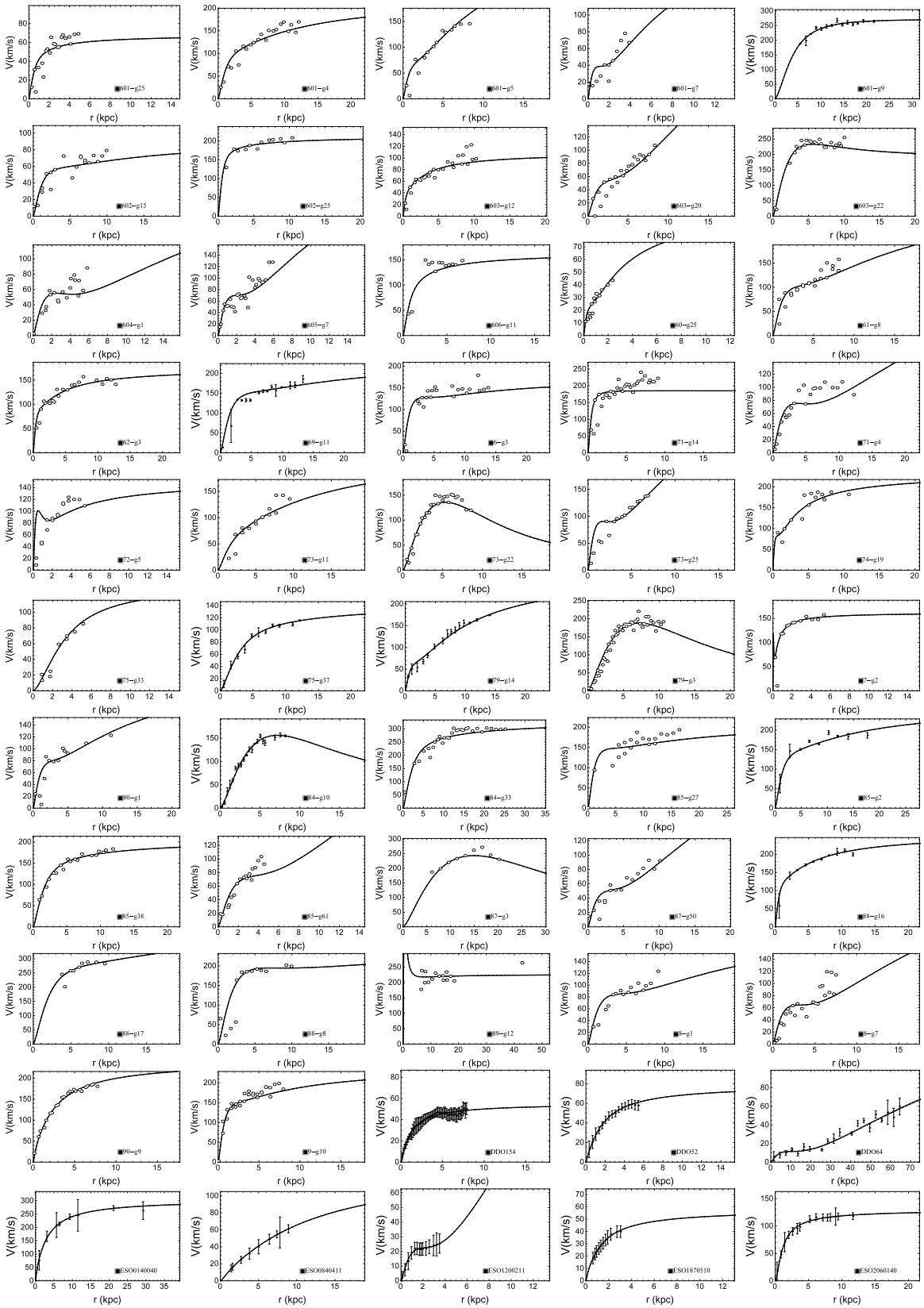
V(km/s)
r (kpc)
601−g25
601−g4
601−g5
601−g7
601−g9
602−g15
602−g25
603−g12
603−g20
603−g22
604−g1
605−g7
606−g11
60−g25
61−g8
62−g3
69−g11
6−g3
71−g14
71−g4
72−g5
73−g11
73−g22
73−g25
74−g19
75−g33
75−g37
79−g14
79−g3
7−g2
80−g1
84−g10
84−g33
85−g27
85−g2
85−g38
85−g61
87−g3
87−g50
88−g16
88−g17
88−g8
89−g12
8−g1
8−g7
90−g9
9−g10
DDO154
DDO52
DDO64
ESO0140040
ESO0840411
ESO1200211
ESO1870510
ESO2060140

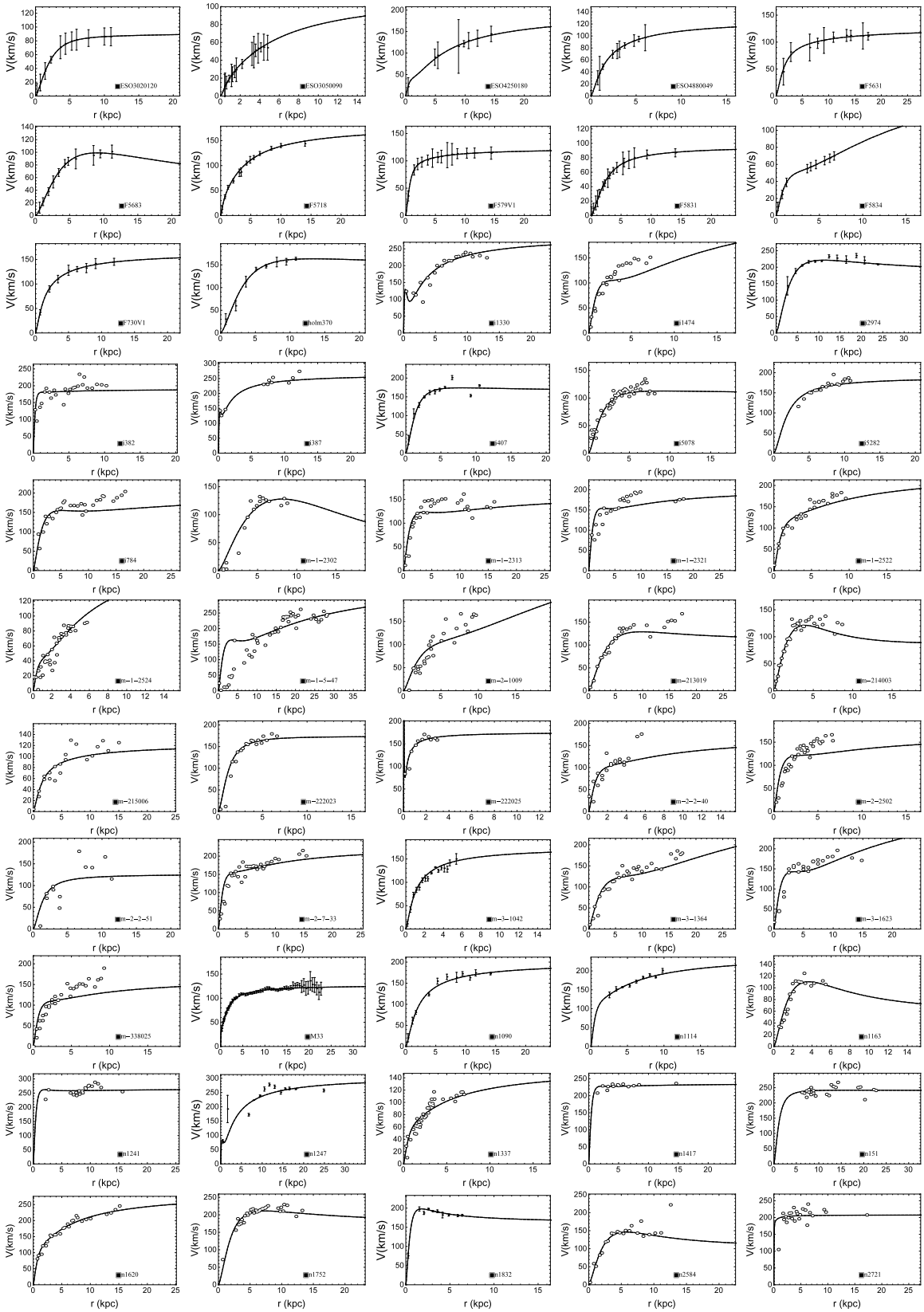
V(km/s)
r (kpc)
ESO3020120
ESO3050090
ESO4250180
ESO4880049
F5631
F5683
F5718
F579V1
F5831
F5834
F730V1
holm370
i1330
i1474
i2974
i382
i387
i407
i5078
i5282
i784
m−1−2302
m−1−2313
m−1−2321
m−1−2522
m−1−2524
m−1−5−47
m−2−1009
m−213019
m−214003
m−215006
m−222023
m−222025
m−2−2−40
m−2−2502
m−2−2−51
m−2−7−33
m−3−1042
m−3−1364
m−3−1623
m−338025
M33
n1090
n1114
n1163
n1241
n1247
n1337
n1417
n151
n1620
n1752
n1832
n2584
n2721

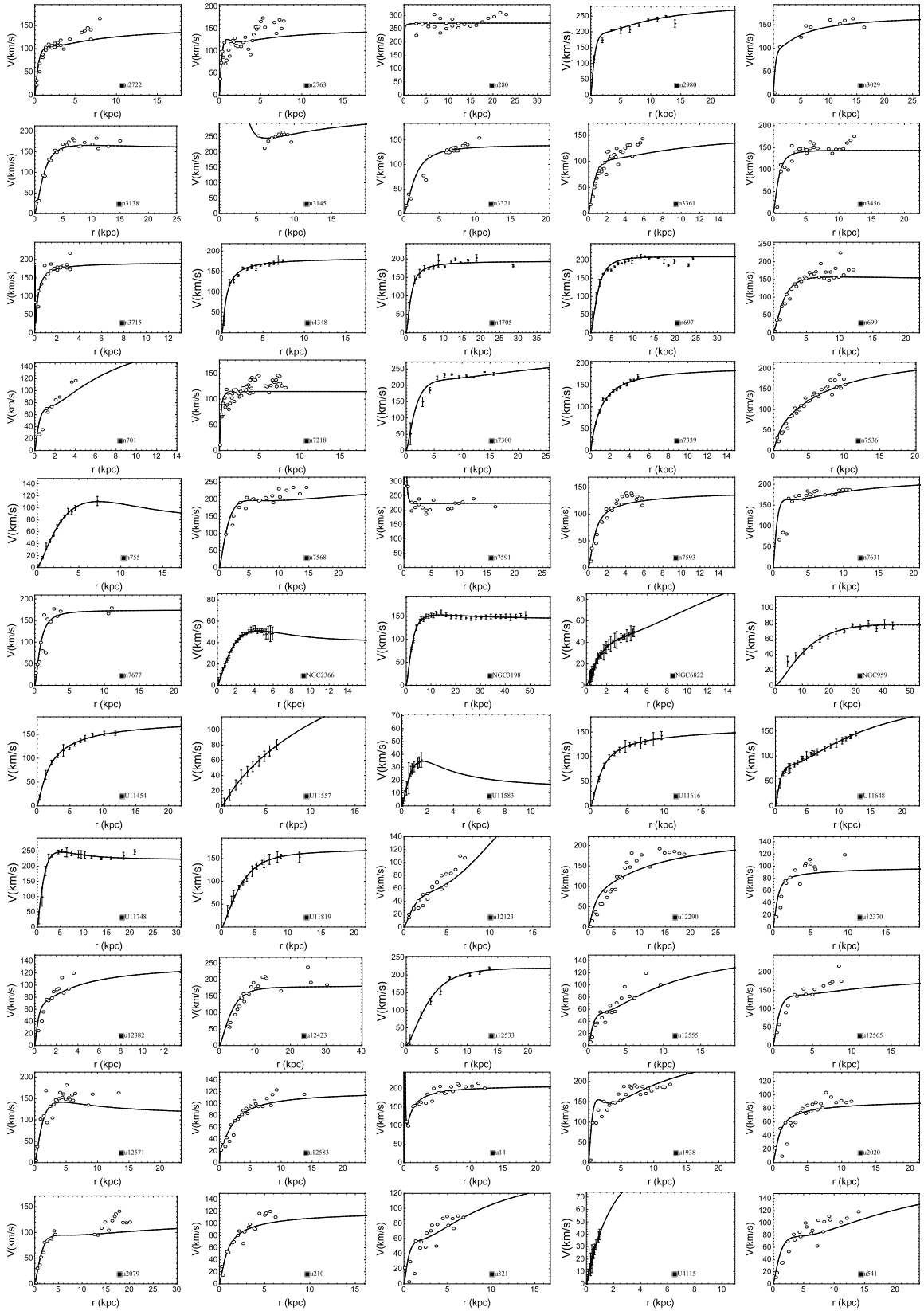
V(km/s)
r (kpc)
n2722
n2763
n280
n2980
n3029
n3138
n3145
n3321
n3361
n3456
n3715
n4348
n4705
n697
n699
n701
n7218
n7300
n7339
n7536
n755
n7568
n7591
n7593
n7631
n7677
NGC2366
NGC3198
NGC6822
NGC959
U11454
U11557
U11583
U11616
U11648
U11748
U11819
u12123
u12290
u12370
u12382
u12423
u12533
u12555
u12565
u12571
u12583
u14
u1938
u2020
u2079
u210
u321
U4115
u541

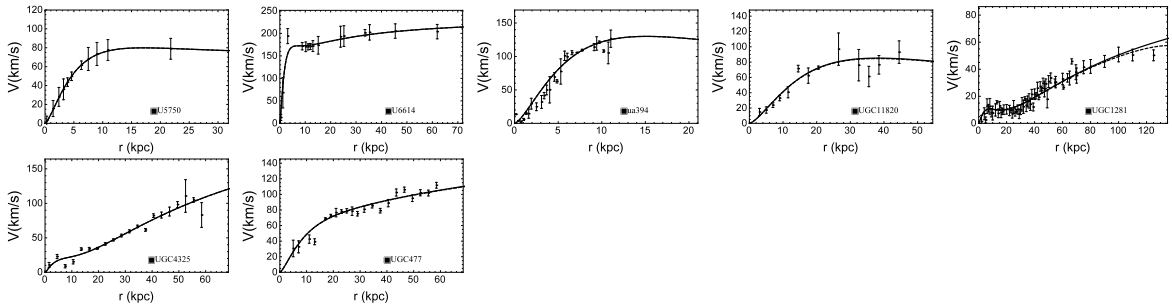

Figure 4.6: Galaxy RCs best fittings using Eq.(4.1).

Galaxy	$\chi^2_{\rm red}$	n	$\langle V_0 \rangle$ (km s^{-1})	$\langle r_c \rangle$ (kpc)	d	$r_{\rm edge}$ (kpc)	M_T (10^{11} M$_\odot$)	Reference
101-g20	0.78	4	173.229 ± 0.001	0.099 ± 0.001	2.685 ± 0.001	176.214 ± 0.005	6.122 ± 0.001	[126]
101-g5	0.45	3	247.172 ± 0.001	5.307 ± 0.001	1.526 ± 0.001	323.124 ± 0.001	20.263 ± 0.001	[126]
102-g10	0.42	2	180.380 ± 0.001	1.627 ± 0.001	1.658 ± 0.001	200.496 ± 0.001	7.387 ± 0.001	[126]
102-g15	0.59	3	203.644 ± 0.001	1.646 ± 0.001	1.905 ± 0.001	209.610 ± 0.007	9.626 ± 0.001	[126]
103-g13	0.20	3	234.151 ± 0.001	0.434 ± 0.002	0.699 ± 0.001	236.231 ± 0.007	14.750 ± 0.001	[126]
103-g15	0.23	3	180.460 ± 0.001	1.613 ± 0.001	1.184 ± 0.001	185.977 ± 0.008	6.504 ± 0.001	[126]
103-g39	0.20	4	213.197 ± 0.002	1.801 ± 0.001	1.326 ± 0.001	205.727 ± 0.009	9.742 ± 0.001	[126]
104-g52	0.23	3	188.682 ± 0.001	2.419 ± 0.001	1.232 ± 0.001	193.461 ± 0.007	7.165 ± 0.001	[126]
105-g20	0.15	1	94.923 ± 0.001	6.060 ± 0.001	2.949 ± 0.001	127.374 ± 0.001	1.651 ± 0.001	[126]
105-g3	0.48	2	167.134 ± 0.001	1.758 ± 0.001	1.566 ± 0.001	181.660 ± 0.001	5.698 ± 0.001	[126]
106-g12	0.16	2	130.908 ± 0.001	1.848 ± 0.001	1.947 ± 0.001	147.968 ± 0.009	2.876 ± 0.001	[126]
106-g8	0.21	2	205.154 ± 0.001	0.964 ± 0.001	1.069 ± 0.001	206.359 ± 0.004	9.832 ± 0.001	[126]
107-g24	0.36	3	228.437 ± 0.001	2.572 ± 0.002	1.346 ± 0.001	221.750 ± 0.006	12.200 ± 0.001	[126]
107-g36	0.75	3	199.274 ± 0.001	0.138 ± 0.001	1.832 ± 0.001	219.329 ± 0.006	10.082 ± 0.001	[126]
108-g11	0.06	2	51.749 ± 0.001	7.903 ± 0.001	5.169 ± 0.001	117.498 ± 0.003	0.907 ± 0.001	[126]
108-g13	0.54	4	299.124 ± 0.001	3.460 ± 0.001	1.373 ± 0.001	295.033 ± 0.003	26.578 ± 0.001	[126]
108-g19	1.14	2	168.911 ± 0.001	0.538 ± 0.001	2.062 ± 0.002	181.362 ± 0.005	5.985 ± 0.001	[126]
108-g6	0.35	3	221.584 ± 0.001	1.551 ± 0.001	1.375 ± 0.001	236.203 ± 0.009	12.759 ± 0.001	[126]
109-g32	0.46	4	223.706 ± 0.001	3.309 ± 0.001	1.247 ± 0.001	229.189 ± 0.002	11.096 ± 0.001	[126]
10-g4	0.70	5	320.243 ± 0.001	4.202 ± 0.001	1.282 ± 0.001	323.717 ± 0.007	31.130 ± 0.001	[126]
111-g9	0.38	4	418.006 ± 0.001	6.243 ± 0.001	1.349 ± 0.001	391.649 ± 0.003	65.420 ± 0.001	[126]
113-g21	0.19	3	144.366 ± 0.001	2.491 ± 0.001	1.266 ± 0.001	135.957 ± 0.001	2.812 ± 0.001	[126]
114-g21	0.88	2	167.903 ± 0.001	1.208 ± 0.001	1.840 ± 0.001	185.512 ± 0.002	5.981 ± 0.001	[126]
116-g12	1.14	4	210.446 ± 0.004	0.834 ± 0.003	1.181 ± 0.009	208.928 ± 0.004	10.204 ± 0.001	[126]
116-g14	0.13	2	169.168 ± 0.001	3.308 ± 0.001	1.471 ± 0.001	186.587 ± 0.003	5.796 ± 0.001	[126]
117-g18	0.15	3	295.172 ± 0.001	1.584 ± 0.001	1.265 ± 0.001	311.818 ± 0.006	30.192 ± 0.001	[126]
117-g19	0.18	1	161.121 ± 0.001	3.178 ± 0.001	1.949 ± 0.001	182.544 ± 0.001	5.662 ± 0.001	[126]
120-g16	0.21	3	216.423 ± 0.001	1.805 ± 0.001	1.263 ± 0.002	219.023 ± 0.002	11.090 ± 0.001	[126]
121-g26	1.55	6	273.042 ± 0.005	0.447 ± 0.001	2.720 ± 0.002	274.926 ± 0.003	23.250 ± 0.001	[126]
121-g6	18.29	4	179.883 ± 0.003	1.250 ± 0.001	1.560 ± 0.001	250.337 ± 0.001	8.885 ± 0.001	[126]
123-g15	0.48	2	213.852 ± 0.001	0.408 ± 0.001	1.111 ± 0.001	228.202 ± 0.005	12.012 ± 0.001	[126]
123-g16	0.05	1	7.899 ± 0.003	3.641 ± 0.001	47.839 ± 0.003	62.808 ± 0.001	0.139 ± 0.001	[126]
123-g23	0.67	3	238.793 ± 0.001	1.837 ± 0.005	1.070 ± 0.003	242.127 ± 0.008	14.921 ± 0.001	[126]
123-g9	0.31	3	214.469 ± 0.001	3.331 ± 0.001	1.513 ± 0.001	214.007 ± 0.001	10.159 ± 0.001	[126]
124-g15	0.39	3	183.513 ± 0.002	1.932 ± 0.001	1.245 ± 0.001	191.146 ± 0.004	6.842 ± 0.001	[126]
13-g16	0.45	4	190.853 ± 0.008	3.760 ± 0.001	1.380 ± 0.001	188.330 ± 0.002	6.269 ± 0.001	[126]
13-g18	0.17	4	413.104 ± 0.001	8.281 ± 0.001	1.063 ± 0.001	361.439 ± 0.009	52.831 ± 0.005	[126]
140-g24	0.10	2	117.951 ± 0.002	5.394 ± 0.001	3.096 ± 0.002	134.934 ± 0.001	2.528 ± 0.001	[126]
140-g25	0.18	1	99.444 ± 0.001	2.003 ± 0.001	1.144 ± 0.001	118.706 ± 0.002	1.331 ± 0.001	[126]
140-g28	0.85	3	114.488 ± 0.004	1.704 ± 0.001	1.764 ± 0.001	155.796 ± 0.009	2.206 ± 0.001	[126]
140-g34	0.18	2	22.536 ± 0.001	3.753 ± 0.002	5.541 ± 0.001	54.303 ± 0.001	0.091 ± 0.001	[126]
141-g20	9.78	1	232.305 ± 0.003	1.826 ± 0.001	1.811 ± 0.005	237.842 ± 0.007	15.054 ± 0.003	[126]
141-g23	0.24	4	351.744 ± 0.001	2.704 ± 0.001	1.160 ± 0.001	340.200 ± 0.004	44.054 ± 0.002	[126]
141-g34	4.74	8	337.264 ± 0.002	0.684 ± 0.001	3.627 ± 0.001	337.099 ± 0.001	42.860 ± 0.002	[126]
141-g37	0.24	2	350.340 ± 0.001	2.125 ± 0.001	1.309 ± 0.001	376.171 ± 0.001	52.267 ± 0.001	[126]
141-g9	0.95	1	219.404 ± 0.002	0.647 ± 0.001	1.827 ± 0.001	224.049 ± 0.007	12.584 ± 0.001	[126]
142-g30	0.19	2	206.152 ± 0.005	2.265 ± 0.001	1.421 ± 0.001	209.544 ± 0.002	9.896 ± 0.001	[126]
142-g35	0.27	1	218.261 ± 0.001	0.462 ± 0.001	1.718 ± 0.001	245.766 ± 0.009	13.632 ± 0.001	[126]
143-g8	0.32	4	131.619 ± 0.001	1.029 ± 0.001	1.356 ± 0.001	146.039 ± 0.006	2.694 ± 0.001	[126]
145-g18	0.45	2	191.596 ± 0.001	0.683 ± 0.001	1.439 ± 0.001	224.975 ± 0.003	9.479 ± 0.001	[126]

Galaxy	$\chi^2_{\rm red}$	n	$\langle V_0 \rangle$ (km s^{-1})	$\langle r_c \rangle$ (kpc)	d	$r_{\rm edge}$ (kpc)	M_T (10^{11} M$_\odot$)	Reference
145-g22	0.20	1	213.723 ± 0.001	1.122 ± 0.001	0.956 ± 0.001	216.615 ± 0.004	11.372 ± 0.001	[126]
146-g6	0.49	3	140.273 ± 0.001	3.473 ± 0.001	1.425 ± 0.001	184.024 ± 0.001	3.622 ± 0.001	[126]
151-g30	0.69	3	206.118 ± 0.001	2.812 ± 0.001	1.747 ± 0.001	284.551 ± 0.002	13.141 ± 0.001	[126]
1547-02	1.85	1	206.744 ± 0.003	3.075 ± 0.004	1.028 ± 0.003	290.927 ± 0.001	14.166 ± 0.002	[126]
155-g6	0.31	5	422.955 ± 0.001	6.826 ± 0.001	1.350 ± 0.003	428.039 ± 0.004	68.748 ± 0.002	[126]
157-g20	0.92	1	111.562 ± 0.001	0.223 ± 0.001	1.938 ± 0.001	131.242 ± 0.008	1.904 ± 0.001	[126]
157-g38	0.10	3	141.833 ± 0.002	0.327 ± 0.001	0.986 ± 0.001	142.920 ± 0.009	3.266 ± 0.001	[126]
160-g2	0.19	4	402.901 ± 0.001	1.331 ± 0.001	1.202 ± 0.001	401.843 ± 0.005	72.603 ± 0.001	[126]
162-g15	0.32	4	160.632 ± 0.001	1.697 ± 0.001	1.478 ± 0.001	169.781 ± 0.005	4.523 ± 0.001	[126]
162-g17	0.52	4	126.004 ± 0.008	2.044 ± 0.001	1.466 ± 0.001	135.809 ± 0.001	2.099 ± 0.001	[126]
163-g11	0.07	1	166.278 ± 0.001	3.203 ± 0.001	2.543 ± 0.001	182.664 ± 0.007	6.273 ± 0.001	[126]
163-g14	0.44	4	154.726 ± 0.001	5.454 ± 0.001	1.826 ± 0.001	150.100 ± 0.001	2.938 ± 0.001	[126]
181-g2	0.46	1	128.820 ± 0.001	8.035 ± 0.001	6.346 ± 0.002	239.626 ± 0.006	7.698 ± 0.002	[126]
183-g14	0.20	3	138.737 ± 0.001	0.446 ± 0.001	0.143 ± 0.001	138.395 ± 0.009	2.966 ± 0.001	[126]
183-g5	0.65	4	159.537 ± 0.001	4.046 ± 0.001	1.483 ± 0.001	196.700 ± 0.005	4.584 ± 0.001	[126]
184-g51	2.47	2	238.865 ± 0.003	5.174 ± 0.005	1.963 ± 0.003	256.925 ± 0.001	16.450 ± 0.004	[126]
184-g54	0.33	2	185.869 ± 0.001	1.577 ± 0.001	1.490 ± 0.001	192.632 ± 0.006	7.492 ± 0.001	[126]
184-g60	0.93	3	108.082 ± 0.001	3.728 ± 0.001	1.585 ± 0.001	141.624 ± 0.001	1.594 ± 0.001	[126]
184-g63	0.38	2	137.181 ± 0.001	2.050 ± 0.001	1.665 ± 0.001	156.044 ± 0.006	3.276 ± 0.001	[126]
184-g67	0.26	3	305.913 ± 0.001	1.375 ± 0.001	1.602 ± 0.001	306.614 ± 0.004	32.252 ± 0.001	[126]
185-g11	0.09	1	224.481 ± 0.001	1.430 ± 0.001	0.169 ± 0.001	242.627 ± 0.001	13.774 ± 0.001	[126]
185-g26	0.33	3	291.243 ± 0.001	1.858 ± 0.001	1.036 ± 0.001	287.647 ± 0.007	26.629 ± 0.001	[126]
185-g36	0.45	3	172.531 ± 0.001	4.147 ± 0.001	1.606 ± 0.001	225.519 ± 0.001	6.836 ± 0.001	[126]
185-g68	0.81	1	85.619 ± 0.001	1.558 ± 0.001	1.498 ± 0.001	87.171 ± 0.001	0.741 ± 0.001	[126]
185-g70	0.25	3	211.168 ± 0.001	2.201 ± 0.001	1.178 ± 0.001	204.952 ± 0.005	9.633 ± 0.001	[126]
186-g21	0.78	1	175.229 ± 0.001	1.065 ± 0.001	1.860 ± 0.001	179.337 ± 0.001	6.453 ± 0.001	[126]
186-g75	0.44	3	97.765 ± 0.001	2.345 ± 0.001	1.609 ± 0.001	127.488 ± 0.001	1.241 ± 0.001	[126]
186-g8	0.21	3	164.549 ± 0.001	1.539 ± 0.001	1.240 ± 0.001	160.734 ± 0.001	4.646 ± 0.001	[126]
187-g8	0.45	4	224.704 ± 0.001	3.831 ± 0.001	1.358 ± 0.001	225.860 ± 0.002	10.777 ± 0.001	[126]
18-g13	0.13	3	350.395 ± 0.001	12.793 ± 0.001	1.627 ± 0.001	311.605 ± 0.001	33.853 ± 0.004	[126]
18-g15	0.91	3	174.083 ± 0.001	2.479 ± 0.001	1.567 ± 0.001	176.333 ± 0.009	5.594 ± 0.001	[126]
196-g11	0.34	3	165.548 ± 0.002	2.736 ± 0.001	1.365 ± 0.001	173.589 ± 0.001	4.855 ± 0.001	[126]
197-g24	0.34	4	346.072 ± 0.001	5.623 ± 0.001	1.384 ± 0.002	316.890 ± 0.009	35.605 ± 0.005	[126]
197-g2	0.33	3	220.701 ± 0.001	2.244 ± 0.001	1.427 ± 0.001	223.977 ± 0.004	11.692 ± 0.001	[126]
1-g7	0.25	3	9.900 ± 0.001	7.924 ± 0.001	5.034 ± 0.001	48.934 ± 0.001	0.066 ± 0.001	[126]
200-g3	0.43	4	170.739 ± 0.001	2.138 ± 0.001	1.411 ± 0.002	178.953 ± 0.003	5.248 ± 0.001	[126]
202-g26	0.67	2	128.478 ± 0.001	0.871 ± 0.001	1.727 ± 0.002	147.916 ± 0.001	2.789 ± 0.001	[126]
202-g35	0.57	4	220.663 ± 0.001	1.782 ± 0.001	1.470 ± 0.001	221.227 ± 0.004	11.374 ± 0.001	[126]
204-g19	0.23	2	137.494 ± 0.001	2.167 ± 0.001	1.397 ± 0.001	156.163 ± 0.008	3.236 ± 0.001	[126]
205-g2	0.42	4	170.698 ± 0.002	1.076 ± 0.001	1.206 ± 0.001	175.418 ± 0.006	5.484 ± 0.001	[126]
208-g31	0.40	4	419.200 ± 0.001	4.021 ± 0.001	1.269 ± 0.001	404.273 ± 0.008	72.769 ± 0.002	[126]
215-g39	0.46	4	313.304 ± 0.001	3.362 ± 0.001	1.404 ± 0.001	298.229 ± 0.006	29.678 ± 0.001	[126]
216-g21	0.29	1	169.697 ± 0.001	1.718 ± 0.006	1.794 ± 0.001	186.845 ± 0.008	6.317 ± 0.001	[126]
216-g8	0.45	3	232.990 ± 0.005	2.527 ± 0.001	1.667 ± 0.001	228.342 ± 0.001	13.321 ± 0.001	[126]
219-g14	0.26	4	530.916 ± 0.003	2.162 ± 0.001	1.503 ± 0.001	550.107 ± 0.003	172.016 ± 0.002	[126]
21-g3	0.19	2	117.330 ± 0.001	1.220 ± 0.001	1.287 ± 0.001	134.018 ± 0.007	2.054 ± 0.001	[126]
21-g5	3.54	5	281.045 ± 0.002	2.272 ± 0.001	1.030 ± 0.001	384.419 ± 0.001	31.781 ± 0.001	[126]
220-g8	0.23	1	94.649 ± 0.001	3.539 ± 0.001	3.594 ± 0.001	108.128 ± 0.001	1.414 ± 0.001	[126]
221-g21	0.28	4	615.000 ± 0.001	4.500 ± 0.001	1.110 ± 0.001	595.892 ± 0.002	236.748 ± 0.002	[126]
221-g22	0.86	2	49.703 ± 0.001	2.843 ± 0.001	2.728 ± 0.001	73.671 ± 0.001	0.228 ± 0.001	[126]

Galaxy	$\chi^2_{\rm red}$	n	$\langle V_0 \rangle$ (km s^{-1})	$\langle r_c \rangle$ (kpc)	d	$r_{\rm edge}$ (kpc)	M_T (10^{11} M$_\odot$)	Reference
22-g3	0.51	3	118.276 ± 0.002	0.854 ± 0.001	1.136 ± 0.001	116.500 ± 0.004	1.769 ± 0.001	[126]
230-g2	0.40	2	132.141 ± 0.001	3.240 ± 0.001	1.329 ± 0.002	176.857 ± 0.001	3.308 ± 0.001	[126]
231-g11	0.19	2	211.058 ± 0.001	2.058 ± 0.001	1.354 ± 0.001	216.240 ± 0.008	10.732 ± 0.001	[126]
231-g23	0.35	3	319.064 ± 0.001	2.401 ± 0.001	1.344 ± 0.001	331.931 ± 0.002	36.939 ± 0.001	[126]
231-g25	0.04	4	599.198 ± 0.001	3.153 ± 0.001	1.117 ± 0.001	589.198 ± 0.005	228.858 ± 0.004	[126]
231-g29	0.28	3	134.655 ± 0.001	2.947 ± 0.001	1.494 ± 0.001	170.667 ± 0.001	3.150 ± 0.001	[126]
231-g6	0.53	3	135.294 ± 0.001	4.130 ± 0.001	1.452 ± 0.001	173.828 ± 0.009	3.076 ± 0.001	[126]
233-g25	0.30	3	355.865 ± 0.004	15.208 ± 0.009	1.144 ± 0.001	418.525 ± 0.009	44.611 ± 0.001	[126]
233-g36	0.30	3	184.129 ± 0.002	2.104 ± 0.001	1.363 ± 0.001	188.759 ± 0.005	6.778 ± 0.001	[126]
233-g41	1.06	1	233.473 ± 0.001	1.297 ± 0.001	2.289 ± 0.001	239.951 ± 0.007	15.458 ± 0.001	[126]
233-g42	0.41	3	111.599 ± 0.001	1.424 ± 0.001	1.695 ± 0.001	128.209 ± 0.001	1.718 ± 0.001	[126]
233-g43	0.59	2	77.486 ± 0.002	2.610 ± 0.001	0.993 ± 0.001	71.1448 ± 0.001	0.403 ± 0.001	[126]
233-g47	0.33	4	295.782 ± 0.001	7.132 ± 0.001	1.391 ± 0.001	366.578 ± 0.003	29.509 ± 0.001	[126]
234-g13	0.25	2	147.871 ± 0.001	1.328 ± 0.001	1.514 ± 0.001	165.598 ± 0.001	4.082 ± 0.001	[126]
2352-14	0.65	3	98.842 ± 0.001	2.303 ± 0.001	1.698 ± 0.001	111.503 ± 0.001	1.101 ± 0.001	[126]
235-g16	1.72	1	186.585 ± 0.004	3.577 ± 0.003	1.850 ± 0.002	265.444 ± 0.004	10.925 ± 0.002	[126]
235-g20	0.40	2	163.320 ± 0.001	1.512 ± 0.001	1.590 ± 0.001	179.947 ± 0.005	5.417 ± 0.001	[126]
236-g37	0.19	2	185.737 ± 0.001	0.991 ± 0.001	1.344 ± 0.001	199.539 ± 0.004	7.823 ± 0.001	[126]
237-g49	0.44	4	251.158 ± 0.001	5.564 ± 0.001	1.241 ± 0.001	218.201 ± 0.001	11.624 ± 0.001	[126]
238-g24	5.96	2	228.000 ± 0.002	2.370 ± 0.001	1.373 ± 0.001	316.359 ± 0.005	18.496 ± 0.001	[126]
239-g17	0.93	3	88.883 ± 0.001	0.882 ± 0.001	1.710 ± 0.005	105.107 ± 0.001	0.910 ± 0.001	[126]
240-g11	2.94	1	228.512 ± 0.004	2.654 ± 0.002	1.603 ± 0.002	236.429 ± 0.008	14.403 ± 0.002	[126]
240-g13	0.68	5	647.320 ± 0.001	3.385 ± 0.008	1.192 ± 0.005	633.706 ± 0.004	281.722 ± 0.032	[126]
241-g21	0.32	4	298.760 ± 0.001	1.273 ± 0.001	1.149 ± 0.001	312.101 ± 0.009	30.669 ± 0.001	[126]
242-g18	0.86	1	70.340 ± 0.001	0.621 ± 0.001	2.396 ± 0.001	88.8651 ± 0.006	0.524 ± 0.001	[126]
243-g36	0.90	3	155.201 ± 0.001	3.087 ± 0.001	1.756 ± 0.001	213.125 ± 0.003	5.420 ± 0.001	[126]
243-g8	0.51	2	215.382 ± 0.001	2.241 ± 0.001	1.136 ± 0.001	218.168 ± 0.001	11.137 ± 0.001	[126]
244-g31	1.35	1	228.697 ± 0.001	1.479 ± 0.001	1.533 ± 0.001	241.838 ± 0.009	14.711 ± 0.001	[126]
244-g43	0.62	5	160.264 ± 0.001	0.155 ± 0.001	1.840 ± 0.001	162.218 ± 0.004	4.776 ± 0.001	[126]
245-g10	0.92	3	190.919 ± 0.001	3.337 ± 0.001	1.717 ± 0.001	195.646 ± 0.003	7.387 ± 0.001	[126]
249-g16	0.50	3	238.312 ± 0.001	2.542 ± 0.001	1.619 ± 0.001	233.441 ± 0.001	14.234 ± 0.001	[126]
249-g35	0.48	5	246.224 ± 0.002	1.798 ± 0.001	1.108 ± 0.001	260.169 ± 0.006	16.256 ± 0.001	[126]
24-g19	0.73	2	158.856 ± 0.002	2.768 ± 0.001	1.188 ± 0.001	215.561 ± 0.006	5.922 ± 0.001	[126]
250-g17	1.56	1	251.355 ± 0.002	1.678 ± 0.001	1.772 ± 0.001	270.057 ± 0.007	19.961 ± 0.001	[126]
251-g10	0.18	3	330.018 ± 0.001	2.761 ± 0.001	1.354 ± 0.001	340.907 ± 0.007	40.308 ± 0.001	[126]
251-g6	0.52	3	197.240 ± 0.001	4.278 ± 0.001	1.479 ± 0.001	261.144 ± 0.006	10.397 ± 0.001	[126]
25-g16	0.81	3	153.866 ± 0.001	2.593 ± 0.001	1.618 ± 0.001	199.432 ± 0.001	4.994 ± 0.001	[126]
264-g43	0.08	3	368.363 ± 0.001	1.707 ± 0.001	1.281 ± 0.001	390.157 ± 0.007	59.217 ± 0.001	[126]
264-g48	0.12	2	187.082 ± 0.002	1.854 ± 0.001	0.947 ± 0.001	194.217 ± 0.001	7.453 ± 0.001	[126]
265-g16	0.40	3	206.780 ± 0.001	5.684 ± 0.001	1.659 ± 0.001	261.409 ± 0.004	11.182 ± 0.001	[126]
266-g8	0.30	3	184.216 ± 0.002	2.685 ± 0.001	1.303 ± 0.001	189.567 ± 0.001	6.625 ± 0.001	[126]
267-g29	0.08	2	239.822 ± 0.001	1.590 ± 0.001	1.342 ± 0.001	259.618 ± 0.008	16.880 ± 0.001	[126]
267-g38	0.17	3	306.638 ± 0.001	1.956 ± 0.001	1.434 ± 0.001	321.379 ± 0.004	33.428 ± 0.001	[126]
268-g11	0.19	3	282.540 ± 0.001	1.613 ± 0.001	1.186 ± 0.001	280.498 ± 0.008	24.693 ± 0.001	[126]
268-g33	0.68	3	267.131 ± 0.001	4.436 ± 0.001	1.713 ± 0.001	348.586 ± 0.007	26.495 ± 0.001	[126]
269-g15	0.11	1	171.472 ± 0.001	4.683 ± 0.001	0.976 ± 0.001	185.662 ± 0.001	6.012 ± 0.001	[126]
269-g19	6.05	3	244.427 ± 0.003	1.507 ± 0.001	1.229 ± 0.002	250.272 ± 0.001	16.466 ± 0.001	[126]
269-g48	0.17	4	160.858 ± 0.001	1.556 ± 0.001	1.295 ± 0.001	171.249 ± 0.001	4.592 ± 0.001	[126]
269-g49	0.08	4	458.600 ± 0.002	2.862 ± 0.001	1.096 ± 0.001	447.711 ± 0.007	100.410 ± 0.003	[126]
269-g61	1.10	1	157.529 ± 0.001	5.868 ± 0.001	4.466 ± 0.001	187.234 ± 0.002	7.344 ± 0.001	[126]

Galaxy	$\chi^2_{\rm red}$	n	$\langle V_0 \rangle$ (km s^{-1})	$\langle r_c \rangle$ (kpc)	d	$r_{\rm edge}$ (kpc)	M_T (10^{11} M$_\odot$)	Reference
269-g63	0.20	2	26.221 ± 0.001	4.568 ± 0.001	6.196 ± 0.001	68.655 ± 0.001	0.181 ± 0.001	[126]
269-g75	0.79	3	123.345 ± 0.001	2.466 ± 0.003	1.728 ± 0.001	161.998 ± 0.001	2.585 ± 0.001	[126]
269-g78	0.54	5	163.790 ± 0.006	1.415 ± 0.002	1.879 ± 0.003	174.015 ± 0.001	4.834 ± 0.001	[126]
269-g82	1.84	2	73.200 ± 0.001	0.633 ± 0.003	2.119 ± 0.004	90.451 ± 0.001	0.558 ± 0.001	[126]
26-g6	0.18	4	461.465 ± 0.002	7.207 ± 0.001	1.090 ± 0.001	434.448 ± 0.002	86.206 ± 0.002	[126]
271-g22	0.25	2	182.374 ± 0.001	1.958 ± 0.004	1.241 ± 0.004	192.033 ± 0.005	7.062 ± 0.001	[126]
271-g4	0.43	6	97.394 ± 0.002	0.292 ± 0.001	1.569 ± 0.001	96.367 ± 0.008	1.001 ± 0.001	[126]
273-g6	0.14	2	168.488 ± 0.002	2.721 ± 0.001	1.557 ± 0.001	166.865 ± 0.002	5.199 ± 0.001	[126]
27-g17	0.57	4	183.918 ± 0.001	0.901 ± 0.001	1.341 ± 0.001	195.926 ± 0.009	7.272 ± 0.001	[126]
27-g24	0.61	2	176.780 ± 0.001	1.755 ± 0.001	1.697 ± 0.001	187.971 ± 0.001	6.637 ± 0.001	[126]
27-g8	8.17	1	117.720 ± 0.002	3.650 ± 0.001	3.597 ± 0.003	182.792 ± 0.009	3.419 ± 0.001	[126]
280-g13	0.14	4	396.151 ± 0.001	3.727 ± 0.004	1.178 ± 0.001	378.585 ± 0.004	60.712 ± 0.001	[126]
281-g38	0.16	1	173.711 ± 0.001	1.990 ± 0.004	2.355 ± 0.001	185.437 ± 0.001	6.733 ± 0.001	[126]
282-g35	0.14	4	251.310 ± 0.001	2.585 ± 0.005	1.174 ± 0.001	252.688 ± 0.006	16.224 ± 0.001	[126]
282-g3	2.11	1	196.041 ± 0.004	2.495 ± 0.002	1.551 ± 0.002	207.742 ± 0.007	9.294 ± 0.002	[126]
284-g13	0.51	3	221.757 ± 0.002	1.750 ± 0.002	1.471 ± 0.001	223.281 ± 0.005	11.991 ± 0.001	[126]
284-g21	0.11	4	360.887 ± 0.002	3.331 ± 0.001	1.092 ± 0.001	344.697 ± 0.009	45.824 ± 0.002	[126]
284-g24	0.80	3	130.624 ± 0.001	2.573 ± 0.006	1.715 ± 0.001	177.040 ± 0.001	3.180 ± 0.001	[126]
284-g29	0.56	3	189.630 ± 0.001	4.965 ± 0.001	1.632 ± 0.001	254.540 ± 0.001	9.270 ± 0.001	[126]
284-g39	0.45	3	133.552 ± 0.002	0.592 ± 0.001	1.525 ± 0.001	133.794 ± 0.002	2.680 ± 0.001	[126]
285-g40	0.41	3	295.427 ± 0.007	3.958 ± 0.001	1.638 ± 0.001	298.416 ± 0.002	27.521 ± 0.002	[126]
286-g16	1.26	2	237.415 ± 0.006	4.134 ± 0.004	1.385 ± 0.003	323.992 ± 0.007	20.097 ± 0.004	[126]
286-g18	0.89	2	295.063 ± 0.001	1.900 ± 0.002	2.122 ± 0.001	328.919 ± 0.001	33.025 ± 0.001	[126]
287-g13	5.63	2	180.873 ± 0.002	4.122 ± 0.001	1.893 ± 0.001	246.668 ± 0.008	9.055 ± 0.001	[126]
290-g22	0.26	2	160.572 ± 0.001	1.028 ± 0.001	1.316 ± 0.001	174.587 ± 0.001	5.091 ± 0.001	[126]
290-g35	0.58	3	254.571 ± 0.001	6.905 ± 0.001	1.346 ± 0.001	322.763 ± 0.008	20.382 ± 0.001	[126]
291-g10	0.79	1	164.551 ± 0.001	0.966 ± 0.001	2.065 ± 0.001	175.817 ± 0.009	5.601 ± 0.001	[126]
291-g24	0.06	3	181.134 ± 0.001	4.315 ± 0.001	1.371 ± 0.001	180.248 ± 0.001	5.663 ± 0.001	[126]
296-g25	0.45	5	178.046 ± 0.004	0.244 ± 0.001	1.579 ± 0.001	179.562 ± 0.003	6.478 ± 0.001	[126]
296-g26	0.58	1	157.943 ± 0.001	8.879 ± 0.002	4.486 ± 0.001	255.503 ± 0.001	10.372 ± 0.001	[126]
297-g37	0.18	1	174.297 ± 0.001	1.361 ± 0.003	1.140 ± 0.001	176.660 ± 0.005	6.169 ± 0.001	[126]
298-g16	0.58	3	300.047 ± 0.001	0.890 ± 0.001	2.089 ± 0.001	303.348 ± 0.002	31.232 ± 0.001	[126]
298-g36	0.35	3	155.028 ± 0.006	2.088 ± 0.001	1.586 ± 0.001	150.114 ± 0.002	3.785 ± 0.001	[126]
298-g8	0.66	2	127.009 ± 0.001	2.038 ± 0.001	1.641 ± 0.001	146.698 ± 0.001	2.631 ± 0.001	[126]
299-g18	0.21	3	187.334 ± 0.001	3.064 ± 0.001	1.259 ± 0.001	246.076 ± 0.005	9.001 ± 0.001	[126]
299-g4	0.37	3	218.309 ± 0.005	1.572 ± 0.005	1.648 ± 0.004	216.739 ± 0.001	11.392 ± 0.001	[126]
2-g12	0.07	6	241.434 ± 0.002	1.012 ± 0.001	0.982 ± 0.001	234.712 ± 0.007	14.467 ± 0.001	[126]
302-g9	0.60	3	71.820 ± 0.001	0.970 ± 0.001	1.613 ± 0.001	85.624 ± 0.009	0.473 ± 0.001	[126]
303-g14	0.17	3	377.399 ± 0.001	2.935 ± 0.001	1.431 ± 0.001	390.497 ± 0.006	60.818 ± 0.001	[126]
304-g16	0.13	1	200.012 ± 0.001	1.028 ± 0.001	1.627 ± 0.001	204.110 ± 0.009	9.514 ± 0.001	[126]
305-g14	0.76	3	156.961 ± 0.001	3.169 ± 0.001	1.761 ± 0.001	165.633 ± 0.004	4.187 ± 0.001	[126]
305-g6	0.27	3	201.417 ± 0.001	0.752 ± 0.001	1.429 ± 0.001	211.703 ± 0.008	9.697 ± 0.001	[126]
306-g2	0.25	3	118.182 ± 0.001	1.519 ± 0.001	1.291 ± 0.001	133.756 ± 0.002	1.969 ± 0.001	[126]
306-g32	1.30	3	236.743 ± 0.007	2.250 ± 0.002	1.420 ± 0.005	236.132 ± 0.006	14.235 ± 0.003	[126]
308-g23	0.35	2	168.376 ± 0.001	0.861 ± 0.001	1.481 ± 0.001	178.599 ± 0.006	5.773 ± 0.001	[126]
309-g17	0.37	3	305.370 ± 0.001	2.028 ± 0.001	1.486 ± 0.001	320.068 ± 0.009	32.994 ± 0.001	[126]
309-g5	0.97	3	86.872 ± 0.001	0.231 ± 0.001	2.011 ± 0.001	104.223 ± 0.007	0.902 ± 0.001	[126]
30-g9	1.17	2	331.980 ± 0.004	4.235 ± 0.003	1.633 ± 0.003	454.957 ± 0.007	56.515 ± 0.008	[126]
310-g2	0.44	2	220.204 ± 0.001	1.319 ± 0.002	1.540 ± 0.001	233.323 ± 0.008	12.876 ± 0.001	[126]
317-g32	1.05	1	214.224 ± 0.003	0.697 ± 0.001	1.604 ± 0.001	232.699 ± 0.007	12.429 ± 0.001	[126]
317-g52	0.61	3	218.210 ± 0.001	2.240 ± 0.001	1.870 ± 0.001	221.006 ± 0.002	11.479 ± 0.001	[126]

Galaxy	$\chi^2_{\rm red}$	n	$\langle V_0 \rangle$ (km s^{-1})	$\langle r_c \rangle$ (kpc)	d	$r_{\rm edge}$ (kpc)	M_T (10^{11} M$_\odot$)	Reference
317-g53	0.77	4	159.323 ± 0.001	5.869 ± 0.001	1.489 ± 0.001	184.648 ± 0.001	3.802 ± 0.001	[126]
319-g16	0.46	3	116.829 ± 0.001	3.199 ± 0.001	1.602 ± 0.001	151.165 ± 0.001	2.061 ± 0.001	[126]
319-g26	0.43	3	130.342 ± 0.001	4.893 ± 0.001	1.431 ± 0.001	162.985 ± 0.001	2.552 ± 0.001	[126]
31-g18	0.35	4	193.889 ± 0.001	0.494 ± 0.001	1.412 ± 0.001	194.566 ± 0.008	8.241 ± 0.001	[126]
31-g5	0.67	1	191.843 ± 0.001	0.820 ± 0.001	1.250 ± 0.001	199.768 ± 0.007	8.511 ± 0.001	[126]
320-g26	0.71	3	227.000 ± 0.001	0.068 ± 0.001	1.812 ± 0.003	231.151 ± 0.002	13.819 ± 0.001	[126]
321-g10	0.26	4	234.197 ± 0.001	1.202 ± 0.001	1.303 ± 0.001	230.965 ± 0.009	13.785 ± 0.001	[126]
321-g17	0.37	4	158.620 ± 0.001	1.012 ± 0.001	1.432 ± 0.001	155.417 ± 0.001	4.200 ± 0.001	[126]
321-g1	0.25	2	83.029 ± 0.001	7.306 ± 0.001	3.304 ± 0.001	136.258 ± 0.001	1.421 ± 0.001	[126]
322-g33	0.99	6	335.597 ± 0.001	2.426 ± 0.001	1.097 ± 0.002	456.970 ± 0.001	53.385 ± 0.002	[126]
322-g36	0.66	4	278.486 ± 0.001	1.419 ± 0.001	1.470 ± 0.003	295.191 ± 0.008	25.12 ± 0.001	[126]
322-g45	0.37	3	147.497 ± 0.001	0.440 ± 0.001	1.245 ± 0.001	164.128 ± 0.003	4.052 ± 0.001	[126]
322-g48	0.05	2	132.885 ± 0.001	6.267 ± 0.001	1.682 ± 0.001	171.065 ± 0.001	3.178 ± 0.001	[126]
322-g55	0.54	5	239.551 ± 0.001	0.675 ± 0.001	1.439 ± 0.001	238.652 ± 0.009	15.208 ± 0.001	[126]
322-g82	6.39	3	252.835 ± 0.006	1.958 ± 0.004	1.735 ± 0.009	250.878 ± 0.003	17.667 ± 0.005	[126]
322-g87	0.71	5	477.622 ± 0.001	2.455 ± 0.001	1.290 ± 0.001	471.525 ± 0.006	114.622 ± 0.001	[126]
322-g93	0.57	4	258.096 ± 0.001	4.252 ± 0.001	1.266 ± 0.001	249.819 ± 0.009	15.613 ± 0.002	[126]
323-g27	0.65	4	366.917 ± 0.001	2.539 ± 0.001	1.543 ± 0.001	375.230 ± 0.001	54.265 ± 0.001	[126]
323-g33	0.34	2	136.994 ± 0.001	1.179 ± 0.001	1.087 ± 0.001	151.682 ± 0.003	3.169 ± 0.	[126]
323-g41	0.74	2	133.730 ± 0.001	1.095 ± 0.001	1.927 ± 0.001	135.139 ± 0.009	2.761 ± 0.001	[126]
323-g42	0.06	3	197.699 ± 0.001	1.602 ± 0.001	1.211 ± 0.002	198.886 ± 0.001	8.402 ± 0.001	[126]
325-g27	0.08	1	44.758 ± 0.002	3.810 ± 0.002	6.336 ± 0.001	66.4859 ± 0.001	0.329 ± 0.001	[126]
325-g50	0.24	2	88.383 ± 0.001	1.215 ± 0.001	1.749 ± 0.001	104.944 ± 0.008	0.923 ± 0.001	[126]
327-g27	0.66	4	328.327 ± 0.001	9.277 ± 0.001	1.341 ± 0.001	279.166 ± 0.001	23.524 ± 0.002	[126]
328-g15	0.90	2	191.145 ± 0.001	0.939 ± 0.001	1.938 ± 0.001	199.360 ± 0.003	8.382 ± 0.001	[126]
328-g3	0.69	4	387.534 ± 0.001	8.091 ± 0.001	1.595 ± 0.001	350.252 ± 0.001	47.359 ± 0.001	[126]
328-g41	0.59	1	183.970 ± 0.001	1.231 ± 0.001	1.271 ± 0.001	186.936 ± 0.003	7.309 ± 0.001	[126]
328-g43	0.36	2	87.032 ± 0.001	1.063 ± 0.002	1.308 ± 0.001	103.315 ± 0.003	0.867 ± 0.001	[126]
328-g46	0.09	1	138.509 ± 0.001	4.826 ± 0.001	4.127 ± 0.001	183.675 ± 0.001	5.187 ± 0.001	[126]
329-g7	0.43	3	316.423 ± 0.001	0.700 ± 0.001	1.679 ± 0.001	319.986 ± 0.008	36.659 ± 0.001	[126]
32-g18	0.54	3	215.401 ± 0.003	1.724 ± 0.001	1.725 ± 0.001	219.143 ± 0.002	11.193 ± 0.001	[126]
336-g13	0.45	5	195.049 ± 0.001	0.092 ± 0.001	1.441 ± 0.001	198.067 ± 0.006	8.694 ± 0.001	[126]
337-g22	0.24	4	336.382 ± 0.001	2.809 ± 0.001	1.377 ± 0.001	338.700 ± 0.009	40.226 ± 0.002	[126]
337-g6	0.22	2	199.657 ± 0.001	1.151 ± 0.001	1.292 ± 0.003	208.192 ± 0.008	9.397 ± 0.001	[126]
338-g22	0.59	4	247.369 ± 0.001	5.249 ± 0.004	1.481 ± 0.001	324.182 ± 0.006	19.078 ± 0.001	[126]
339-g36	0.83	3	166.385 ± 0.001	2.481 ± 0.001	1.829 ± 0.001	222.731 ± 0.001	6.673 ± 0.001	[126]
33-g22	0.35	3	169.599 ± 0.001	3.734 ± 0.004	1.144 ± 0.001	178.487 ± 0.001	4.933 ± 0.001	[126]
33-g32	0.46	3	212.912 ± 0.001	1.071 ± 0.001	1.725 ± 0.001	213.244 ± 0.001	10.850 ± 0.001	[126]
340-g8	0.40	4	188.161 ± 0.001	0.746 ± 0.001	1.263 ± 0.001	199.150 ± 0.004	7.810 ± 0.001	[126]
342-g43	0.17	4	379.778 ± 0.001	1.843 ± 0.001	1.425 ± 0.001	398.262 ± 0.003	63.109 ± 0.001	[126]
343-g18	0.15	3	267.996 ± 0.002	4.369 ± 0.001	1.126 ± 0.001	252.160 ± 0.004	17.940 ± 0.001	[126]
343-g28	0.12	1	93.903 ± 0.002	1.921 ± 0.001	1.754 ± 0.001	116.191 ± 0.002	1.208 ± 0.001	[126]
344-g20	0.04	2	15.880 ± 0.003	10.277 ± 0.001	9.330 ± 0.002	96.161 ± 0.001	0.497 ± 0.001	[126]
346-g14	3.98	4	266.432 ± 0.003	3.222 ± 0.002	1.136 ± 0.005	253.521 ± 0.003	17.685 ± 0.004	[126]
346-g1	0.04	2	1.259 ± 0.003	6.727 ± 0.003	25.477 ± 0.009	51.317 ± 0.002	0.076 ± 0.001	[126]
346-g26	0.49	3	134.317 ± 0.001	1.713 ± 0.001	1.451 ± 0.001	149.830 ± 0.009	2.868 ± 0.001	[126]
347-g28	0.69	3	88.576 ± 0.001	1.071 ± 0.001	1.788 ± 0.001	104.022 ± 0.001	0.886 ± 0.001	[126]
347-g33	8.20	1	153.076 ± 0.002	1.609 ± 0.001	2.518 ± 0.001	162.764 ± 0.002	4.605 ± 0.001	[126]
347-g34	0.57	3	137.660 ± 0.001	1.300 ± 0.001	1.708 ± 0.001	154.294 ± 0.008	3.205 ± 0.001	[126]

Galaxy	$\chi^2_{\rm red}$	n	$\langle V_0 \rangle$ (km s^{-1})	$\langle r_c \rangle$ (kpc)	d	$r_{\rm edge}$ (kpc)	M_T (10^{11} M$_\odot$)	Reference
349-g32	0.38	1	231.682 ± 0.004	5.925 ± 0.001	2.872 ± 0.001	260.587 ± 0.0001	18.151 ± 0.001	[126]
349-g33	0.08	1	201.244 ± 0.001	2.160 ± 0.001	1.568 ± 0.001	205.332 ± 0.0025	9.686 ± 0.001	[126]
34-g12	0.16	2	241.085 ± 0.001	2.124 ± 0.001	1.491 ± 0.001	254.421 ± 0.0001	16.637 ± 0.001	[126]
350-g23	7.66	1	228.430 ± 0.002	1.110 ± 0.001	1.279 ± 0.003	232.334 ± 0.006	14.032 ± 0.001	[126]
351-g18	0.69	3	149.817 ± 0.001	3.281 ± 0.001	1.602 ± 0.001	160.251 ± 0.007	3.61 ± 0.001	[126]
351-g1	0.23	2	9.900 ± 0.002	11.533 ± 0.002	7.749 ± 0.002	68.3362 ± 0.0003	0.179 ± 0.001	[126]
352-g14	1.25	2	187.269 ± 0.001	1.321 ± 0.001	2.062 ± 0.001	189.824 ± 0.0001	7.653 ± 0.001	[126]
352-g15	0.14	4	281.480 ± 0.001	2.629 ± 0.001	1.432 ± 0.001	281.695 ± 0.0094	23.183 ± 0.001	[126]
352-g24	0.26	4	378.287 ± 0.001	1.222 ± 0.001	1.334 ± 0.001	377.811 ± 0.003	60.34 ± 0.002	[126]
352-g27	0.85	2	165.736 ± 0.001	2.776 ± 0.001	1.931 ± 0.001	181.919 ± 0.001	5.636 ± 0.001	[126]
352-g50	0.71	1	111.812 ± 0.001	1.607 ± 0.001	2.500 ± 0.001	136.900 ± 0.001	2.079 ± 0.001	[126]
352-g53	1.76	2	264.541 ± 0.003	0.267 ± 0.001	0.718 ± 0.001	278.414 ± 0.002	22.495 ± 0.001	[126]
353-g14	0.42	2	132.212 ± 0.001	1.665 ± 0.001	1.493 ± 0.007	150.920 ± 0.002	2.939 ± 0.001	[126]
353-g2	0.25	1	78.664 ± 0.002	1.734 ± 0.001	2.732 ± 0.002	99.8382 ± 0.001	0.776 ± 0.001	[126]
354-g17	0.44	3	226.787 ± 0.001	2.993 ± 0.001	1.704 ± 0.009	220.604 ± 0.004	12.012 ± 0.001	[126]
354-g46	0.66	3	264.978 ± 0.001	1.719 ± 0.001	1.719 ± 0.001	282.608 ± 0.006	22.106 ± 0.001	[126]
354-g47	0.73	6	211.467 ± 0.001	0.183 ± 0.001	4.019 ± 0.005	214.641 ± 0.001	11.064 ± 0.001	[126]
355-g26	0.21	2	132.230 ± 0.001	1.710 ± 0.001	1.540 ± 0.001	147.901 ± 0.004	2.881 ± 0.001	[126]
356-g15	0.55	3	246.579 ± 0.001	6.259 ± 0.001	1.748 ± 0.001	322.403 ± 0.001	20.057 ± 0.001	[126]
356-g18	0.55	6	680.158 ± 0.003	1.967 ± 0.001	1.000 ± 0.001	676.648 ± 0.007	341.409 ± 0.001	[126]
357-g16	1.30	4	201.161 ± 0.009	1.265 ± 0.001	1.034 ± 0.003	202.124 ± 0.007	8.724 ± 0.001	[126]
357-g19	0.56	4	224.886 ± 0.001	2.120 ± 0.001	1.412 ± 0.001	220.374 ± 0.004	11.528 ± 0.001	[126]
357-g3	0.46	3	177.309 ± 0.001	2.481 ± 0.001	1.373 ± 0.001	184.297 ± 0.001	6.026 ± 0.001	[126]
358-g17	0.53	3	308.863 ± 0.006	0.781 ± 0.002	1.556 ± 0.007	335.227 ± 0.009	36.512 ± 0.002	[126]
358-g58	0.23	4	183.857 ± 0.001	0.532 ± 0.001	1.438 ± 0.001	184.133 ± 0.009	6.985 ± 0.001	[126]
358-g63	0.16	2	135.694 ± 0.005	3.103 ± 0.001	1.819 ± 0.001	134.660 ± 0.009	2.732 ± 0.001	[126]
358-g9	0.88	3	87.975 ± 0.001	2.067 ± 0.001	1.751 ± 0.007	112.591 ± 0.001	0.898 ± 0.001	[126]
359-g6	0.13	4	480.884 ± 0.002	2.708 ± 0.003	0.956 ± 0.001	477.948 ± 0.006	118.632 ± 0.004	[126]
35-g18	0.50	4	288.783 ± 0.001	2.105 ± 0.001	1.407 ± 0.004	297.329 ± 0.002	26.436 ± 0.003	[126]
35-g3	0.43	3	91.966 ± 0.001	0.757 ± 0.001	1.260 ± 0.001	110.277 ± 0.001	1.02 ± 0.001	[126]
361-g12	0.14	3	205.478 ± 0.003	3.709 ± 0.001	1.192 ± 0.003	209.598 ± 0.007	8.779 ± 0.003	[126]
362-g11	8.95	1	117.405 ± 0.003	2.118 ± 0.001	1.954 ± 0.002	121.347 ± 0.001	1.999 ± 0.001	[126]
363-g23	1.01	3	143.000 ± 0.001	0.029 ± 0.001	3.043 ± 0.001	145.732 ± 0.003	3.463 ± 0.001	[126]
363-g7	0.05	1	16.180 ± 0.003	4.891 ± 0.002	23.839 ± 0.001	77.575 ± 0.008	0.261 ± 0.001	[126]
365-g28	0.43	3	239.131 ± 0.001	4.075 ± 0.001	1.713 ± 0.001	238.745 ± 0.001	14.137 ± 0.001	[126]
366-g4	0.08	3	169.994 ± 0.001	1.991 ± 0.002	1.125 ± 0.001	163.729 ± 0.003	4.911 ± 0.001	[126]
366-g9	0.07	3	153.752 ± 0.001	0.352 ± 0.001	0.965 ± 0.001	154.930 ± 0.004	4.161 ± 0.001	[126]
36-g19	0.68	3	248.579 ± 0.001	3.661 ± 0.001	1.811 ± 0.001	247.992 ± 0.006	16.205 ± 0.001	[126]
373-g12	0.31	3	93.949 ± 0.008	1.734 ± 0.001	1.695 ± 0.001	124.561 ± 0.001	1.161 ± 0.001	[126]
373-g21	0.74	4	231.094 ± 0.001	4.126 ± 0.001	1.294 ± 0.001	226.897 ± 0.004	11.232 ± 0.001	[126]
373-g29	0.16	2	9.900 ± 0.001	5.411 ± 0.001	10.041 ± 0.001	58.196 ± 0.001	0.11 ± 0.001	[126]
374-g10	0.42	3	201.076 ± 0.001	2.182 ± 0.001	1.462 ± 0.001	196.092 ± 0.005	8.437 ± 0.001	[126]
374-g11	0.25	2	158.879 ± 0.001	1.183 ± 0.001	1.045 ± 0.001	168.795 ± 0.007	4.757 ± 0.001	[126]
374-g26	0.56	4	255.895 ± 0.001	2.298 ± 0.001	1.431 ± 0.001	256.525 ± 0.007	17.524 ± 0.001	[126]
374-g27	5.44	3	275.896 ± 0.007	0.862 ± 0.001	1.671 ± 0.001	278.074 ± 0.001	24.058 ± 0.001	[126]
374-g29	0.56	4	295.487 ± 0.002	3.006 ± 0.001	1.495 ± 0.001	373.311 ± 0.003	34.445 ± 0.001	[126]
374-g3	0.48	2	70.802 ± 0.001	3.659 ± 0.001	2.651 ± 0.001	98.997 ± 0.001	0.612 ± 0.001	[126]
374-g49	0.52	4	348.596 ± 0.001	2.488 ± 0.001	1.486 ± 0.001	356.578 ± 0.009	46.358 ± 0.001	[126]
374-g8	0.32	4	341.821 ± 0.002	2.333 ± 0.001	0.964 ± 0.003	331.650 ± 0.002	40.815 ± 0.004	[126]
375-g12	0.81	3	227.858 ± 0.001	10.791 ± 0.001	2.169 ± 0.002	210.618 ± 0.001	10.454 ± 0.001	[126]

Galaxy	$\chi^2_{\rm red}$	n	$\langle V_0 \rangle$ (km s^{-1})	$\langle r_c \rangle$ (kpc)	d	$r_{\rm edge}$ (kpc)	M_T (10^{11} M$_\odot$)	Reference
375-g26	0.18	4	187.071 ± 0.001	0.541 ± 0.001	1.084 ± 0.001	186.963 ± 0.008	7.312 ± 0.001	[126]
375-g29	0.49	5	600.00 ± 0.001	3.791 ± 0.001	1.262 ± 0.001	587.551 ± 0.007	220.625 ± 0.003	[126]
375-g2	0.04	1	138.750 ± 0.002	1.464 ± 0.001	1.751 ± 0.001	156.705 ± 0.002	3.537 ± 0.001	[126]
375-g47	0.02	1	153.345 ± 0.001	1.793 ± 0.001	1.250 ± 0.002	181.934 ± 0.005	4.922 ± 0.001	[126]
375-g60	0.69	5	1.453 ± 0.004	4.915 ± 0.001	3.862 ± 0.001	16.1876 ± 0.001	0.002 ± 0.001	[126]
376-g2	0.47	2	186.616 ± 0.001	1.571 ± 0.001	1.443 ± 0.001	191.843 ± 0.006	7.509 ± 0.001	[126]
377-g10	0.39	4	394.738 ± 0.001	2.238 ± 0.009	1.469 ± 0.001	388.694 ± 0.008	65.706 ± 0.017	[126]
377-g11	0.72	2	9.900 ± 0.009	8.852 ± 0.001	11.339 ± 0.001	81.404 ± 0.001	0.302 ± 0.001	[126]
377-g31	0.89	3	173.792 ± 0.004	1.886 ± 0.001	1.755 ± 0.001	183.187 ± 0.001	6.000 ± 0.001	[126]
378-g11	0.13	3	214.419 ± 0.002	2.514 ± 0.001	1.194 ± 0.001	213.597 ± 0.009	10.263 ± 0.001	[126]
379-g6	1.57	1	200.070 ± 0.011	3.753 ± 0.001	1.037 ± 0.002	202.155 ± 0.001	9.081 ± 0.002	[126]
380-g14	1.21	2	166.167 ± 0.001	0.979 ± 0.003	1.984 ± 0.001	177.175 ± 0.001	5.626 ± 0.001	[126]
380-g19	0.14	2	285.801 ± 0.001	2.131 ± 0.008	0.929 ± 0.002	284.616 ± 0.003	25.796 ± 0.002	[126]
380-g23	0.09	1	40.848 ± 0.005	5.118 ± 0.001	9.864 ± 0.001	101.261 ± 0.001	0.581 ± 0.001	[126]
380-g24	0.09	4	213.680 ± 0.001	0.919 ± 0.001	1.380 ± 0.001	212.033 ± 0.007	10.666 ± 0.001	[126]
380-g2	0.42	2	47.973 ± 0.004	1.152 ± 0.001	2.008 ± 0.001	59.9848 ± 0.001	0.156 ± 0.001	[126]
381-g51	0.43	4	367.358 ± 0.009	2.505 ± 0.001	1.565 ± 0.001	374.114 ± 0.005	54.311 ± 0.004	[126]
382-g32	1.36	3	267.394 ± 0.001	9.782 ± 0.001	1.793 ± 0.001	341.539 ± 0.001	23.790 ± 0.001	[126]
382-g41	0.40	4	0.689 ± 0.002	5.410 ± 0.001	5.951 ± 0.002	19.7724 ± 0.006	0.004 ± 0.001	[126]
382-g4	0.35	4	156.290 ± 0.001	1.667 ± 0.001	1.394 ± 0.001	164.632 ± 0.004	4.131 ± 0.001	[126]
382-g58	0.11	1	174.920 ± 0.001	7.152 ± 0.001	4.680 ± 0.001	287.152 ± 0.001	13.389 ± 0.001	[126]
383-g2	1.24	1	162.716 ± 0.001	2.277 ± 0.001	2.322 ± 0.001	175.255 ± 0.001	5.611 ± 0.001	[126]
383-g55	0.21	2	280.254 ± 0.001	1.486 ± 0.001	1.177 ± 0.001	309.815 ± 0.004	27.585 ± 0.001	[126]
383-g67	0.31	4	284.548 ± 0.001	2.821 ± 0.002	1.236 ± 0.001	280.854 ± 0.003	23.232 ± 0.001	[126]
383-g88	0.85	2	177.908 ± 0.001	1.091 ± 0.001	1.574 ± 0.001	186.744 ± 0.001	6.727 ± 0.001	[126]
385-g12	0.21	1	4.835 ± 0.001	9.546 ± 0.001	82.590 ± 0.001	92.7764 ± 0.001	0.447 ± 0.001	[126]
385-g8	0.20	3	217.815 ± 0.001	5.889 ± 0.001	1.437 ± 0.001	211.532 ± 0.001	9.403 ± 0.001	[126]
386-g43	0.28	3	370.320 ± 0.001	1.314 ± 0.001	1.516 ± 0.001	398.065 ± 0.009	61.830 ± 0.002	[126]
386-g44	0.94	2	176.385 ± 0.001	0.290 ± 0.001	1.391 ± 0.001	179.146 ± 0.004	6.433 ± 0.001	[126]
386-g6	0.12	2	170.483 ± 0.001	1.096 ± 0.001	1.073 ± 0.002	185.738 ± 0.009	6.070 ± 0.001	[126]
386-g9	0.87	1	206.284 ± 0.001	0.423 ± 0.001	2.615 ± 0.001	211.193 ± 0.005	10.540 ± 0.001	[126]
387-g20	0.27	2	43.085 ± 0.001	5.334 ± 0.001	4.721 ± 0.001	87.994 ± 0.001	0.381 ± 0.001	[126]
387-g26	0.40	3	282.105 ± 0.001	3.749 ± 0.001	1.798 ± 0.001	377.385 ± 0.006	32.703 ± 0.001	[126]
387-g4	0.99	2	233.664 ± 0.001	0.284 ± 0.001	2.029 ± 0.001	251.564 ± 0.003	15.933 ± 0.001	[126]
38-g12	0.16	1	152.862 ± 0.002	0.779 ± 0.001	0.842 ± 0.004	171.66 ± 0.007	4.607 ± 0.001	[126]
397-g18	0.27	2	238.098 ± 0.001	4.999 ± 0.001	1.046 ± 0.001	235.151 ± 0.003	13.756 ± 0.001	[126]
398-g20	0.09	1	108.406 ± 0.002	4.097 ± 0.001	4.100 ± 0.009	126.958 ± 0.001	2.290 ± 0.002	[126]
399-g23	0.34	1	214.382 ± 0.001	1.284 ± 0.001	0.830 ± 0.001	216.788 ± 0.004	11.400 ± 0.001	[126]
3-g3	0.77	4	309.320 ± 0.001	3.076 ± 0.001	1.485 ± 0.001	309.745 ± 0.006	30.631 ± 0.001	[126]
3-g4	0.43	3	271.597 ± 0.001	2.918 ± 0.001	1.372 ± 0.001	278.37 ± 0.003	21.874 ± 0.001	[126]

Galaxy	$\chi^2_{\rm red}$	n	$\langle V_0 \rangle$ (km s^{-1})	$\langle r_c \rangle$ (kpc)	d	$r_{\rm edge}$ (kpc)	M_T (10^{11} M$_\odot$)	Reference
400-g21	0.42	4	321.943 ± 0.001	5.965 ± 0.001	1.274 ± 0.001	304.343 ± 0.002	28.698 ± 0.002	[126]
400-g37	0.50	3	137.458 ± 0.001	1.194 ± 0.001	1.606 ± 0.001	154.851 ± 0.008	3.212 ± 0.001	[126]
400-g5	0.26	3	196.193 ± 0.001	0.997 ± 0.001	1.540 ± 0.001	213.279 ± 0.002	9.204 ± 0.001	[126]
401-g3	0.40	2	250.127 ± 0.001	2.554 ± 0.001	1.710 ± 0.001	266.863 ± 0.001	18.859 ± 0.001	[126]
403-g16	0.48	4	217.507 ± 0.001	0.258 ± 0.001	1.260 ± 0.001	238.329 ± 0.001	12.925 ± 0.001	[126]
403-g31	0.11	4	245.160 ± 0.001	2.811 ± 0.001	1.075 ± 0.001	230.149 ± 0.006	13.640 ± 0.001	[126]
404-g18	0.19	5	231.337 ± 0.002	2.498 ± 0.001	1.100 ± 0.002	258.078 ± 0.006	13.569 ± 0.001	[126]
404-g31	0.58	2	42.893 ± 0.001	5.318 ± 0.001	3.945 ± 0.001	61.9362 ± 0.001	0.266 ± 0.001	[126]
404-g45	0.57	4	313.706 ± 0.001	5.621 ± 0.001	1.442 ± 0.001	287.901 ± 0.001	26.161 ± 0.001	[126]
406-g26	0.43	4	215.963 ± 0.001	2.973 ± 0.001	1.429 ± 0.002	218.779 ± 0.009	10.079 ± 0.002	[126]
406-g33	0.10	2	154.704 ± 0.002	2.076 ± 0.001	1.381 ± 0.001	168.747 ± 0.001	4.452 ± 0.001	[126]
40-g12	1.00	1	190.290 ± 0.002	3.011 ± 0.005	1.994 ± 0.003	201.195 ± 0.007	8.697 ± 0.002	[126]
410-g19	0.29	1	145.463 ± 0.001	0.524 ± 0.001	2.673 ± 0.001	173.381 ± 0.005	4.325 ± 0.001	[126]
410-g27	0.60	2	152.710 ± 0.002	2.149 ± 0.001	1.792 ± 0.001	173.021 ± 0.001	4.541 ± 0.001	[126]
411-g10	1.64	2	134.297 ± 0.001	0.922 ± 0.001	1.957 ± 0.001	151.257 ± 0.002	3.132 ± 0.001	[126]
411-g3	0.37	3	184.215 ± 0.001	6.386 ± 0.001	2.168 ± 0.001	173.668 ± 0.001	5.861 ± 0.001	[126]
412-g21	0.92	2	157.310 ± 0.008	1.510 ± 0.001	1.963 ± 0.001	175.885 ± 0.001	4.975 ± 0.001	[126]
413-g14	0.56	3	389.127 ± 0.003	2.197 ± 0.001	1.359 ± 0.001	404.245 ± 0.002	67.953 ± 0.001	[126]
413-g16	0.70	2	259.047 ± 0.001	3.197 ± 0.002	1.844 ± 0.001	277.996 ± 0.006	21.093 ± 0.001	[126]
413-g23	0.77	3	156.446 ± 0.001	3.209 ± 0.002	1.620 ± 0.001	212.751 ± 0.001	5.429 ± 0.001	[126]
414-g25	0.70	1	148.578 ± 0.001	1.923 ± 0.001	2.275 ± 0.001	172.825 ± 0.001	4.580 ± 0.001	[126]
414-g8	2.34	2	185.117 ± 0.003	6.815 ± 0.001	0.780 ± 0.001	164.751 ± 0.003	5.003 ± 0.001	[126]
415-g10	0.17	1	109.886 ± 0.001	0.957 ± 0.003	0.551 ± 0.001	129.267 ± 0.005	1.764 ± 0.001	[126]
415-g15	0.10	2	248.585 ± 0.001	0.640 ± 0.001	1.233 ± 0.001	273.078 ± 0.005	19.386 ± 0.001	[126]
415-g28	0.91	5	457.530 ± 0.001	3.669 ± 0.001	1.285 ± 0.001	451.076 ± 0.007	95.855 ± 0.002	[126]
416-g20	0.65	2	279.227 ± 0.001	0.263 ± 0.002	2.276 ± 0.001	306.602 ± 0.007	27.768 ± 0.001	[126]
416-g33	0.49	2	127.363 ± 0.007	1.893 ± 0.001	1.533 ± 0.001	175.473 ± 0.001	3.179 ± 0.001	[126]
416-g37	0.57	2	204.554 ± 0.001	0.854 ± 0.001	1.813 ± 0.001	216.093 ± 0.001	10.400 ± 0.001	[126]
416-g41	0.87	1	138.786 ± 0.001	2.947 ± 0.001	3.076 ± 0.001	149.561 ± 0.001	3.743 ± 0.001	[126]
417-g18	0.55	2	146.906 ± 0.001	1.526 ± 0.005	1.783 ± 0.001	197.136 ± 0.005	4.842 ± 0.001	[126]
418-g15	0.15	2	169.970 ± 0.001	2.052 ± 0.001	1.872 ± 0.001	170.888 ± 0.008	5.584 ± 0.001	[126]
418-g1	0.55	4	233.473 ± 0.001	1.661 ± 0.001	1.439 ± 0.001	240.474 ± 0.006	14.017 ± 0.001	[126]
418-g8	0.23	5	394.119 ± 0.008	1.405 ± 0.001	1.126 ± 0.004	410.229 ± 0.004	69.784 ± 0.006	[126]
419-g3	0.61	4	267.989 ± 0.001	4.435 ± 0.001	1.505 ± 0.001	250.659 ± 0.001	17.051 ± 0.001	[126]
419-g4	0.81	1	165.781 ± 0.001	1.195 ± 0.001	1.851 ± 0.002	182.106 ± 0.004	5.869 ± 0.001	[126]
41-g6	0.55	6	0.740 ± 0.001	13.985 ± 0.001	3.915 ± 0.001	31.5739 ± 0.001	0.018 ± 0.001	[126]
41-g9	1.76	2	248.775 ± 0.006	7.596 ± 0.003	1.371 ± 0.004	237.383 ± 0.001	14.967 ± 0.007	[126]
420-g3	0.28	1	159.143 ± 0.001	0.992 ± 0.001	1.191 ± 0.001	161.587 ± 0.002	4.721 ± 0.001	[126]
422-g10	1.15	1	209.741 ± 0.001	0.501 ± 0.001	1.864 ± 0.001	230.158 ± 0.009	11.807 ± 0.001	[126]
422-g12	0.78	3	263.179 ± 0.001	2.130 ± 0.001	1.448 ± 0.001	274.371 ± 0.002	20.750 ± 0.001	[126]
426-g8	0.46	3	214.354 ± 0.001	4.951 ± 0.001	1.509 ± 0.001	278.931 ± 0.001	13.013 ± 0.001	[126]
427-g14	1.04	2	78.999 ± 0.001	0.435 ± 0.002	2.042 ± 0.001	96.014 ± 0.002	0.691 ± 0.001	[126]
427-g2	0.83	2	201.490 ± 0.001	0.928 ± 0.009	1.854 ± 0.001	213.264 ± 0.001	9.956 ± 0.001	[126]
42-g10	0.13	3	237.414 ± 0.001	1.168 ± 0.001	1.265 ± 0.002	252.252 ± 0.009	15.864 ± 0.001	[126]
42-g3	0.39	1	195.902 ± 0.001	1.475 ± 0.001	2.749 ± 0.001	203.189 ± 0.007	9.386 ± 0.001	[126]
433-g10	0.11	4	282.689 ± 0.001	1.094 ± 0.001	1.245 ± 0.001	280.973 ± 0.009	24.819 ± 0.001	[126]
433-g15	0.77	4	192.085 ± 0.001	2.776 ± 0.001	1.508 ± 0.001	194.469 ± 0.004	7.064 ± 0.001	[126]
433-g17	0.54	6	478.990 ± 0.001	3.155 ± 0.001	2.065 ± 0.001	459.824 ± 0.001	108.782 ± 0.001	[126]
434-g23	0.31	4	373.658 ± 0.001	3.194 ± 0.001	1.267 ± 0.001	367.497 ± 0.004	53.387 ± 0.001	[126]
435-g10	0.66	4	181.747 ± 0.001	2.983 ± 0.001	1.491 ± 0.001	184.867 ± 0.004	5.881 ± 0.001	[126]

Galaxy	$\chi^2_{\rm red}$	n	$\langle V_0 \rangle$ (km s^{-1})	$\langle r_c \rangle$ (kpc)	d	$r_{\rm edge}$ (kpc)	M_T (10^{11} M$_\odot$)	Reference
435-g14	0.42	3	241.200 ± 0.001	4.312 ± 0.003	1.453 ± 0.001	232.517 ± 0.009	13.595 ± 0.001	[126]
435-g19	0.39	3	181.414 ± 0.001	1.535 ± 0.004	1.203 ± 0.002	185.674 ± 0.008	6.591 ± 0.001	[126]
435-g24	0.12	2	172.201 ± 0.001	1.751 ± 0.004	1.926 ± 0.004	183.082 ± 0.001	6.185 ± 0.001	[126]
435-g25	0.36	2	318.931 ± 0.001	12.837 ± 0.003	1.015 ± 0.002	403.78 ± 0.005	39.907 ± 0.002	[126]
435-g34	0.76	2	130.721 ± 0.001	0.913 ± 0.001	1.932 ± 0.004	150.31 ± 0.001	2.947 ± 0.001	[126]
435-g50	0.18	2	90.9706 ± 0.002	1.337 ± 0.002	1.018 ± 0.001	107.969 ± 0.003	0.967 ± 0.001	[126]
435-g51	0.07	2	161.529 ± 0.005	0.756 ± 0.002	0.986 ± 0.003	173.484 ± 0.005	5.126 ± 0.001	[126]
435-g5	0.29	3	283.034 ± 0.001	4.488 ± 0.003	1.202 ± 0.001	267.684 ± 0.005	21.461 ± 0.001	[126]
436-g34	0.49	2	299.509 ± 0.001	2.237 ± 0.001	1.157 ± 0.001	320.177 ± 0.009	32.176 ± 0.001	[126]
436-g39	0.65	5	381.965 ± 0.001	10.485 ± 0.001	1.502 ± 0.003	299.023 ± 0.001	29.916 ± 0.001	[126]
436-g3	0.61	4	328.495 ± 0.001	2.086 ± 0.001	1.378 ± 0.002	339.033 ± 0.009	39.415 ± 0.001	[126]
437-g18	0.18	4	403.547 ± 0.002	2.986 ± 0.001	1.058 ± 0.001	400.929 ± 0.003	68.572 ± 0.001	[126]
437-g22	0.25	1	88.309 ± 0.001	3.354 ± 0.004	3.709 ± 0.001	101.591 ± 0.001	1.173 ± 0.001	[126]
437-g25	0.10	3	194.063 ± 0.002	0.476 ± 0.001	1.161 ± 0.001	195.576 ± 0.005	8.371 ± 0.001	[126]
437-g31	0.26	2	113.239 ± 0.001	1.559 ± 0.004	1.481 ± 0.001	131.742 ± 0.006	1.875 ± 0.001	[126]
437-g35	0.41	9	104.281 ± 0.001	0.083 ± 0.002	3.817 ± 0.003	105.352 ± 0.001	1.308 ± 0.001	[126]
437-g47	0.37	4	194.932 ± 0.002	2.789 ± 0.001	1.295 ± 0.001	195.409 ± 0.007	7.219 ± 0.001	[126]
437-g54	0.31	3	200.000 ± 0.001	2.275 ± 0.002	1.418 ± 0.001	194.399 ± 0.008	8.220 ± 0.001	[126]
437-g71	0.72	5	215.483 ± 0.001	1.865 ± 0.001	1.173 ± 0.001	230.412 ± 0.006	10.828 ± 0.001	[126]
437-g72	0.06	3	17.200 ± 0.001	8.244 ± 0.001	4.577 ± 0.001	59.7863 ± 0.002	0.120 ± 0.001	[126]
438-g15	0.45	3	211.455 ± 0.001	3.375 ± 0.004	1.535 ± 0.001	273.335 ± 0.002	12.932 ± 0.001	[126]
438-g18	0.57	3	202.050 ± 0.001	3.367 ± 0.003	1.677 ± 0.001	193.938 ± 0.001	8.162 ± 0.001	[126]
439-g11	0.38	3	104.112 ± 0.001	1.038 ± 0.001	1.290 ± 0.002	120.708 ± 0.004	1.411 ± 0.001	[126]
439-g18	0.22	2	135.959 ± 0.001	8.390 ± 0.002	3.556 ± 0.001	218.822 ± 0.004	5.862 ± 0.001	[126]
439-g20	0.85	1	183.009 ± 0.001	1.791 ± 0.004	2.449 ± 0.001	189.73 ± 0.006	7.642 ± 0.001	[126]
439-g9	0.26	3	215.078 ± 0.001	9.922 ± 0.002	2.269 ± 0.001	201.729 ± 0.001	9.185 ± 0.001	[126]
43-g8	1.14	2	270.046 ± 0.001	0.599 ± 0.002	1.896 ± 0.001	288.66 ± 0.004	24.350 ± 0.001	[126]
440-g51	0.10	2	120.841 ± 0.003	0.753 ± 0.001	0.950 ± 0.002	137.299 ± 0.009	2.253 ± 0.001	[126]
441-g11	0.48	3	70.668 ± 0.002	1.390 ± 0.002	1.474 ± 0.002	96.1461 ± 0.004	0.498 ± 0.001	[126]
441-g2	0.33	2	123.260 ± 0.001	0.767 ± 0.005	1.610 ± 0.001	142.834 ± 0.002	2.476 ± 0.001	[126]
442-g24	0.65	3	142.219 ± 0.001	2.315 ± 0.004	1.844 ± 0.002	190.967 ± 0.001	4.158 ± 0.001	[126]
442-g2	0.77	5	317.601 ± 0.007	4.782 ± 0.001	1.191 ± 0.004	317.077 ± 0.007	28.822 ± 0.002	[126]
443-g38	0.79	3	310.618 ± 0.001	3.989 ± 0.002	1.464 ± 0.003	310.958 ± 0.003	31.512 ± 0.001	[126]
443-g41	0.58	1	217.644 ± 0.001	1.462 ± 0.002	2.717 ± 0.002	225.249 ± 0.002	12.787 ± 0.001	[126]
443-g42	0.31	4	493.089 ± 0.001	3.783 ± 0.001	0.952 ± 0.001	485.562 ± 0.007	122.999 ± 0.002	[126]
443-g59	0.11	4	199.496 ± 0.001	1.961 ± 0.001	1.263 ± 0.001	190.437 ± 0.002	7.727 ± 0.001	[126]
443-g80	0.85	3	93.805 ± 0.001	1.203 ± 0.003	1.698 ± 0.003	109.108 ± 0.003	1.033 ± 0.001	[126]
444-g14	0.23	5	306.505 ± 0.001	2.002 ± 0.001	1.315 ± 0.003	295.349 ± 0.001	28.826 ± 0.001	[126]
444-g1	0.30	2	35.719 ± 0.001	4.718 ± 0.001	6.413 ± 0.001	86.4928 ± 0.001	0.362 ± 0.001	[126]
444-g21	0.21	4	201.751 ± 0.001	2.550 ± 0.001	1.314 ± 0.001	189.06 ± 0.002	7.561 ± 0.001	[126]
444-g33	0.56	3	65.866 ± 0.001	1.291 ± 0.002	1.676 ± 0.001	62.5484 ± 0.002	0.274 ± 0.001	[126]
444-g47	0.26	4	336.067 ± 0.001	2.973 ± 0.003	1.298 ± 0.001	327.142 ± 0.005	38.296 ± 0.001	[126]
444-g86	0.40	2	223.074 ± 0.001	0.853 ± 0.002	1.338 ± 0.003	241.668 ± 0.001	13.754 ± 0.001	[126]
445-g15	1.24	3	239.760 ± 0.001	2.912 ± 0.003	1.871 ± 0.001	241.738 ± 0.001	14.987 ± 0.001	[126]
445-g19	0.21	2	203.892 ± 0.001	1.527 ± 0.003	1.435 ± 0.001	209.247 ± 0.007	9.810 ± 0.001	[126]
445-g39	1.12	3	353.386 ± 0.001	1.789 ± 0.001	1.615 ± 0.002	353.489 ± 0.007	49.421 ± 0.001	[126]
446-g18	0.91	3	191.370 ± 0.001	4.910 ± 0.002	1.794 ± 0.002	255.971 ± 0.001	9.642 ± 0.001	[126]
446-g1	0.75	3	232.072 ± 0.008	2.864 ± 0.005	1.828 ± 0.002	227.211 ± 0.001	13.124 ± 0.001	[126]
446-g23	0.52	3	211.409 ± 0.004	7.838 ± 0.001	1.999 ± 0.002	273.31 ± 0.001	12.216 ± 0.001	[126]
446-g2	0.53	3	127.539 ± 0.007	4.237 ± 0.002	2.289 ± 0.003	121.814 ± 0.002	2.022 ± 0.001	[126]

Galaxy	$\chi^2_{\rm red}$	n	$\langle V_0 \rangle$ (km s^{-1})	$\langle r_c \rangle$ (kpc)	d	$r_{\rm edge}$ (kpc)	M_T (10^{11} M$_\odot$)	Reference
446-g44	5.62	3	224.131 ± 0.002	1.588 ± 0.002	0.903 ± 0.002	220.127 ± 0.006	11.934 ± 0.001	[126]
446-g51	0.54	2	134.966 ± 0.001	2.279 ± 0.001	1.272 ± 0.001	153.412 ± 0.001	3.028 ± 0.001	[126]
446-g53	0.53	4	85.677 ± 0.002	0.828 ± 0.001	1.480 ± 0.001	99.481 ± 0.006	0.769 ± 0.001	[126]
446-g58	0.08	6	270.916 ± 0.001	0.249 ± 0.001	2.441 ± 0.001	320.076 ± 0.004	26.966 ± 0.001	[126]
447-g17	0.76	5	311.868 ± 0.001	1.544 ± 0.001	2.933 ± 0.001	324.417 ± 0.001	34.972 ± 0.001	[126]
447-g19	0.05	1	172.352 ± 0.001	4.563 ± 0.001	2.547 ± 0.002	195.680 ± 0.007	7.361 ± 0.001	[126]
447-g21	0.26	3	291.092 ± 0.004	5.721 ± 0.001	1.695 ± 0.001	276.630 ± 0.009	23.685 ± 0.001	[126]
447-g23	0.38	3	211.042 ± 0.001	1.807 ± 0.001	1.666 ± 0.001	208.549 ± 0.001	10.149 ± 0.001	[126]
448-g13	0.21	1	222.259 ± 0.003	1.277 ± 0.002	1.842 ± 0.001	227.377 ± 0.004	13.153 ± 0.001	[126]
44-g13	0.11	1	69.007 ± 0.001	7.226 ± 0.001	9.087 ± 0.004	158.626 ± 0.001	2.240 ± 0.001	[126]
44-g1	0.92	3	161.490 ± 0.004	2.421 ± 0.001	1.795 ± 0.004	172.530 ± 0.001	4.775 ± 0.001	[126]
452-g8	0.42	3	167.222 ± 0.001	3.625 ± 0.001	1.561 ± 0.001	224.671 ± 0.004	6.477 ± 0.001	[126]
459-g14	0.36	2	139.005 ± 0.001	1.585 ± 0.001	1.356 ± 0.001	160.576 ± 0.001	3.452 ± 0.001	[126]
459-g6	0.41	4	447.981 ± 0.004	2.022 ± 0.001	1.480 ± 0.001	444.347 ± 0.003	98.163 ± 0.001	[126]
460-g29	0.24	2	201.285 ± 0.003	7.655 ± 0.001	2.904 ± 0.001	292.301 ± 0.001	14.690 ± 0.001	[126]
460-g31	0.66	3	264.379 ± 0.003	5.376 ± 0.001	1.743 ± 0.003	354.589 ± 0.009	26.032 ± 0.001	[126]
460-g8	0.14	1	164.436 ± 0.001	2.269 ± 0.001	1.824 ± 0.001	168.905 ± 0.007	5.392 ± 0.001	[126]
461-g10	0.79	4	275.042 ± 0.001	7.959 ± 0.001	1.471 ± 0.003	342.608 ± 0.001	23.016 ± 0.001	[126]
461-g25	0.47	1	114.932 ± 0.001	2.919 ± 0.001	3.630 ± 0.001	127.607 ± 0.001	2.325 ± 0.001	[126]
461-g3	0.28	1	73.887 ± 0.003	5.405 ± 0.001	9.713 ± 0.001	122.668 ± 0.001	2.065 ± 0.001	[126]
461-g44	0.21	4	503.137 ± 0.001	4.129 ± 0.001	1.303 ± 0.001	495.559 ± 0.009	131.278 ± 0.003	[126]
462-g16	0.61	3	162.529 ± 0.001	2.539 ± 0.001	1.579 ± 0.001	223.679 ± 0.004	6.311 ± 0.001	[126]
463-g25	0.64	3	266.120 ± 0.001	8.867 ± 0.001	1.882 ± 0.001	336.366 ± 0.006	23.747 ± 0.001	[126]
466-g13	0.98	3	214.067 ± 0.001	4.655 ± 0.001	1.726 ± 0.001	280.166 ± 0.001	13.346 ± 0.001	[126]
466-g14	0.17	1	26.849 ± 0.001	4.164 ± 0.001	13.484 ± 0.001	62.7647 ± 0.001	0.277 ± 0.001	[126]
466-g27	1.29	4	440.048 ± 0.001	2.198 ± 0.001	1.533 ± 0.001	450.260 ± 0.003	95.703 ± 0.001	[126]
466-g28	0.81	3	73.537 ± 0.001	11.829 ± 0.003	2.523 ± 0.001	105.318 ± 0.001	0.654 ± 0.001	[126]
466-g5	0.22	3	179.513 ± 0.001	1.254 ± 0.003	1.502 ± 0.001	185.368 ± 0.003	6.584 ± 0.001	[126]
467-g11	0.65	4	334.593 ± 0.001	5.936 ± 0.001	1.178 ± 0.001	315.827 ± 0.004	32.236 ± 0.001	[126]
467-g23	0.07	2	232.296 ± 0.001	3.411 ± 0.001	1.884 ± 0.001	233.020 ± 0.006	14.157 ± 0.001	[126]
467-g27	0.77	3	221.297 ± 0.001	2.417 ± 0.001	1.786 ± 0.001	223.117 ± 0.003	11.824 ± 0.001	[126]
467-g36	0.80	9	178.557 ± 0.001	0.044 ± 0.001	3.713 ± 0.001	190.119 ± 0.001	7.009 ± 0.001	[126]
468-g11	0.28	2	180.550 ± 0.001	0.622 ± 0.002	1.051 ± 0.001	182.231 ± 0.005	6.771 ± 0.001	[126]
468-g23	0.43	4	217.296 ± 0.001	2.713 ± 0.001	1.303 ± 0.001	216.593 ± 0.003	10.162 ± 0.001	[126]
46-g8	0.45	4	219.458 ± 0.001	2.745 ± 0.002	1.293 ± 0.001	216.521 ± 0.003	10.337 ± 0.001	[126]
471-g2	0.37	1	180.659 ± 0.001	6.295 ± 0.002	2.765 ± 0.001	197.046 ± 0.008	8.560 ± 0.001	[126]
472-g10	0.10	3	2.073 ± 0.001	13.168 ± 0.001	8.814 ± 0.001	59.803 ± 0.001	0.12 ± 0.	[126]
474-g39	0.06	2	208.348 ± 0.001	2.777 ± 0.001	1.146 ± 0.001	204.916 ± 0.007	9.627 ± 0.001	[126]
474-g5	0.32	3	152.009 ± 0.001	4.971 ± 0.001	1.682 ± 0.001	159.410 ± 0.001	3.485 ± 0.001	[126]
476-g15	8.72	2	170.336 ± 0.004	1.541 ± 0.001	1.023 ± 0.002	238.804 ± 0.005	7.756 ± 0.001	[126]
476-g16	0.96	3	234.095 ± 0.001	5.473 ± 0.001	1.828 ± 0.001	305.483 ± 0.002	17.388 ± 0.001	[126]
476-g25	0.08	2	197.258 ± 0.001	3.880 ± 0.001	2.016 ± 0.001	198.060 ± 0.009	8.693 ± 0.001	[126]
476-g5	0.34	3	333.392 ± 0.001	4.473 ± 0.001	1.541 ± 0.001	330.071 ± 0.007	38.488 ± 0.002	[126]
477-g16	0.26	2	114.884 ± 0.001	1.284 ± 0.001	1.596 ± 0.001	132.032 ± 0.006	1.959 ± 0.001	[126]
477-g18	0.75	2	191.945 ± 0.001	0.925 ± 0.001	1.762 ± 0.001	204.535 ± 0.001	8.647 ± 0.001	[126]
478-g11	4.49	4	155.380 ± 0.005	0.832 ± 0.001	1.079 ± 0.001	152.619 ± 0.004	3.978 ± 0.001	[126]
47-g10	0.08	4	413.974 ± 0.001	4.945 ± 0.001	1.100 ± 0.001	403.484 ± 0.007	68.229 ± 0.005	[126]
481-g11	0.26	2	149.124 ± 0.005	2.296 ± 0.004	1.262 ± 0.001	166.055 ± 0.001	4.018 ± 0.001	[126]
481-g13	5.95	2	190.988 ± 0.003	2.943 ± 0.001	1.359 ± 0.003	268.286 ± 0.009	10.837 ± 0.002	[126]
481-g21	2.01	6	288.754 ± 0.002	1.478 ± 0.001	1.054 ± 0.001	277.854 ± 0.009	24.001 ± 0.001	[126]

Galaxy	$\chi^2_{\rm red}$	n	$\langle V_0 \rangle$ (km s^{-1})	$\langle r_c \rangle$ (kpc)	d	$r_{\rm edge}$ (kpc)	M_T (10^{11} M$_\odot$)	Reference
481-g2	2.05	2	189.128 ± 0.003	2.988 ± 0.003	1.081 ± 0.003	263.969 ± 0.004	10.306 ± 0.001	[126]
481-g30	0.51	3	142.240 ± 0.002	2.674 ± 0.006	1.062 ± 0.002	150.445 ± 0.005	2.989 ± 0.001	[126]
482-g16	0.98	1	61.019 ± 0.001	0.811 ± 0.001	4.752 ± 0.001	80.050 ± 0.001	0.392 ± 0.001	[126]
482-g1	0.29	2	160.170 ± 0.001	1.190 ± 0.001	1.404 ± 0.001	174.906 ± 0.001	5.066 ± 0.001	[126]
482-g35	0.37	3	172.249 ± 0.001	2.377 ± 0.001	1.537 ± 0.001	178.022 ± 0.009	5.548 ± 0.001	[126]
482-g41	0.36	1	53.051 ± 0.001	3.198 ± 0.001	9.571 ± 0.001	94.848 ± 0.008	0.688 ± 0.001	[126]
482-g43	0.04	3	226.276 ± 0.001	3.159 ± 0.002	1.619 ± 0.001	223.287 ± 0.003	11.997 ± 0.001	[126]
482-g46	0.67	3	100.214 ± 0.001	2.119 ± 0.001	1.707 ± 0.001	137.022 ± 0.003	1.439 ± 0.001	[126]
483-g12	1.27	3	170.022 ± 0.001	1.426 ± 0.001	1.871 ± 0.001	168.739 ± 0.001	5.376 ± 0.001	[126]
483-g2	0.58	4	202.214 ± 0.001	3.829 ± 0.001	1.474 ± 0.001	251.538 ± 0.002	9.997 ± 0.001	[126]
483-g6	0.74	1	140.371 ± 0.005	1.668 ± 0.001	2.265 ± 0.004	145.438 ± 0.001	3.442 ± 0.001	[126]
484-g25	0.06	3	264.940 ± 0.001	0.951 ± 0.001	1.037 ± 0.001	265.352 ± 0.007	20.905 ± 0.001	[126]
485-g12	0.64	4	262.224 ± 0.004	3.294 ± 0.001	1.497 ± 0.001	254.602 ± 0.005	17.489 ± 0.001	[126]
485-g24	0.05	5	174.410 ± 0.001	0.569 ± 0.001	1.454 ± 0.002	173.137 ± 0.007	5.807 ± 0.001	[126]
485-g4	0.23	3	158.524 ± 0.001	2.602 ± 0.001	1.423 ± 0.001	216.690 ± 0.002	5.744 ± 0.001	[126]
487-g19	0.83	3	87.385 ± 0.001	0.791 ± 0.001	1.782 ± 0.001	103.437 ± 0.003	0.872 ± 0.001	[126]
487-g2	0.17	3	300.997 ± 0.001	2.108 ± 0.001	1.232 ± 0.001	297.208 ± 0.007	29.374 ± 0.001	[126]
488-g44	0.80	4	175.569 ± 0.001	1.620 ± 0.001	1.532 ± 0.001	181.080 ± 0.002	5.845 ± 0.001	[126]
488-g54	0.26	4	462.072 ± 0.001	3.147 ± 0.001	1.358 ± 0.001	469.192 ± 0.009	107.141 ± 0.003	[126]
489-g11	0.98	2	86.6872 ± 0.001	1.949 ± 0.001	2.121 ± 0.001	119.137 ± 0.001	1.021 ± 0.001	[126]
489-g26	1.27	3	280.767 ± 0.001	1.692 ± 0.001	2.446 ± 0.001	282.768 ± 0.001	25.297 ± 0.	[126]
489-g47	0.24	1	162.144 ± 0.002	2.412 ± 0.001	3.215 ± 0.001	186.052 ± 0.001	6.176 ± 0.001	[126]
489-g6	0.44	3	145.042 ± 0.001	1.957 ± 0.001	1.626 ± 0.001	158.903 ± 0.008	3.554 ± 0.001	[126]
48-g8	0.66	1	197.023 ± 0.001	1.685 ± 0.001	1.987 ± 0.001	275.529 ± 0.002	12.576 ± 0.001	[126]
490-g10	0.82	5	299.978 ± 0.001	3.546 ± 0.002	1.266 ± 0.001	309.508 ± 0.003	26.750 ± 0.002	[126]
490-g14	0.31	3	133.605 ± 0.001	3.351 ± 0.001	1.702 ± 0.001	176.363 ± 0.002	3.217 ± 0.001	[126]
490-g28	0.41	5	165.078 ± 0.002	2.251 ± 0.002	1.251 ± 0.002	181.085 ± 0.001	4.661 ± 0.001	[126]
490-g36	0.28	5	739.947 ± 0.002	3.707 ± 0.001	1.114 ± 0.001	925.984 ± 0.006	549.596 ± 0.007	[126]
490-g45	0.36	4	186.817 ± 0.002	2.567 ± 0.001	1.407 ± 0.001	174.245 ± 0.003	5.919 ± 0.001	[126]
496-g19	0.49	4	204.051 ± 0.001	2.626 ± 0.002	1.526 ± 0.001	207.565 ± 0.001	8.675 ± 0.001	[126]
497-g14	1.58	1	224.145 ± 0.001	0.346 ± 0.002	2.041 ± 0.001	228.839 ± 0.007	13.408 ± 0.001	[126]
497-g18	0.72	4	386.056 ± 0.001	6.536 ± 0.004	1.570 ± 0.001	516.825 ± 0.006	77.500 ± 0.001	[126]
497-g34	0.38	2	205.978 ± 0.002	0.818 ± 0.001	1.467 ± 0.001	229.266 ± 0.006	11.144 ± 0.001	[126]
498-g3	0.51	4	257.135 ± 0.001	1.134 ± 0.003	1.580 ± 0.001	273.902 ± 0.009	20.066 ± 0.001	[126]
499-g22	0.39	3	124.660 ± 0.001	1.195 ± 0.004	1.610 ± 0.001	140.758 ± 0.006	2.388 ± 0.001	[126]
499-g26	0.69	5	401.061 ± 0.001	6.484 ± 0.001	1.210 ± 0.001	369.067 ± 0.005	51.420 ± 0.001	[126]
499-g39	0.59	1	176.223 ± 0.001	0.689 ± 0.001	1.543 ± 0.001	190.814 ± 0.007	6.892 ± 0.001	[126]
499-g4	0.50	9	143.231 ± 0.001	0.144 ± 0.001	3.566 ± 0.002	159.971 ± 0.002	3.735 ± 0.001	[126]
499-g5	7.49	1	148.020 ± 0.002	1.097 ± 0.001	1.927 ± 0.005	214.268 ± 0.005	5.503 ± 0.001	[126]
4-g19	0.86	3	133.628 ± 0.001	1.078 ± 0.001	1.843 ± 0.001	150.652 ± 0.009	2.986 ± 0.001	[126]
501-g11	0.14	1	82.9424 ± 0.001	4.085 ± 0.001	4.275 ± 0.002	115.438 ± 0.002	1.269 ± 0.001	[126]
501-g1	0.26	1	91.1524 ± 0.001	2.099 ± 0.001	2.122 ± 0.001	112.883 ± 0.002	1.136 ± 0.001	[126]
501-g68	1.21	2	138.794 ± 0.001	1.424 ± 0.003	2.068 ± 0.001	155.582 ± 0.008	3.436 ± 0.001	[126]
501-g69	0.31	5	486.018 ± 0.001	3.878 ± 0.001	1.122 ± 0.001	468.783 ± 0.008	111.538 ± 0.003	[126]
501-g75	0.72	3	196.471 ± 0.001	3.390 ± 0.001	1.731 ± 0.009	262.543 ± 0.001	10.792 ± 0.005	[126]
501-g80	0.67	6	717.740 ± 0.001	3.111 ± 0.001	1.000 ± 0.001	981.351 ± 0.007	548.231 ± 0.005	[126]
501-g86	0.09	3	256.229 ± 0.006	2.460 ± 0.002	1.426 ± 0.001	266.557 ± 0.001	18.873 ± 0.001	[126]
501-g97	0.27	1	207.479 ± 0.001	0.885 ± 0.003	1.143 ± 0.001	210.843 ± 0.003	10.487 ± 0.001	[126]
502-g12	0.09	3	167.799 ± 0.001	0.716 ± 0.001	1.075 ± 0.001	178.473 ± 0.002	5.620 ± 0.001	[126]
502-g13	0.71	3	138.467 ± 0.001	1.896 ± 0.001	1.831 ± 0.001	134.986 ± 0.001	2.752 ± 0.001	[126]

Galaxy	$\chi^2_{\rm red}$	n	$\langle V_0 \rangle$ (km s^{-1})	$\langle r_c \rangle$ (kpc)	d	$r_{\rm edge}$ (kpc)	M_T (10^{11} M$_\odot$)	Reference
502-g2	1.00	2	200.963 ± 0.001	0.517 ± 0.003	1.938 ± 0.001	221.418 ± 0.004	10.342 ± 0.001	[126]
503-g22	0.66	5	66.306 ± 0.001	0.112 ± 0.001	0.001 ± 0.001	81.126 ± 0.005	0.402 ± 0.	[126]
505-g8	0.68	4	145.947 ± 0.001	1.092 ± 0.001	1.362 ± 0.001	156.352 ± 0.003	3.550 ± 0.001	[126]
506-g4	1.07	1	197.026 ± 0.001	4.008 ± 0.001	3.487 ± 0.002	229.780 ± 0.004	11.755 ± 0.001	[126]
507-g11	0.17	1	199.689 ± 0.001	3.688 ± 0.001	2.109 ± 0.001	212.797 ± 0.006	10.243 ± 0.001	[126]
507-g2	0.17	2	9.900 ± 0.007	7.936 ± 0.001	9.580 ± 0.002	67.871 ± 0.001	0.175 ± 0.001	[126]
507-g56	0.25	3	272.108 ± 0.001	4.144 ± 0.001	1.553 ± 0.001	267.393 ± 0.005	20.495 ± 0.001	[126]
507-g62	0.35	3	215.395 ± 0.001	1.740 ± 0.001	1.413 ± 0.001	217.938 ± 0.009	11.009 ± 0.001	[126]
508-g11	0.57	3	138.241 ± 0.001	4.548 ± 0.001	1.473 ± 0.003	174.071 ± 0.002	3.169 ± 0.001	[126]
508-g60	0.03	4	341.162 ± 0.003	9.293 ± 0.001	1.416 ± 0.001	294.430 ± 0.006	27.581 ± 0.005	[126]
509-g35	0.22	1	13.720 ± 0.001	5.498 ± 0.001	30.135 ± 0.001	81.884 ± 0.001	0.307 ± 0.001	[126]
509-g44	0.05	1	239.677 ± 0.004	3.314 ± 0.001	1.014 ± 0.001	255.728 ± 0.008	16.646 ± 0.001	[126]
509-g45	0.64	3	158.069 ± 0.001	3.662 ± 0.001	1.643 ± 0.001	206.244 ± 0.009	5.285 ± 0.001	[126]
509-g74	0.47	4	372.991 ± 0.001	4.137 ± 0.001	1.405 ± 0.001	354.194 ± 0.003	49.717 ± 0.001	[126]
509-g91	0.18	3	174.882 ± 0.001	1.688 ± 0.002	0.935 ± 0.004	169.493 ± 0.008	5.448 ± 0.003	[126]
511-g46	0.34	3	146.852 ± 0.002	3.255 ± 0.001	1.742 ± 0.001	158.148 ± 0.001	3.463 ± 0.001	[126]
512-g12	0.27	2	35.390 ± 0.001	7.673 ± 0.001	5.595 ± 0.001	94.5044 ± 0.004	0.472 ± 0.001	[126]
514-g10	0.27	3	211.218 ± 0.001	2.348 ± 0.004	1.571 ± 0.001	215.206 ± 0.005	10.284 ± 0.001	[126]
515-g13	1.09	1	326.956 ± 0.001	3.201 ± 0.002	1.656 ± 0.001	337.334 ± 0.004	42.135 ± 0.002	[126]
515-g3	0.96	4	502.325 ± 0.001	4.809 ± 0.001	1.511 ± 0.001	490.848 ± 0.002	128.346 ± 0.001	[126]
516-g8	0.60	5	645.369 ± 0.001	4.427 ± 0.001	1.217 ± 0.001	625.429 ± 0.006	268.554 ± 0.004	[126]
51-g18	0.78	2	78.423 ± 0.001	0.866 ± 0.001	1.800 ± 0.001	98.0238 ± 0.001	0.685 ± 0.001	[126]
526-g11	0.59	3	143.251 ± 0.001	2.589 ± 0.001	1.502 ± 0.001	157.002 ± 0.001	3.300 ± 0.001	[126]
527-g11	0.46	2	199.697 ± 0.001	4.943 ± 0.002	2.053 ± 0.001	276.175 ± 0.001	12.484 ± 0.001	[126]
527-g19	0.85	5	710.670 ± 0.001	6.562 ± 0.001	1.218 ± 0.001	667.704 ± 0.007	332.013 ± 0.004	[126]
527-g21	0.62	4	203.372 ± 0.001	1.325 ± 0.001	1.493 ± 0.001	199.271 ± 0.003	8.854 ± 0.001	[126]
528-g17	0.45	3	155.867 ± 0.001	4.279 ± 0.001	1.474 ± 0.001	207.324 ± 0.003	4.993 ± 0.001	[126]
528-g34	0.65	2	150.907 ± 0.001	1.162 ± 0.001	1.339 ± 0.002	168.837 ± 0.004	4.332 ± 0.001	[126]
530-g34	0.57	2	212.134 ± 0.003	1.440 ± 0.001	1.646 ± 0.002	226.067 ± 0.001	11.579 ± 0.001	[126]
531-g22	3.84	3	293.244 ± 0.006	2.805 ± 0.001	1.014 ± 0.002	284.812 ± 0.004	25.850 ± 0.002	[126]
531-g25	0.12	4	424.433 ± 0.002	3.916 ± 0.002	1.093 ± 0.001	420.164 ± 0.003	77.616 ± 0.001	[126]
532-g14	0.49	6	567.021 ± 0.002	3.721 ± 0.001	1.069 ± 0.001	773.485 ± 0.005	260.561 ± 0.005	[126]
533-g37	0.44	5	306.581 ± 0.001	1.826 ± 0.001	1.144 ± 0.003	310.039 ± 0.009	30.596 ± 0.002	[126]
533-g48	0.13	3	149.974 ± 0.002	0.376 ± 0.005	0.001 ± 0.001	166.625 ± 0.008	4.221 ± 0.001	[126]
533-g4	0.64	2	218.739 ± 0.001	2.720 ± 0.003	0.993 ± 0.004	214.775 ± 0.004	11.085 ± 0.003	[126]
533-g53	22.84	3	238.706 ± 0.001	1.582 ± 0.001	1.181 ± 0.001	245.073 ± 0.008	15.300 ± 0.001	[126]
533-g6	1.03	1	172.040 ± 0.002	0.850 ± 0.001	2.289 ± 0.001	176.658 ± 0.005	6.169 ± 0.001	[126]
533-g8	0.54	4	367.585 ± 0.001	1.714 ± 0.001	1.465 ± 0.001	364.213 ± 0.005	54.057 ± 0.001	[126]
534-g24	0.58	4	306.565 ± 0.001	2.550 ± 0.001	1.460 ± 0.001	310.971 ± 0.002	30.796 ± 0.001	[126]
534-g31	0.45	4	269.543 ± 0.002	4.286 ± 0.006	1.494 ± 0.001	252.241 ± 0.001	17.482 ± 0.003	[126]
534-g3	0.06	4	226.489 ± 0.007	1.049 ± 0.001	1.144 ± 0.001	223.752 ± 0.008	12.534 ± 0.001	[126]
534-g9	0.80	3	206.611 ± 0.001	2.732 ± 0.001	1.939 ± 0.001	288.750 ± 0.001	13.537 ± 0.001	[126]
535-g15	0.27	4	258.423 ± 0.001	0.727 ± 0.001	1.354 ± 0.001	258.812 ± 0.009	19.397 ± 0.001	[126]
539-g14	0.47	4	286.078 ± 0.001	4.724 ± 0.001	1.415 ± 0.001	287.439 ± 0.001	22.459 ± 0.001	[126]
539-g5	0.14	2	172.677 ± 0.001	1.987 ± 0.002	1.633 ± 0.006	172.715 ± 0.009	5.765 ± 0.002	[126]
53-g2	0.11	2	159.901 ± 0.001	6.728 ± 0.001	1.612 ± 0.004	152.779 ± 0.002	3.990 ± 0.001	[126]
540-g10	0.61	3	144.719 ± 0.004	1.458 ± 0.001	1.296 ± 0.004	157.632 ± 0.002	3.542 ± 0.001	[126]
540-g16	8.72	3	136.988 ± 0.004	3.570 ± 0.001	1.489 ± 0.002	183.237 ± 0.001	3.442 ± 0.001	[126]
541-g1	0.79	2	221.147 ± 0.004	3.358 ± 0.001	1.741 ± 0.001	294.120 ± 0.001	16.188 ± 0.001	[126]
541-g4	0.58	4	293.537 ± 0.001	2.901 ± 0.001	1.459 ± 0.001	281.345 ± 0.007	24.917 ± 0.001	[126]
543-g12	6.87	4	220.515 ± 0.009	0.785 ± 0.001	1.318 ± 0.002	219.749 ± 0.009	11.873 ± 0.001	[126]

Galaxy	$\chi^2_{\rm red}$	n	$\langle V_0 \rangle$ (km s^{-1})	$\langle r_c \rangle$ (kpc)	d	$r_{\rm edge}$ (kpc)	M_T (10^{11} M$_\odot$)	Reference
544-g27	0.64	3	127.403 ± 0.001	1.607 ± 0.001	1.575 ± 0.001	142.901 ± 0.008	2.479 ± 0.001	[126]
544-g32	0.69	4	287.349 ± 0.001	4.865 ± 0.001	1.471 ± 0.001	266.242 ± 0.004	20.635 ± 0.001	[126]
545-g11	0.79	1	179.674 ± 0.001	0.393 ± 0.001	1.519 ± 0.001	193.690 ± 0.004	7.270 ± 0.001	[126]
545-g21	0.71	1	153.322 ± 0.003	2.533 ± 0.001	2.565 ± 0.001	181.464 ± 0.001	5.239 ± 0.001	[126]
545-g3	0.63	4	85.718 ± 0.002	0.836 ± 0.002	1.382 ± 0.001	107.551 ± 0.005	0.835 ± 0.001	[126]
545-g5	0.70	4	279.242 ± 0.004	2.311 ± 0.002	1.147 ± 0.005	274.892 ± 0.009	22.290 ± 0.003	[126]
546-g15	0.15	1	338.037 ± 0.004	2.364 ± 0.003	0.928 ± 0.001	361.046 ± 0.004	47.243 ± 0.002	[126]
546-g29	0.27	3	207.337 ± 0.002	5.207 ± 0.001	1.697 ± 0.001	205.417 ± 0.003	8.670 ± 0.001	[126]
546-g31	0.41	2	209.665 ± 0.001	2.272 ± 0.003	1.678 ± 0.001	226.026 ± 0.007	11.194 ± 0.001	[126]
546-g36	0.65	3	106.714 ± 0.001	1.551 ± 0.001	1.423 ± 0.001	120.781 ± 0.005	1.441 ± 0.001	[126]
546-g37	1.00	1	73.453 ± 0.001	0.609 ± 0.004	2.364 ± 0.001	92.396 ± 0.002	0.592 ± 0.001	[126]
547-g14	1.09	3	179.226 ± 0.001	0.302 ± 0.001	2.724 ± 0.001	182.224 ± 0.001	6.770 ± 0.001	[126]
547-g1	0.52	3	118.047 ± 0.001	1.610 ± 0.004	1.382 ± 0.001	133.529 ± 0.001	1.958 ± 0.001	[126]
547-g24	0.43	2	93.544 ± 0.001	0.389 ± 0.001	1.812 ± 0.001	94.827 ± 0.005	0.954 ± 0.001	[126]
547-g31	0.35	1	147.554 ± 0.001	0.202 ± 0.002	0.946 ± 0.001	150.176 ± 0.008	3.790 ± 0.001	[126]
547-g32	0.06	1	150.359 ± 0.001	2.436 ± 0.001	2.187 ± 0.001	177.276 ± 0.009	4.823 ± 0.001	[126]
547-g4	0.60	3	80.806 ± 0.001	0.496 ± 0.004	1.360 ± 0.001	80.239 ± 0.006	0.578 ± 0.001	[126]
548-g21	0.93	6	1127.770 ± 0.001	3.974 ± 0.001	0.928 ± 0.001	1131.290 ± 0.006	1547.134 ± 0.002	[126]
548-g31	0.54	4	190.749 ± 0.002	0.078 ± 0.001	1.768 ± 0.001	215.975 ± 0.005	9.099 ± 0.001	[126]
548-g32	0.81	4	113.791 ± 0.006	1.143 ± 0.002	1.035 ± 0.004	129.143 ± 0.006	1.722 ± 0.001	[126]
548-g50	0.13	5	111.333 ± 0.002	1.075 ± 0.001	1.403 ± 0.001	104.450 ± 0.009	1.275 ± 0.001	[126]
548-g63	0.16	1	2.818 ± 0.003	3.242 ± 0.001	97.890 ± 0.002	47.620 ± 0.003	0.060 ± 0.001	[126]
548-g71	0.17	5	424.073 ± 0.002	2.220 ± 0.001	1.138 ± 0.001	430.055 ± 0.002	82.213 ± 0.001	[126]
548-g77	0.14	2	94.976 ± 0.001	0.862 ± 0.001	1.025 ± 0.001	111.246 ± 0.004	1.115 ± 0.001	[126]
549-g18	0.92	4	242.520 ± 0.001	3.393 ± 0.003	1.541 ± 0.001	230.117 ± 0.005	13.282 ± 0.001	[126]
549-g22	0.54	3	211.570 ± 0.001	2.156 ± 0.001	1.391 ± 0.001	211.387 ± 0.009	10.111 ± 0.001	[126]
549-g40	0.36	2	213.452 ± 0.001	4.927 ± 0.001	2.444 ± 0.001	218.471 ± 0.001	11.667 ± 0.001	[126]
54-g21	0.60	1	57.192 ± 0.009	0.553 ± 0.001	1.169 ± 0.001	57.919 ± 0.001	0.217 ± 0.001	[126]
550-g7	0.59	4	140.117 ± 0.002	1.902 ± 0.001	1.434 ± 0.001	150.402 ± 0.005	2.950 ± 0.001	[126]
550-g9	0.22	3	199.155 ± 0.001	2.099 ± 0.002	1.229 ± 0.001	198.484 ± 0.007	8.328 ± 0.001	[126]
551-g13	0.81	5	736.731 ± 0.001	8.154 ± 0.002	1.250 ± 0.001	685.541 ± 0.007	354.556 ± 0.007	[126]
551-g31	0.45	5	323.158 ± 0.001	1.725 ± 0.004	1.217 ± 0.001	314.381 ± 0.002	34.766 ± 0.001	[126]
552-g43	0.52	2	184.393 ± 0.001	3.238 ± 0.002	1.400 ± 0.001	192.356 ± 0.004	7.087 ± 0.001	[126]
553-g26	0.76	4	434.331 ± 0.001	7.698 ± 0.001	1.470 ± 0.001	398.893 ± 0.005	69.815 ± 0.002	[126]
553-g3	0.54	3	207.759 ± 0.001	1.729 ± 0.001	1.658 ± 0.001	214.559 ± 0.006	10.159 ± 0.001	[126]
554-g10	0.82	2	221.504 ± 0.001	0.432 ± 0.001	1.978 ± 0.002	225.335 ± 0.005	12.802 ± 0.001	[126]
554-g19	0.29	3	161.497 ± 0.001	0.493 ± 0.001	1.296 ± 0.001	175.537 ± 0.005	5.192 ± 0.001	[126]
554-g24	0.42	3	166.686 ± 0.001	1.013 ± 0.001	1.390 ± 0.001	175.888 ± 0.009	5.414 ± 0.001	[126]
554-g28	0.65	5	279.243 ± 0.001	1.832 ± 0.001	1.215 ± 0.001	282.442 ± 0.009	22.932 ± 0.001	[126]
554-g29	0.57	5	486.027 ± 0.007	5.399 ± 0.001	1.231 ± 0.001	461.337 ± 0.007	104.076 ± 0.006	[126]
554-g34	0.12	2	201.949 ± 0.001	3.512 ± 0.001	1.737 ± 0.001	200.941 ± 0.002	9.078 ± 0.001	[126]
555-g16	8.40	2	252.860 ± 0.003	2.678 ± 0.001	1.660 ± 0.001	258.457 ± 0.007	18.585 ± 0.002	[126]
555-g29	0.41	4	306.351 ± 0.001	2.618 ± 0.001	1.368 ± 0.001	305.903 ± 0.002	30.027 ± 0.001	[126]
555-g2	0.75	5	143.238 ± 0.001	0.079 ± 0.001	1.893 ± 0.001	159.430 ± 0.002	3.775 ± 0.001	[126]
555-g8	0.44	4	332.883 ± 0.001	2.525 ± 0.001	1.059 ± 0.001	328.335 ± 0.009	38.087 ± 0.001	[126]
556-g23	0.06	1	164.777 ± 0.001	1.645 ± 0.001	0.909 ± 0.001	177.722 ± 0.007	5.487 ± 0.001	[126]
556-g5	0.85	1	142.787 ± 0.001	1.352 ± 0.001	2.129 ± 0.001	147.137 ± 0.007	3.564 ± 0.001	[126]
55-g29	0.09	2	180.017 ± 0.001	2.597 ± 0.001	1.599 ± 0.002	179.045 ± 0.007	6.422 ± 0.001	[126]
55-g4	0.16	4	9.900 ± 0.002	11.480 ± 0.002	3.940 ± 0.001	51.522 ± 0.001	0.077 ± 0.001	[126]
562-g14	0.49	3	254.651 ± 0.001	3.640 ± 0.001	1.708 ± 0.001	246.780 ± 0.001	16.816 ± 0.001	[126]

Galaxy	$\chi^2_{\rm red}$	n	$\langle V_0 \rangle$ (km s^{-1})	$\langle r_c \rangle$ (kpc)	d	$r_{\rm edge}$ (kpc)	M_T (10^{11} M$_\odot$)	Reference
563-g11	0.91	1	236.122 ± 0.001	1.870 ± 0.001	1.927 ± 0.001	254.211 ± 0.007	16.673 ± 0.001	[126]
563-g13	0.80	3	162.740 ± 0.001	2.240 ± 0.001	1.870 ± 0.001	224.939 ± 0.009	6.505 ± 0.001	[126]
563-g14	2.41	2	205.195 ± 0.005	1.645 ± 0.003	1.000 ± 0.006	213.349 ± 0.001	9.976 ± 0.002	[126]
563-g17	0.62	3	321.921 ± 0.001	1.890 ± 0.001	1.734 ± 0.001	339.040 ± 0.007	39.294 ± 0.001	[126]
563-g21	0.36	2	331.855 ± 0.001	4.848 ± 0.001	1.645 ± 0.001	335.289 ± 0.001	40.990 ± 0.001	[126]
563-g28	0.11	6	521.514 ± 0.002	1.481 ± 0.001	1.323 ± 0.001	516.073 ± 0.002	153.786 ± 0.001	[126]
564-g20	8.22	4	241.411 ± 0.002	3.323 ± 0.002	1.275 ± 0.001	326.210 ± 0.008	19.420 ± 0.001	[126]
564-g23	0.35	3	195.069 ± 0.008	4.179 ± 0.001	1.509 ± 0.001	263.736 ± 0.003	10.332 ± 0.001	[126]
564-g31	0.76	3	193.772 ± 0.004	3.222 ± 0.006	1.783 ± 0.001	265.032 ± 0.003	10.677 ± 0.001	[126]
564-g35	0.33	4	207.378 ± 0.005	0.894 ± 0.001	1.442 ± 0.001	205.884 ± 0.009	9.765 ± 0.001	[126]
564-g36	0.31	1	54.433 ± 0.003	4.279 ± 0.003	9.662 ± 0.002	115.177 ± 0.001	0.939 ± 0.001	[126]
566-g14	0.11	2	159.745 ± 0.001	2.817 ± 0.001	1.524 ± 0.001	157.606 ± 0.009	4.380 ± 0.001	[126]
566-g22	3.55	3	180.345 ± 0.003	0.506 ± 0.003	0.993 ± 0.001	181.279 ± 0.004	6.665 ± 0.001	[126]
566-g26	6.09	2	227.765 ± 0.005	1.014 ± 0.001	1.088 ± 0.001	229.303 ± 0.005	13.490 ± 0.001	[126]
566-g30	0.22	4	311.049 ± 0.001	2.430 ± 0.001	1.313 ± 0.001	301.369 ± 0.004	30.625 ± 0.001	[126]
566-g9	0.13	2	206.804 ± 0.001	0.982 ± 0.001	1.042 ± 0.001	207.934 ± 0.005	10.059 ± 0.001	[126]
567-g26	0.76	1	140.024 ± 0.001	1.431 ± 0.001	2.775 ± 0.001	163.474 ± 0.001	3.888 ± 0.001	[126]
567-g45	0.50	1	260.284 ± 0.001	3.162 ± 0.001	1.852 ± 0.001	267.310 ± 0.008	21.371 ± 0.001	[126]
567-g6	0.70	3	119.423 ± 0.006	1.890 ± 0.001	1.579 ± 0.001	134.357 ± 0.009	2.007 ± 0.001	[126]
569-g22	0.27	2	243.007 ± 0.002	2.528 ± 0.001	1.465 ± 0.001	242.594 ± 0.007	15.974 ± 0.001	[126]
570-g2	0.35	3	178.896 ± 0.001	1.024 ± 0.003	1.428 ± 0.001	186.418 ± 0.002	6.630 ± 0.001	[126]
571-g12	0.15	2	233.861 ± 0.001	3.525 ± 0.003	1.587 ± 0.001	232.265 ± 0.007	14.019 ± 0.001	[126]
571-g15	0.17	4	449.967 ± 0.001	4.736 ± 0.004	1.241 ± 0.001	441.116 ± 0.006	90.472 ± 0.002	[126]
571-g16	0.29	4	342.681 ± 0.001	2.732 ± 0.002	1.297 ± 0.001	341.751 ± 0.007	42.167 ± 0.002	[126]
572-g18	0.44	3	114.072 ± 0.001	0.684 ± 0.001	1.531 ± 0.001	130.764 ± 0.005	1.899 ± 0.001	[126]
572-g22	0.11	2	99.128 ± 0.007	2.401 ± 0.001	1.581 ± 0.001	96.982 ± 0.003	1.021 ± 0.001	[126]
573-g12	0.90	3	274.720 ± 0.001	2.170 ± 0.001	2.046 ± 0.001	389.757 ± 0.009	33.132 ± 0.001	[126]
573-g14	0.35	3	162.597 ± 0.001	2.688 ± 0.001	1.623 ± 0.001	170.575 ± 0.002	4.681 ± 0.001	[126]
573-g6	0.76	5	478.937 ± 0.001	7.213 ± 0.003	1.265 ± 0.001	425.609 ± 0.008	85.758 ± 0.004	[126]
574-g28	0.76	4	217.852 ± 0.001	3.189 ± 0.002	1.384 ± 0.001	214.076 ± 0.005	9.856 ± 0.001	[126]
574-g32	0.49	5	381.733 ± 0.001	2.834 ± 0.004	1.278 ± 0.003	379.732 ± 0.004	56.785 ± 0.008	[126]
574-g33	0.13	3	9.900 ± 0.001	10.794 ± 0.001	6.101 ± 0.001	69.844 ± 0.003	0.191 ± 0.	[126]
576-g11	0.64	3	167.628 ± 0.001	3.438 ± 0.001	1.708 ± 0.001	158.925 ± 0.001	4.491 ± 0.001	[126]
576-g12	0.98	5	501.335 ± 0.001	5.430 ± 0.001	1.239 ± 0.003	478.236 ± 0.003	115.499 ± 0.002	[126]
576-g14	0.33	5	752.003 ± 0.001	7.311 ± 0.001	1.286 ± 0.003	728.235 ± 0.002	405.187 ± 0.004	[126]
576-g26	0.44	4	248.130 ± 0.001	3.776 ± 0.001	1.164 ± 0.001	256.049 ± 0.004	15.115 ± 0.001	[126]
576-g32	0.20	1	128.567 ± 0.001	0.739 ± 0.001	0.001 ± 0.001	144.758 ± 0.006	2.698 ± 0.	[126]
576-g39	0.72	6	745.921 ± 0.001	5.251 ± 0.002	1.038 ± 0.001	701.085 ± 0.007	385.562 ± 0.014	[126]
576-g3	8.07	3	197.249 ± 0.004	4.231 ± 0.001	1.253 ± 0.002	265.202 ± 0.001	10.435 ± 0.001	[126]
576-g48	0.45	1	177.098 ± 0.001	1.639 ± 0.001	2.198 ± 0.001	182.664 ± 0.008	6.819 ± 0.001	[126]
576-g51	0.79	3	188.435 ± 0.003	2.566 ± 0.001	1.786 ± 0.001	194.271 ± 0.003	7.353 ± 0.001	[126]
577-g1	1.14	3	174.978 ± 0.004	1.807 ± 0.001	1.766 ± 0.001	239.521 ± 0.006	8.101 ± 0.001	[126]
579-g9	0.41	1	85.219 ± 0.001	2.049 ± 0.001	2.817 ± 0.002	91.510 ± 0.001	0.857 ± 0.001	[126]
57-g80	0.76	3	173.212 ± 0.001	3.650 ± 0.001	1.849 ± 0.001	232.279 ± 0.008	7.346 ± 0.001	[126]
580-g29	0.51	3	67.286 ± 0.002	6.554 ± 0.001	2.677 ± 0.001	94.161 ± 0.001	0.477 ± 0.001	[126]
580-g37	0.22	2	217.735 ± 0.002	2.224 ± 0.001	1.115 ± 0.001	215.813 ± 0.004	11.246 ± 0.001	[126]
580-g41	0.84	3	100.734 ± 0.009	1.479 ± 0.003	1.849 ± 0.001	97.952 ± 0.001	1.052 ± 0.001	[126]
580-g45	0.74	5	378.203 ± 0.009	6.995 ± 0.001	1.231 ± 0.001	340.701 ± 0.002	40.296 ± 0.003	[126]
580-g49	0.37	4	236.406 ± 0.001	3.077 ± 0.001	1.320 ± 0.001	239.432 ± 0.002	13.255 ± 0.001	[126]
580-g6	0.54	4	315.470 ± 0.001	2.825 ± 0.001	1.413 ± 0.001	318.552 ± 0.008	33.088 ± 0.001	[126]

Galaxy	$\chi^2_{\rm red}$	n	$\langle V_0 \rangle$ (km s^{-1})	$\langle r_c \rangle$ (kpc)	d	$r_{\rm edge}$ (kpc)	M_T (10^{11} M$_\odot$)	Reference
581-g10	0.29	3	152.859 ± 0.001	0.924 ± 0.003	1.541 ± 0.001	168.905 ± 0.001	4.398 ± 0.001	[126]
581-g11	0.06	3	9.995 ± 0.001	7.227 ± 0.001	4.757 ± 0.001	44.322 ± 0.001	0.049 ± 0.001	[126]
581-g15	0.92	8	165.866 ± 0.001	0.144 ± 0.001	2.576 ± 0.001	187.641 ± 0.009	5.893 ± 0.001	[126]
581-g4	0.12	2	36.499 ± 0.001	9.738 ± 0.001	4.339 ± 0.001	89.233 ± 0.002	0.397 ± 0.001	[126]
581-g6	0.26	5	824.619 ± 0.002	7.344 ± 0.001	1.000 ± 0.001	1121.160 ± 0.009	788.410 ± 0.02	[126]
582-g12	0.82	3	155.085 ± 0.007	0.706 ± 0.001	1.933 ± 0.003	168.913 ± 0.003	4.602 ± 0.001	[126]
582-g13	0.71	2	203.942 ± 0.004	4.481 ± 0.003	2.249 ± 0.001	282.268 ± 0.001	13.513 ± 0.001	[126]
582-g21	0.26	2	90.383 ± 0.001	6.171 ± 0.009	3.701 ± 0.001	111.172 ± 0.001	1.537 ± 0.001	[126]
582-g4	0.13	2	108.429 ± 0.002	2.014 ± 0.001	1.732 ± 0.002	107.707 ± 0.002	1.398 ± 0.001	[126]
583-g2	0.64	3	233.523 ± 0.001	1.938 ± 0.003	1.711 ± 0.001	231.169 ± 0.002	13.822 ± 0.001	[126]
583-g7	0.77	3	365.765 ± 0.003	3.519 ± 0.001	1.648 ± 0.002	375.612 ± 0.009	54.599 ± 0.002	[126]
584-g4	0.89	3	227.623 ± 0.003	1.012 ± 0.002	1.873 ± 0.001	228.753 ± 0.009	13.393 ± 0.001	[126]
586-g2	0.32	4	240.907 ± 0.001	5.774 ± 0.001	1.344 ± 0.001	309.783 ± 0.002	16.639 ± 0.001	[126]
58-g25	0.22	4	284.406 ± 0.001	2.381 ± 0.001	1.551 ± 0.001	275.739 ± 0.008	23.457 ± 0.001	[126]
58-g28	0.60	4	201.786 ± 0.002	3.670 ± 0.001	1.311 ± 0.001	201.835 ± 0.003	7.627 ± 0.001	[126]
58-g30	0.10	1	149.642 ± 0.002	1.554 ± 0.001	2.856 ± 0.004	156.466 ± 0.002	4.286 ± 0.001	[126]
58-g3	0.45	2	124.532 ± 0.001	1.644 ± 0.001	1.518 ± 0.001	140.978 ± 0.003	2.433 ± 0.001	[126]
593-g3	0.48	3	214.230 ± 0.001	2.369 ± 0.001	1.517 ± 0.001	225.388 ± 0.002	11.086 ± 0.001	[126]
594-g8	0.35	2	187.762 ± 0.001	3.843 ± 0.001	1.404 ± 0.001	199.241 ± 0.001	7.540 ± 0.001	[126]
595-g10	0.19	2	139.066 ± 0.009	4.534 ± 0.001	1.959 ± 0.002	138.172 ± 0.006	2.951 ± 0.001	[126]
596-g9	0.29	2	139.209 ± 0.001	1.500 ± 0.001	1.336 ± 0.001	156.066 ± 0.001	3.366 ± 0.001	[126]
59-g23	0.64	3	203.410 ± 0.001	3.803 ± 0.001	1.642 ± 0.001	275.583 ± 0.005	12.010 ± 0.001	[126]
59-g24	0.48	1	135.556 ± 0.001	4.902 ± 0.003	3.789 ± 0.001	155.838 ± 0.004	4.234 ± 0.001	[126]
601-g19	0.39	4	335.511 ± 0.001	3.654 ± 0.001	1.415 ± 0.001	324.684 ± 0.001	37.081 ± 0.001	[126]
601-g25	0.60	2	68.339 ± 0.001	0.742 ± 0.001	1.384 ± 0.001	83.927 ± 0.001	0.438 ± 0.001	[126]
601-g4	0.21	3	226.208 ± 0.001	2.802 ± 0.002	1.416 ± 0.001	225.649 ± 0.001	12.136 ± 0.001	[126]
601-g5	0.11	4	345.987 ± 0.001	2.301 ± 0.001	1.198 ± 0.001	337.281 ± 0.001	42.930 ± 0.001	[126]
601-g7	0.63	5	244.486 ± 0.001	1.666 ± 0.001	1.221 ± 0.001	245.851 ± 0.008	15.228 ± 0.001	[126]
601-g9	1.63	1	269.000 ± 0.004	5.062 ± 0.002	1.671 ± 0.002	388.898 ± 0.006	32.955 ± 0.005	[126]
602-g15	0.44	3	94.559 ± 0.002	2.942 ± 0.001	1.617 ± 0.001	125.494 ± 0.002	1.106 ± 0.001	[126]
602-g25	0.63	2	212.205 ± 0.001	0.963 ± 0.002	1.625 ± 0.001	228.007 ± 0.008	11.764 ± 0.001	[126]
603-g12	0.24	3	109.608 ± 0.001	0.826 ± 0.001	1.360 ± 0.001	127.680 ± 0.001	1.688 ± 0.001	[126]
603-g20	0.34	5	549.463 ± 0.001	4.584 ± 0.001	1.088 ± 0.001	748.455 ± 0.005	235.961 ± 0.004	[126]
603-g22	0.24	2	190.204 ± 0.001	3.797 ± 0.001	2.443 ± 0.001	213.123 ± 0.001	9.003 ± 0.001	[126]
604-g1	0.93	5	275.305 ± 0.001	4.376 ± 0.001	1.293 ± 0.001	280.887 ± 0.004	19.153 ± 0.001	[126]
605-g7	0.53	5	449.773 ± 0.001	2.953 ± 0.001	1.215 ± 0.001	449.447 ± 0.009	94.532 ± 0.002	[126]
606-g11	0.87	2	165.537 ± 0.009	1.146 ± 0.001	1.336 ± 0.001	174.460 ± 0.007	5.393 ± 0.001	[126]
60-g25	0.36	4	104.975 ± 0.002	0.785 ± 0.002	1.230 ± 0.001	119.154 ± 0.008	1.402 ± 0.001	[126]
61-g8	0.48	4	323.194 ± 0.001	3.694 ± 0.001	1.369 ± 0.001	314.036 ± 0.001	33.006 ± 0.001	[126]
62-g3	0.27	3	175.526 ± 0.001	1.003 ± 0.001	1.498 ± 0.001	174.903 ± 0.001	5.987 ± 0.001	[126]
69-g11	12.86	3	242.803 ± 0.003	3.950 ± 0.001	1.631 ± 0.002	318.771 ± 0.004	19.977 ± 0.002	[126]
6-g3	0.57	3	177.500 ± 0.001	2.562 ± 0.001	1.762 ± 0.002	187.982 ± 0.001	6.289 ± 0.001	[126]
71-g14	0.83	1	184.724 ± 0.001	0.505 ± 0.001	1.587 ± 0.001	197.043 ± 0.003	7.823 ± 0.001	[126]
71-g4	0.61	5	409.476 ± 0.001	6.148 ± 0.001	1.267 ± 0.001	362.853 ± 0.003	53.453 ± 0.005	[126]
72-g5	0.81	4	152.986 ± 0.001	0.803 ± 0.001	1.732 ± 0.001	164.807 ± 0.002	4.251 ± 0.001	[126]
73-g11	0.24	3	237.975 ± 0.001	3.751 ± 0.004	1.215 ± 0.001	227.474 ± 0.004	12.935 ± 0.001	[126]
73-g22	0.22	4	12.248 ± 0.001	11.121 ± 0.001	3.703 ± 0.001	51.226 ± 0.002	0.075 ± 0.001	[126]
73-g25	0.36	5	499.957 ± 0.001	2.863 ± 0.001	1.262 ± 0.001	494.386 ± 0.006	130.324 ± 0.002	[126]
74-g19	0.32	4	232.905 ± 0.001	0.730 ± 0.002	1.425 ± 0.003	232.891 ± 0.007	14.133 ± 0.001	[126]
75-g33	0.20	1	138.904 ± 0.001	3.507 ± 0.001	1.000 ± 0.001	153.813 ± 0.006	3.293 ± 0.001	[126]

Galaxy	$\chi^2_{\rm red}$	n	$\langle V_0 \rangle$ (km s^{-1})	$\langle r_c \rangle$ (kpc)	d	$r_{\rm edge}$ (kpc)	M_T (10^{11} M$_\odot$)	Reference
75-g37	1.75	2	147.718 ± 0.005	4.557 ± 0.002	1.460 ± 0.003	193.292 ± 0.002	4.479 ± 0.002	[126]
79-g14	1.64	4	284.383 ± 0.003	2.365 ± 0.008	1.236 ± 0.005	274.203 ± 0.009	23.067 ± 0.003	[126]
79-g3	0.14	3	10.100 ± 0.001	11.637 ± 0.001	6.016 ± 0.004	72.515 ± 0.001	0.213 ± 0.	[126]
7-g2	0.15	5	161.872 ± 0.001	0.082 ± 0.001	1.721 ± 0.004	164.376 ± 0.008	4.969 ± 0.001	[126]
80-g1	0.45	4	253.055 ± 0.001	3.174 ± 0.001	1.368 ± 0.004	252.549 ± 0.001	16.115 ± 0.001	[126]
84-g10	2.42	3	30.805 ± 0.003	10.773 ± 0.002	3.808 ± 0.003	78.441 ± 0.004	0.270 ± 0.001	[126]
84-g33	0.34	2	331.015 ± 0.006	3.515 ± 0.001	1.496 ± 0.002	342.862 ± 0.002	41.973 ± 0.002	[126]
85-g27	0.75	3	214.319 ± 0.001	3.033 ± 0.001	1.715 ± 0.004	218.494 ± 0.001	10.610 ± 0.001	[126]
85-g2	13.05	3	268.065 ± 0.001	3.450 ± 0.001	1.516 ± 0.002	265.284 ± 0.001	20.052 ± 0.002	[126]
85-g38	0.21	2	206.834 ± 0.001	2.530 ± 0.001	1.476 ± 0.001	210.434 ± 0.009	9.982 ± 0.001	[126]
85-g61	0.30	5	600.210 ± 0.001	5.537 ± 0.001	1.149 ± 0.004	610.777 ± 0.004	218.864 ± 0.004	[126]
87-g3	0.42	3	9.900 ± 0.001	24.372 ± 0.001	6.622 ± 0.002	120.780 ± 0.001	0.986 ± 0.001	[126]
87-g50	0.54	5	396.675 ± 0.001	4.878 ± 0.002	1.158 ± 0.001	387.930 ± 0.001	57.244 ± 0.002	[126]
88-g16	1.86	3	258.562 ± 0.003	1.341 ± 0.001	1.456 ± 0.002	258.076 ± 0.002	19.232 ± 0.001	[126]
88-g17	0.44	3	475.564 ± 0.002	5.576 ± 0.001	1.570 ± 0.002	463.408 ± 0.007	111.346 ± 0.003	[126]
88-g8	0.33	3	265.430 ± 0.003	5.068 ± 0.001	1.780 ± 0.002	270.992 ± 0.001	19.671 ± 0.001	[126]
89-g12	1.23	3	226.859 ± 0.003	0.707 ± 0.001	2.618 ± 0.001	260.201 ± 0.006	15.423 ± 0.001	[126]
8-g1	0.43	4	232.867 ± 0.001	4.506 ± 0.001	1.437 ± 0.001	220.391 ± 0.008	10.915 ± 0.001	[126]
8-g7	0.50	5	395.587 ± 0.001	4.540 ± 0.001	1.228 ± 0.001	391.390 ± 0.001	58.585 ± 0.001	[126]
90-g9	0.04	3	241.630 ± 0.001	0.840 ± 0.002	1.065 ± 0.002	242.189 ± 0.009	15.894 ± 0.001	[126]
9-g10	0.57	3	245.136 ± 0.001	1.852 ± 0.001	1.608 ± 0.001	242.906 ± 0.007	16.036 ± 0.001	[126]
DDO154	0.22	2	55.551 ± 0.003	0.696 ± 0.002	0.939 ± 0.008	54.448 ± 0.001	0.181 ± 0.001	[20]
DDO52	0.13	3	79.121 ± 0.002	0.591 ± 0.006	0.939 ± 0.008	77.589 ± 0.006	0.523 ± 0.001	[20]
DDO64	2.83	6	227.195 ± 0.008	19.177 ± 0.002	1.023 ± 0.006	156.922 ± 0.001	0.920 ± 0.004	[127, 128]
ESO0140040	0.22	3	305.050 ± 0.006	1.060 ± 0.005	1.074 ± 0.003	305.775 ± 0.008	31.988 ± 0.002	[25]
ESO0840411	0.03	3	140.620 ± 0.004	3.850 ± 0.009	0.969 ± 0.009	171.657 ± 0.002	3.166 ± 0.005	[25]
ESO1200211	0.05	6	507.776 ± 0.003	3.934 ± 0.002	0.996 ± 0.004	480.812 ± 0.005	120.561 ± 0.082	[25]
ESO1870510	0.03	3	58.081 ± 0.003	0.481 ± 0.002	1.036 ± 0.008	56.809 ± 0.005	0.205 ± 0.001	[25]
ESO2060140	0.15	1	129.776 ± 0.001	0.852 ± 0.002	0.437 ± 0.007	130.458 ± 0.002	2.484 ± 0.001	[25]
ESO3020120	0.02	2	96.040 ± 0.009	3.950 ± 0.003	1.799 ± 0.008	93.589 ± 0.009	0.917 ± 0.01	[25]
ESO3050090	0.03	3	117.641 ± 0.003	1.830 ± 0.002	1.077 ± 0.004	110.912 ± 0.008	1.527 ± 0.001	[25]
ESO4250180	0.05	4	198.176 ± 0.001	1.600 ± 0.009	1.203 ± 0.007	191.293 ± 0.009	7.832 ± 0.002	[25]
ESO4880049	0.02	2	129.106 ± 0.009	1.301 ± 0.002	0.994 ± 0.002	144.947 ± 0.005	2.663 ± 0.003	[25]
F5631	0.13	2	127.111 ± 0.002	2.170 ± 0.005	1.363 ± 0.006	124.776 ± 0.001	2.174 ± 0.002	[25]
F5683	0.11	1	27.018 ± 0.001	5.942 ± 0.002	12.718 ± 0.002	87.116 ± 0.002	0.37 ± 0.002	[25]
F5718	0.58	3	182.131 ± 0.004	1.274 ± 0.004	1.130 ± 0.002	179.572 ± 0.001	6.479 ± 0.001	[25]
F579V1	0.01	2	123.216 ± 0.002	1.090 ± 0.002	1.533 ± 0.004	143.626 ± 0.005	2.464 ± 0.001	[25]
F5831	0.07	1	97.061 ± 0.002	2.343 ± 0.009	0.925 ± 0.004	96.160 ± 0.002	0.995 ± 0.001	[25]
F5834	0.21	4	189.772 ± 0.006	3.275 ± 0.003	1.302 ± 0.002	171.881 ± 0.009	5.682 ± 0.004	[25]
F730V1	0.13	2	165.326 ± 0.005	1.144 ± 0.005	1.016 ± 0.009	179.541 ± 0.008	5.495 ± 0.002	[25]
holm370	1.50	1	137.337 ± 0.005	4.588 ± 0.002	2.789 ± 0.009	208.169 ± 0.001	5.047 ± 0.004	[126]
i1330	0.17	5	289.764 ± 0.004	0.611 ± 0.001	1.547 ± 0.008	290.503 ± 0.002	27.431 ± 0.002	[126]
i1474	0.58	4	280.148 ± 0.001	2.977 ± 0.001	1.451 ± 0.003	277.462 ± 0.002	22.266 ± 0.001	[126]
i2974	2.74	1	171.519 ± 0.006	4.475 ± 0.003	3.257 ± 0.007	188.111 ± 0.001	7.448 ± 0.005	[126]
i382	0.88	2	189.659 ± 0.003	0.457 ± 0.001	1.941 ± 0.001	199.154 ± 0.001	8.286 ± 0.001	[126]
i387	0.13	4	265.343 ± 0.004	0.341 ± 0.001	1.622 ± 0.002	286.002 ± 0.002	23.090 ± 0.001	[126]
i407	13.77	1	162.742 ± 0.002	1.853 ± 0.002	2.160 ± 0.005	174.497 ± 0.004	5.515 ± 0.001	[126]
i5078	0.28	1	105.856 ± 0.002	2.087 ± 0.001	2.134 ± 0.003	110.215 ± 0.002	1.498 ± 0.001	[126]
i5282	0.53	1	190.451 ± 0.002	1.981 ± 0.003	1.060 ± 0.001	195.453 ± 0.009	8.093 ± 0.001	[126]
i784	0.75	3	204.083 ± 0.001	4.187 ± 0.001	1.813 ± 0.002	279.136 ± 0.003	12.278 ± 0.001	[126]
m-1-2302	0.16	3	9.900 ± 0.001	12.969 ± 0.001	5.300 ± 0.001	67.144 ± 0.002	0.169 ± 0.001	[126]

Galaxy	$\chi^2_{\rm red}$	n	$\langle V_0 \rangle$ (km s^{-1})	$\langle r_c \rangle$ (kpc)	d	$r_{\rm edge}$ (kpc)	M_T (10^{11} M$_\odot$)	Reference
m-1-2313	0.64	3	164.110 ± 0.001	2.809 ± 0.001	1.804 ± 0.001	158.067 ± 0.001	4.419 ± 0.001	[126]
m-1-2321	0.67	3	206.198 ± 0.001	2.062 ± 0.002	1.798 ± 0.003	215.811 ± 0.005	10.016 ± 0.001	[126]
m-1-2522	0.47	3	235.686 ± 0.001	2.271 ± 0.001	1.503 ± 0.001	240.569 ± 0.001	14.430 ± 0.001	[126]
m-1-2524	0.32	4	203.975 ± 0.008	1.459 ± 0.002	1.209 ± 0.001	198.181 ± 0.004	8.709 ± 0.001	[126]
m-1-5-47	0.48	4	366.183 ± 0.002	4.499 ± 0.001	1.539 ± 0.001	346.289 ± 0.001	46.462 ± 0.001	[126]
m-2-1009	0.55	4	454.155 ± 0.001	7.074 ± 0.002	1.250 ± 0.001	423.654 ± 0.005	82.215 ± 0.002	[126]
m-213019	0.26	2	111.244 ± 0.001	6.198 ± 0.001	2.339 ± 0.001	155.654 ± 0.001	2.261 ± 0.001	[126]
m-214003	0.24	3	97.460 ± 0.001	4.682 ± 0.001	2.250 ± 0.001	91.014 ± 0.001	0.844 ± 0.001	[126]
m-215006	0.33	2	123.671 ± 0.001	1.804 ± 0.001	1.239 ± 0.001	142.749 ± 0.002	2.386 ± 0.001	[126]
m-222023	0.13	1	173.495 ± 0.001	1.390 ± 0.001	1.524 ± 0.001	192.065 ± 0.004	6.723 ± 0.001	[126]
m-222025	0.17	6	175.562 ± 0.001	0.044 ± 0.001	2.052 ± 0.001	178.560 ± 0.009	6.370 ± 0.001	[126]
m-2-2-40	0.49	3	175.077 ± 0.001	1.780 ± 0.001	1.584 ± 0.002	171.689 ± 0.002	5.663 ± 0.001	[126]
m-2-2502	0.84	3	171.474 ± 0.001	1.936 ± 0.001	1.744 ± 0.002	178.146 ± 0.001	5.656 ± 0.001	[126]
m-2-2-51	0.74	1	126.638 ± 0.001	1.559 ± 0.004	1.239 ± 0.001	128.227 ± 0.001	2.359 ± 0.001	[126]
m-2-7-33	0.43	3	231.079 ± 0.001	1.968 ± 0.001	1.696 ± 0.001	232.899 ± 0.005	13.622 ± 0.001	[126]
m-3-1042	3.05	2	176.519 ± 0.003	0.710 ± 0.001	0.917 ± 0.002	177.674 ± 0.003	6.276 ± 0.001	[126]
m-3-1364	0.47	4	373.222 ± 0.001	7.385 ± 0.007	1.393 ± 0.001	336.293 ± 0.001	41.881 ± 0.007	[126]
m-3-1623	0.49	4	350.214 ± 0.001	3.768 ± 0.001	1.495 ± 0.001	334.059 ± 0.007	41.711 ± 0.002	[126]
m-338025	0.65	3	167.649 ± 0.001	1.762 ± 0.001	1.673 ± 0.001	178.428 ± 0.008	5.435 ± 0.001	[126]
M33	0.67	4	127.476 ± 0.007	0.286 ± 0.002	1.361 ± 0.004	150.981 ± 0.002	2.785 ± 0.003	[105, 121]
n1090	2.25	2	200.410 ± 0.004	1.142 ± 0.001	0.772 ± 0.002	200.319 ± 0.008	8.994 ± 0.001	[126]
n1114	3.94	3	245.295 ± 0.002	1.413 ± 0.002	1.463 ± 0.002	244.281 ± 0.002	16.31 ± 0.001	[126]
n1163	0.30	2	52.051 ± 0.001	3.308 ± 0.001	3.517 ± 0.001	73.973 ± 0.001	0.301 ± 0.001	[126]
n1241	1.09	2	265.427 ± 0.001	0.873 ± 0.001	2.024 ± 0.001	269.747 ± 0.009	21.961 ± 0.001	[126]
n1247	19.38	5	306.964 ± 0.002	0.661 ± 0.001	1.386 ± 0.001	307.422 ± 0.008	32.508 ± 0.001	[126]
n1337	0.40	3	157.513 ± 0.001	1.373 ± 0.001	1.365 ± 0.002	168.681 ± 0.009	4.544 ± 0.001	[126]
n1417	0.91	2	236.493 ± 0.001	0.809 ± 0.001	1.967 ± 0.001	254.819 ± 0.008	16.459 ± 0.001	[126]
n151	0.94	1	240.080 ± 0.001	1.446 ± 0.001	1.670 ± 0.001	245.163 ± 0.009	16.487 ± 0.001	[126]
n1620	0.10	3	289.136 ± 0.001	1.779 ± 0.001	1.372 ± 0.002	302.042 ± 0.007	27.935 ± 0.002	[126]
n1752	0.44	1	165.667 ± 0.002	2.912 ± 0.001	3.182 ± 0.001	177.579 ± 0.001	6.266 ± 0.001	[126]
n1832	2.26	1	159.843 ± 0.002	0.664 ± 0.002	3.020 ± 0.002	164.888 ± 0.003	5.016 ± 0.001	[126]
n2584	0.23	2	100.389 ± 0.001	4.447 ± 0.001	2.764 ± 0.001	148.983 ± 0.001	1.850 ± 0.001	[126]
n2721	0.96	2	207.717 ± 0.001	0.081 ± 0.001	1.792 ± 0.001	216.994 ± 0.009	10.872 ± 0.001	[126]
n2722	0.58	3	150.984 ± 0.001	1.282 ± 0.001	1.720 ± 0.001	166.356 ± 0.009	4.179 ± 0.001	[126]
n2763	0.79	3	152.549 ± 0.001	0.869 ± 0.001	1.887 ± 0.002	166.139 ± 0.009	4.348 ± 0.001	[126]
n280	0.96	1	270.980 ± 0.001	0.031 ± 0.001	1.021 ± 0.001	276.178 ± 0.003	23.569 ± 0.001	[126]
n2980	3.94	3	303.311 ± 0.004	1.773 ± 0.001	1.663 ± 0.001	316.731 ± 0.006	32.529 ± 0.001	[126]
n3029	0.50	3	173.457 ± 0.001	1.027 ± 0.001	1.562 ± 0.001	172.838 ± 0.001	5.777 ± 0.001	[126]
n3138	0.15	1	154.770 ± 0.006	2.280 ± 0.001	2.165 ± 0.001	160.501 ± 0.001	4.626 ± 0.001	[126]
n3145	1.22	8	342.635 ± 0.001	0.799 ± 0.001	3.929 ± 0.001	341.951 ± 0.001	44.738 ± 0.001	[126]
n3321	0.15	1	140.667 ± 0.001	1.858 ± 0.001	1.372 ± 0.007	159.340 ± 0.001	3.641 ± 0.001	[126]
n3361	0.55	3	162.162 ± 0.001	1.865 ± 0.001	1.649 ± 0.004	171.519 ± 0.009	4.850 ± 0.001	[126]
n3456	0.39	1	143.104 ± 0.001	1.040 ± 0.001	1.628 ± 0.001	146.099 ± 0.001	3.489 ± 0.001	[126]
n3715	0.32	12	192.428 ± 0.002	0.020 ± 0.001	2.417 ± 0.001	195.728 ± 0.005	8.390 ± 0.001	[126]
n4348	2.77	13	184.594 ± 0.002	0.037 ± 0.002	1.263 ± 0.002	192.431 ± 0.006	7.551 ± 0.003	[126]
n4705	3.79	1	194.989 ± 0.004	1.497 ± 0.001	1.241 ± 0.001	197.949 ± 0.004	8.678 ± 0.001	[126]
n697	31.37	1	207.744 ± 0.001	2.240 ± 0.002	1.657 ± 0.001	212.349 ± 0.002	10.714 ± 0.001	[126]
n699	0.27	1	147.800 ± 0.001	2.206 ± 0.001	2.121 ± 0.001	167.378 ± 0.002	4.380 ± 0.001	[126]
n701	0.62	4	227.265 ± 0.001	1.550 ± 0.001	1.368 ± 0.001	235.746 ± 0.004	13.047 ± 0.001	[126]
n7218	0.82	1	114.817 ± 0.001	0.221 ± 0.003	1.571 ± 0.001	135.403 ± 0.002	2.076 ± 0.001	[126]

Galaxy	$\chi^2_{\rm red}$	n	$\langle V_0\rangle$ (km s^{-1})	$\langle r_c\rangle$ (kpc)	d	$r_{\rm edge}$ (kpc)	M_T (10^{11} M$_\odot$)	Reference
n7300	27.62	3	329.698 ± 0.001	5.031 ± 0.001	1.676 ± 0.001	457.145 ± 0.007	53.446 ± 0.002	[126]
n7339	2.77	3	194.193 ± 0.009	0.365 ± 0.002	1.017 ± 0.003	212.940 ± 0.002	9.177 ± 0.001	[126]
n7536	0.15	3	247.510 ± 0.001	2.276 ± 0.001	1.202 ± 0.001	241.771 ± 0.002	15.812 ± 0.001	[126]
n755	0.70	4	144.130 ± 0.005	11.874 ± 0.003	1.809 ± 0.004	147.518 ± 0.001	1.796 ± 0.003	[126]
n7568	0.71	3	264.116 ± 0.001	4.232 ± 0.001	1.795 ± 0.001	366.483 ± 0.001	27.553 ± 0.001	[126]
n7591	0.94	7	224.870 ± 0.001	0.054 ± 0.001	6.518 ± 0.001	236.824 ± 0.001	13.909 ± 0.001	[126]
n7593	0.37	2	144.524 ± 0.001	1.114 ± 0.001	1.467 ± 0.001	158.803 ± 0.002	3.748 ± 0.001	[126]
n7631	0.53	3	221.614 ± 0.001	1.557 ± 0.001	1.786 ± 0.001	229.184 ± 0.005	12.502 ± 0.001	[126]
n7677	0.39	1	174.333 ± 0.001	1.002 ± 0.003	1.458 ± 0.001	177.594 ± 0.004	6.267 ± 0.001	[126]
NGC2366	0.44	3	48.588 ± 0.007	4.883 ± 0.005	2.101 ± 0.008	44.336 ± 0.001	0.091 ± 0.001	[20, 122]
NGC3198	0.54	1	140.533 ± 0.001	3.482 ± 0.008	2.261 ± 0.004	207.311 ± 0.001	4.984 ± 0.003	[120]
NGC6822	0.09	4	200.122 ± 0.002	4.679 ± 0.002	1.225 ± 0.001	188.966 ± 0.001	6.437 ± 0.001	[123]
NGC959	1.50	2	73.765 ± 0.005	25.880 ± 0.002	2.173 ± 0.003	112.484 ± 0.001	0.796 ± 0.002	[127, 128]
U11454	0.37	2	182.924 ± 0.006	1.567 ± 0.005	1.047 ± 0.005	193.845 ± 0.006	7.199 ± 0.001	[25]
U11557	0.03	3	238.977 ± 0.008	4.200 ± 0.007	1.002 ± 0.008	232.254 ± 0.002	12.928 ± 0.008	[25]
U11583	0.03	2	12.442 ± 0.007	1.560 ± 0.009	4.139 ± 0.007	23.962 ± 0.002	0.008 ± 0.001	[25]
U11616	0.14	2	164.774 ± 0.009	2.177 ± 0.002	1.412 ± 0.009	176.449 ± 0.003	5.289 ± 0.005	[25]
U11648	0.38	4	260.699 ± 0.008	2.936 ± 0.004	1.366 ± 0.006	247.025 ± 0.004	16.866 ± 0.007	[25]
U11748	1.02	2	223.564 ± 0.003	3.021 ± 0.002	2.245 ± 0.003	313.796 ± 0.007	18.096 ± 0.003	[25]
U11819	0.36	2	184.055 ± 0.009	5.572 ± 0.009	1.764 ± 0.007	180.682 ± 0.001	6.600 ± 0.006	[25]
u12123	0.44	5	780.509 ± 0.003	5.663 ± 0.001	1.000 ± 0.001	1073.250 ± 0.008	691.6 ± 0.021	[126]
u12290	0.46	3	234.607 ± 0.001	3.2445 ± 0.001	1.330 ± 0.001	238.836 ± 0.001	13.624 ± 0.001	[126]
u12370	0.73	2	99.284 ± 0.001	1.046 ± 0.001	1.628 ± 0.001	118.290 ± 0.004	1.316 ± 0.001	[126]
u12382	0.46	3	137.900 ± 0.001	0.866 ± 0.004	1.494 ± 0.001	150.618 ± 0.005	3.181 ± 0.001	[126]
u12423	0.41	2	189.675 ± 0.001	6.858 ± 0.001	1.882 ± 0.001	253.199 ± 0.001	10.035 ± 0.001	[126]
u12533	2.64	1	205.370 ± 0.003	5.302 ± 0.001	2.132 ± 0.002	301.964 ± 0.007	15.403 ± 0.003	[126]
u12555	0.54	4	178.874 ± 0.006	2.279 ± 0.001	1.351 ± 0.001	186.680 ± 0.003	5.972 ± 0.001	[126]
u12565	0.73	3	200.508 ± 0.001	2.183 ± 0.001	1.708 ± 0.001	202.613 ± 0.001	8.788 ± 0.001	[126]
u12571	0.66	1	106.699 ± 0.001	1.807 ± 0.001	3.416 ± 0.001	114.921 ± 0.001	1.698 ± 0.001	[126]
u12583	0.16	4	121.582 ± 0.002	0.494 ± 0.001	1.241 ± 0.001	141.118 ± 0.008	2.317 ± 0.001	[126]
u14	0.36	8	208.848 ± 0.002	0.098 ± 0.001	2.903 ± 0.001	219.504 ± 0.006	11.019 ± 0.001	[126]
u1938	0.49	4	308.447 ± 0.001	2.116 ± 0.001	1.597 ± 0.001	302.048 ± 0.003	30.833 ± 0.001	[126]
u2020	0.42	2	92.743 ± 0.001	1.278 ± 0.001	1.411 ± 0.005	113.436 ± 0.001	1.082 ± 0.001	[126]
u2079	0.42	3	129.786 ± 0.001	4.237 ± 0.001	1.778 ± 0.001	173.146 ± 0.009	2.904 ± 0.001	[126]
u210	0.31	2	121.511 ± 0.001	1.068 ± 0.002	1.304 ± 0.001	138.437 ± 0.004	2.292 ± 0.001	[126]
u321	0.59	4	178.892 ± 0.001	2.081 ± 0.001	1.379 ± 0.001	169.138 ± 0.007	5.414 ± 0.001	[126]
U4115	0.01	3	129.643 ± 0.007	0.705 ± 0.007	0.983 ± 0.002	128.572 ± 0.001	2.378 ± 0.001	[126]
u541	0.61	4	212.051 ± 0.001	4.600 ± 0.001	1.441 ± 0.004	270.497 ± 0.008	11.557 ± 0.001	[126]
U4115	0.01	3	129.643 ± 0.008	0.705 ± 0.008	0.983 ± 0.002	128.572 ± 0.001	2.378 ± 0.001	[25]
u541	0.61	4	212.051 ± 0.001	4.600 ± 0.001	1.441 ± 0.001	270.497 ± 0.008	11.557 ± 0.001	[126]
U5750	0.02	2	72.406 ± 0.005	10.050 ± 0.006	2.247 ± 0.008	105.912 ± 0.002	0.676 ± 0.012	[25]
U6614	1.02	3	237.681 ± 0.009	4.852 ± 0.009	1.769 ± 0.004	326.234 ± 0.001	19.424 ± 0.003	[25]
ua394	36.47	1	28.822 ± 0.002	10.182 ± 0.002	15.996 ± 0.001	120.188 ± 0.006	0.971 ± 0.001	[126]
UGC11820	2.62	1	4.330 ± 0.008	27.870 ± 0.004	74.569 ± 0.009	115.254 ± 0.001	0.856 ± 0.003	[127, 128]
UGC1281	2.47	6	125.004 ± 0.007	18.956 ± 0.003	1.129 ± 0.005	143.478 ± 0.002	0.235 ± 0.001	[124, 125]
UGC4325	5.78	5	275.876 ± 0.009	14.329 ± 0.002	1.022 ± 0.002	243.449 ± 0.001	8.072 ± 0.004	[127, 128]
UGC477	4.69	3	183.986 ± 0.003	23.777 ± 0.003	1.359 ± 0.005	170.217 ± 0.003	2.759 ± 0.001	[127, 128]

Table 4.1: Best fitting dynamical parameters $\langle V_0\rangle$, $\langle r_c\rangle, d$, n, $r_{\rm edge}$ and the total mass M_T given by Eq.(4.13).

4.4 Connecting dark matter and classical gravity

Given the accurate results from the fittings with the circular velocity profile given by Eq.(4.1) with the Newtonian renormalization prescription by Eq.(4.12), extrapolating towards the center of the galaxy and to the outside of the RC, giving in this last regime the Keplerian behavior, one may ask from a geometrical question: how modified a static and spherically symmetric space-time should be, in order to keep a free massive particle moving with the velocity profile Eq.(4.1)? The solution of this problem can be easily tackled since only involves fixing a gauge for the velocity and solve the geodesic equations for such specific space-time model.

4.4.1 Geodesic equations

As a simplified model, one could write the line element of a static and spherically symmetric $3+1$ space-time, just as to get the well known Schwarzschild solution:

$$ds^2 = -e^{\nu(r)}dt^2 + e^{-\nu(r)}dr^2 + r^2 d\Omega^2, \tag{4.19}$$

where $\nu(r)$ is a function depending only on the radial coordinate r, and $d\Omega^2 = d\theta^2 + \sin^2\theta d\phi^2$ corresponds to the typical solid angle differential element. This metric solution was also implemented in [94] to describe galaxy RCs in the $f(R) = R^n$ framework. The metric tensor[2]

$$g_{\mu\nu} = \text{diag}(-e^{\nu(r)}, e^{-\nu(r)}, r^2, r^2\sin^2\theta), \tag{4.20}$$

is diagonal and doesn't depend on t nor Ω, which mean that there are two conserved quantities E and L associated to the energy and the angular momentum (measured by an observer at infinity), and they are given respectively by

$$E = -e^{\nu(r)}\dot{t}, \tag{4.21}$$

$$L = r^2\dot{\Omega}, \tag{4.22}$$

where the dot-derivative is with respect to the proper time τ defined by $d\tau^2 = -ds^2$.

Suppose now one puts a free test massive particle ($m = 1$) to move in such a space-time. The equations of motion for such a particle can be derived from the Lagrangian, which is written as

$$\mathcal{L}_{\text{m}} = -\frac{1}{2}e^{\nu(r)}\dot{t}^2 + \frac{1}{2}e^{-\nu(r)}\dot{r}^2 + \frac{1}{2}r^2\dot{\Omega}^2. \tag{4.23}$$

Notice that since this space-time is by definition static and spherically symmetric, the only geodesic solution corresponding to the $\theta-$coordinate is $\theta = \pi/2$, that's why one can leave all the equations in terms of the angular variable Ω and not separately in θ and ϕ.

Since the particle is freely moving, the normalization of its 4-velocity $u^\mu u_\mu = -1$ gives $\mathcal{L}_{\text{m}} = -1/2$ and Eq.(4.23) becomes:

$$-1 = -e^{\nu(r)}\dot{t}^2 + e^{-\nu(r)}\dot{r}^2 + r^2\dot{\Omega}^2. \tag{4.24}$$

Substituting Eq.(4.21) and Eq.(4.22) into Eq.(4.24), one arrives to

$$E^2 = \dot{r}^2 + e^{\nu(r)}\left(1 + \frac{L^2}{r^2}\right), \tag{4.25}$$

from where one can recognize the effective potential $V_{\text{eff}}(r)$:

$$V_{\text{eff}}(r) = e^{\nu(r)}\left(1 + \frac{L^2}{r^2}\right). \tag{4.26}$$

[2]The expression $\text{diag}(a, b, c, d)$ is a 4×4 matrix whose diagonal elements are a, b, c, d.

Stable orbits

The knowledge of the effective potential $V_{\rm eff}(r)$ by Eq.(4.26) allows to determine the stable orbits in which the particle can move: they are the minimum solutions of the extremal problem for $V_{\rm eff}(r)$. The extremal solutions satisfy:

$$\frac{L^2}{r^2} = \frac{r\nu'(r)/2}{1 - r\nu'(r)/2}, \tag{4.27}$$

as long as $1 - r\nu'(r)/2 \neq 0$, and the prime-derivative is with respect to the radial coordinate r.

In the proper reference system, $r\dot{\Omega}$ is the circular velocity in the $\theta = \pi/2$ plane, then one can write:

$$(r\dot{\Omega})^2 = \dot{t}^2 \left(r\frac{d\Omega}{dt} \right)^2 = \dot{t}^2 V_\Omega^2(r), \tag{4.28}$$

$$= E^2 e^{-2\nu(r)} V_\Omega^2(r), \tag{4.29}$$

where in this case $V_\Omega(r)$ is the circular velocity measured by an external observer.

Substituting Eq.(4.27) and Eq.(4.29) into Eq.(4.25), one arrives to the equation

$$\frac{r}{2}\frac{d}{dr}\left(e^{\nu(r)}\right) = V_\Omega^2(r), \tag{4.30}$$

which defines the metric coefficient $e^{\nu(r)}$ in terms of the measured circular velocity from an external observer. The line element, with the right units, becomes

$$ds^2 = -c^2 e^{\nu(r)} dt^2 + e^{-\nu(r)} dr^2 + r^2 d\Omega^2. \tag{4.31}$$

$$\frac{d\, e^{\nu(r)}}{dr} = \frac{2V_\Omega^2(r)}{c^2 r}. \tag{4.32}$$

Before integrating Eq.(4.32), one should notice that in the weak field limit: $e^{\nu(r)} \simeq 1 + 2\Phi(r)/c^2$ one obtains the expected result

$$\frac{d\Phi(r)}{dr} = \frac{V_\Omega^2(r)}{r} \tag{4.33}$$

for the centripetal acceleration in terms of the gravitational potential $\Phi(r)$.

Setting $V_\Omega^2(r)$ equals to the velocity profile $V_n^2(r)$ in Eq.(4.1), one is forcing every massive particle, freely moving in such space-time (luminous and DM) in circular orbits, to move with a circular velocity $V_n(r)$. Since the renormalization prescription described in the previous section gives at large distances the Keplerian behavior for $V_n(r)$, then one can choose

$$e^{\nu(r)} = 1 - \int_r^{+\infty} \frac{2V_n^2(s)\, ds}{c^2 s}, \tag{4.34}$$

and the line element becomes

$$ds^2 = -c^2\left(1 - \int_r^{+\infty} \frac{2V_n^2(s)\,ds}{c^2 s}\right)dt^2 + \left(1 - \int_r^{+\infty} \frac{2V_n^2(s)\,ds}{c^2 s}\right)^{-1} dr^2 + r^2 d\Omega^2. \tag{4.35}$$

Notice that the line element Eq.(4.19) is completely determined, which gives that any massive particle in a circular orbit will move with the desired circular velocity profile.

At large distances, the line element coincides with the Schwarzschild solution for a BH of mass M_T, where M_T is the total mass introduced in Eq.(4.13).

The obtained results are as exact as a general relativistic expression, valid for static and spherically symmetric 3+1 space-times, and since the motion of the test particles is defined via the geodesic equations, these relations are totally independent of any theory of gravity; even if one allows the modified theory of gravity to contain arbitrary contractions of the Ricci and Riemann tensors, the above equations would still hold exactly.

4.4.2 Einstein and continuity equations

Given the metric tensor, one can compute directly the geometrical quantities associated with this space-time, i.e. Christoffel symbols, Riemann and Ricci tensors, scalar curvature and the Einstein tensor. The non-vanishing Christoffel symbols are:

$$\Gamma^0_{10} = \frac{\nu'(r)}{2}, \quad \Gamma^1_{00} = \frac{c^2}{2}e^{2\nu(r)}\nu'(r), \quad \Gamma^1_{11} = -\frac{\nu'(r)}{2}, \tag{4.36}$$

$$\Gamma^1_{22} = -r\,e^{\nu(r)}, \quad \Gamma^1_{33} = -r\,e^{\nu(r)}\sin^2\theta, \quad \Gamma^2_{12} = \frac{1}{r}, \tag{4.37}$$

$$\Gamma^2_{33} = -\sin\theta\cos\theta, \quad \Gamma^3_{31} = \frac{1}{r}, \quad \Gamma^3_{23} = \cot\theta. \tag{4.38}$$

The non vanishing components of the Riemann tensor are

$$R^0_{110} = \frac{e^{-\nu(r)}}{2}\frac{d^2}{dr^2}\left(e^{\nu(r)} - 1\right), \quad R^0_{220} = \frac{r}{2}\frac{d}{dr}\left(e^{\nu(r)} - 1\right), \quad R^0_{330} = R^0_{220}\sin^2(\theta) \tag{4.39}$$

$$R^1_{010} = \frac{c^2 e^{\nu(r)}}{2}\frac{d^2}{dr^2}\left(e^{\nu(r)} - 1\right), \quad R^1_{221} = R^0_{220}, \quad R^1_{331} = R^0_{220}\sin^2(\theta) \tag{4.40}$$

$$R^2_{020} = \frac{c^2 e^{\nu(r)}}{2r}\frac{d}{dr}\left(e^{\nu(r)} - 1\right), \quad R^2_{121} = -\frac{e^{-\nu(r)}}{2r}\frac{d}{dr}\left(e^{\nu(r)} - 1\right), \quad R^2_{333} = R^3_{232}\sin^2(\theta) \tag{4.41}$$

$$R^3_{030} = R^2_{020}, \quad R^3_{131} = R^2_{121}, \quad R^3_{232} = -\left(e^{\nu(r)} - 1\right). \tag{4.42}$$

The Ricci tensor is diagonal and its components are

$$R_{00} = \frac{c^2 e^{\nu(r)}}{2r}\frac{d^2}{dr^2}\left(r\left(e^{\nu(r)}-1\right)\right), \quad R_{11} = -\frac{e^{-\nu(r)}}{2r}\frac{d^2}{dr^2}\left(r\left(e^{\nu(r)}-1\right)\right) \tag{4.43}$$

$$R_{22} = -\frac{d}{dr}\left(r\left(e^{\nu(r)}-1\right)\right), \quad R_{33} = R_{22}\sin^2(\theta), \tag{4.44}$$

$$\tag{4.45}$$

and the scalar curvature $R = g^{\mu\nu}R_{\mu\nu}$ is

$$R = -\frac{1}{r^2}\frac{d^2}{dr^2}\left(r^2\left(e^{\nu(r)}-1\right)\right). \tag{4.46}$$

Moreover, the Einstein tensor components $G_{\mu\nu} = R_{\mu\nu} - g_{\mu\nu}R/2$ are given by:

$$G_{00} = -\frac{c^2 e^{\nu(r)}}{r^2}\frac{d}{dr}\left(r\left(e^{\nu(r)}-1\right)\right), \quad G_{11} = \frac{e^{-\nu(r)}}{r^2}\frac{d}{dr}\left(r\left(e^{\nu(r)}-1\right)\right), \tag{4.47}$$

$$G_{22} = \frac{r}{2}\frac{d^2}{dr^2}\left(r\left(e^{\nu(r)}-1\right)\right), \quad G_{33} = G_{22}\sin^2\theta. \tag{4.48}$$

Since when deriving the metric coefficient $e^{\nu(r)}$ by gauging the circular velocity, luminous and DM were treated in equal footing, we consider the covariant stress-energy tensor of a perfect fluid in spherical coordinates with pressure anisotropies that describes the dynamics of total matter content, i.e. luminous and DM; the components are given by:

$$T_{\mu\nu} = \mathrm{diag}\left(c^4\rho(r)e^{\nu(r)}, p_r(r)e^{-\nu(r)}, p_\theta(r)r^2, p_\theta(r)r^2\sin^2\theta\right), \tag{4.49}$$

where $\rho(r)$ is the total matter density (luminous and DM matter) contained in this space time, $p_r(r)$ is a radial pressure and $p_\theta(r)$ is the angular pressure of the fluid in the $\hat{\theta}$ direction (going outside from the $\theta = \pi/2$ plane).

The first two Einstein equations $G_{\mu\nu} = \frac{8\pi G}{c^2}T_{\mu\nu}$ will give:

$$\rho(r) = -\frac{c^2}{8\pi G r^2}\frac{d}{dr}\left(r\left(e^{\nu(r)}-1\right)\right), \quad p_r(r) = \frac{c^4}{8\pi G r^2}\frac{d}{dr}\left(r\left(e^{\nu(r)}-1\right)\right). \tag{4.50}$$

Notice that from the above equations one gets $p_r(r) = -c^2\rho(r)$, which in the case of only DM, corresponds to a cosmological constant equation of state. The third Einstein equation gives

$$p_\theta(r) = \frac{c^4}{16\pi G r}\frac{d^2}{dr^2}\left(r\left(e^{\nu(r)}-1\right)\right). \tag{4.51}$$

For the above mentioned stress-energy tensor, the conservation equation reads as $\nabla_\mu T^{\mu\nu} = 0$, which in this case it is a constrain or compatibility equation, since all the components are

already fixed. Given the symmetries of our problem (static and isotropy), there's only one compatibility equation which is: $\partial_1 T^{\mu\nu} + \Gamma^{\mu}_{1\mu} T^{11} + \Gamma^{1}_{\mu\mu} T^{\mu\mu} = 0$. The contravariant components of the stress-energy tensor are

$$T^{\mu\nu} = g^{\mu\rho} g^{\nu\sigma} T_{\rho\sigma} = diag(\rho(r) e^{-\nu(r)}, p_r(r) e^{\nu}, r^{-2} p_\theta(r), r^{-2} \sin^{-2}\theta p_\theta(r)). \tag{4.52}$$

From this, we get

$$p_\theta(r) = \frac{r}{2} \frac{d\, p_r(r)}{dr} + p_r(r). \tag{4.53}$$

But notice from the second Einstein equation, computing the radial derivative, one gets

$$\frac{d}{dr}\left(\frac{d}{dr}\left(r\left(e^{\nu(r)} - 1\right)\right)\right) = \frac{8\pi G}{c^4} \frac{d(p_r(r) r^2)}{dr} = \frac{8\pi G}{c^4} r^2 \frac{d\, p_r(r)}{dr} + \frac{16\pi G}{c^4} r p_r(r), \tag{4.54}$$

therefore, looking at the third Einstein equation, one obtains back the compatibility relation

$$p_\theta(r) = \frac{r}{2} \frac{d\, p_r(r)}{dr} + p_r(r). \tag{4.55}$$

This means that with the chosen metric and stress-energy tensors, the Einstein equations form a complete system, where all the unknown dynamical functions are uniquely determined.

The above computed density $\rho(r)$ and the radial and angular pressures $p_r(r)$, $p_\theta(r)$ contain the information of the whole matter composing the galaxy, luminous and dark. Assuming no interactions between the luminous and DM components, one can make the separation:

$$\rho(r) = \rho_L(r) + \rho_D(r), \quad p_r(r) = p_{r\,L}(r) + p_{r\,D}(r), \quad p_\theta(r) = p_{\theta\,L}(r) + p_{\theta\,D}(r), \tag{4.56}$$

where the luminous matter component is labeled by the letter L and the DM component labeled by D respectively.

Spiral galaxies are the final state of the galaxy sequence evolution and they are in mechanical equilibrium. DM is supposed to be made by WIMPs, then, since their interactions are very weak compared to the luminous matter, then one wouldn't expect an azimuthal pressure for the DM fluid, otherwise it wouldn't distribute isotropically within the galaxy. From this, one should expect that $p_{\theta\,D}(r)/p_{\theta\,L}(r) \ll 1$. Moreover, since there are no strong visible signs of luminous matter moving radially within the galaxy, then one should expect $p_{r\,L}(r)/p_{r\,D}(r) \ll 1$. From these two conditions, one has

$$\rho(r) = \rho_L(r) + \rho_D(r), \quad p_r(r) = p_{r\,D}(r), \quad p_\theta(r) = p_{\theta\,L}(r), \tag{4.57}$$

or

$$\rho(r) = \rho_L(r) + \rho_D(r), \quad p_{r\,D}(r) = -c^2(\rho_L(r) + \rho_D(r)), \quad p_{\theta\,L}(r) = \frac{r}{2} \frac{d\, p_{r\,D}(r)}{dr} + p_{r\,D}(r), \tag{4.58}$$

From the above equations one can extract the following information:

- Since around the optical disk length scale $R_{\rm opt}$, the luminous matter density has a sharp fall-off, then, in the range $R_{\rm opt} \lesssim r \lesssim r_{\rm edge}$, the DM follows an equation of state identical as the cosmological constant $p_{r\,D}(r) = -c^2\rho_D(r)$. Moreover, since beyond $r = r_{\rm edge}$ one recovers the Schwarzschild metric solution $\rho(r \simeq r_{\rm edge}) = 0$, then, around $r \simeq r_{\rm edge}$ one has $p_{r\,D}(r \simeq r_{\rm edge}) = 0$ describing the DM halo as a self-gravitating object in mechanical equilibrium.

- The luminous matter is distributed anisotropically with two angular pressures, one in the $\hat{\theta}$ direction and another one in the equatorial plane $\hat{\phi}$: $p_\phi(r) = p_\theta(r)\sin^2\theta$, which make the luminous matter rotate around the galactic center and move vertically in the plane of the galaxy.

- Since the radial pressure due to only DM determines the angular one by Eq.(4.58), then the DM gives the shape of the luminous matter distribution.

To compute the total density $\rho(r)$ and radial pressure $p_r(r)$ with Eq.s(4.50), and the anisotropic or azimuthal pressure $p_\theta(r)$ Eq.(4.51), the only needed ingredient is the velocity profile $V_n(r)$ from Eq.(4.1) and the renormalization prescription in Eq.(4.12). In Figs.(4.7) are shown the dependence of the total density $\rho_n(r)/\rho_0$ with the distance from the galactic center r, being $\rho_0 = \dfrac{\langle V_0\rangle^2}{4\pi G\langle r_c\rangle^2}$, for $d = 0.7$ (left panel), $d = 1.3$ (right panel) and $r_{\rm edge}/\langle r_c\rangle = 12$. As one may see from the graphics, the density has a steep-slope for $r \leq \langle r_c\rangle$, and for $r \simeq r_{\rm edge}$, a sharp fall-off is expected. For a same value of r, in all its allowed range of variation, the density decreases with the increasing values of n, independently of the parameter d. This means beyond the length scale where the luminous matter contribution to the total density is already negligible, this last is lower for increasing n.

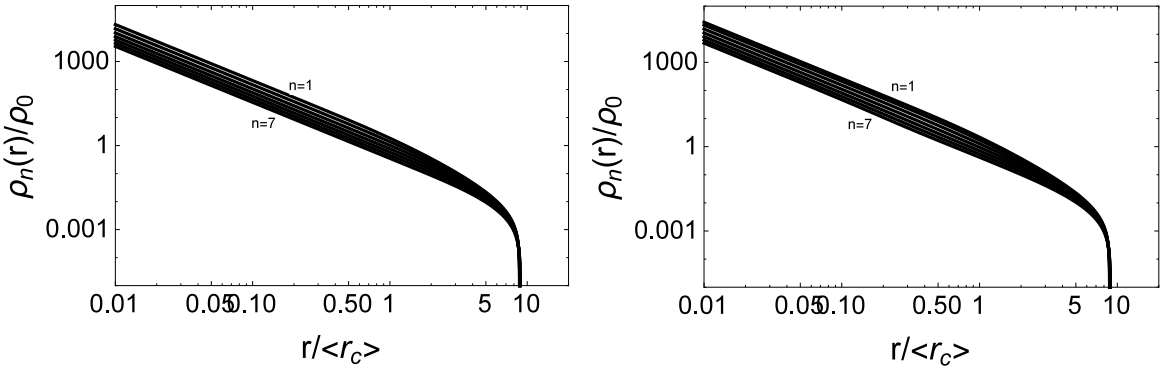

Figure 4.7: Radial dependence of the total density $\rho(r)/\rho_0$ as computed with Eq.(4.50) for the velocity profile $V_n(r)$, with the renormalization prescription Eq.(4.12). The ratio $r_{\rm edge}/\langle r_c\rangle = 12$ was taken; $d = 0.7$ (for the left panel), $d = 1.3$ (for the right panel), and $n = 1, 2, 3, 4, 5, 6, 7$ (from top to bottom) as shown in both panels.

On the other hand, in Figs.(4.8) are shown the radial dependence of the radial and azimuthal pressures $p_r(r)/p_0$ (continuous lines), $p_\theta(r)/p_0$ (dashed lines), being $p_{r\,0} = c^2\rho_0$. In both cases, using $d = 0.7$ (left panel), $d = 1.3$ (right panel) and $r_{\rm edge}/\langle r_c\rangle = 12$, one can see that both pressures tend to zero at large r, while towards the center, both present singularities due to the steep slope of the density. The radial pressure $p_r(r)/p_0$ is always negative, being the DM the only component feeling this effect. Below $2\langle r_c\rangle$ the effects of the negative radial pressures are more pronounced, while after $2\langle r_c\rangle$, the negative radial pressure becomes negligible, reaching a sphere $r \simeq r_{\rm edge}$ where the mechanical equilibrium $p_r(r) = 0$ holds. The azimuthal pressure $p_\theta(r)/p_0$ is shown in Fig.(4.8) as well, and as to this pressure only contributes the luminous matter, it is shown in Fig.(4.8) for different values of n, that this last should be distributed within the galaxy as forming a flattened disk at large r, with a small bulge below $2\langle r_c\rangle$. Since $p_\theta(r)$ is totally determined by $p_r(r)$, and since $p_r(r)$ is uniquely dominated by the DM, then the shape of the luminous matter is fixed by the DM environment.

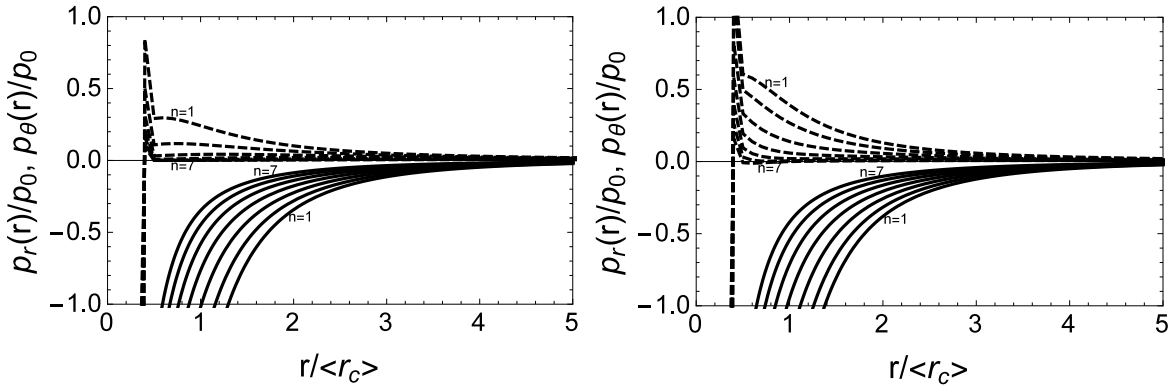

Figure 4.8: Radial dependence of the radial and azimuthal pressures $p_r(r)/p_0$ (continuous line), $p_\theta(r)/p_0$ (dashed lines), using $r_{\rm edge}/\langle r_c\rangle = 12$, $d = 0.7$ (left panel) and $d = 1.3$ (right panel).

Conclusions

In this thesis we have studied the main methods of galaxy RC fittings, coming from MOG and the structure and dynamics of galactic DM halos inferred by their mass density profiles. A new method was introduced, which breaks routinely the before mentioned methods in the sense that no previous theory is assumed, but a generic velocity formula to fit 887 RCs of galaxies with different morphologies.

A direct application of these methods was performed on the galaxy M33, where the highly resoluted and extended RC of this spiral galaxy was already obtained in [105] using the combined data of the optical RC in the innermost regions and the extended 21-cm kinematical data. The luminous mass content was determined as well in [105], and then modelled as a thin disk composed by stars, atomic and molecular gases, these lasts corrected by a factor of 1.33 to take into account the presence of Helium. No bulge, nor prominent bars are observed, so the only uncertainties that could be introduced come from the constant stellar mass-to-light ratio, which is considered as a constant free parameter, but constrained by the BVIgi mass maps.

While still waiting for the experimental confirmation on the existence of the DM particles, the MOG models propose a simple scenario to explain the flatness of galaxy RCs by modifying the equations of General Relativity at larger scales than the Solar System without adding more mass than the one observed in galaxy photometric measurements. Particularly, we analyzed the well extended and high spatial resoluted RC of the galaxy M33 in the MOND and $f(R) = R^n$ theory frameworks. In MOND, for the standard interpolating function (2.9), the fit is incompatible with the BVIgi mass maps, while for the simple interpolating function , although less favorable than the first, was found compatible. The fits in both cases don't improve by increasing the stellar disk mass. For the $f(R) = R^n$ theory, by fixing either $\beta = 0.70$ or $\beta = 0.87$ (see Eq.(2.30)) the best fitting values are compatible with the BVIgi mass maps but the probabilities reject these two power-law models. As a conclusion, for the galaxy M33, MOND is favored against $f(R) = R^n$.

Assuming a DM halo model surrounding the galaxy M33, we studied two different methods to explain the flatness of its RC and derive the properties of the corresponding DM halo. For the spiral galaxy M33 we studied first the standard mass modeling method with the cuspy NFW and the cored BRK DM halo mass density profiles, which lead the core-cusp controversy. We confirm the results obtained in [105] as the NFW DM density profile provides a better fit to the RC when combined in quadrature with the luminous mass circular velocity contribution.

However, the BRK fitting solution cannot be washed out since the uncertainties in stellar mass-to-light ratio make both DM mass models compatible with the data, which can be explained by the fact that even in the outermost parts of this galaxy, the influence of the luminous matter is not negligible. To avoid this degeneracy, the local density method, introduced in [103], was used to determine the properties of the DM halo relying only on the experimental data and removing the uncertainties introduced by the stellar mass-to-light ratio. This method assumes in advance the knowledge of an analytical formula to represent the RC data, as to compute the total local density is needed. We introduced a simple rational velocity formula to fit the circular velocity data, which gives a steeply rising and flattish RC that fits better the data than with the previously mentioned methods. In this case, the cored BRK DM halo distribution provided a better fit for the M33 galaxy than the NFW DM profile, but still compatible. One may conclude then that this galaxy may harbor a cored DM halo, but the degeneracy still persists since both methods used in modelling the RC data of this spiral galaxy favour different DM density distributions and halo masses.

The main limitation of the local density method is that one needs to provide an analytical and model-independent formula to represent the experimental data of the RC to compute the total local density. For the galaxy M33, it was introduced Eq.(3.7) which solved our problem. However, there are many situations in which this formula doesn't provide a good representation of the experimental data, for example, when dealing with galaxies with only increasing RCs, slightly decreasing ones, prominent bulges or other galactic substructures. We gave a solution to this problem by postulating an empirical circular velocity formula Eq.(4.1) as a function of the galactic radius, which at large distances gives a flat RC and fulfills the necessities above mentioned. We fitted 887 different galaxy RCs with an unprecedented degree of accuracy. Given the goodness of the fits in the experimental data range, we promoted this empirical formula as valid as an extrapolation function to the regions where there are no more experimental points. Since an asymptotically flat RC will give rise to an ill-defined gravitational potential, a renormalization method of the scale length r_c and velocity V_0 was implemented in such a way that for distances greater than a sliding scale $r_{\rm edge} > r_c$ the circular velocity profile converges to the keplerian one, making available the computation of the total gravitational potential, and hence, make predictions on the mass enclosed by the galaxy. In particular, we computed the estimated mass of the spiral M33 and it was found compatible with the estimated mass taking into account the NFW and BRK DM halo models, but the BRK total mass is more in agreement.

For future works regarding my thesis I am eager to deepen into the phenomenology of the velocity profiles given by Eq.(4.1) since it fits with unprecedent precision many rotation curves of different morphological types of galaxies without needing in advance the luminous matter distribution. With highly spatial resolute and more extended RCs in order to understand better the correlations between the parameters and make better predictions that may help understanding the nature of the DM itself. Since the DM halo hosting a galaxy is approximately spherical, using the velocity formula with the later renormalization procedure of the gravitational potential to get the Keplerian result after some length scale, inside the halo region one can apply the

techniques of Stellar Astrophysics and General Relativity to compute the stress-energy tensor of the interior mass and look for possible Equations of State for the DM, which at the same time will allow to disentangle the nature of these invisible particles and their interactions.

Bibliography

[1] Öpik E., Bull. de la Soc. Astro. de Russie, 21:150.

[2] Oort, J. H. (1932), Bull. Astron. Inst. Netherlands, 6:249.

[3] Zwicky, F., Helvetica Physica Acta, (1933), $6 : 110 - 127$.

[4] Babcock, H. W., Lick Observatory Bulletin, (1939), 19:41-51.

[5] Bosma, A., PhD Thesis, Groningen Univ., 1978.

[6] Bosma A. and van der Kruit P. C., Astron.Astrophys., **79** (1979) 281.

[7] Rubin V. C., Thonnard N. and Ford W. K. Jr., Astrophys. J. **238** (1980) 471.

[8] Silk J., The Big Bang (Freeman, 1988 edition).

[9] Metcalf R.B. and Silk J., Phys. Rev. Lett. **98** (2007) 071302.

[10] Goddard Space Flight Center (May 14, 2004). Dark Matter may be Black Hole Pinpoints. NASA's Imagine the Universe.

[11] Di Cintio A., Brook C. B., Macciò A. V., Stinson G. S., Knebe A., Dutton A. A. and Wadsley J., Mon. Not. Roy. Astron. Soc. **437** (2014) no.1, 415.

[12] Navarro J. F., Frenk C. S. and White S. D. M., Astrophys. J. **462** (1996) 563.

[13] Navarro J. F., Frenk C. S. and White S. D. M., Astrophys. J. **490** (1997) 493.

[14] Moore B., Nature **370** (1994) 629.

[15] Salucci P. and Burkert A., Astrophys. J. **537** (2000) L9.

[16] de Blok W. J. G. and Bosma A., Astron. Astrophys. **385** (2002) 816.

[17] de Blok W. J. Walter G., Brinks F. E., Trachternach C., Oh S. H. and Kennicutt R. C. Jr., Astron. J. **136** (2008) 2648.

[18] Gentile G., Salucci P., Klein U., Vergani D. and Kalberla P., Mon. Not. Roy. Astron. Soc. **351** (2004) 903.

[19] Gentile G., Burkert A., Salucci P., Klein U. and Walter F., Astrophys. J. Lett. **634** (2005) L145.

[20] Oh S. H. *et al.*, Astron. J. **149** (2015) 180.

[21] Salucci P., Lapi A., Tonini C., Gentile G., Yegorova I. and Klein U., Mon. Not. Roy. Astron. Soc. **378** (2007) 41.

[22] Donato F. *et al.*, Mon. Not. Roy. Astron. Soc. **397** (2009) 1169.

[23] Karukes E. V. and Salucci P., Mon. Not. Roy. Astron. Soc. **465** (2017) no.4, 4703.

[24] Chan T. K., Kereš D., Oñorbe J., Hopkins P. F., Muratov A. L., Faucher-Giguère C. A. and Quataert E., Mon. Not. Roy. Astron. Soc. **454** (2015) no.3, 2981.

[25] de Blok E., McGaugh S. and Rubin V., [arXiv:0107366].

[26] Spergel D. N. and Steinhardt P. J., Phys. Rev. Lett. **84** (2000) 3760.

[27] Boehm C., Fayet P. and Schaeffer R., Phys. Lett. B **518** (2001) 8.

[28] Boehm C., Riazuelo A., Hansen S. H. and Schaeffer R., Phys. Rev. D **66** (2002) 083505.

[29] Dvorkin C., Blum K. and Kamionkowski M., Phys. Rev. D **89** (2014) no.2, 023519.

[30] Lovell M. R., Frenk C. S., Eke V. R., Jenkins A., Gao L. and Theuns T., Mon. Not. Roy. Astron. Soc. **439** (2014) 300.

[31] de Vega H. J., Salucci P. and Sanchez N. G., Mon. Not. Roy. Astron. Soc. **442** (2014) no.3, 2717.

[32] Colin P., Valenzuela O. and Avila-Reese V., Astrophys. J. **673** (2008) 203.

[33] Kuzio de Naray R., Martinez G. D., Bullock J. S. and Kaplinghat M., Astrophys. J. **710** (2010) L161.

[34] Maccio A. V., Paduroiu S., Anderhalden D., Schneider A. and Moore B., Mon. Not. Roy. Astron. Soc. **424** (2012) 1105.

[35] Bernabei R. *et al.*, Phys. Lett. B **424** (1998) 195.

[36] Beringer J. *et al.*, Phys. Rev. D **86** (2012) 010001.

[37] Ahmed Z. *et al.*, Science **327** (2010) 1619.

[38] Aalseth C. E. *et al.*, Phys. Rev. D **88** (2013) 012002.

[39] McCabe C., Phys. Rev. D **84** (2011) 043525.

[40] Herrero-Garcia J., Schwetz T. and Zupan J., Phys. Rev. Lett. **109** (2012) 141301.

[41] Angloher G. *et al.*, Eur. Phys. J. C **72** (2012) 1971.

[42] Adriani O. *et al.*, Nature **458** (2009) 607.

[43] Adriani O. *et al.*, Phys. Rev. Lett. **102** (2009) 051101.

[44] D. S. Akerib *et al.* , Nucl. Instrum. Meth. A **704** (2013) 111.

[45] D. S. Akerib *et al.*, Phys. Rev. Lett. **116** (2016) no.16, 161302.

[46] E. Aprile *et al.*, arXiv:1705.06655.

[47] Milgrom, M. Astrophys. J. **270** (1983) 365.

[48] Bekenstein J. D., Phys. Rev. D **70** (2004) 083509, Erratum: [Phys. Rev. D **71** (2005) 069901].

[49] Buchdahl H. A., Mon. Not. Roy. Astron. Soc. **150** (1970) 1.

[50] Clowe D., Bradac M., Gonzalez A. H., Markevitch M., Randall S. W., Jones C. and Zaritsky D., Astrophys. J. **648** (2006) L109.

[51] Angus G. W., Shan H., Zhao H. and Famaey B., Astrophys. J. **654** (2007) L13.

[52] Sanders R. H., Mon. Not. Roy. Astron. Soc. **380** (2007) 331.

[53] Angus G. W., Famaey B. and Buote D. A., Mon. Not. Roy. Astron. Soc. **387** (2008) 1470.

[54] Angus G. W., Mon. Not. Roy. Astron. Soc. **394** (2009) 527.

[55] Angus G. W., Diaferio A., Famaey B. and van der Heyden K. J., Mon. Not. Roy. Astron. Soc. **436** (2013) 202.

[56] Alcubierre M., Guzman F. S., Matos T., Nunez D., Urena-Lopez L. A. and Wiederhold P., Class. Quant. Grav. **19** (2002) 5017.

[57] Alcubierre M., Guzman F. S., Matos T., Nunez D., Urena-Lopez L. A. and Wiederhold P., [arXiv:0204307].

[58] Bernal A. and Siddhartha Guzman F., Phys. Rev. D **74** (2006) 103002.

[59] Bernal A. and Guzman F. S., Phys. Rev. D **74** (2006) 063504.

[60] Rodriguez-Meza M. A. and Cervantes-Cota J. L., Mon. Not. Roy. Astron. Soc. **350** (2004) 671.

[61] Sobouti Y., Astron. Astrophys. **464** (2007) 921, Erratum: [Astron. Astrophys. **472** (2007) 833].

[62] Mendoza S. and Rosas-Guevara Y. M., Astron. Astrophys. **472** (2007) 367.

[63] Sotiriou T. P. and Faraoni V., Rev. Mod. Phys. **82** (2010) 451.

[64] Holmberg, E., Meddelanden fran Lunds Astronomiska Observatorium Serie II (1958) A13.

[65] Roberts, M.S. 1975a. Proc. IAU Symp. 69:331.

[66] Toomre A., Astrophys. J. **138** (1963) 385.

[67] Brandt, John C. Astrophysical Journal, **131**, (1960), p.293.

[68] Kent S. M., Astron. J. **93** (1987) 816.

[69] Freeman K. C., Astrophys. J. **160** (1970) 811.

[70] Tully R. B. and Fisher J. R., Astron. Astrophys. **54** (1977) 661.

[71] Athanassoula E., Bosma A. and Papaioannou S., Astron.Astrophys. **179**, (1987) 23.

[72] Persic M. and Salucci P., Mon. Not. Roy. Astron. Soc. **234** (1988) 131.

[73] Palunas P. and Williams T. B., Astron. J. **120** (2000) no.6, 2284.

[74] Salucci P. and Persic M., Astron. Astrophys. **351** (1999) 442.

[75] Begeman K. G., Broeils A. H. and Sanders R. H., Mon. Not. Roy. Astron. Soc. **249** (1991) 523.

[76] Famaey B., Gentile G., Bruneton J. P. and Zhao H. S., Phys. Rev. D **75** (2007) 063002.

[77] Bekenstein J. and Milgrom M., Astrophys. J. **286** (1984) 7.

[78] Milgrom M., Mon. Not. Roy. Astron. Soc. **403** (2010) 886.

[79] Sanders R. H. and McGaugh S. S., Ann. Rev. Astron. Astrophys. **40** (2002) 263.

[80] Kent S. M., Astron. J. **91** (1986) 1301.

[81] Sanders R. H., Astrophys. J. **473** (1996) 117.

[82] de Blok W. J. G. and McGaugh S. S., Astrophys. J. **508** (1998) 132.

[83] McGaugh S. S., Astrophys. J. **609** (2004) 652.

[84] McGaugh S. S., Astrophys. J. **632** (2005) 859.

[85] Clifton T., Ferreira P. G., Padilla A. and Skordis C., Phys. Rept. **513** (2012) 1.

[86] Slosar A., Melchiorri A. and Silk J., Phys. Rev. D **72** (2005) 101301.

[87] Seifert M. D., Phys. Rev. D **76** (2007) 064002.

[88] Zhang P., Liguori M., Bean R. and Dodelson S., Phys. Rev. Lett. **99** (2007) 141302.

[89] Starobinsky A. A., Phys. Lett. **91B** (1980) 99.

[90] Flanagan E. E., Class. Quant. Grav. **21** (2004) 3817.

[91] Iglesias A., Kaloper N., Padilla A. and Park M., Phys. Rev. D **76** (2007) 104001.

[92] Barausse E., Sotiriou T. P. and Miller J. C., Class. Quant. Grav. **25** (2008) 062001.

[93] Olmo G. J., Phys. Rev. Lett. **95** (2005) 261102.

[94] Capozziello S., Cardone V. F. and Troisi A., Mon. Not. Roy. Astron. Soc. **375** (2007) 1423.

[95] Klypin A., Kravtsov A. V., Bullock J. and Primack J., Astrophys. J. **554** (2001) 903.

[96] Hayashi E. *et al.*, [arXiv:0408132].

[97] Diemand J., Zemp M., Moore B., Stadel J. and Carollo M., Mon. Not. Roy. Astron. Soc. **364** (2005) 665.

[98] Caimmi R. and Marmo C., Serb. Astron. J. **169** (2004) 11.

[99] Burkert A., IAU Symp. **171** (1996) 175, [Astrophys. J. **447** (1995) L25].

[100] Bullock J. S., Kolatt T. S., Sigad Y., Somerville R. S., Kravtsov A. V., Klypin A. A., Primack J. R. and Dekel A., Mon. Not. Roy. Astron. Soc. **321** (2001) 559.

[101] Dutton A. A. and Macciò A. V., Mon. Not. Roy. Astron. Soc. **441** (2014) no.4, 3359.

[102] Ade P. A. R. *et al.*, Astron. Astrophys. **594** (2016) A13.

[103] Salucci P., Nesti F., Gentile G. and Martins C. F., Astron. Astrophys. **523** (2010) A83.

[104] Corbelli E., Mon. Not. Roy. Astron. Soc. **342** (2003) 199.

[105] Corbelli E., Thilker D., Zibetti S., Giovanardi C. and Salucci P., Astron. Astrophys. **572** (2014) A23.

[106] Corbelli E. and Walterbos R. A. M., Astrophys. J. **669** (2007) 315.

[107] Bevington P. R. and Robinson K. D., Data reduction and error analysis for the physical sciences, McGraw-Hill, 2003.

[108] Bell E. F. and de Jong R. S., Astrophys. J. **550** (2001) 212.

[109] Portinari L. and Salucci P., Astron. Astrophys. **521** (2010) A82.

[110] Zibetti S., Charlot S. and Rix H. W., Mon. Not. Roy. Astron. Soc. **400** (2009) 1181.

[111] González Delgado R. M. *et al.*, Astron. Astrophys. **562** (2014) A47.

[112] Massey P., Olsen K. A. G., Hodge P. W., Strong S. B., Jacoby G. H., Schlingman W. and Smith R. C., Astron. J. **131** (2006) 2478.

[113] York D. G. *et al.*, Astron. J. **120** (2000) 1579.

[114] Casertano S., Mon Not R Astron Soc (1983) **203** 203 (3): 735.

[115] Gratier P. *et al.*, Astron. Astrophys. **522** (2010) A3.

[116] Druard C., Braine J., Schuster K. F., Schneider N., *et. al.*, Astron. Astrophys. **567** (2014) A118.

[117] Corbelli E. and Schneider S. E., Astrophys. J. **479** (1997) 244.

[118] Martins C. F. and Salucci P., Mon. Not. Roy. Astron. Soc. **381** (2007) 1103.

[119] Salucci P., Martins C. F. and Karukes E., Int. J. Mod. Phys. D **23** (2014) no.12, 1442005.

[120] Karukes E. V., Salucci P. and Gentile G., Astron. Astrophys. **578** (2015) A13.

[121] Fune E. L., Salucci P. and Corbelli E., Mon. Not. R. Astron. Soc. **468** (2017), 147.

[122] Lelli F., Verheijen M. and Fraternali F., Astron. Astrophys. **566** (2014) A71.

[123] Weldrake D., de Blok E. and Walter F., Mon. Not. Roy. Astron. Soc. **340** (2003) 12.

[124] Moiseev A. V., Astrophys. Bull. **69** (2014) 1.

[125] Swaters R. A., Sancisi R., van Albada T. S. and van der Hulst J. M., Astron. Astrophys. **493** (2009) 871.

[126] Persic M. and Salucci P., Astrophys. J. Suppl. **99** (1995) 501.

[127] Kuzio de Naray R., McGaugh S. S., de Blok W. J. G. and Bosma A., Astrophys. J. Suppl. **165** (2006) 461.

[128] Kuzio de Naray R., McGaugh S. S. and de Blok W. J. G., Astrophys. J. **676** (2008) 920.